6-22-2018

New Platinum(II) and Rhenium(I) Complexes of "Linear" Chelate Ligands Terminated with Pyridyl or Imidazolyl N-Donor Groups

Himali Kokila Ranasinghe Pilana Vithanage
Louisiana State University and Agricultural and Mechanical College, himaliran@gmail.com

NEW PLATINUM(II) AND RHENIUM(I) COMPLEXES OF "LINEAR" CHELATE LIGANDS TERMINATED WITH PYRIDYL OR IMIDAZOLYL N-DONOR GROUPS

A Dissertation

Submitted to the Graduate Faculty of the
Louisiana State University and
Agricultural and Mechanical College
in partial fulfillment of the
requirements for the degree of
Doctor of Philosophy

in

The Department of Chemistry

by
Himali Kokila Ranasinghe Pilana Vithanage
B.Sc. University of Sri Jayewardenepura, Sri Lanka, 2012
August 2018

We must not forget that when radium was discovered no one knew that it would prove useful in hospitals. The work was one of pure science. And this is a proof that scientific work must not be considered from the point of view of the direct usefulness of it. It must be done for itself, for the beauty of science, and then there is always the chance that a scientific discovery may become like the radium a benefit for humanity.

– Marie Curie

Lecture at Vassar College, Poughkeepsie, New York (14 May 1921)

ACKNOWLEDGMENTS

First of all, I would like to thank my research advisor, Dr. Luigi Marzilli, for his guidance and support throughout my doctoral work. His knowledge and expertise in the field of Inorganic Chemistry always inspire me to work harder each day in the lab and to read more about the subject. I would also like to thank Dr. Patricia Marzilli for her kindness and patience shown throughout by endlessly correcting my manuscripts. I should gratefully mention my undergraduate supervisor, Dr. Theshini Perera, for being the first and the main inspiration of my decision to pursue a PhD. I specially thank my committee members, Dr. Megan Macnaughtan, Dr. Weiwei Xie, Dr. William Crowe and Dr. David Baker for their support and for offering advice when needed.

I would like to thank Dr. Frank Fronczek and Dr. Svetlana Pakhomova for their X-ray structure determinations and Dr. Thomas Weldeghiorghis and Dr. Fengli for their useful NMR discussions. Further, I would like to thank all the other faculty and staff members and friends at LSU who have helped me in many ways. Especially, I would like to thank my former labmates, Drs. Nerissa Lewis, Chase Andrepont and Pramuditha Abhayawardhana for the support given to me since the very first day I began my journey in the Marzilli Lab.

Last but not least, I would like to thank my family for being there with me (physically or mentally) throughout this tough journey. I am eternally grateful to my parents for loving me unconditionally and for giving me all the freedom in the world to dream and achieve big. I appreciate the love and support given by my younger siblings, Sanka and Neeliya. I must also thank my parents-in-law for taking me as their own and for encouraging me to achieve my goals. My deepest appreciation goes to my husband, Asela, for taking a detour from his career to be here with me in USA and for the endless support given to keep my life in proper balance during past few years.

TABLE OF CONTENTS

LIST OF TABLES

LIST OF FIGURES

LIST OF ABBREVIATIONS

Abbreviation	Definition
NMR	nuclear magnetic resonance
ESI	electrospray ionization
min	minutes
h	hours
Hz	hertz
MHz	megahertz
ppm	parts per million
mM	milimolar
mL	milliliter
μL	microliter
mmol	milimoles
d	doublet
s	singlet
m	multiplet
equiv	equivalent
TMS	trimethylsilane
DMSO	deuterated dimethyl sulfoxide
D_2O	deuterated water
1D	one-dimentional
2D	two-dimentional
RT	room temperature

ABSTRACT

The overall goal of this dissertation research is to design, synthesize, and study new Pt(II) and Re(I) complexes relevant to biomedical applications. One of the projects involves the assessment of the interactions of bulky tridentate carrier ligands with a bound guanine nucleobase derivative (**G**) in platinum complexes, with a goal of developing chemistry potentially relevant to active anti-cancer Pt drugs. In another project, the *fac*-$[Re^{I}(CO)_3]^+$ core is used to prepare novel Re(I) complexes with the purpose of developing new linking chemistry relevant to ^{99m}Tc and ^{187}Re radiopharmaceuticals. This research explores the use of three different types of linear carrier-ligands in approaches directed toward achieving the stated goals.

The first type of linear tridentate carrier ligand employed (*N*(R)1,1′-Me_2dma, when R = H, bis(1-methyl-2-methylimidazolyl)amine) is terminated by imidazolyl rings and has a central N-donor with an NH or an N−C bond. High in-plane steric bulk in monofunctional Pt(II) complexes is a feature associated with increased anti-cancer activity. Therefore, understanding carrier-ligand steric effects is crucial in designing new platinum drugs. For that purpose, the new *N*(R)1,1′-Me_2dma ligands were utilized to synthesize [Pt(II)(*N*(R)1,1′-Me_2dma)Cl]Cl complexes. The chemical behavior of adducts of simple purine derivatives (**G**) made with these monofunctional Pt(II) complexes was studied. The ligands and complexes were characterized using NMR spectroscopy, single-crystal X-ray crystallography and ESI mass spectrometry. Solution NMR spectroscopy was used as the primary tool to study the Pt(II)(*N*(R)1,1′-Me_2dma)**G** adducts. During this work, the 3′-GMP mono adduct of [Pt(*N*(H)1,1′-Me_2dma)Cl]Cl complex was crystallized, allowing the first crystallographic molecular structure determination for a 3′-GMP platinum(II) complex.

The other two types of linear tridentate ligands have the central N donor in a sulfonamide linkage. New ligands terminated with either two pyridyl rings (second type, *N*(SO_2R)3,3′,5,5′-Me_4dpa and *N*(SO_2R)6,6′-Me_2dpa, derivatives of 2-dipicolylamine) or with two imidazolyl rings (third type, *N*(SO_2R)1,1′-Me_2dma) were prepared. Pt(II) and Re(I) complexes of these new ligands were synthesized and their chemical properties studied.

CHAPTER 1. INTRODUCTION

Transition metal complexes play an important role in modern medicine.[1-2] Anticancer activity in Pt(II) complexes,[3] radio-diagnostic properties of ^{99m}Tc complexes,[4] radio-therapeutic properties of ^{187}Re complexes,[4] anti-metastatic activity of Ru(III) complexes[1] and antiarthritic properties of Au(I) complexes[1] are some common examples illustrating the involvement of metal compounds in therapeutic and diagnostic pharmaceuticals. In metal-mediated pharmaceuticals, the metal atom is often chelated by a carrier ligand. In addition to coordinating to the metal atom, a carrier-ligand can introduce new properties to the pharmaceutical agent. As an example, by linking a targeting moiety onto the carrier ligand, a drug molecule can be delivered to a specific destination in the body such as a tumor (Figure 1.1).

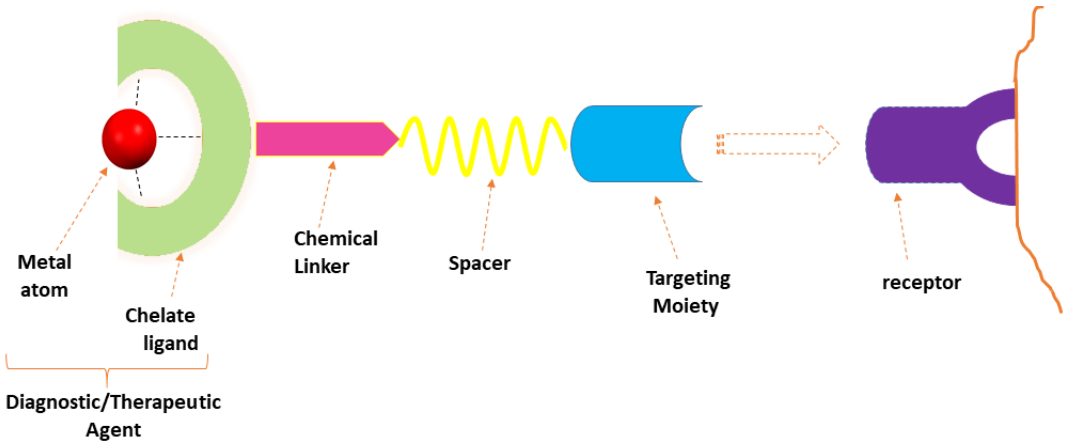

Figure 1.1. Schematic representation of a target-specific metal-mediated therapeutic or diagnostic drug molecule.

Therefore, developing new linking strategies relevant to the chelating ligands is crucial in designing new metal-mediated pharmaceuticals with specific chemical properties. Furthermore, steric factors of the carrier ligands can be directly associated with the structure-activity relationship of certain drug molecules. In such cases, understanding carrier ligand steric effects is important in designing new drugs; one such example is the anticancer activity in platinum(II) complexes.[5-7]

1.1 Carrier-Ligand Bulk and Anticancer Activity in Platinum(II) Complexes

Platinum complexes exclusively bind at the N7 atom in purine bases (preferably guanine) of DNA. There are two major types of platinum−DNA adducts: intrastrand cross-links and monofunctional adducts (Figure 1.2).[8-10] Predominantly, the 1,2 intrastrand G*G* cross-link lesion is considered as the active lesion responsible for the anticancer activity of cisplatin.[11-17] G* represents G residues in DNA or oligomers with a Pt(II) bound to N7.

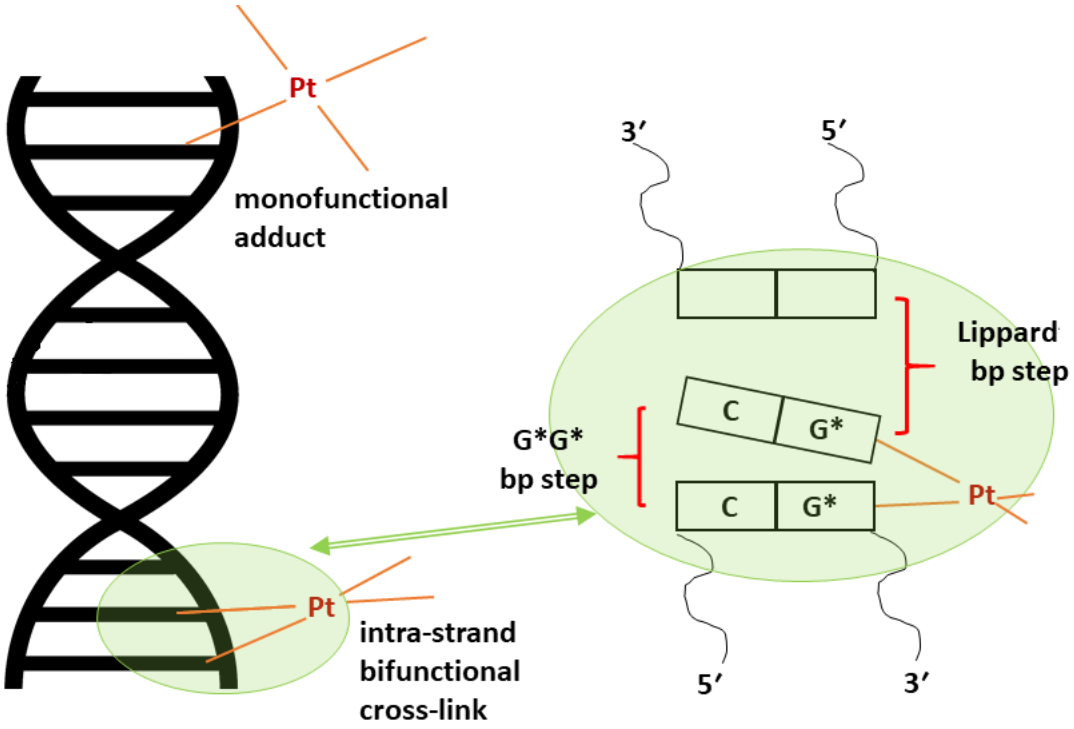

Figure 1.2. Chart showing common Pt−DNA binding modes and the distorted G*G* and Lippard's base pair steps in intrastrand cross-link lesions.

Studies of an HMG-bound 16-mer duplex studied by X-ray methods[18] and a 9-mer duplex studied by NMR methods in solution[19] reveal that the DNA distortion induced by cisplatin (G*G* cross-link lesion) extends over two base pair (bp) steps (Figure 1.2), the cross-link bp step (between the 5′-G*·C bp and the 3′-G*·C bp) and the adjacent bp step (also referred to as the Lippard bp step,[20] between the 5′-G*·C bp and the next bp in the 5′-direction along the duplex).

Both bp steps are highly distorted. Both solid-state and solution studies have revealed that the Lippard bp step has a large shift and a large slide.[18-19,21] Therefore, the Lippard bp step could possibly play a more important role in anticancer activity than the G*G* cross-link bp step.[19-22]

1.2 Monofunctional Platinum Complexes and Pt(L^{tri})G Adducts

Monofunctional platinum complexes were considered as inactive in early days.[23-24] Because the monofunctional agents studied previously contained small carrier ligands (such as [Pt(diethylenetriamine)Cl]Cl and [Pt(NH_3)$_3$Cl]Cl),[18,25-27] the small distortion to the DNA structure created by these compounds is insufficient to inhibit cancer cell growth. Later, certain monofunctional platinum complexes containing bulky carrier ligands were found to be anticancer active (pyriplatin and phenanthriplatin);[28] this finding increased interest in developing monofunctional platinum anticancer agents. A distortion very similar to that found in the Lippard bp step of DNA having the cisplatin lesion was later also observed in an X-ray structure of an oligomer adduct of the bulky monofunctional platinum anticancer agent, *cis*-[Pt(NH_3)$_2$(pyridine)Cl]$^+$ (pyriplatin).[29-30] This finding indicates that the monofunctional platinum agents can be anticancer active, if enough bulk is present at one cis position to induce distortion in the adjacent bp step in DNA. Therefore, studying carrier-ligand steric effects is key in designing such new monofunctional platinum drugs and in understanding their mechanism of action.

Studying DNA duplexes bearing Pt drug lesions can be very complicated. Work from this laboratory[19] showed many mistakes were made in such studies and the nature of the distortion reported in several papers was not correct. Historically, simple models (adducts with small oligomers, or with single stranded DNA, etc.) are often employed to execute preliminary studies of new platinum complexes.[18-19,31-34] Adducts of platinum complexes with unlinked guanine/hypoxanthine derivatives (**G**) are the simplest models;[31,35-36] hence, they provide an

accurate starting point to study the chemical and physical properties of new platinum agents. Also, such simple models allow one to employ invaluable characterization techniques such as NMR spectroscopy or X-ray crystallography.[5-7,16,37] In the studies presented here, we assess the interactions of **G** with newly designed platinum(II) complexes (bifunctional and monofunctional), specifically the influence of carrier-ligand bulk on the properties of the formed **G** adducts.

The nucleobase (**G**) in Pt(L^{tri})**G** type adducts (L^{tri} = a tridentate, one bidentate and one monodentate, or three monodentate ligands) orients roughly perpendicular to the coordination plane defined by Pt and the four ligating atoms N, N′, N″, and Cl or N7(**G**). The nucleobase can rotate around the Pt–N7 single bond and acquire two possible orientations (Figure 1.3, arrow up and arrow down). When N, N′, and N″ are symmetric with respect to the coordination plane and N equals N″, both orientations lead to one rotamer, if R′ is not chiral. If N is not equal to N″, the two orientations represent two rotamers. If N′ is not symmetric with respect to the coordination plane, two rotamers are possible regardless of whether or not N is equal to N″.

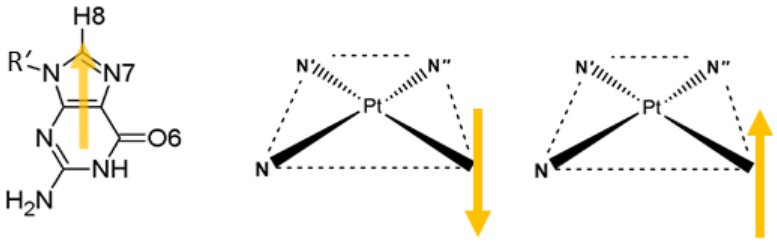

Figure 1.3. The two possible orientations of **G** in Pt(L^{tri})**G** type adducts. Note that the nucleobase is represented by an arrow with the tip at the H8 of the purine.

If the rotation of **G** around the Pt–N7 bond is too fast relative to the NMR time scale, only one set of signals for the two rotamers of the Pt(L^{tri})**G** adduct can be observed. However, if the L^{tri} carrier ligand is bulky enough to impede the nucleobase rotation, two separate sets of signals for each rotamer can be observed. NMR spectroscopy can thus be used effectively to assess whether a L^{tri} ligand is bulky enough to interact with **G** (and interfere with its free rotation) in a Pt(L^{tri})**G**

type adduct. Such information can provide insight into how that monofunctional platinum complex would influence the structure of Pt−DNA adducts on the cellular level.

1.3 Rhenium Complexes as Models for Diagnostic and Therapeutic Radiopharmaceuticals

Nuclear medicine is a powerful, non-invasive tool, which can be used for diagnostic and therapeutic medical processes for many diseases. Technetium-99m (^{99m}Tc) is one of the most widely used radio-imaging agents.[4,38-39] The radioactive isotope of rhenium, ^{187}Re, has also received much attention owing to its useful therapeutic properties.[4,38-39] Rhenium and technetium are members of the same group in the periodic table and share similar chemical and physical properties. Therefore, non-radioactive Re(I) complexes (^{185}Re) are commonly used as models in developing new radiopharmaceuticals of ^{99m}Tc and ^{187}Re.[38-39] In such developments, *fac*-$[M^{I}(CO)_3]^+$ core plays a major role because of its many ideal properties relevant to medicinal applications (such as high *in vivo* robustness, stable association of the low oxidation numbered metal atom, water-soluble precursor complex, *fac*-$[M^{I}(CO)_3(H_2O)_3]^+$, etc.).[4,40] Many carrier-ligand systems coordinated to the *fac*-$[M^{I}(CO)_3]^+$ core have been studied.[4,38-39,41] However, developing new linking strategies with different bioconjugation possibilities is useful in designing new radiopharmaceuticals.

1.4 References

1. Guo, Z.; Sadler, P. J. *Angew. Chem. Int. Ed.* **1999,** *38* (11), 1512-1531.

2. Bagchi, A.; Mukherjee, P.; Raha, A. *Int. j. adv. pharm.* **2015,** *5*, 171-180.

3. Lippert, B., *Cisplatin. Chemistry and Biochemistry of a Leading Anticancer Drug*. 1999.

4. Paulo, A.; Morais, G. R.; Santos, I. In *Advances in Organometallic Chemistry and Catalysis*, Pombeiro, A. J., Ed. 2014.

5. Andrepont, C.; Marzilli, P. A.; Marzilli, L. G. *Inorg. Chem.* **2012,** *51* (21), 11961-11970.

6. Andrepont, C.; Marzilli, P. A.; Pakhomova, S.; Marzilli, L. G. *J. Inorg. Biochem.* **2015,** *153*, 219-230.

7. Andrepont, C.; Pakhomova, S.; Marzilli, P. A.; Marzilli, L. G. *Inorg. Chem.* **2015,** *54*, 4895-4908.

8. Eastman, A. In *Cisplatin. Chemistry and Biochemistry of a Leading Anticancer Drug*, Lippert, B., Ed. Wiley-VCH: Weinheim, 1999.

9. Takahara, P. M.; Frederick, C. A.; Lippard, S. J. *J. Am. Chem. Soc.* **1996,** *118* (49), 12309-12321.

10. Spingler, B.; Whittington, D. A.; Lippard, S. J. *Inorg. Chem.* **2001,** *40* (22), 5596-5602.

11. Bloemink, M. J.; Reedijk, J.; Sigel, A.; Sigel, H., *Metal Ions in Biological Systems*. Marcel Dekker, Inc: New York, 1996; Vol. 32, p 641-685.

12. Saad, J. S.; Natile, G.; Marzilli, L. G. *J. Am. Chem. Soc.* **2009,** *131*, 12314-12324.

13. Reedijk, J. *Chem. Commun.* **1996,** (7), 801-806.

14. Todd, R. C.; Lippard, S. J. *J. Inorg. Biochem.* **2010,** *104*, 902-908.

15. Ober, M.; Lippard, S. J. *J. Am. Chem. Soc.* **2008,** *130*, 2851-2861.

16. Bhattacharyya, D.; Marzilli, P. A.; Marzilli, L. G. *Inorg. Chem.* **2005,** *44* (21), 7644-7651.

17. Malina, J.; Novakova, O.; Vojtiskova, M.; Natile, G.; Brabec, V. *Biophys. J.* **2007,** *93* (11), 3950-3962.

18. Ohndorf, U.-M.; Rould, M. A.; He, Q.; Pabo, C. O.; Lippard, S. J. *Nature* **1999,** *399* (6737), 708-712.

19. Marzilli, L. G.; Saad, J. S.; Kuklenyik, Z.; Keating, K. A.; Xu, Y. *J. Am. Chem. Soc.* **2001,** *123* (12), 2764-2770.

20. Sullivan, S. T.; Ciccarese, A.; Fanizzi, F. P.; Marzilli, L. G. *J. Am. Chem. Soc.* **2001,** *123*, 9345-9355.

21. Sullivan, S. T.; Saad, J. S.; Fanizzi, F. P.; Marzilli, L. G. *J Am Chem Soc* **2002,** *124* (8), 1558-1559.

22. Saad, J. S.; Benedetti, M.; Natile, G.; Marzilli, L. G. *Inorg. Chem.* **2011,** *50*, 4559-4571.

23. Macquet, J.-P.; Butour, J.-L. *J. Natl. Cancer Inst.* **1983,** *70* (5), 899-905.

24. Cleare, M. J.; Hoeschele, J. D. *Bioinorg. Chem.* **1973,** *2* (3), 187-210.

25. Wang, Z.; Yu, H.; Gou, S.; Chen, F.; Fang, L. *Inorg. Chem.* **2016,** *55* (9), 4519-4528.

26. Reily, M. D.; Marzilli, L. G. *J. Am. Chem. Soc.* **1985,** *107*, 4916-4924.

27. Marzilli, L. G.; Reily, M. D.; Heyl, B. L.; McMurray, C. T.; Wilson, W. D. *FEBS Lett.* **1984,** *176* (2), 389-392.

28. Johnstone, T. C.; Suntharalingam, K.; Lippard, S. J. *Phil. Trans. R. Soc. A* **2015,** *373* (2037).

29. Lovejoy, K. S.; Todd, R. C.; Zhang, S.; McCormick, M. S.; D'Aquino, J. A.; Reardon, J. T.; Sancar, A.; Giacomini, K. M.; Lippard, S. J. *Proc. Natl. Acad. Sci.* **2008,** *105* (26), 8902-8907.

30. Todd, R. C.; Lippard, S. J.; Bonetti, A.; Leone, R.; Muggia, F. M.; Howell, S. B., *Platinum and Other Heavy Metal Compounds in Cancer Chemotherapy*. Humana Press: New York, 2009; p 67-72.

31. Ano, S. O. K., Z.; Marzilli, L. G. In *Cisplatin: Chemistry and Biochemistry of a Leading Anticancer Drug*, Lippert, B., Ed. Wiley-VCH: Weinheim, 1999; pp 247–291.

32. Berners-Price, S. J.; Ranford, J. D.; Sadler, P. *Inorg. Chem.* **1994,** *33*, 5842-5846.

33. Kelland, L. *Nature (London)* **2007,** *7* (8), 573-584.

34. Wilson, J. J.; Lippard, S. J. *J. Med. Chem.* **2012,** *55*, 5326-5336.

35. Cramer, R. E.; Dahlstrom, P. L.; Seu, M. J. T.; Norton, T.; Kashiwagi, M. *Inorg. Chem.* **1980,** *19* (1), 148-154.

36. Cramer, R. E.; Dahlstrom, P. L. *J. Am. Chem. Soc.* **1979,** *101* (13), 3679-3681.

37. Maheshwari, V.; Marzilli, P. A.; Marzilli, L. G. *Inorg. Chem.* **2008,** *47* (20), 9303-9313.

38. Perera, T.; Abhayawardhana, P.; Marzilli, P. A.; Fronczek, F. R.; Marzilli, L. G. *Inorg. Chem.* **2013,** *52*, 2412−2421.

39. Abhayawardhana, P.; Marzilli, P. A.; Perera, T.; Fronczek, F. R.; Marzilli, L. G. *Inorg. Chem.* **2012,** *51* (13), 7271-7283.

40. Bartholoma, M.; Valliant, J.; Maresca, K. P.; Babichc, J.; Zubieta, J. *Chem. Commun.* **2009,** *5*, 493-512.

41. Wei, L.; Babich, J. W.; Ouellette, W.; Zubieta, J. *Inorg. Chem* **2006,** *45* (7), 3057-3066.

CHAPTER 2. A VERY RARE EXAMPLE OF A STRUCTURALLY CHARACTERIZED 3′-GMP METAL COMPLEX. NMR AND SYNTHESTIC ASSESSMENT OF ADDUCTS FORMED BY GUANINE DERIVATIVES WITH [Pt(L^{tri})Cl]Cl COMPLEXES WITH AN N,N′,N″ TRIDENTATE LIGAND (L^{tri}) TERMINATED BY IMIDAZOLE RINGS*

2.1 Introduction

High carrier-ligand bulk leads to decreases in anticancer activity and increases in toxicity of bifunctional platinum(II) anticancer agents,[42-46] whereas for monofunctional platinum(II) agents we believe[5-6,12,47] that high carrier-ligand bulk correlates with increased anticancer activity.[12,25,29,48-50] Bifunctional agents, such as cisplatin, form G*G* intrastrand cross-link lesions and cause large distortions in DNA structure, manifest in large changes in CD[51] and NMR[26-27] spectra. (G residues in DNA or oligomers with a Pt(II) center bound to N7 are designated as G*). In contrast, small monofunctional platinum agents, such as [Pt(dien)Cl]Cl (dien = diethylenetriamine) and [Pt(NH_3)$_3$Cl]Cl, cause minimal changes in the DNA CD[14,18] and NMR[26-27] spectra, indicating that monofunctional agents with small carrier ligands are unable to distort the DNA structure greatly upon adduct formation.[5] Studies of oligomer duplexes having one G*G* cross-link lesion (an HMG-bound 16-mer duplex studied by X-ray methods[18] and a 9-mer duplex studied by NMR methods in solution[19]) reveal that the DNA distortion induced by bifunctional Pt(II) agents extends over two base pair (bp) steps. The cross-link bp step (between the 5′-G*•C bp and the 3′-G*•C bp) and the adjacent bp step (between the 5′-G*•C bp and the next bp in the 5′-direction along the duplex) are both highly distorted.

---

*Reproduced with permission from American Chemical Society: Ranasinghe, Kokila.; Marzilli, Patricia A.; Pakhomova, Svetlana.; Marzilli, Luigi G. "A Very Rare Example of a Structurally Characterized 3′-GMP Metal Complex. NMR and Synthetic Assessment of Adducts Formed by Guanine Derivatives with [Pt(L^{tri})Cl]Cl Complexes with an N,N′,N″ Tridentate Ligand (L^{tri}) Terminated by Imidazole Rings." *Inorg. Chem.* (2017), 56(14), 8462-8477. Copyright 2017 American Chemical Society.

Both solid-state and solution structural studies have revealed that the adjacent bp step has a large shift and a large slide.[18-19,21] Therefore, we considered the possibility that this highly distorted bp step could play an important role in anticancer activity.[19-20]A very similar distortion as found in this adjacent bp step was later observed in an X-ray structure of an oligomer adduct of a bulky monofunctional platinum anticancer agent.[29-30] Such findings indicate that a monofunctional agent with bulky carrier ligands could manifest anticancer activity by forming DNA adducts with a highly distorted bp step similar to that found in DNA adducts formed by non bulky bifunctional agents such as cisplatin. Understanding carrier-ligand steric effects is thus key in designing new platinum drugs. Adducts formed between the Pt agents and **G** ligands (bold **G** = monodentate *N*9-substituted guanine or hypoxanthine derivative, Figure 2.1) have been studied by NMR methods in order to assess carrier-ligand bulk.[22,47,52]

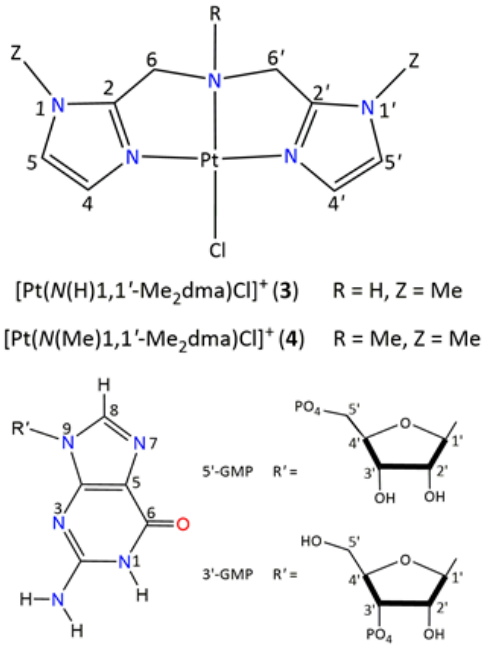

Figure 2.1. *Top*: Numbering scheme for [Pt(*N*(R)1,1′-Me_2dma)Cl]$^+$ complexes containing carrier ligands based on di-(2-methylimidazolyl)amine, *N*(H)dma (R = H, Z = H). To our knowledge, no complexes of *N*(H)dma with Pt are known. *Bottom*: Numbering scheme for the guanine nucleobase and for 3′-GMP and 5′-GMP. Ino and 5′-IMP contain hypoxanthine, having a hydrogen instead of the amino group at position 2 of the purine ring. The atom-numbering schemes depicted here are employed in the NMR discussion.

In order to gain a fundamental understanding of the steric effects within monofunctional Pt(II) **G** adducts, this laboratory has used NMR techniques to assess the properties of Pt(L^{tri})**G** adducts **(**L^{tri} = an *N,N′,N″* tridentate carrier ligand**)** formed by monofunctional platinum agents with L^{tri} ligands based on di-(2-picolyl)amine [*N*(H)dpa] or dien.[5-7,53-54] The present study focuses on the preparation of water-soluble [Pt(II)(L^{tri})Cl]Y complexes of tridentate imidazolyl ligands and on identifying the adducts that these complexes form in solution with various purine derivatives. We utilize both di-(1-methyl-2-methylimidazolyl)amine [*N*(H)1,1′-Me_2dma (**1**)] and a ligand new to the literature, *N*-(methyl)-di-(1-methyl-2-methylimidazolyl)amine [*N*(Me)1,1′-Me_2dma (**2**)]; we designate these ligands as *N*(R)1,1′-Me_2dma (Figure 2.1, R = H, Me). The tridentate ligand, *N*(H)1,1′-Me_2dma, and its derivatives (with a substituent on the central N; e.g., –CH_2CH_2OH) have been used to synthesize complexes of various metals (e.g., Re, Cu, Tc, Fe) usually intended for biomedical applications.[55-62]

We describe the synthesis of [Pt(*N*(H)1,1′-Me_2dma)Cl]Y (**3**) and [Pt(*N*(Me)1,1′-Me_2dma)Cl]Y (**4**) [Y = Cl^- (**3a** and **4a**) and BF_4^- (**3b** and **4b**)] and the structural characterization of their cations by ^{1}H NMR spectroscopy and single-crystal X-ray diffraction. We then use ^{1}H NMR spectroscopy to examine Pt(*N*(R)1,1′-Me_2dma)**G** adducts formed from [Pt(*N*(R)1,1′-Me_2dma)Cl]Cl complexes and compare the results to those of other Pt(L^{tri})**G** adducts. In the present study, the crystallization of one product, [Pt(*N*(H)1,1′-Me_2dma)(3′-GMPH)]NO_3•$5H_2O$ (**5**), allowed characterization by single-crystal X-ray diffraction.

Structures of metal 3′-GMP complexes are particularly rare. Only two molecular structures of complexes with 3′-GMP are described in the literature, and both are Cu(II) complexes. One, [Cu(3′-GMP)(phen)(H_2O)]$_2$•$7H_2O$,[63] lacks M─N7 bonding, and the other, ([Cu_3(3′-GMP)$_2$(3′-GMPH)$_2$(H_2O)$_5$]•$7H_2O$)$_n$,[64] is a polymeric compound exhibiting nucleotide metal coordination

through both the N7 atoms and the phosphate groups. Thus, to our knowledge **5** is the first crystallographically characterized complex with any metal in which 3′-GMP is bound through only an M─N7 bond. Other relevant structures with one Pt─N7 bond do not contain a nucleotide; these are [Pt(dien)(guanosine)]$(ClO_4)_2$,[65] [Pt(dien)(inosine)]$(NO_3)_2$•H_2O,[66] [Pt$(NH_3)_3$(9-methylhypoxanthine)]Cl(NO_3)•1.5H_2O,[67] [Pt$(NH_3)_3$(9-ethylhypoxanthine)]Cl(NO_3)•H_2O,[67] and *cis*-[Pt$(NH_3)_2$(N^2,N^2-dimethyl-9-methylguanine)Cl]PF_6.[68] In contrast, there are many reported structures of complexes with two cis Pt─N7 bonds to **G** ligands, quite often 5′-GMP.[35,44,69-78]

In studies of Pt(*N*(H)dpa)**G** adducts, no quality crystals for single-crystal X-ray structures could be obtained to support the conclusions reached by using NMR methods.[5-7,53] The structure of [Pt(*N*(H)1,1′-Me_2dma)(3′-GMPH)]NO_3•5H_2O (**5**) gives us deeper insights into previous findings on Pt(*N*(H)dpa)**G** adducts, in addition to confirming and supporting our previous analysis of solution results for Pt(*N*(H)dpa)**G** adducts.

2.2 Experimental Section

Starting Materials. Sodium salts of **G** nucleotides [5′-guanosine monophosphate (5′-GMP), 5′-guanosine diphosphate (5′-GDP), 5′-guanosine triphosphate (5′-GTP), 5′-inosine monophosphate (5′-IMP), and 3′-guanosine monophosphate (3′-GMP)], neutral purine derivatives [inosine (Ino), 1-methylguanosine (1-MeGuo), and 9-ethylguanine (9-EtG)], $K_2[PtCl_4]$, 1-methyl-2-imidazolecarboxaldehyde, and methylamine hydrochloride ($MeNH_3Cl$) were used as received from Sigma-Aldrich. *cis*-Pt$(DMSO)_2Cl_2$,[79] *N*(H)1,1′-Me_2dma (**1**),[58] and 2-(chloromethyl)-1-methylimidazole hydrochloride[80] were prepared by known methods. Because the protonation state and hence the charge of the Pt(*N*(R)1,1′-Me_2dma)**G** adducts in which **G** = a nucleotide are not well defined, we omit charges for the adducts. However, charges are specified for structurally characterized isolated complexes.

NMR Measurements. NMR spectra were recorded on an Avance-III Prodigy 500 MHz Bruker spectrometer. Peak positions are relative to TMSP-d_4 in D_2O or to solvent residual peak with TMS as reference. A presaturation pulse to suppress the water peak was employed when necessary. All NMR data were processed with TopSpin and MestReNova 10.0.0 software. The pH values of D_2O or 65:35 D_2O:DMSO-d_6 solutions examined by NMR spectroscopy are stated as measured and not corrected for D_2O. The pH (uncorrected) of all solutions, including reaction mixtures, was adjusted when necessary with DNO_3 or NaOD (0.5 M) D_2O solutions.

Mass Spectrometric Measurements. High resolution mass spectra were recorded on an Agilent 6210 ESI TOF LCMS mass spectrometer.

X-ray Data Collection and Structure Determination. Diffraction data were collected on a Bruker Kappa Apex-II DUO CCD diffractometer with Mo Kα radiation (λ = 0.71073 Å), equipped with an Oxford Cryosystems Cryostream. All X-ray structures were determined by direct methods and difference Fourier techniques and refined by full-matrix least-squares by using *SHELXL2014*[81] with H atoms in idealized positions.

***N*-(methyl)-di-(1-methyl-2-methylimidazolyl)amine [*N*(Me)1,1′-Me$_2$dma, 2].** A solution of 2-(chloromethyl)-1-methylimidazole hydrochloride (1.00 g, 6 mmol), K_2CO_3 (1.7 g, 12 mmol), and $MeNH_3Cl$ (0.16 g, 2.4 mmol) in acetonitrile (100 mL) was heated at reflux under nitrogen for 18 h. After the mixture was allowed to cool to room temperature and filtered, the solvent was removed under reduced pressure. The resulting pale yellow residue was dissolved in eluent A [acetone:5.0 M NH_4OH (80:20)] and purified by chromatography on a silica column with eluent A. The fractions collected were spotted and analyzed on TLC plates by using eluent A. The cleanest fractions, as assessed by ^{1}H NMR spectroscopy, were combined and taken to dryness by rotary evaporation to afford a colorless oil (0.21 g, 40% yield). ^{1}H NMR signals (ppm) in D_2O (pH

8.3): 7.09 (s, 2H, H5/5′), 6.96 (s, 2H, H4/4′), 3.68 (s, 4H, CH_2), 3.56 (s, 6H, CH_3), 2.25 (s, 3H, CH_3). ^{1}H NMR signals (ppm) in DMSO-d_6: 7.07 (s, 2H, H5/5′), 6.76 (s, 2H, H4/4′), 3.52 (s, 4H, CH_2), 3.48 (s, 6H, CH_3), 2.06 (s, 3H, CH_3). ESI-MS (*m/z*): $[M + H]^+$ calcd for $C_{11}H_{17}N_5$, 220.1557; found, 220.1558.

[Pt(*N*(H)1,1′-Me$_2$dma)Cl]Y (3a and 3b). A solution of *N*(H)1,1′-Me$_2$dma (21 mg, 0.1 mmol) in methanol (1 mL) was added to a methanol solution of *cis*-Pt(DMSO)$_2$Cl$_2$ (42 mg, 0.1 mmol, in 5 mL) and the mixture was heated at 50 °C overnight. The pale yellow [Pt(*N*(H)1,1′-Me$_2$dma)Cl]Cl (**3a**) solid (24 mg, 55% yield) formed was collected by filtration, washed with cold methanol, then with ether, and air dried. ^{1}H NMR signals (ppm) in D_2O (pH 4): 7.03 (d, J = 1.5 Hz, 2H), 6.85 (d, J = 1.6 Hz, 2H, H4/4′), 4.63 (d, J = 15.4 Hz, 2H, CH_2), 3.67 (s, 6H, CH_3); one of the methylene signals is masked by the solvent peak. ^{1}H NMR signals (ppm) in DMSO-d_6: 8.31 (bs, 1H, NH), 7.38 (s, 2H, H5/5′), 6.93 (s, 2H, H4/4′), 4.56 (d, J = 15.3 Hz, 2H, CH_2), 4.53 (d, J = 15.0 Hz, 2H, CH_2), 3.73 (s, 6H, CH_3). ESI-MS (*m/z*): $[M + H]^+$ calcd for $C_{10}H_{15}ClN_5Pt$, 436.0737; found, 436.0639. An aqueous solution of [Pt(*N*(H)1,1′-Me$_2$dma)Cl]Cl (**3a**) (80 mg, 2 mL) was treated with an excess of $NaBF_4$ (30 mg) to yield a yellow solid. A solution of this solid in acetone (50 mg, 2 mL) was allowed to stand at room temperature, and slow evaporation produced pale yellow, X-ray quality crystals of [Pt(*N*(H)1,1′-Me$_2$dma)Cl]BF_4 (**3b**) formed after 4 d. ^{1}H NMR signals (ppm) in DMSO-d_6: 8.12 (bs, 1H, NH), 7.38 (2H, H5/5′), 6.93 (2H, H4/4′), 4.55 (d, J = 15.3 Hz, 2H, CH_2), 4.53 (d, J = 15.3 Hz, 2H, CH_2), 3.73 (s, 6H, CH_3).

[Pt(*N*(Me)1,1′-Me$_2$dma)Cl]Y (4a and 4b). A solution of *N*(Me)1,1′-Me$_2$dma (22 mg, 0.1 mmol) in methanol (1 mL) was added to a methanol solution of *cis*-Pt(DMSO)$_2$Cl$_2$ (42 mg, 0.1 mmol, in 5 mL), and the mixture was heated at 50 °C overnight. The pale yellow solid (29 mg, 61% yield) that formed was collected by filtration, washed with cold methanol, then with ether,

and air dried. X-ray quality crystals of [Pt(*N*(Me)1,1′-Me_2dma)Cl]Cl (**4a**) were obtained by mixing equal volumes (1 mL) of acetonitrile solutions of *cis*-Pt$(DMSO)_2Cl_2$ (10 mg, 12.5 mM) and the ligand (5 mg, 12.5 mM) and allowing the resulting solution to stand at room temperature. Pale yellow, needle-like crystals that separated overnight were characterized by single-crystal X-ray crystallography. ^{1}H NMR signals (ppm) in D_2O (pH 4, uncorrected for D_2O): 7.15 (d, *J* = 1.5 Hz, 2H, H5/5′), 7.01 (d, *J* = 1.6 Hz, 2H, H4/4′), 4.97 (d, *J* = 15.4 Hz, 2H, CH_2), 4.64 (d, *J* = 15.4 Hz, 2H, CH_2), 3.73 (s, 6H, CH_3), 3.12 (s, 3H, CH_3). ^{1}H NMR signals (ppm) in DMSO-d_6: 7.43 (d, *J* = 1.6 Hz, 2H, H5/5′), 6.97 (d, *J* = 1.6 Hz, 2H, H4/4′), 4.87 (d, *J* = 15.1 Hz, 2H, CH_2), 4.72 (d, *J* = 15.4 Hz, 2H, CH_2), 3.77 (s, 6H, CH_3), 2.99 (s, 3H, CH_3). An aqueous solution of **4a** (87 mg, 2 mL) was treated with an excess of $NaBF_4$ (30 mg) to yield a yellow solid. When a solution of this solid in acetone (50 mg, 2 mL) was allowed to stand at room temperature, slow evaporation afforded X-ray quality, pale yellow crystals of [Pt(*N*(Me)1,1′-Me_2dma)Cl]BF_4 (**4b**) after 2 d. ^{1}H NMR signals (ppm) in DMSO-d_6: 7.43 (d, *J* = 1.7 Hz, 2H, H5/5′), 6.96 (d, *J* = 1.7 Hz, 2H, H4/4′), 4.86 (d, *J* = 15.3 Hz, 2H, CH_2), 4.71 (d, *J* = 15.3 Hz, 2H, CH_2), 3.77 (s, 6H, CH_3), 2.99 (s, 3H, CH_3).

G Adduct Formation with [Pt(*N*(R)1,1′-Me_2dma)Cl]Cl. A 10 mM solution of [Pt(*N*(R)1,1′-Me_2dma)Cl]Cl (R = H or Me) in D_2O at pH 4 (uncorrected) was treated with 2.5 molar equiv of **G** (**G** = 5′-GMP, 5′-GTP, 3′-GMP, 5′-IMP and Ino for R = H or Me, and with **G** = 5′-GDP, 1-MeGuo and 9-EtG for R = H). The solution was maintained at 25 °C and at pH 4 and monitored by ^{1}H NMR spectroscopy until the [Pt(*N*(R)1,1′-Me_2dma)Cl]Cl signals completely disappeared. The signals of the reactants are shifted by stacking interactions between free **G** and the [Pt(*N*(R)1,1′-Me_2dma)Cl]$^+$ cation. As the adduct formed (decreasing the concentrations of the reactants), the resulting decrease in the extent of stacking interactions between the reactants caused

the slight shift changes. Similar results were found in studies of Pt(*N*(H)dpa)**G** adducts, and a more complete explanation can be found in the published report.[5]

In order to compare properties for the [Pt(*N*(H)1,1′-Me$_2$dma)Cl]$^+$ cation and Pt(*N*(H)1,1′-Me$_2$dma)**G** adducts with those reported in a D$_2$O:DMSO-d_6 (65:35) solvent mixture for the [Pt(*N*(H)dpa))Cl]$^+$ cation and Pt(*N*(H)dpa)**G** adducts,[5] the formation of selected Pt(*N*(H)1,1′-Me$_2$dma)**G** adducts (**G** = 5′-GMP and 5′-GTP) from [Pt(*N*(H)1,1′-Me$_2$dma)Cl]$^+$ was studied in this solvent mixture at pH 4 (uncorrected) (Supporting Information, Table A.2).

Crystallization of [Pt(*N*(H)1,1′-Me$_2$dma)(3′-GMPH)]NO$_3$•5H$_2$O (5). In order to obtain X-ray quality crystals of the Pt(*N*(H)1,1′-Me$_2$dma)(3′-GMP) adduct, 12.2 mg of 3′-GMP (2.5 molar equiv) was added to a 20 mM solution (5.2 mg/600 μL) of [Pt(*N*(H)1,1′-Me$_2$dma)Cl]Cl in D$_2$O, and the pH was adjusted to 4. The solution was allowed to stand at room temperature. Pale yellow, needle-like crystals were collected after two weeks.

2.3 Results and Discussion

Synthesis of *N*(R)1,1′-Me$_2$dma and [Pt(*N*(R)1,1′-Me$_2$dma)Cl]Y (Y = Cl or BF$_4$). *N*(H)1,1′-Me$_2$dma (**1**) was synthesized by hydrogenation of the 1-methyl-2-imidazolecarboxaldehyde oxime as reported in the literature.[58] Several procedures are known[57,59,82] for coupling the appropriate amine derivative with two equiv of 1-methyl-2-imidazolecarboxaldehyde in the presence of sodium triacetoxyborohydride in order to synthesize tridentate imidazolyl ligands having different substituents at the central nitrogen. However, the attempt to synthesize the *N*(Me)1,1′-Me$_2$dma (**2**) ligand by this method was unsuccessful. Therefore, we employed a coupling method known to produce tridentate pyridyl derivatives, which involves coupling the appropriate amine with 2-(chloromethyl)pyridine.[83] Correspondingly, the coupling of methylamine with two equiv of 2-(chloromethyl)-1-methylimidazole under basic

conditions produced *N*(Me)1,1′-Me_2dma (**2**) in acceptable yield. Several platinum precursors, such as *cis*-Pt(DMSO)$_2Cl_2$, $K_2[PtCl_4]$ and Pt(1,5-cyclooctadiene)Cl_2, have been used in synthesizing platinum complexes of pyridyl or imidazolyl ligands.[84-88] The procedures with the latter two precursors use water as the solvent. Because our complexes are highly soluble in water, we employed *cis*-Pt(DMSO)$_2Cl_2$ in methanol and obtained [Pt(*N*(R)1,1′-Me_2dma)Cl]Cl (**3a** and **4a**) in 55−61% yields.

Structural Results. Crystal data and details of the structural refinement for [Pt(*N*(H)1,1′-Me_2dma)Cl]BF_4 (**3b**), [Pt(*N*(Me)1,1′-Me_2dma)Cl]Cl•H_2O (**4a**), [Pt(*N*(Me)1,1′-Me_2dma)Cl]BF_4 (**4b**), and [Pt(*N*(H)1,1′-Me_2dma)(3′-GMPH)]NO_3•$5H_2O$ (**5**) are summarized in Table 2.1. Selected bond lengths and angles are reported in Table 2.2, along with data for [Pt(*N*(H)dpa)Cl]Cl[89] and [Pt(*N*(Me)dpa)Cl]Cl[90] for comparison. The ORTEP plots for cations of [Pt(*N*(H)1,1′-Me_2dma)Cl]BF_4 (**3b**), [Pt(*N*(Me)1,1′-Me_2dma)Cl]BF_4 (**4b**), and [Pt(*N*(H)1,1′-Me_2dma)(3′-GMPH)]NO_3•$5H_2O$ (**5**) (Figure 2.2; the **4a** structure is similar to **4b** and not shown here) show the numbering system used to describe the solid-state data. Crystals of **3b** contain two independent complexes in the asymmetric unit, only one (A) of which is shown in Figure 2.2 and used in the discussion. The N2 atom of the cation [Pt(*N*(H)1,1′-Me_2dma)Cl]$^+$ is disordered over two almost equivalent positions with occupancies of 0.51:0.49 (1A:2A). Compound **4b** is a non-merohedral twin. Compound **5** was losing solvent rapidly during crystal harvesting. The resulting crystal structure has a disordered nitrate anion and water molecules. Hydrogen atoms of water molecules and the phosphate moiety were not located in the difference Fourier map. In the discussions related to the 3′-GMPH group in complex **5**, the standard numbering system for guanine derivatives (Figure 2.1) is employed to allow comparisons with known structures.

Table 2.1. Crystal Data and Structure Refinement for [Pt(*N*(H)1,1′-Me_2dma)Cl]BF_4 (**3b**), [Pt(*N*(Me)1,1′-Me_2dma)Cl]Cl•H_2O (**4a**), [Pt(*N*(Me)1,1′-Me_2dma)Cl]BF_4 (**4b**), and [Pt(*N*(H)1,1′-Me_2dma)(3′-GMPH)]NO_3•5H_2O (**5**)

	3b	**4a**	**4b**	**5**
	$C_{10}H_{15}ClN_5Pt\cdot BF_4$	$C_{11}H_{17}Cl_2N_5Pt\cdot OH_2$	$C_{11}H_{17}ClN_5Pt\cdot BF_4$	$C_{20}H_{27}N_{10}O_8PPt\cdot NO_3\cdot 5(H_2O)$
fw	522.62	503.30	536.65	913.66
crystal system	triclinic	monoclinic	monoclinic	orthorhombic
space group	$P\bar{1}$	$P2_1/c$	$C2/c$	$P2_12_12_1$
a (Å)	7.4468(4)	10.7948(6)	22.684(3)	9.0409(6)
b (Å)	12.5154(7)	11.5052(6)	12.5272(17)	16.7570(12)
c (Å)	17.0151(11)	12.2870(7)	11.2101(15)	20.8873(15)
α (deg)	110.894(2)	90	90	90
β (deg)	92.093(3)	97.773(3)	95.074(6)	90
γ (deg)	97.991(3)	90	90	90
V ($Å^3$)	1460.77(15)	1537.19(15)	3173.1(7)	3164.4(4)
T (K)	106	90	90	90
Z	4	4	8	4
ρ_{calc} (mg/m^3)	2.376	2.175	2.247	1.918
abs coeff (mm^{-1})	9.83	9.48	9.06	4.58
$2\theta_{max}$ (°)	52.8	61.0	71.8	51.4
R[F2 > 2σ(F2)][a]	0.035	0.030	0.030	0.037
Rw[b]	0.071	0.089	0.089	0.084
res. dens. (e $Å^{-3}$)	1.46, -0.90	4.90, -2.56	2.39, -1.60	1.68, -0.94
data/parameters	5955/430	4689/190	7527/212	5877/457

[a] $R = (\sum||F_o| - |F_c||)/\sum|F_o|$. [b] $Rw = [\sum[w(F_o^2 - F_c^2)^2]/\sum[w(F_o^2)^2]]^{1/2}$, in which $w = 1/[\sigma^2(F_o^2) + (dP)^2 + (eP)]$ and $P = (F_o^2 + 2F_c^2)$.

Table 2.2. Selected Bond Distances (Å) and Angles (deg) for [Pt(*N*(H)1,1′-Me_2dma)Cl]BF_4 (**3b**), [Pt(*N*(Me)1,1′-Me_2dma)Cl]Cl•H_2O (**4a**), [Pt(*N*(Me)1,1′-Me_2dma)Cl]BF_4 (**4b**), [Pt(*N*(H)1,1′-Me_2dma)(3′-GMPH)]NO_3•$5H_2O$ (**5**), [Pt(*N*(H)dpa)Cl]Cl[a], and [Pt(*N*(Me)dpa)Cl]Cl[b]

	3b	**4a**	**4b**	**5**	[Pt(*N*(H)dpa)Cl]Cl	[Pt(*N*(Me)dpa)Cl]Cl
			bond distances			
Pt–N1	1.992(6)	1.992(3)	1.978(4)	2.004(8)	2.008(6)	2.006(3)
Pt–N2	2.035(13), 2.069(13)	2.042(3)	2.041(3)	2.031(9)	2.009(12)	2.017(3)
Pt–N3	1.98(2)	1.998(3)	2.002(4)	1.995(9)	2.011(5)	2.007(3)
Pt–Cl or N6	2.317(6)	2.3065(7)	2.2793(10)	2.007(8)	2.301(2)	2.3048(10)
			bond angles			
N1–Pt–N3	164.6(2)	164.27(14)	165.32(14)	164.5(4)	166.0(2)	166.0(2)
N1–Pt–Cl or N6	97.08(18)	96.21(9)	96.85(11)	96.4(4)	97.2(2)	96.62(9)
N2–Pt–Cl or N6	167.6(6), 169.9(5)	176.63(8)	176.53(9)	178.0(6)	168.7(6)	179.52(9)
N3–Pt–Cl or N6	98.27(17)	98.63(9)	97.12(12)	98.7(4)	97.8(2)	96.82(9)
N2–Pt–N1	83.1(4), 81.5(4)	82.67(12)	83.60(15)	81.6(3)	83.3(3)	83.35(12)
N2–Pt–N3	81.8(4), 83.5(4)	82.80(11)	82.73(15)	83.3(3)	83.3(3)	83.4(2)
Pt–N3–C6[c]	113.1(5)	111.9(2)	111.6(3)	110.6(7)	112.7(4)[d]	114.1(5)[d]
Pt–N3–C8[c]	139.4(5)	141.0(3)	139.5(3)	140.9(8)	127.2(5)[d]	128.7(5)[d]
C6–N3–C8[c]	107.1(6)	106.8(3)	108.8(4)	108.3(10)	120.1(6)[d]	117.0(6)[d]

[a]Data from ref.[89] [b]Data from ref.[90] [c]The angles for the other ring are similar to the values reported here. [d]For [Pt(*N*(H)dpa)Cl]Cl and [Pt(*N*(Me)dpa)Cl]Cl the C6 and C8 numbering in the table represents the C2 and C6 atoms, respectively, in NMR discussions.

[Pt(*N*(H)1,1′-Me$_2$dma)Cl]BF$_4$ (3b) and [Pt(*N*(Me)1,1′-Me$_2$dma)Cl]Y (4a, Y = Cl, and 4b, Y = BF$_4$). Cations of **3b, 4a** and **4b** have a pseudo square planar geometry. The four coordination sites are occupied by the N1, N2 and N3 atoms of the tridentate ligands and by a Cl atom (trans to N2). The Pt─Cl and Pt─N bond distances and N1─Pt─N3 bite angles in **3b**, **4a** and **4b** are not significantly different from the values reported for their [Pt(*N*(H)dpa)Cl]$^{+}$[89] and [Pt(*N*(Me)dpa)Cl]$^{+}$[90] analogs (Table 2.2). In these complexes, all of the Pt─N bond distances lie within the ranges expected for Pt─N(sp^2) bond distances (1.99─2.08 Å)[7,84,91] or Pt─N(sp^3) bond distances (2.01─2.12 Å).[7,54,92-93]

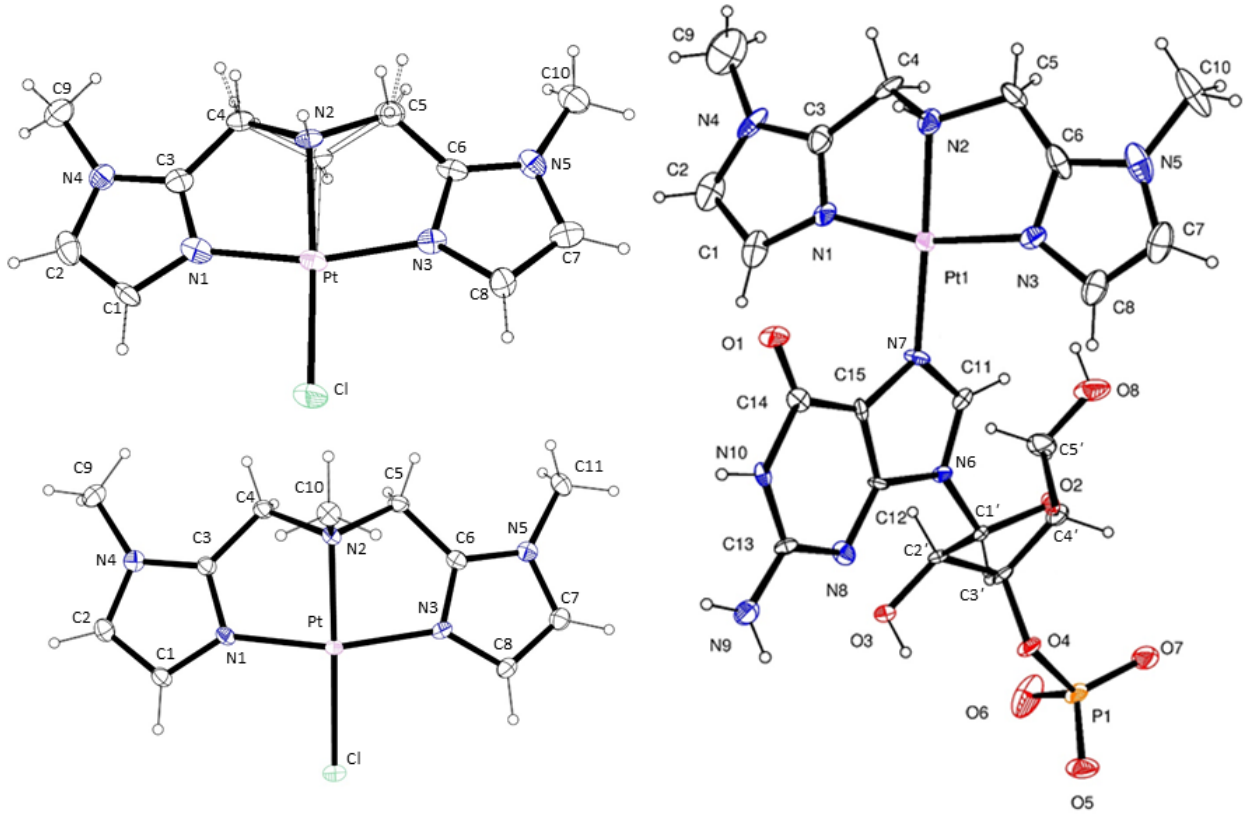

Figure 2.2. ORTEP plots showing the cations of [Pt(*N*(H)1,1′-Me$_2$dma)Cl]BF$_4$ (**3b**, *top left*), [Pt(*N*(Me)1,1′-Me$_2$dma)Cl]BF$_4$ (**4b**, *bottom left*), and [Pt(*N*(H)1,1′-Me$_2$dma)(3′-GMPH)]NO$_3$•5H$_2$O (**5**, *right*). Thermal ellipsoids are drawn with 50% probability.

For the cations in **3b**, **4a** and **4b**, the sp^3 geometry of the central N atom places the two methylene groups on the side of the coordination plane opposite to the NH or N(Me) groups (Figure 2.3 and Figure A.1 in Supporting Information). As a result, the plane of the imidazolyl

rings (defined by the 3 C and 2 N atoms in the ring) is tilted with respect to the coordination plane (defined by Pt and the four ligating atoms N1, N3, N2 and Cl/(**G**)N7). The average tilt angles for rings in [Pt(*N*(H)1,1′-Me_2dma)Cl]BF_4 (**3b**), [Pt(N(H)dpa)Cl]Cl,[89] and [Pt(N(H)6,6′-Me_2dpa)Cl]Cl[7] structures are 7.1°, 5.4° and 5.2°, respectively. Addition of a methyl group on the central nitrogen appears to force the CH_2 groups to be farther below the coordination plane (Figures A1 and A2 in Supporting Information); consequently, the average tilt angles approximately double to 12.4°, 12.9° and 12.3° in [Pt(*N*(Me)1,1′-Me_2dma)Cl]Cl (**4a**), [Pt(*N*(Me)1,1′-Me_2dma)Cl]BF_4 (**4b**), and [Pt(N(Me)dpa)Cl]Cl,[90] respectively. The tilting of all the imidazolyl rings with respect to the coordination plane results in the H4/4' protons projecting toward the same side of the coordination plane as the NH or N(Me) groups (Figure 2.3).

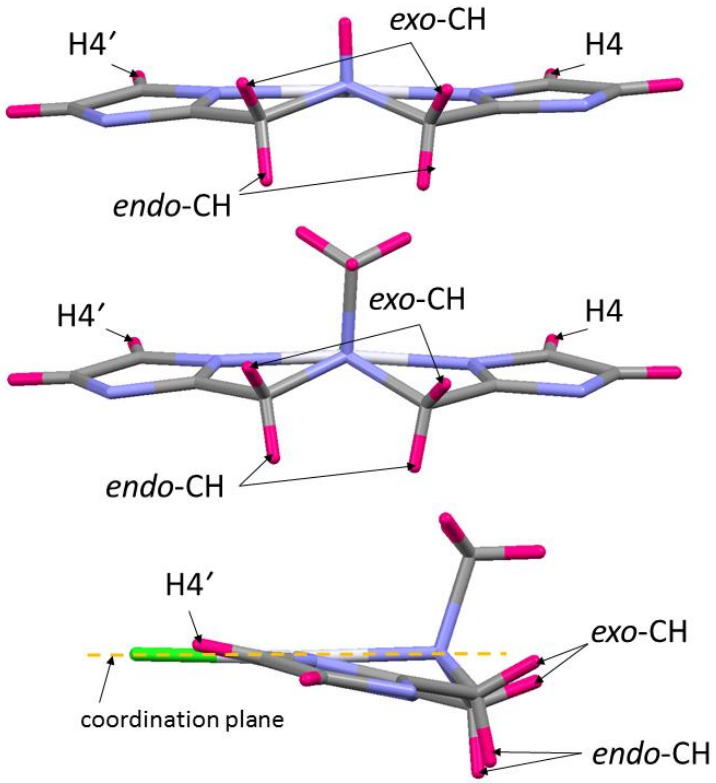

Figure 2.3. Orientation of the H4/4′ protons, methylene groups, and the imidazolyl rings in the [Pt(*N*(R)1,1′-Me_2dma)Cl]BF_4 cations [*top*: **3b** (R = H), *middle* and *bottom*: **4b** (R = Me)] viewed along the coordination plane. Also shown are designations of the *endo*-CH and the *exo*-CH protons. For clarity, the N-Me groups of the imidazolyl rings are hidden.

[Pt(*N*(H)1,1′-Me$_2$dma)(3′-GMPH)]NO$_3$•5H$_2$O (5). The Pt─N1, Pt─N2, and Pt─N3 (Table 2.2) bond distances of this pseudo square planar Pt(II) complex do not differ significantly from the values for **3b**. Also, the N1─Pt─N3 bite angle of **5** (164.5(4)°) is comparable to the value for [Pt(*N*(H)1,1′-Me$_2$dma)Cl]$^+$ in **3b** (164.6(2)°, Table 2.2). Compared to the tilting observed for **3b** (7.1°), the imidazolyl rings in **5** have a greater degree of tilting. One of the imidazolyl rings is tilted by 19.1° and the other ring by 10.0°. The Pt─N7(**G**) bond of 2.007(8) Å in **5** falls within the typical Pt─N7(**G**) bond distance ranges reported for mono adducts[65-68] (1.99─2.07 Å) and for bis adducts[35,44,69-78] (2.02─2.08 Å). The metric parameters and conformational features of the 3′-GMPH ligand are normal and are described in the Supporting Information.

The difference, Pt–N7–C5 bond angle minus the Pt–N7–C8 bond angle, in structures of Pt(II) complexes of G (G = any derivative of guanine) is defined as the 'rocking angle'.[94] The typical range of the rocking angle, identified some years ago as being about -2° to +11°,[94] indicates that the Pt–N7–C8 angle is normally smaller than the Pt–N7–C5 angle. Rocking angles in more recent structures also almost always fall in this range.[67,69,71-72,74-76] Mono adducts tend to be at the lower end of this range. Small rocking angles usually are observed when the structure has no clear intramolecular interactions, as in [Pt(*N*(H)1,1′-Me$_2$dma)(3′-GMPH)]$^+$ (**5**), which has a positive rocking angle of 1.4°. Rare examples of highly negative values for the rocking angle occur only when the carrier ligand has high bulk, such as for Pt(*N*,*N*,*N*′,*N*′-tetramethylethylenediamine)**G**$_2$ complexes, with values of -3.2° (**G** = 5′-GMP)[70] and -6.8° (**G** = 9-MeG).[44]

An analysis by Yao et al. of crystallographic data for *cis*-[PtL$_2$G$_2$] type structures available at the time demonstrated a linear correlation (R = 0.897) between the rocking angle and the Pt–O6 non bonded distance.[94] The linear correlation also accounts for the Pt–O6 distance in **5** (3.40 Å)

and in all relevant structures published after the report by Yao et al.[94] and discussed here.[67,69-72,74-76]

Canting is another parameter used to compare structural features of Pt(II) complexes of coordinated purines. If the dihedral angle between the plane of a base and the coordination plane is close to 90°, the base is not canted. The smaller the dihedral angle, the greater the canting. This dihedral angle in **5** is 66.5°, indicating moderate canting. As previously reported,[78,95] 6-oxopurine Cu(II) complexes exhibit an interesting relationship between the dihedral angle and intramolecular hydrogen bonding interactions of the 6-oxo group with protons in *cis*-carrier ligands. If the proton can project out of the coordination plane, such as a proton on a ligating sp^3 N cis to the purine, a hydrogen bond is then possible. When a hydrogen bond is present, the dihedral angle falls in a highly canted 40−60° range. In the absence of such an interaction, the angle is usually greater than 65° and in the moderately canted range. Except for a few Pt(II) complexes exhibiting strong intramolecular base-base stacking between two adjacent cis purines,[69,72-73,77] all published Pt(II) 6-oxopurine complexes also seem to follow this relationship.[44,65-68,70-71,74-76,78] Accordingly, the small canting value exhibited by **5** (characteristic of the absence of intramolecular hydrogen bond interactions) is consistent with the closest proton in the carrier ligand being a partially positive CH atom lying essentially in the coordination plane.

NMR Spectroscopy. ^{1}H NMR spectroscopy was used to characterize the *N*(Me)1,1′-Me_2dma ligand (in D_2O and DMSO-d_6), the [Pt(*N*(R)1,1′-Me_2dma)Cl]$^+$ complexes (in D_2O and DMSO-d_6), and the Pt(*N*(R)1,1′-Me_2dma)**G** adducts (in D_2O) reported here. NMR signals were assigned by analyzing their chemical shifts, splitting pattern, integration, and data from 2D NMR experiments. Selected 1D ^{1}H and ^{13}C NMR data and assignments in D_2O for [Pt(*N*(H)1,1′-Me_2dma)Cl]Cl, [Pt(*N*(Me)1,1′-Me_2dma)Cl]Cl, and their **G** adducts are collected in Tables 2.3, 2.4

and 2.5. The atom-numbering scheme in Figure 2.1 is employed in the NMR discussion. ^{1}H NMR results in D_2O/DMSO-d_6 (65:35) for Pt(*N*(H)1,1′-Me_2dma)**G** adducts (**G** = 5′-GMP and 5′-GTP) appear in the Supporting Information.

Table 2.3. ^{1}H NMR Data (ppm) for the *N*(R)1,1′-Me_2dma Carrier Ligands in Pt(*N*(R)1,1′-Me_2dma)**G** and in [Pt(*N*(R)1,1′-Me_2dma)Cl]Cl (D_2O, pH 4.0, 25 °C)

R	Cl or **G**	t (days)[a]	H4/4′		H5/5′	1/1′-Me	N-Me
			syn	anti			
H	Cl[b]		6.85		7.03	3.67	-
H	5′-GMP[c]	6	6.53, 6.52	6.57, 6.55	7.07[d]	3.75	-
H	5′-GTP[c]	6	6.52, 6.51	6.56, 6.54	7.07[d]	3.74	-
H	3′-GMP[c]	10	6.56, 6.53	6.58, 6.57	7.09[d]	3.75	-
H	5′-IMP[c]	6	6.50, 6.47	6.53, 6.52	7.08[d]	3.76	-
H	5′-GDP[c]	4	6.52, 6.51	6.57, 6.55	7.07[d]	3.74	-
H	Ino[c]	10	6.51, 6.49	6.54, 6.52	7.09[d]	3.77	-
H	1-MeGuo[c]	10	6.52, 6.51	6.55	7.09[d]	3.77	-
H	9-EtG[c]	10	6.52	6.54	7.10[d]	3.77	-
Me	Cl[e]		7.01		7.15	3.73	3.12
Me	5′-GMP[c]	10	6.58, 6.57	6.65, 6.63	7.12[d]	3.79	3.18
Me	5′-GTP[c]	10	6.58, 6.56	6.66, 6.65	7.13[d]	3.79	3.18
Me	3′-GMP[c]	10	6.61, 6.58	6.66, 6.64	7.14[d]	3.80	3.20
Me	5′-IMP[c]	10	6.54, 6.51	6.59, 6.58	7.12[d]	3.79	3.20
Me	Ino[c]	10	6.55, 6.53	6.59, 6.57	7.13[d]	3.79	3.22

[a]t = reaction completion time. [b]*endo*-H6/6′ signal is masked by the solvent peak and *exo*-H6/6′ signal is 4.63 ppm (15.4 Hz). [c]*exo*- and *endo*-H6/6′ signals are masked by the solvent peak. [d]syn and anti signals are overlapped. [e]*endo*- and *exo*-H6/6′ are 4.97 and 4.64 ppm, respectively.

Table 2.4. Selected ^{1}H NMR Data (ppm) for the **G** Ligand in Pt(*N*(R)1,1′-Me$_2$dma)**G** Adducts (D_2O, pH 4.0, 25 °C)

R	**G**	H8 free	H8 syn	H8 anti	H1′ free	H1′ syn	H1′ anti	$\Delta\delta^a$	syn:anti ratio
H	5′-GMP	8.10	8.69	9.00	5.91	6.05	6.10	0.31	1.07:1
H	5′-GTP	8.19	8.74	9.05	5.92	6.05	6.09	0.31	1.01:1
H	3′-GMP	8.01	8.65	8.95	5.93	6.05	6.09	0.30	1.18:1
H	5′-IMP[b]	8.44	9.08	9.40	6.12	6.28	6.31	0.32	1.05:1
H	5′-GDP	8.12	8.71	9.01	5.91	6.04	6.09	0.30	1.02:1
H	Ino[c]	8.34	9.04	9.35	6.09	6.23	6.27	0.31	1.22:1
H	1-MeGuo	7.96	8.63	8.92	5.88	6.02	6.07	0.29	1.25:1
H	9-EtG[d]	7.91	8.43	8.74	-	-	-	0.31	1.30:1
Me	5′-GMP	8.11	8.66	8.98	5.91	6.05	6.09	0.32	1.60:1
Me	5′-GTP	8.14	8.69	9.01	5.93	6.05	6.09	0.32	1.63:1
Me	3′-GMP	8.01	8.61	8.97	5.94	6.04	6.10	0.36	1.57:1
Me	5′-IMP[e]	8.44	9.04	9.36	6.14	6.27	6.31	0.32	1.65:1
Me	Ino[f]	8.33	8.97	9.33	6.08	6.26	6.20	0.36	1.26:1

[a]Shift difference between the H8 signals of the syn and anti rotamers (cf. text). [b]H2: 8.21 (free), 8.40 (syn), and 8.34 ppm (anti). [c]H2: 8.21 (free), 8.40 (syn), and 8.34 ppm (anti). [d]CH_2: 4.08 (free), 4.26 (syn), 4.21 ppm (anti); CH_3: 1.41 (free), 1.48 (syn), 1.54 ppm (anti). [e]H2: 8.21 (free), 8.40 (syn) and 8.32 ppm (anti). [f]H2: 8.21 (free), 8.40 (syn), and 8.33 ppm (anti).

Table 2.5. 1D ^{13}C NMR Data (ppm) for [Pt(*N*(R)1,1′-Me_2dma)Cl]Cl [**3a** (R = H) and **4a** (R = Me)] and for Their 5′-GMP Adducts (D_2O, pH 4.0, 25 °C)

carbons[a]	**3a**	adduct		**4a**	adduct	
		syn	anti		syn	anti
5′-GMP C8		139.96	140.03		139.96	140.04
5′-GMP C1′		87.97			88.03	
		87.94			87.95	
C5/5′	122.32	122.48		122.36	122.78	
		122.40			122.70	
C4/4′	123.42	124.40		124.33	124.73	
		124.29			124.70	
		124.20			124.59	
					124.52	
C2/2′	153.92	153.80		152.87	152.46	
C6/6′	51.02	51.50		61.95	61.94	
		51.44			61.90	
		51.39			61.88	
C1/1′	34.58	34.62		34.72	34.74	
N(Me)	-	-		52.72	52.24	

[a]Free 5′-GMP: C8, 137.48 ppm; C1′, 86.85 ppm.

[Pt(*N*(R)1,1′-Me_2dma)Cl]Cl Assignments. Complexes **3** (R = H) and **4** (R = Me) both have two downfield ^1H NMR signals (Figure 2.4), as expected for the H4/4′ and H5/5′ aromatic protons. However, the small coupling constant of ∼1.5 Hz, combined with the effect of the nearby quadrupolar nitrogen atoms, causes the signals to appear as singlets in some spectra. In a ROESY

spectrum (Supporting Information) in D_2O for [Pt(*N*(H)1,1′-Me_2dma)Cl]Cl (**3a)**, a strong NOE cross-peak from the 1/1′-Me signal at 3.67 ppm to the most downfield signal (7.03 ppm) allows the signal to be assigned to H5/5′. The other aromatic peak (6.85 ppm) can thus be assigned to H4/4′, an assignment supported by the absence of any NOE cross-peak from the H4/4′ signal to any other peak except to the H5/5′ signal.

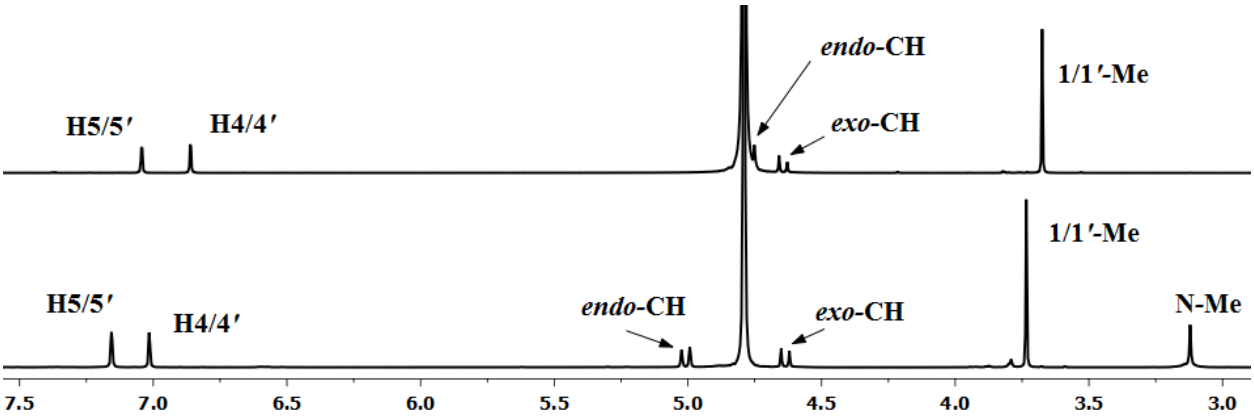

Figure 2.4. ^{1}H NMR spectra (25 °C, D_2O, pH 4) of [Pt(*N*(H)1,1′-Me_2dma)Cl]Cl (**3a**) *(top)* and [Pt(*N*(Me)1,1′-Me_2dma)Cl]Cl (**4a**) (*bottom*) complexes (shifts in ppm).

The two protons in each methylene group in the [Pt(*N*(R)1,1′-Me_2dma)Cl]$^+$ cations are not magnetically equivalent; these are designated as *endo*-CH and *exo*-CH (Figure 2.3). The two ^{1}H NMR methylene signals are doublets. Analysis of NOE cross-peaks led us to assign the upfield and downfield [Pt(*N*(R)1,1′-Me_2dma)Cl]Cl doublets to the *exo*-CH and *endo*-CH signals, respectively. A similar relationship was found for [Pt(*N*(H)dpa)Cl]Cl.[5] The ^{13}C NMR shifts were determined from 1D NMR spectra (Table 2.5). The ^{13}C NMR signals for the C4/4′, C5/5′, and C1/1′ carbons of [Pt(*N*(H)1,1′-Me_2dma)Cl]Cl (**3a**) were assigned (Table 2.5) with the aid of cross-peaks (in ppm) involving the H4/4′ (6.85−123.4), H5/5′ (7.03−122.3), and 1/1′-Me (3.67−34.6) signals, respectively, in an HSQC experiment (Supporting Information). Cross-peaks from the *endo*-CH and *exo*-CH signals assign the ^{13}C NMR signal at 51.5 ppm to C6/6′. The only signal with no HSQC cross-peak (153.92 ppm) is assigned to C2/2′. As described in Supporting

Information, this approach for assigning the signals of **3a** was also used to assign the ^{1}H and ^{13}C NMR signals (Tables 2.3 and 2.5) for [Pt(*N*(Me)1,1′-Me$_2$dma)Cl]Cl (**4a**).

Although the **3a** and **4a** structures are similar except for the different substituent on the central N atom, the methylene signals (in DMSO-d_6) are separated by only 0.03 ppm for **3a** (an AB pattern, *endo*-CH at 4.56 and *exo*-CH at 4.53 ppm), whereas the separation between the two doublets of **4a** is 0.15 ppm (in DMSO-d_6, *endo*-CH at 4.87 and *exo*-CH at 4.72 ppm). These separations of methylene signals in [Pt(*N*(R)1,1′-Me$_2$dma)Cl]Cl are significantly less than the values reported for their [Pt(*N*(R)dpa)Cl]Cl analogs (in DMSO-d_6, 0.32[5] and 0.64[90] ppm for R = H and Me, respectively). However, the coupling constants for all four platinum complexes are ~15 Hz regardless of the carrier ligand or the substituent at the central N.

The robustness of [Pt(*N*(H)1,1′-Me$_2$dma)Cl]Cl (**3a**) in D_2O (pH 7), in DMSO-d_6, and in strongly acidic (0.2 M HCl) conditions was monitored by using ^{1}H NMR spectroscopy. The spectra revealed no change even 10 days after addition of HCl (Supporting Information).

Pt(*N*(R)1,1′-Me$_2$dma)G Adducts. NMR Background for Determining Rotamer Conformation in Adducts. In simple Pt(L^{tri})**G** adducts, the inductive effect of the Pt(II) center causes the H8, H2 (in hypoxanthine derivatives, cf. Figure 2.1), and ribose H1′ peaks of bound **G** to be shifted downfield compared to these signals for free **G**.[96-97] Two **G** base orientations and hence two rotamers are possible for Pt(L^{tri})**G** adducts having L^{tri} ligands that are unsymmetrical with respect to the coordination plane but symmetrical about a plane perpendicular to the coordination plane (Figure 2.5). By convention,[96] the rotamer of Pt(L^{tri})**G** adducts having the R group and the guanine O6 on the same side of the coordination plane is named syn, and the rotamer having these groups on opposite sides of this plane is named anti (Figure 2.5). The syn and anti rotamers interconvert by rotation about the Pt–N7 bond.[19,43,97-99] Furthermore, neither rotamer has

a plane of symmetry in an adduct formed by **G** derivatives having a chiral ribose, such as 5′-GMP. Therefore, in each rotamer the corresponding protons in the two halves of the carrier ligand are not magnetically equivalent. When NMR evdience is found that Pt(L^{tri})**G** rotamers exist, only two signals are found for each type of **G** proton but as many as four signals can be observed for each proton type of carrier-ligand proton. Such a situation in fact applies to the new Pt(*N*(R)1,1′-Me_2dma)**G** adducts studied here (Figure 2.6).

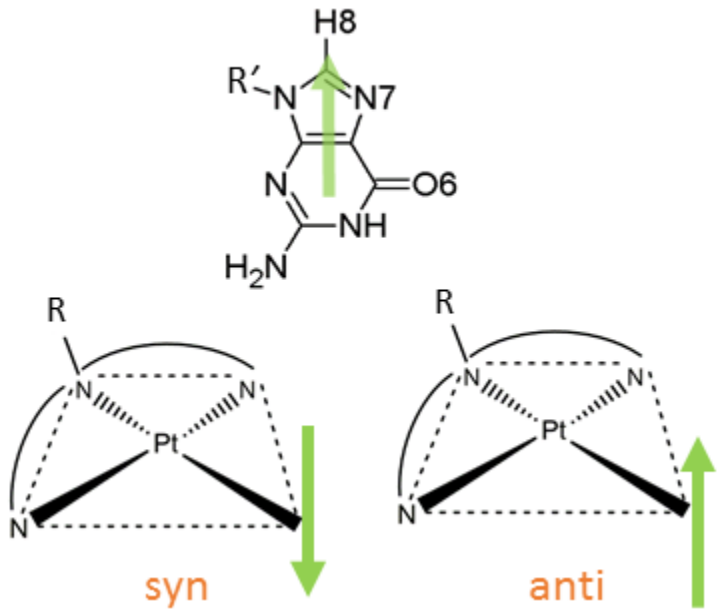

Figure 2.5. The two possible purine orientations for Pt(L^{tri})**G** adducts when the tridentate carrier ligand (L^{tri}) is unsymmetrical with respect to the coordination plane but symmetrical about a plane perpendicular to the coordination plane. Note that the nucleobase is represented by an arrow with the tip at the H8 of the purine. R can be any substituent such as H or Me.

For separate sets of NMR signals of the syn and anti rotamers to be observed, the carrier ligand must be bulky enough to slow the rotation rate of the nucleobase on the NMR time scale.[36-37,96-102] For example, Pt(Me_5dien)**G** adducts (Me_5dien = *N*,*N*,*N*′,*N*″,*N*‴-pentamethyldiethylenetriamine) exhibit two sharp H8 NMR signals, one for each rotamer, indicating that the presence of terminal dimethylamino groups provides enough bulk to hinder nucleobase rotation about the Pt–N7 bond.[96] In contrast, because of the relatively low bulk of dien,

the H8 proton of the Pt(dien)**G** adducts shows only one sharp **G** H8 NMR peak, indicating fast rotation of the guanine base about the Pt—N7 bond.[5] Recently, the *N*(H)dpa ligand was found to possess enough bulk to impede the rotation of the guanine nucleobase in Pt(*N*(H)dpa)**G** adducts.[5-6] Similarly, all new Pt(*N*(R)1,1′-Me_2dma)**G** adducts examined in the present study have spectra with two sharp downfield H8 NMR signals (Figure 2.7 and Supporting Information), a finding consistent with hindered rotation of the purine base.

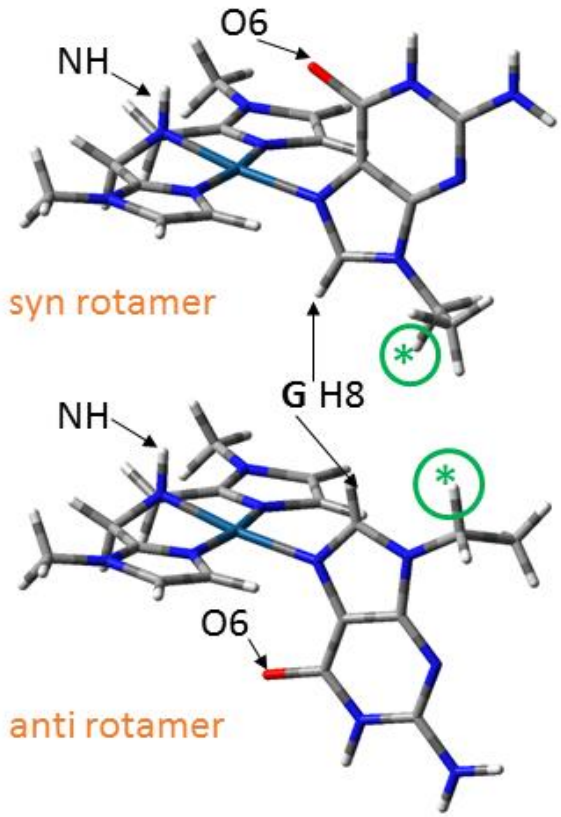

Figure 2.6. Models of the two possible rotamers for Pt(L^{tri})**G** complexes with tridentate ligands (L^{tri}) unsymmetrical with respect to the coordination plane but symmetrical about a plane perpendicular to the coordination plane, illustrated for L^{tri} = *N*(H)1,1′-Me_2dma and **G** = 9-EtG. Rotation of the ethyl group around the N9–CH_2 bond creates a time-averaged mirror plane, preserving the symmetry of the Pt(*N*(H)1,1′-Me_2dma) moiety. However, if a chiral *N*-9 substituent is created by replacing one methylene proton (circled), then the two halves of the Pt(*N*(H)1,1′-Me_2dma) moiety become magnetically inequivalent.

The main factor influencing the downfield shift of ^{1}H NMR signals on complex formation is the Pt(II) inductive effect, and this effect is expected to fall off as the number of bonds between

the proton and the Pt(II) increases. However, the inductive effect is not expected to be different for the two rotamers. Indeed, the shift difference (Δδ) between the H8 signals of the syn and anti rotamers is only ~0.04 ppm for the Pt(Me_5dien)(5′-GMP) adduct and Δδ = 0 for H2 in almost all closely related 5′-IMP adducts.[96] In contrast, the aromatic rings terminating both ends of the tridentate ligand lead to large Δδ values for H8 of ~0.36 ppm for the Pt(*N*(H)dpa)**G** adducts.[5] The syn H8 signal is upfield to the anti H8 signal. These observations for Pt(*N*(H)dpa)**G** adducts were explained by invoking models with a relatively uncanted guanine nucleobase in both rotamers. In such a model, H8 is closer to the shielding region of tilted anisotropic pyridyl groups of the carrier ligand in the syn rotamer than in the anti rotamer, accounting for the syn rotamer having the more upfield H8 signal.[5] As we discuss below, this explanation can be evaluated with the help of the structure of **5** because the H8 signals of Pt(*N*(R)1,1′-Me_2dma)**G** adducts exhibit NMR features similar to those of Pt(*N*(H)dpa)**G** adducts.

Pt(*N*(H)1,1′-Me_2dma)(5′-GMP) Adduct. Spectra of the reaction mixture of [Pt(*N*(H)1,1′-Me_2dma)Cl]Cl (**3a**) and 2.5 molar equiv of 5′-GMP in D_2O (pH 4) showed new ^{1}H NMR signals clearly detectable about 1 h after mixing. The signals for **3a** disappeared in ~6 days (Figure 2.7), indicating that the reaction was complete. Compared to the H8 signal for free 5′-GMP at 8.10 ppm, two sharp downfield H8 singlets characteristic of Pt(II)-bound 5′-GMP were observed. As discussed above, two H8 singlets (Figure 2.7) provide evidence for impeded rotation of the guanine nucleobase in two rotamers of the Pt(*N*(H)1,1′-Me_2dma)(5′-GMP) adduct; for reasons given above, the H8 signals at 9.00 and 8.69 ppm are assigned to the anti and syn rotamers, respectively. Furthermore, strong EXSY cross-peaks between the syn and anti H8 signals in the ROESY spectrum of the Pt(*N*(H)1,1′-Me_2dma)(5′-GMP) adduct (Figure 2.8) add further strong evidence that the two H8 signals arise from slow exchange between two rotamers. In contrast, ROESY

spectra of Pt(*N*(H)dpa)**G** adducts show no EXSY cross-peaks,[5] indicating that the exchange between Pt(*N*(H)dpa)**G** rotamers occurs relatively more slowly than exchange between Pt(*N*(H)1,1′-Me_2dma)**G** rotamers.

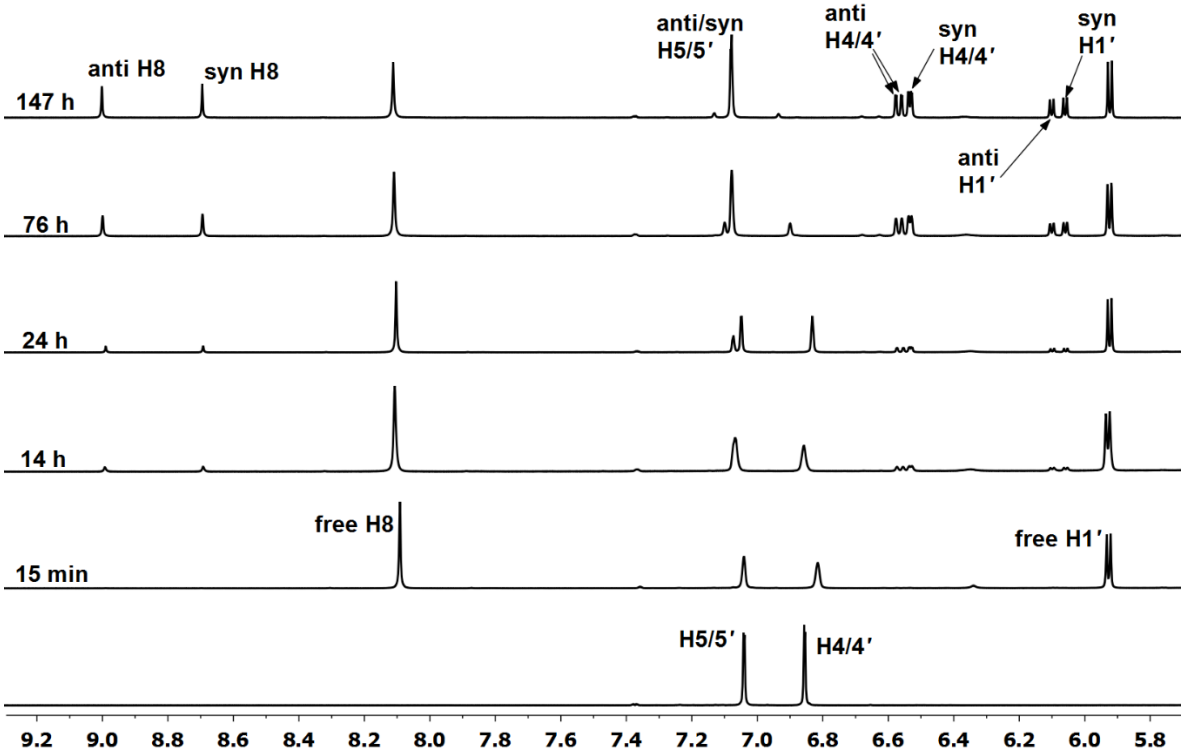

Figure 2.7. Aromatic and H1′ region of the ^{1}H NMR spectra (25 °C, D_2O, pH 4) of [Pt(*N*(H)1,1′-Me_2dma)Cl]$^+$(10 mM, bottom) and of the reaction mixture forming Pt(*N*(H)1,1′-Me_2dma)(5′-GMP) recorded 15 min, 14 h, 24 h, 76 h, and 147 h after adding 2.5 molar equiv of 5′-GMP (shifts in ppm).

The two rotamers of the Pt(*N*(H)1,1′-Me_2dma)(5′-GMP) adduct each have an H1′ doublet shifted downfield similarly (~0.2 ppm) by metal coordination. The NOE cross-peak between the downfield anti H8 signal and the downfield H1′ doublet (6.10 ppm) in the ROESY spectrum (Figure 2.8) assigns this H1′ doublet to the anti rotamer. The NOE cross-peak from the syn H8 signal to the doublet at 6.05 ppm confirms its assignment as syn H1′. Because both the H1′ and H8 protons are associated with the five-membered ring of the guanine base, the H1′ and H8 signals are shielded more by the tilted imidazolyl rings in the syn rotamer than in the anti rotamer. A

similar relationship was found to be caused by the tilted pyridyl rings in the Pt(*N*(H)dpa)**G** class of adducts.[5]

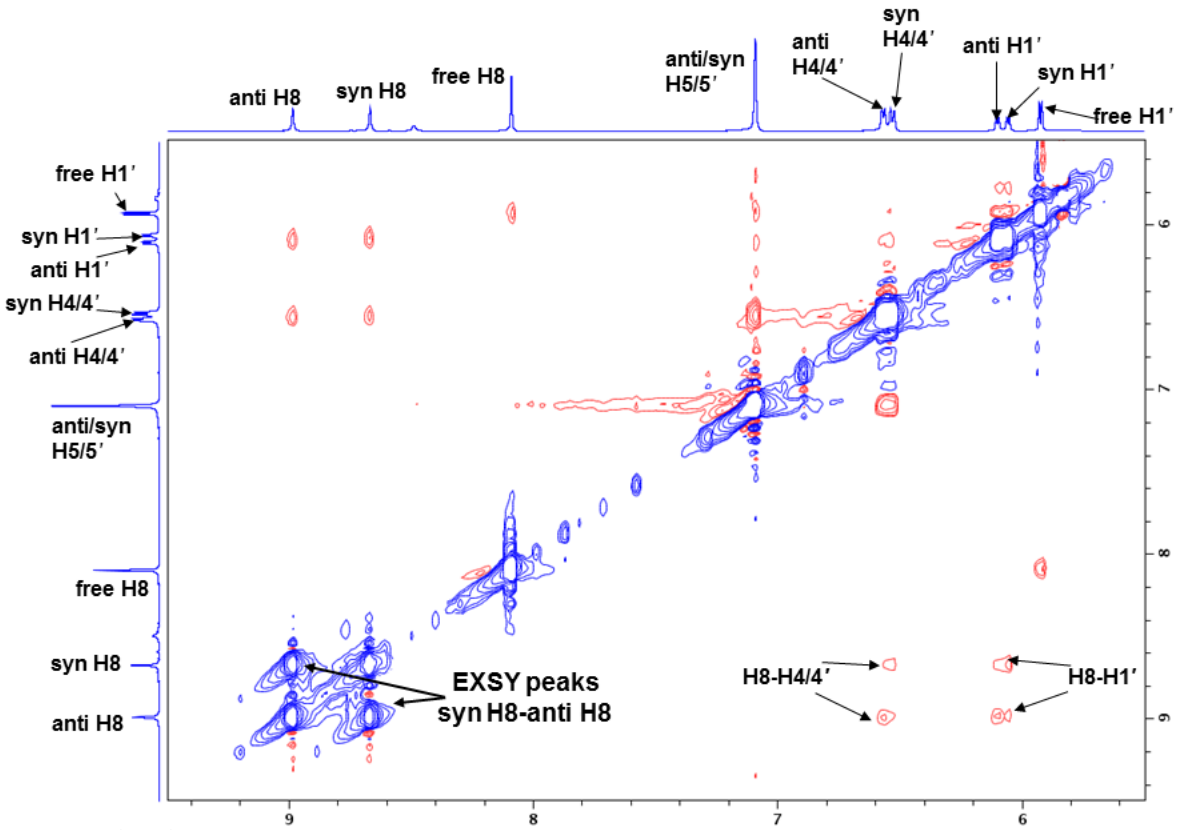

Figure 2.8. ^{1}H–^{1}H ROESY spectrum of Pt(*N*(H)1,1′-Me$_2$dma)(5′-GMP), showing syn H8-anti H8 EXSY cross-peaks and H8–H4/4′ and H8–H1′ NOE cross-peaks (D$_2$O, pH 4.0, 25 °C, shifts in ppm).

The above rotamer assignments rely on shifts of the bound 5′-GMP signals as described previously.[5] The NMR features of Pt(*N*(R)1,1′-Me$_2$dma)**G** adducts and the molecular structure of **5** allow the use of NOE cross-peaks between the bound **G** H8 and the carrier-ligand signals to remove any doubt about previous assignments. From its characteristic shift and the integration, the singlet at 3.75 ppm is unambiguously assigned to the 1/1′-Me signal of the Pt(*N*(H)1,1′-Me$_2$dma)(5′-GMP) adduct. The 1/1′-Me signal shows a strong cross-peak to an apparent singlet at 7.07 ppm in the ROESY spectrum (Supporting Information), allowing the assignment of the 7.07 ppm signal to H5/5′. This H5/5′ singlet has a strong, broad cross-peak to four closely bunched

singlets near 6.57–6.52 ppm (Figure 2.8). The four singlets together integrate as having the same intensity as the H5/5′ singlet, and thus all can be assigned to the H4/4′ protons. These signals exhibit no cross-peaks with the 1/1′-Me signal, confirming the H4/4′ assignment. As mentioned above, the two halves of the carrier ligand are not magnetically equivalent when the *N*9-substituent is chiral (Figure 2.6).

In the ROESY spectra of both Pt(*N*(H)1,1′-Me_2dma)(5′-GMP) (Figure 2.8) and Pt(*N*(Me)1,1′-Me_2dma)(5′-GMP) (Supporting Information), the H8-H4/4′ NOE cross-peaks are stronger for the anti rotamer than for the syn rotamer. To understand this difference in NOE cross-peaks, we used the GaussView 5.0.8 software program to construct a model of the anti rotamer (Figure A.3 in Supporting Information) from the molecular structure of the syn rotamer in [Pt(*N*(H)1,1′-Me_2dma)(3′-GMPH)]NO_3•5H_2O (**5**). The 3′-GMP ligand of the syn rotamer in **5** was rotated by 180° about the Pt−N7 bond and the C8—N7—Pt angle adjusted to that of the syn rotamer (126.78°). The **G** H8 proton and carrier-ligand H4/4′ protons are farther apart in the syn rotamer structure (~3.5 Å) than in the model of the anti rotamer (~2.8 Å). Thus, the NOE intensities confirm the rotamer assignments using the reasoning in previous work[5] based on the effects on H8 shifts of the anisotropy of the tilted carrier-ligand aromatic rings.

The anisotropic guanine in Pt(*N*(Me)dpa)**G**,[53] Pt(*N*(H)dpa)**G**[5] and Pt(5,5′-Me_2bipy)$\mathbf{G}_2$[37] (5,5′-Me_2bipy = 5,5′-dimethyl-2,2′-bipyridine) adducts caused large upfield shifts (~1.1 ppm) of the signals of the carrier-ligand protons closest (H6/6′) to the coordinated **G**. Similarly, in the **G** adducts of **3a** and **4a**, the signals of the protons closest (H4/4′) to the coordinated **G** are affected the most (upfield shifts of ~0.3 to 0.4 ppm as compared to the H4/4′ signal for **3a**) by adduct formation. The non bonded distance from the chloride atom to the H4/4′ protons in **3b** is ~0.4 Å longer than the corresponding distance to the H6/6′ protons in [Pt(*N*(H)dpa)Cl]Cl.[89] Therefore,

the coordinated guanine must be closer to the H6/6′ protons in Pt(*N*(H)dpa)**G** adducts as compared to the H4/4′ protons in Pt(*N*(H)1,1′-Me_2dma)**G** adducts (Figure 2.9). Hence, the guanine nucleobase will undoubtedly cause more upfield shifting of the H6/6′ signals than the H4/4′ signals, as observed.

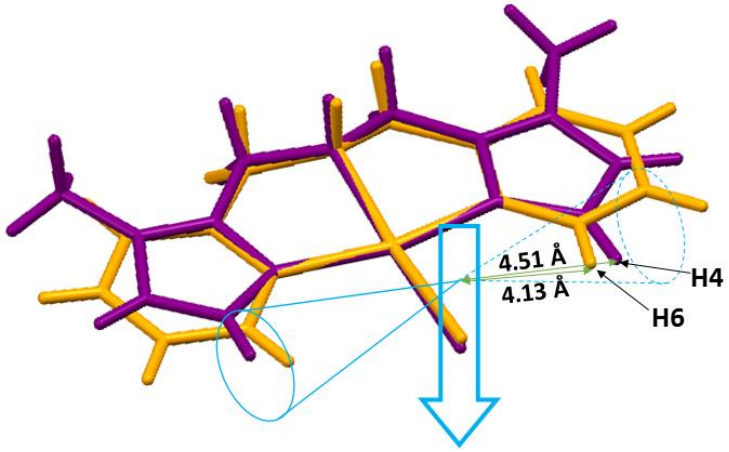

Figure 2.9. Overlap of stick drawings of [Pt(*N*(H)1,1′-Me_2dma)Cl]$^+$ (purple) and [Pt(*N*(H)dpa)Cl]$^+$ (gold) cations (by superimposing the Pt, N1, N2 and N3 atoms). By using GaussView 5.0.8 software, 9-methylguanine (9-MeG) adduct models were constructed from the X-ray data by replacing the coordinated Cl atoms with a 9-MeG having a Pt—N7 distance of 2.007 Å (the distance in **5**) in the plane bisecting the two halves of the cations. These two halves are almost but not exactly equivalent (Table 2.2). For simplicity, the illustration replaces the purine with a blue arrow. The syn orientation is shown. Cones qualitatively indicate that the H4/4′ and H6/6′ atoms lie within the shielding region of the purine base. The thin green arrows span the distances to the center of the purine six-membered ring from the H4 and the H6 atoms in one half of the carrier ligand. The average of distances (Å) of the H4/4′ and H6/6′ atoms to the center of the 9-MeG rings measured using Mercury 3.7 software follow: for the [Pt(*N*(H)1,1′-Me_2dma)(9-MeG)]$^{2+}$ models (6-membered ring, syn 4.51 and anti 4.54; 5-membered ring, syn 3.63 and anti 3.63) and for the [Pt(*N*(H)dpa)(9-MeG)]$^{2+}$ models (6-membered ring, syn 4.13 and anti 4.13; 5-membered ring, syn 3.14 and anti 3.14). Thus, for a given adduct and a given ring, the distances are virtually identical in both the syn and the anti 9-MeG orientations. In all cases, distances are ~0.4–0.5 Å longer for the [Pt(*N*(H)1,1′-Me_2dma)(9-MeG)]$^{2+}$ model.

As described above, the chiral ribose in 5′-GMP makes the two halves of the carrier ligand of each Pt(*N*(H)1,1′-Me_2dma)(5′-GMP) rotamer inequivalent. The effect of chirality is small. Likewise, the difference in orientation of the nucleobase leads to only small differences in shifts of carrier-ligand signals. As stated in Figure 2.9, the distances from H4/4′ to the center of the guanine rings in the syn rotamer are almost all identical to the respective distances in the anti

rotamer. Thus, resolution of the four possible signals can be observed only for signals of nuclei close to the anisotropic nucleobase of the chiral **G**. The two rotamers of Pt(*N*(H)1,1′-Me_2dma)(5′-GMP) exhibit four closely spaced H4/4′ signals. NOE cross-peaks (Figure 2.8) from the anti H8 and syn H8 singlets to the two most downfield and the two most upfield H4/4′ signals, respectively, assign the H4/4′ signals (Table 2.3). The H5/5′ protons in Pt(*N*(H)1,1′-Me_2dma)(5′-GMP) are far from the coordinated 5′-GMP and exhibit an apparent singlet with a very small downfield shift change (0.04 ppm) compared to the H5/5′ signal for **3a**.

The ^{13}C NMR shifts were determined from 1D NMR spectra (Table 2.5). All of the carrier-ligand carbons are farther from the anisotropic nucleobase than are the H4/4′ protons; thus, there are usually fewer than the four possible detectable ^{13}C NMR signals arising from the two chiral rotamers of the Pt(*N*(H)1,1′-Me_2dma)(5′-GMP) adduct. For example, only three peaks are assignable to C4/4′ in an HSQC experiment for Pt(*N*(H)1,1′-Me_2dma)(5′-GMP) (Supporting Information) in which four clustered H4/4′ signals exhibit one strong cross-peak to the ^{13}C NMR peaks at 124.4, 124.3, and 124.2 ppm. Similarly, the H5/5′ signal has a strong cross-peak to only two closely associated peaks at 122.5 and 122.4 ppm for C5/5′. In addition, the 1/1′-Me ^{1}H NMR signal shows a cross-peak to the C1/1′ signal at 34.6 ppm (Table 2.5).

The HSQC spectrum of the Pt(*N*(H)1,1′-Me_2dma)(5′-GMP) adduct (Supporting Information) is in turn useful in locating the methylene *endo*-CH signals, which fall close to the HOD solvent peak and are suppressed by presaturation of the HOD signal. The two strong cross-peaks observed involve the C6/6′ signal (at 51 ppm, a characteristic shift for such methylene carbons[5,7,58]) and the cluster of peaks at 4.60 ppm and the suppressed signals near 4.73 ppm (Supporting Information). We can confidently assign these ^{1}H NMR clusters respectively to the

exo-CH and *endo*-CH protons because *endo*-CH signals are invariably downfield, as discussed above.

Other Pt(*N*(H)1,1′-Me$_2$dma)G Adducts. With the progression of the reaction between [Pt(*N*(H)1,1′-Me$_2$dma)Cl]$^+$ and 3′-GMP (molar ratio = 1:2.5) in D_2O at pH 4, the adduct separated as pale yellow crystals. The carrier-ligand signals in the Pt(*N*(H)1,1′-Me$_2$dma)(3′-GMP) adduct have shifts similar to those observed for the 5′-GMP, 5′-GDP and 5′-GTP adducts (Table 2.3). These observations suggest that the location of the phosphate groups at the 3′ or 5′ position of the sugar groups does not appear to have a major effect on the properties of the adducts.

For the Pt(*N*(H)1,1′-Me$_2$dma)(5′-IMP) adduct, the H8 singlets are at 9.40 (anti) and 9.08 ppm (syn), and the H2 signals are at 8.40 (syn) and 8.34 (anti) ppm (Figure 2.10, Table 2.4). The opposite order of shifts of the H2 and H8 signals in the anti vs the syn rotamer arises because the imidazolyl anisotropy affects mainly the six-membered ring signals in the anti rotamer and mainly the five-membered ring signals in the syn rotamer. A similar opposite directional influence on the H2 and H8 signals by a nearby anisotropic ring was found for other 5′-IMP adducts.[5,100] Because the rotamer abundance for the Pt(*N*(H)1,1′-Me$_2$dma)(5′-IMP) adduct is very close to 1:1 (Figure 2.10), the relative intensities of the two H1′ signals of the adduct were not useful for assigning the H1′ signals. The Pt(*N*(Me)1,1′-Me$_2$dma)(5′-IMP) adduct has a syn:anti intensity ratio of 1.65:1, and the relative intensities of the peaks show that the syn H1′ signal is upfield and the anti H1′ signal is downfield (Supporting Information); this is the expected shift relationship because H1′ is on the five-membered ring. By analogy, the more upfield H1′ signal for Pt(*N*(H)1,1′-Me$_2$dma)(5′-IMP) is assigned to the syn rotamer. For these two Pt(*N*(R)1,1′-Me$_2$dma)(5′-IMP) adducts, the order of shifts of the H2 signal compared to the H8 and H1′ signals is opposite in the anti vs the syn rotamer. The effect of ring anisotropy is largest on H8 shifts and smallest on H1′ shifts. All

these shift relationships were found also for Pt(*N*(H)dpa)(5′-IMP) (in a solvent mixture),[5] but the shift difference between rotamers for all three types of signals is greatest for Pt(*N*(H)dpa)(5′-IMP), consistent with our conclusion below that the anisotropy of the pyridyl ring is greater than that of the imidazolyl ring in these adducts.

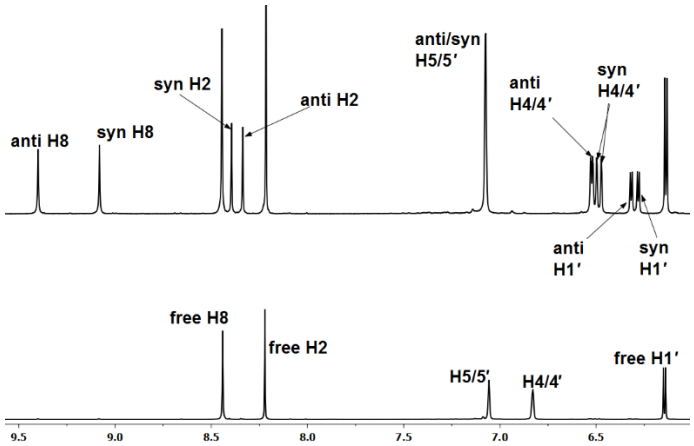

Figure 2.10. ^{1}H NMR spectra (25 °C, D_2O, pH 4) of the mixture of [Pt(*N*(H)1,1′-Me_2dma)Cl]$^{+}$ and 5′-IMP at 15 min after mixing (*bottom*) and of the Pt(*N*(H)1,1′-Me_2dma)(5′-IMP) adduct 6 days after mixing (*top*) (shifts in ppm). The spectral region was selected to show the H8 and H2 signals.

[Pt(*N*(H)1,1′-Me_2dma)(9-EtG)]$^{2+}$, [Pt(*N*(H)1,1′-Me_2dma)(Ino)]$^{2+}$ and [Pt(*N*(H)1,1′-Me_2dma)(1-MeGuo)]$^{2+}$ adducts were studied to assess the influence of the phosphate group on the formation and properties of the adducts. Complete formation of Pt(*N*(H)1,1′-Me_2dma)**G** adducts by reaction of **3a** with neutral nucleobases/nucleosides required ~10 days, a longer time than for nucleotides (Table 2.3); the relatively shorter reaction times observed for the **3a** cation with anionic nucleotides can be attributed to the electrostatic attraction between the reactants.

The ^{1}H NMR chemical shifts, Δδ values, and syn:anti ratios for these three [Pt(*N*(H)1,1′-Me_2dma)**G**]$^{2+}$ adducts are similar to those of the adducts with nucleotides (Tables 2.3 and 2.4 and Supporting Information), indicating that phosphate and ribose groups have at best a small influence on Δδ and on impeding nucleobase rotation. The absence of the chiral sugar group in the [Pt(*N*(H)1,1′-Me_2dma)(9-EtG)]$^{2+}$ adduct results in only one H4/4′ signal for each rotamer, giving a total of two H4/4′ signals, not four as found with adducts in which **G** has a ribose group.

Furthermore, correlating the abundance of the two sets of CH_2 and CH_3 signals with that of the H8 signals establishes that the anti rotamer has the more downfield signals for all of the protons associated with the five-membered guanine ring (Table 2.4).

Comparison between Pt(*N*(H)dpa)G and Pt(*N*(H)1,1′-Me$_2$dma)G Adducts. In order to compare the properties of the new adducts with those found previously for the Pt(*N*(H)dpa)**G** adducts,[5] we conducted a few studies of Pt(*N*(H)1,1′-Me$_2$dma)**G** adducts (**G** = 5′-GMP and 5′-GTP) in the solvent mixture (65:35 D_2O:DMSO-d_6 at pH 4) used previously for the Pt(*N*(H)dpa)**G** adducts.[5] The results for both classes of adducts, such as the syn:anti ratios, are comparable (Supporting Information). Also, the Δδ values (in 65:35 D_2O:DMSO-d_6) for **G** = 5′-GMP and 5′-GTP are ~0.4 ppm for Pt(*N*(H)dpa)**G** adducts and are ~0.3 ppm for Pt(*N*(H)1,1′-Me$_2$dma)**G** adducts. The non bonded distances between the bound Cl and the center of the aromatic rings found in the molecular structures are shorter to the imidazolyl rings (~4.2 Å) of the [Pt(*N*(R)1,1′-Me$_2$dma)Cl]$^+$ cations than to the pyridyl rings (~4.4 Å) of the [Pt(*N*(R)dpa)Cl]$^+$ cations.[89-90] The difference in these distances suggests that H8 in adducts is farther from the center of the pyridyl rings than from the center of the imidazolyl rings. Together with the Δδ values for these adducts in the solvent mixture, the difference in these distances leaves little doubt that the anisotropy of the pyridyl ring is greater than that of the imidazolyl ring.

Upon adduct formation, the downfield shift changes of the H8 and H1′ NMR signals (relative to free **G**) are comparatively smaller for Pt(*N*(H)1,1′-Me$_2$dma)**G** than for Pt(*N*(H)dpa)**G** adducts. As an example, from data in Supporting Information, the H8 shift changes upon adduct formation are 0.62 and 0.91 ppm for the syn and anti rotamers of Pt(*N*(H)1,1′-Me$_2$dma)(5′-GMP), respectively, vs. 0.76 and 1.12 ppm[5] for the corresponding rotamers of Pt(*N*(H)dpa)(5′-GMP). Because the anisotropic effect of the pyridyl rings on H8 is greater than that of the imidazolyl

rings, the conclusion is clear that the Pt(II) center exerts a stronger electron-withdrawing effect on the nucleobase in the Pt(*N*(H)dpa)**G** than in the Pt(*N*(H)1,1′-Me_2dma)**G** adducts. The strength of this Pt(II) inductive effect provides a rough estimate of the relative electron-donating ability of the bound aromatic rings. Thus, the imidazolyl rings have a relatively higher donating ability than the pyridyl rings, as might be expected. This difference, which undoubtedly occurs also in the chlorido complexes, may be the reason that complete formation of the Pt(*N*(H)dpa)(5′-GMP) adduct requires less time (~2 d) than that needed for the Pt(*N*(H)1,1′-Me_2dma)(5′-GMP) adduct (≥4 d) in either D_2O (100%) or D_2O:DMSO-d_6 (65:35).

Pt(*N*(Me)1,1′-Me_2dma)G Adducts. To examine the influence of increased bulk at the central nitrogen of the carrier ligand, we evaluated the properties of the Pt(*N*(Me)1,1′-Me_2dma)**G** adducts (Table 2.4). The Pt(*N*(Me)1,1′-Me_2dma)(5′-GMP) adduct showed sharp H8 singlets for the syn (upfield H8 signal at 8.66 ppm) and the anti (downfield H8 signal at 8.98 ppm) rotamers (Supporting Information, Table 2.4). The Δδ for the two H8 signals (0.32 ppm) is comparable to that of Pt(*N*(H)1,1′-Me_2dma)(5′-GMP) (0.31 ppm). The chemical shifts for H1′ doublets of the syn and anti rotamers of the Pt(*N*(Me)1,1′-Me_2dma)(5′-GMP) adduct are similar to what is observed for the Pt(*N*(H)1,1′-Me_2dma)(5′-GMP) adduct (Table 2.4). Similarly, the Pt(*N*(Me)1,1′-Me_2dma)(5′-GTP), Pt(*N*(Me)1,1′-Me_2dma)(3′-GMP), Pt(*N*(Me)1,1′-Me_2dma)(5′-IMP), and Pt(*N*(Me)1,1′-Me_2dma)(Ino) adducts have shifts (Tables 2.3 and 2.4 and Supporting Information) very similar to those of the corresponding Pt(*N*(H)1,1′-Me_2dma)**G** adducts. However, the EXSY cross-peaks connecting the syn and anti H8 signals in a ROESY spectrum of the Pt(*N*(Me)1,1′-Me_2dma)(5′-GMP) adduct (Supporting Information) are relatively smaller than those of the Pt(*N*(H)1,1′-Me_2dma)(5′-GMP) adduct (Figure 2.8), suggesting that base rotation is more facile in the latter.

Another difference between the Pt(*N*(Me)1,1′-Me_2dma)**G** adducts and the Pt(*N*(H)1,1′-Me_2dma)**G** adducts was the relative abundance of the rotamers in D_2O when **G** = 5′-GMP, 5′-GTP, 3′-GMP, and 5′-IMP. The Pt(*N*(Me)1,1′-Me_2dma)**G** adducts have a high syn:anti ratio (≥1.5:1), whereas the Pt(*N*(H)1,1′-Me_2dma)**G** adducts have rotamers of nearly equal abundance (Table 2.4). Comparison of the model of the anti rotamer (Figure A.3 in Supporting Information) with the molecular structure of the syn rotamer in [Pt(*N*(H)1,1′-Me_2dma)(3′-GMPH)]NO_3•5H_2O (**5**) did not show any steric interactions that would favor either rotamer, consistent with the similar abundance of the rotamers. Finally, it is interesting to note 1) that the imidazole ring has a greater degree of tilting in **5** than in the chlorido complexes and 2) that a methyl group on the central nitrogen increases tilting. Thus, the greater abundance of the syn rotamer typically found for Pt(*N*(Me)1,1′-Me_2dma)**G** adducts than for Pt(*N*(H)1,1′-Me_2dma)**G** adducts may arise in part because the tilting is already greater in the starting [Pt(*N*(Me)1,1′-Me_2dma)Cl]Cl complex.

Relationship of the Phosphate Group to Pt(II) and N7 in GMP Complexes. The molecular structure of [Pt(*N*(H)1,1′-Me_2dma)(3′-GMPH)]NO_3•5H_2O (**5**) allows us to compare the proximity of the phosphate group to Pt(II) and N7 to such distances in structurally characterized 5′-GMP complexes, all of which are bis adducts.[69-72,77] Non-bonded distances were obtained from crystallographically determined molecular structures by using Mercury 3.7 software. For our purposes, we use the central P atom to gauge the distance of the phosphate group to the other atoms. The Pt-to-P non bonded distance (9.7 Å) in the 3′-GMP complex (**5**) is much longer than in the 5′-GMP complexes (5.0-6.2 Å). The NMR and structural data for such bis 5′-GMP adducts, especially for the ΔHT conformation (head-to-tail orientation of the two bases and right-handed chirality), suggest that the phosphate group of 5′-GMP interacts electrostatically with the Pt(II)

center or the carrier ligand.[70-71] Thus, the most abundant conformers often differ between bis adducts formed by 5′-GMP and those formed by 3′-GMP.[102]

The spatial position of the 3′-phosphate group in 3′-GMP bound via N7 to a metal center separates the centers of charge. This separation may explain why so few 3′-GMP complexes have been crystallized. The large number of known structures of 5′-GMP complexes of many metals may indicate that charge neutralization resulting from the close proximity of the 5′-phosphate group to the metal center facilitates crystallization.

Furthermore, the inability of 3′-GMP to form such electrostatic interactions explains why formation of the Pt(*N*(R)1,1′-Me_2dma)(3′-GMP) adduct requires 10 d vs the 6 d or less needed to form the 5′-GMP, 5′-GDP, 5′-GTP, and 5′-IMP adducts, in which a phosphate group is closer to the Pt(II) center. The N7-to-P non bonded distance in **5** is 8.0 Å. The attraction of the negative 3′-phosphate to the positive Pt(II) center during adduct formation positions the N7 of 3′-GMP too far from Pt(II) to facilitate N7-to-Pt bond formation. In contrast, the N7-to-P non bonded distances in 5′-GMP adducts range from 5.1 to 6.3 Å.[69-72,77] The attraction of the negative 5′-phosphate group to the positive Pt(II) center positions the N7 of GMP closer to Pt(II) during adduct formation by 5′-GMP than during adduct formation by 3′-GMP. This positioning probably accounts for the shorter times observed for reactions of 5′-GMP than of 3′-GMP.

2.4 Conclusions

The presence of EXSY cross-peaks in the ROESY spectra of Pt(*N*(R)1,1′-Me_2dma)(5′-GMP) adducts but not in the ROESY spectrum of the Pt(*N*(H)dpa)(5′-GMP) adduct[5] revealed that rotamer interchange is more facile for Pt(*N*(H)1,1′-Me_2dma)**G** adducts than for Pt(*N*(H)dpa)**G** adducts; we conclude that this finding establishes that the *N*(R)1,1′-Me_2dma carrier-ligand steric effect is relatively lower than the *N*(H)dpa carrier-ligand steric effect. We believe that this lower

steric effect is a consequence of the greater distance of the H4/4′ protons from the **G** nucleobase in Pt(*N*(H)1,1′-Me_2dma)**G** adducts as compared to the distance of the corresponding H6/6′ protons in Pt(*N*(H)dpa)**G** adducts.

The structural data for [Pt(*N*(H)1,1′-Me_2dma)(3′-GMPH)]NO_3•5H_2O (**5**) confirm that the 3′-phosphate group is too far from the carrier ligand or the positive Pt(II) center to influence the properties of the complex. This finding nicely complements a study with Pt(Me_5dien)(5′/3′-GMP) adducts, which exhibited properties independent of the 3′ or 5′ position of the phosphate group on the ribose.[96] The Me_5dien carrier ligand has considerable steric bulk projecting out of the coordination plane, and the 5′-phosphate group cannot easily approach the positive Pt(II) center. In analogs of Pt(Me_5dien)(5′/3′-GMP) adducts in which protons occupied the positions of some of the carrier-ligand N-Me groups,[96-97] the rotamer distribution greatly favored the rotamer in which the 5′-phosphate group could form a hydrogen bond to the carrier-ligand NH proton. The solid-state structure of **5** in the present study thus fully supports previous less direct evidence regarding the role of the phosphate group in influencing rotamer abundance when the carrier ligand has NH groups in the cis position.

Finally, the structure of [Pt(*N*(H)1,1′-Me_2dma)(3′-GMPH)]NO_3•5H_2O (**5**) establishes the validity of features deduced from NMR results for Pt(*N*(H)dpa)**G** adducts[5] that have a related tridentate ligand. In particular, the structure of **5** shows that the **G** nucleobase has low canting and that the carrier-ligand aromatic rings in a **G** adduct are tilted, as found in the parent chlorido complexes. In studies of Pt(*N*(H)dpa)**G** adducts,[5] the tilting of the pyridyl rings served to assign signals to the syn or anti rotamer. The structure of **5** provides a basis for creating models of the syn and anti rotamers. These models indicate that the H8-to-H4/4′ distance is longer in the syn than in the anti rotamer. The relevant cross-peak intensity is larger for the anti than for the syn

signals, a finding that provides strong support for the validity of previous rotamer assignments[5] based on the effect of carrier-ligand anisotropic groups on H8 chemical shifts.

2.5 References

1. Hambley, T. W. *J. Chem. Soc., Dalton Trans.* **2001,** *19*, 2711-2718.

2. Beljanski, V.; Villanueva, J. M.; Doetsch, P. W.; Natile, G.; Marzilli, L. G. *J. Am. Chem. Soc.* **2005,** *127*, 15833-15842.

3. Orbell, J. D.; Taylor, M. R.; Birch, S. L.; Lawton, S. E.; Vilkins, L. M.; Keefe, L. J. *Inorg. Chim. Acta* **1988,** *152*, 125-134.

4. Benedetti, M.; Malina, J.; Kasparkova, J.; Brabec, V.; Natile, G. *Environ. Health Perspect.* **2002,** *110*, 779-782.

5. Hirano, T.; Inagaki, K.; Fukai, T.; Alink, M.; Nakahara, H.; Kidani, Y. *Chem. Pharm. Bull.* **1990,** *38*, 2850-2852.

6. Andrepont, C.; Marzilli, P. A.; Marzilli, L. G. *Inorg. Chem.* **2012,** *51* (21), 11961-11970.

7. Andrepont, C.; Marzilli, P. A.; Pakhomova, S.; Marzilli, L. G. *J. Inorg. Biochem.* **2015,** *153*, 219-230.

8. Saad, J. S.; Marzilli, P. A.; Intini, F. P.; Natile, G.; Marzilli, L. G. *Inorg. Chem.* **2011,** *50* (17), 8608-8620.

9. Saad, J. S.; Natile, G.; Marzilli, L. G. *J. Am. Chem. Soc.* **2009,** *131*, 12314-12324.

10. Park, G. Y.; Wilson, J. J.; Song, Y.; Lippard, S. J. *Proc. Natl. Acad. Sci. U.S.A.* **2012,** *109* (30), 11987-11992.

11. Johnstone, T. C.; Wilson, J. J.; Lippard, S. J. *Inorg. Chem.* **2013,** *52* (21), 12234-12249.

12. Zhu, G.; Myint, M.; Ang, W. H.; Song, L.; Lippard, S. J. *Cancer Res.* **2012,** *72* (3), 790-800.

13. Lovejoy, K. S.; Todd, R. C.; Zhang, S.; McCormick, M. S.; D'Aquino, J. A.; Reardon, J. T.; Sancar, A.; Giacomini, K. M.; Lippard, S. J. *Proc. Natl. Acad. Sci.* **2008,** *105* (26), 8902-8907.

14. Wang, Z.; Yu, H.; Gou, S.; Chen, F.; Fang, L. *Inorg. Chem.* **2016,** *55* (9), 4519-4528.

15. Macquet, J. P.; Butour, J. L. *Eur. J. Biochem.* **1978,** *83*, 375-387.

16. Marzilli, L. G.; Reily, M. D.; Heyl, B. L.; McMurray, C. T.; Wilson, W. D. *FEBS Lett.* **1984,** *176* (2), 389-392.

17. Reily, M. D.; Marzilli, L. G. *J. Am. Chem. Soc.* **1985,** *107*, 4916-4924.

18. Ohndorf, U.-M.; Rould, M. A.; He, Q.; Pabo, C. O.; Lippard, S. J. *Nature* **1999,** *399* (6737), 708-712.

19. Marzilli, L. G.; Saad, J. S.; Kuklenyik, Z.; Keating, K. A.; Xu, Y. *J. Am. Chem. Soc.* **2001,** *123* (12), 2764-2770.

20. Sullivan, S. T.; Saad, J. S.; Fanizzi, F. P.; Marzilli, L. G. *J Am Chem Soc* **2002,** *124* (8), 1558-1559.

21. Sullivan, S. T.; Ciccarese, A.; Fanizzi, F. P.; Marzilli, L. G. *J. Am. Chem. Soc.* **2001,** *123*, 9345-9355.

22. Todd, R. C.; Lippard, S. J.; Bonetti, A.; Leone, R.; Muggia, F. M.; Howell, S. B., *Platinum and Other Heavy Metal Compounds in Cancer Chemotherapy*. Humana Press: New York, 2009; p 67-72.

23. Saad, J. S.; Benedetti, M.; Natile, G.; Marzilli, L. G. *Inorg. Chem.* **2011,** *50*, 4559-4571.

24. Maheshwari, V.; Marzilli, P. A.; Marzilli, L. G. *Inorg. Chem.* **2011,** *50*, 6626-6636.

25. Andrepont, C. New Platinum Complexes with Tridentate Ligands as Models for Active Monofunctional Anticancer Drugs. Ph.D. Dissertation, Louisiana State University, Baton Rouge, LA, Baton Rouge, Louisiana, May 2015.

26. Andrepont, C.; Pakhomova, S.; Marzilli, P. A.; Marzilli, L. G. *Inorg. Chem.* **2015,** *54*, 4895-4908.

27. Ndinguri, M. W.; Fronczek, F. R.; Marzilli, P. A.; Crowe, W. E.; Hammer, R. P.; Marzilli, L. G. *Inorg. Chim. Acta* **2010,** *363* (8), 1796-1804.

28. Tshentu, Z. R.; Gerber, T. I. A.; Walmsley, R.; Mayer, P. *Polyhedron* **2008,** *27* (1), 406-410.

29. Oberhausen, K. J.; Richardson, J. F.; Buchanan, R. M.; Pierce, W. *Polyhedron* **1989,** *8* (5), 659-668.

30. Maresca, K. P.; Kronauge, J. F.; Zubieta, J.; Babich, J. W. *Inorg. Chem. Commun.* **2007,** *10* (12), 1409-1412.

31. Banerjee, S. R.; Levadala, M. K.; Lazarova, N.; Wei, L.; Valliant, J. F.; Stephenson, K. A.; Babich, J. W.; Maresca, K. P.; Zubieta, J. *Inorg. Chem.* **2002,** *41*, 6417-6425.

32. Lu, G.; Hillier, S. M.; Maresca, K. P.; Zimmerman, C. N.; Eckelman, W. C.; Joyal, J. L.; Babich, J. W. *J. Med. Chem.* **2013,** *56*, 510-520.

33. Maresca, K. P.; Marquis, J. C.; Hillier, S. M.; Lu, G.; Femia, F. J.; Zimmerman, C. N.; Eckelman, W. C.; Joyal, J. L.; Babich, J. W. *Bioconjug. Chem.* **2010,** *21* (6), 1032-1042.

34. Karlin, K.; Cruse, R.; McKown, J.; Hayes, J.; Dahlstrom, P.; Zubieta, J. *Transit. Metal Chem.* **1984,** *9* (10), 404-405.

35. Rodriguez, M.-C.; Morgenstern-Badarau, I.; Cesario, M.; Guilhem, J.; Keita, B.; Nadjo, L. *Inorg. Chem.* **1996,** *35* (26), 7804-7810.

36. Wei, C.-Y.; Fischer, B. E.; Bau, R. *J. Chem. Soc., Chem. Commun* **1978,** (23), 1053-1055.

37. Sheldrick, W. S. *Z. Naturforsch.* **1983,** *38 b*, 16-19.

38. Melanson, R.; Rochon, F. D. *Can. J. Chem.* **1979,** *57* (1), 57-61.

39. Melanson, R.; Rochon, F. D. *Acta Crystallogr., Sect. B: Struct. Sci.* **1978,** *34* (12), 3594-3598.

40. Ibáñez, S.; Albertí, F. M.; Sanz Miguel, P. J.; Lippert, B. *Chem. -Eur. J.* **2011,** *17* (34), 9283-9287.

41. Orbell, J. D.; Solorzano, C.; Marzilli, L. G.; Kistenmacher, T. J. *Inorg. Chem.* **1982,** *21* (10), 3806-3810.

42. Barnham, K. J.; Bauer, C. J.; Djuran, M. I.; Mazid, M. A.; Rau, T.; Sadler, P. J. *Inorg. Chem.* **1995,** *34* (11), 2826-2832.

43. Benedetti, M.; Tamasi, G.; Cini, R.; Marzilli, L. G.; Natile, G. *Chem. -Eur. J.* **2007,** *13* (11), 3131-3142.

44. Benedetti, M.; Tamasi, G.; Cini, R.; Natile, G. *Chem. -Eur. J.* **2003,** *9* (24), 6122-6132.

45. Djuran, M. I.; Milinkovic, S. U.; Habtemariam, A.; Parsons, S.; Sadler, P. J. *J. Inorg. Biochem.* **2002,** *88* (3–4), 268-273.

46. Kistenmacher, T. J.; Chiang, C. C.; Chalilpoyil, P.; Marzilli, L. G. *J. Am. Chem. Soc.* **1979,** *101* (5), 1143-1148.

47. Cramer, R. E.; Dahlstrom, P. L.; Seu, M. J. T.; Norton, T.; Kashiwagi, M. *Inorg. Chem.* **1980,** *19* (1), 148-154.

48. Cini, R.; Grabner, S.; Bukovec, N.; Cerasino, L.; Natile, G. *Eur. J. Inorg. Chem.* **2000,** *2000* (7), 1601-1607.

49. Grabner, S.; Plavec, J.; Bukovec, N.; Di Leo, D.; Cini, R.; Natile, G. *Dalton Trans* **1998,** (9), 1447-1452.

50. Schroder, G.; Lippert, B.; Sabat, M.; Lock, C. J. L.; Faggiani, R.; Song, B.; Sigel, H. *Dalton Trans* **1995,** (23), 3767-3775.

51. Marzilli, L. G.; Chalilpoyil, P.; Chiang, C. C.; Kistenmacher, T. J. *J. Am. Chem. Soc.* **1980,** *102* (7), 2480-2482.

52. Heyl, B. L.; Shinozuka, K.; Miller, S. K.; VanDerveer, D. G.; Marzilli, L. G. *Inorg Chem* **1985,** *24* (5), 661-666.

53. Price., J. H.; Williamson, A. N.; Robert, F. S.; Bradford, B. W. *Inorg. Chem.* **1972,** *11*, 1280-1284.

54. Gautier, F.-M.; Jones, S.; Martin, S. J. *Org. Biomol. Chem.* **2009,** *7* (2), 229-231.

55. Sheldrick, G. *Acta Crystallogr. Sect. A* **2008,** *64* (1), 112-122.

56. An, Y.; Li, X.-F.; Sun, J.-J.; Tong, S.-F.; Yang, H.; Yang, S.-P.; Dong, L.-H.; Yin, Y.-S. *Inorg. Chem. Commun.* **2014,** *40*, 211-214.

57. Choi, K.-Y.; Jeon, Y.-M.; Ryu, H.; Oh, J.-J.; Lim, H.-H.; Kim, M.-W. *Polyhedron* **2004,** *23* (6), 903-911.

58. Pitteri, B.; Marangoni, G.; Cattalini, L.; Visentin, F.; Bertolasi, V.; Gilli, P. *Polyhedron* **2001,** *20* (9–10), 869-880.

59. Grehl, M.; Krebs, B. *Inorg. Chem.* **1994,** *33*, 3877-3885.

60. Ravera, M.; Gabano, E.; Sardi, M.; Ermondi, G.; Caron, G.; McGlinchey, M. J.; Müller-Bunz, H.; Monti, E.; Gariboldi, M. B.; Osella, D. *J. Inorg. Biochem.* **2011,** *105* (3), 400-409.

61. Ludwig, T.; Fakih, S.; Bertram, H.; Krebs, B.; Oberleithner, H. *Cell Biochem. Biophys.* **2006,** *45* (1), 31-41.

62. Bloemink, M. J.; Engelking, H.; Karentzopoulos, S.; Krebs, B.; Reedijk, J. *Inorg. Chem.* **1996,** *35* (3), 619-627.

63. Pitteri, B.; Annibale, G.; Marangoni, G.; Bertolasi, V.; Ferretti, V. *Polyhedron* **2002,** *21*, 2283-2291.

64. Seubert, K.; Böhme, D.; Kösters, J.; Shen, W.-Z.; Freisinger, E.; Müller, J. *Z. Anorg. Allg. Chem.* **2012,** *638* (11), 1761-1767.

65. Maheshwari V.; Bhattacharyya D.; Fronczek F. R.; Marzilli P. A.; Marzilli L. G. *Inorg. Chem.* **2006,** *45,* 7182-7190.

66. Britten, J. F.; Lock, C. J. L.; Pratt, W. M. C. *Acta Crystallogr. Sect. B* **1982,** *38* (8), 2148-2155.

67. Lonnon, D. G.; Craig, D. C.; Colbran, S. B. *J. Chem. Soc., Dalton Trans.* **2006,** (31), 3785-3797.

68. Yao, S.; Plastaras, J. P.; Marzilli, L. G. *Inorg Chem* **1994,** *33* (26), 6061-6077.

69. Marzilli, L. G.; Kistenmacher, T. J. *Acc Chem Res* **1977,** *10* (4), 146-152.

70. Carlone, M.; Fanizzi, F. P.; Intini, F. P.; Margiotta, N.; Marzilli, L. G.; Natile, G. *Inorg. Chem.* **2000,** *39* (4), 634-641.

71. Carlone, M.; Marzilli, L. G.; Natile, G. *Inorg. Chem.* **2004,** *43,* 584-592.

72. Carlone, M.; Marzilli, L. G.; Natile, G. *Eur. J. Inorg. Chem.* **2005**, 1264-1273.

73. Sandlin, R. D.; Starling, M. P.; Williams, K. M. *J. Inorg. Biochem.* **2010,** *104*, 214.

74. Saad, J. S.; Scarcia, T.; Natile, G.; Marzilli, L. G. *Inorg. Chem.* **2002,** *41* (19), 4923-4935.

75. Maheshwari, V.; Marzilli, P. A.; Marzilli, L. G. *Inorg. Chem.* **2008,** *47* (20), 9303-9313.

76. Cramer, R. E.; Dahlstrom, P. L. *J. Am. Chem. Soc.* **1979,** *101* (13), 3679-3681.

77. Cramer, R. E.; Dahlstrom, P. L. *Inorg. Chem.* **1985,** *24* (21), 3420-3424.

78. Xu, Y.; Natile, G.; Intini, F. P.; Marzilli, L. G. *J. Am. Chem. Soc.* **1990,** *112* (22), 8177-8179.

CHAPTER 3. NNN-TRIDENTATE LIGANDS WITH CENTRAL SULFONAMIDE AND TERMINAL PYRIDYL RING N-DONORS. COMPARISON OF FACTORS AFFECTING LIGAND COORDINATION MODE AND BINDING STRENGTH TO *fac*-$[Re(I)(CO)_3]^+$ AND $Pt(II)Cl_2$ "CORES" AS ELUCIDATED BY X-RAY STRUCTURAL AND NMR SPECTRAL METHODS

3.1 Introduction

New properties can be introduced into metal complexes by linking dangling groups with targeting moieties or fluorophores onto carrier ligands. Typically, the most useful linking chemistry avoids creating new asymmetric centers in the complexes, especially when the ultimate goal is to identify a diagnostic or therapeutic agent. One common approach is to attach the dangling group to the central N atom of *N*,*N'*,*N''*-donor tridentate ligands (Figure 3.1).[1-15] Various metal complexes of tridentately bound ligand derivatives of 2-dipicolylamine (*N*(H)dpa) (Figure 3.2), di-(2-methylimidazolyl)amine (*N*(H)dma), or diethylenetriamine (dien) with a suitable group attached to the central N possess useful properties, such as enhanced targeting ability,[2,7-8] fluorescence,[3,10,13] high anticancer/antitumor activity,[9,11-12] or new bioconjugation chemistry.[4-6] In almost all cases, the dangling group is attached to the chelate ligand via an N–C bond. As one example, naphthalimide derivatives (R) are attached via an N–C bond to the central N atom of the *N*(R)dpa ligand in *fac*-$[Re(CO)_3(N(R)dpa)]BF_4$ complexes, which have promising cell-imaging properties.[3] In particular, complexes of Pt(II) with chelate ligands having dangling groups[9-17] have been widely explored because such complexes often exhibit anticancer or antiviral activity.[9,11-12,17]

Recent studies from our laboratory have shown that *N*(SO_2R)dpa (Figure 3.2) or *N*(SO_2R)dien type ligands, in which the central *N*-donor atom is part of a tertiary sulfonamide group, function as a new class of tridentate ligands and form Re(I) complexes, *fac*-$[Re(CO)_3(N(SO_2R)dpa)]PF_6$[4] and *fac*-$[Re(CO)_3(N(SO_2R)dien)]PF_6$[5] (R = Me and Tol (*p*-tolyl)). Such ligands, in which the dangling group is attached via an N–S bond to the central N atom,

expand the scope of dangling-group properties that can be employed. The relevance of such Re(I) compounds to the development of ^{99m}Tc(I) and Re(I) radiopharmaceutical diagnostic and therapeutic agents has been discussed.[4-5]

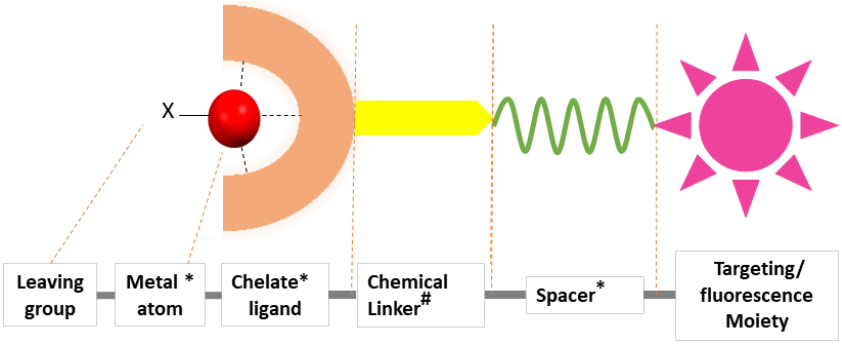

Figure 3.1. Components of a biological targeting therapeutic or diagnostic metal-containing agent. *Component with no geometrical or optical isomers. #Non-chiral linking component attached to the central donor of the chelate ligand, thereby avoiding the introduction of geometrical or optical isomers.

The *fac*-[Re(CO)$_3$(*N*(SO$_2$R)dpa)]$^+$ and *fac*-[Re(CO)$_3$(*N*(SO$_2$R)dien)]$^+$ cations are the first examples of any metal complex with the sulfonamide as part of a noncyclic linear tridentate ligand having a normal metal-to-sulfonamide nitrogen bond length (~2.2 Å).[4-5] More recently, closely related complexes of Mn(I) have been described.[18-19] Resonance stabilization within the sulfonamide group results in the sulfonamide nitrogen lacking a readily available lone pair of electrons for metal coordination. For a M–N bond to form, the bond must be energetically favorable enough to convert the hybridization of the sulfonamide N from sp^2 (resonance stabilized) to sp^3 (stabilized by the M–N bond). A key factor favoring coordination of the tertiary sulfonamide N of *N*(SO$_2$R)dpa- and *N*(SO$_2$R)dien-type ligands to Re(I) is the formation of two adjacent 5-membered chelate rings, the most favorable ring size for chelate formation. In this study, we investigate whether the normally highly favorable Pt–N bond could also form when the N atom is within the sulfonamide group in *N*(SO$_2$R)dpa-type ligands; in such a case, new types of dangling

groups could be employed with Pt(II) complexes that possess a metal center forming agents known to have widespread use in biomedicine.

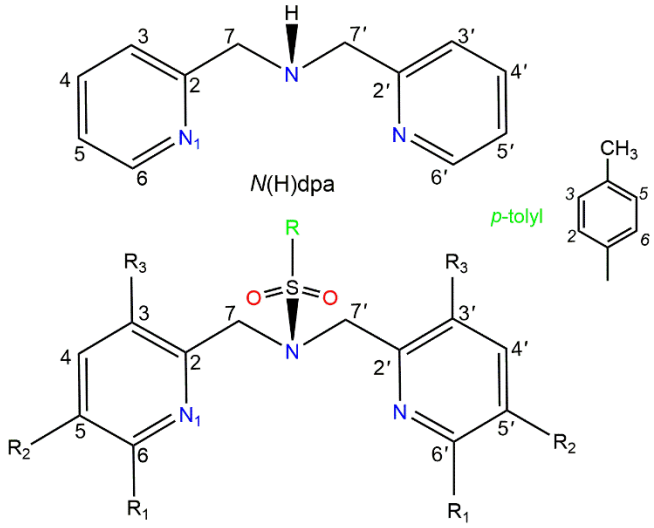

		R_1	R_2	R_3	R
P	*N*(SO_2R)dpa	H	H	H	
1	*N*(SO_2Me)3,3′,5,5′-Me_4dpa	H	Me	Me	Me
2	*N*(SO_2Tol)3,3′,5,5′-Me_4dpa	H	Me	Me	*p*-tolyl
3	*N*(SO_2Me)6,6′-Me_2dpa	Me	H	H	Me
4	*N*(SO_2Tol)6,6′-Me_2dpa	Me	H	H	*p*-tolyl

Figure 3.2. Line drawing and numbering scheme for *N*(SO_2R)Me_ndpa ligands based on the parent (***P***) ligand framework, *N*(SO_2R)dpa: *N*,*N*-di(3,5-dimethyl-2-picolyl)methanesulfonamide, *N*(SO_2Me)3,3′,5,5′-Me_4dpa (**1**); *N*,*N*-di(3,5-dimethyl-2-picolyl)-*p*-tolylsulfonamide, *N*(SO_2Tol)3,3′,5,5′-Me_4dpa (**2**); *N*,*N*-di(6-methyl-2-picolyl)methanesulfonamide, *N*(SO_2Me)6,6′-Me_2dpa (**3**); and *N*,*N*-di(6-methyl-2-picolyl)-*p*-tolylsulfonamide, *N*(SO_2Tol)6,6′-Me_2dpa (**4**). Note that the *p*-tolyl group numbering is *italicized* to prevent confusion with the pyridyl ring numbering.

Unlike the situation with the Re(I) complexes, for which adduct formation with biological molecules is usually not a key feature for biological applications, Pt(II) complexes typically act by forming adducts and require one or two leaving groups for functionality. Because aromatic protons have ^{1}H NMR signals complicating such studies, we chose to prepare and study *N*(SO_2R)dpa-type ligands with methyl groups replacing some of the aromatic protons characteristic of known ligands. Furthermore, methyl groups can increase the steric bulk on the carrier ligand, a factor influencing anticancer activity of Pt(II) compounds.[20-25] Therefore, we prepared Pt(II) complexes utilizing four new *N*(SO_2R)Me_ndpa ligands (Figures 3.2 and 3.3, R = Me or Tol and with n

indicating different methyl substitution patterns on the pyridyl ring). *fac*-[Re(CO)$_3$(*N*(SO$_2$R)Me$_n$dpa)]PF$_6$ complexes of these new ligands were synthesized to confirm that they are capable of binding tridentately to Re(I), despite the presence of methyl substituents on the pyridyl ring, especially for *N*(SO$_2$R)6,6′-Me$_2$dpa. All of the *fac*-[Re(CO)$_3$(chelate)]PF$_6$ complexes discussed below have facial geometry, and thus from this point onward we omit the *fac*- designation when discussing specific compounds.

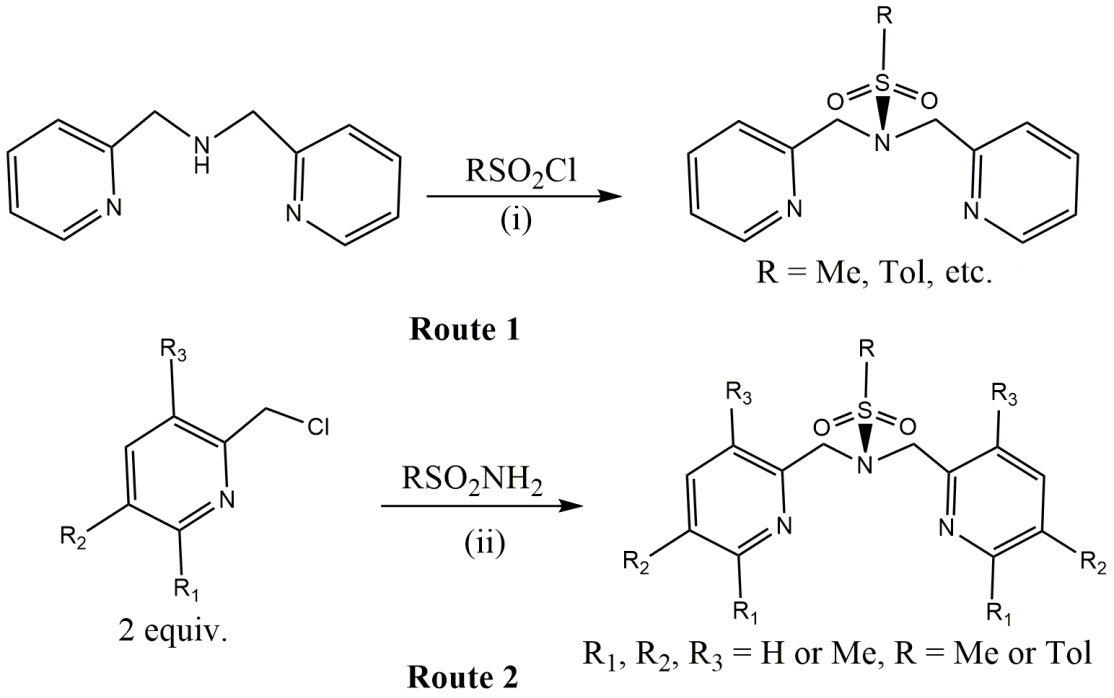

Figure 3.3. Synthetic routes for the ligands, *N*(SO$_2$R)dpa (Route 1) and *N*(SO$_2$R)Me$_n$dpa (Route 2). (i) dioxane, RT, 24 h. (ii) K$_2$CO$_3$, acetonitrile at reflux, N$_2$, 18 h.

Previous studies from this laboratory have shown that the *N*(R)dpa and *N*(R)1,1′-Me$_2$dma ligands (R = H or Me) readily bind to the Pt(II) metal center in a tridentate fashion to form [Pt(L^{tri})Cl]$^+$ (L^{tri} = *N*,*N*′,*N*″-donor tridentate carrier ligand) complexes.[26-27] However, the new *N*(SO$_2$R)Me$_n$dpa ligands form Pt(II) complexes with bidentate *N*(SO$_2$R)Me$_n$dpa ligands having an 8-membered chelate ring with the tertiary sulfonamide nitrogen not bound directly to Pt(II) but serving as an atom in the chain of the chelate ring. Structural characterizations of Pt(II) complexes with bidentate ligands having 8-membered chelate rings such as those found here are very few in

number, as compared to bifunctional Pt(II) complexes with smaller 5-, 6-, and 7-membered chelate rings of bidentate pyridyl/imidazolyl ligands[28-50] or with two pyridyl/imidazolyl monodentate ligands.[51-55] The rarity and unusual properties of the new bifunctional Pt(II) compounds with a large 8-membered chelate ring in the current work led us to compare their structural features with these features in related bifunctional Pt(II) complexes. The relevance of binding at G residues in DNA by anticancer-active Pt(II) compounds[28,33,43-44,55] has led to many studies of adduct formation of guanine derivatives with mono- and bi-functional Pt(II) complexes bearing carrier ligands with 5- and 6-membered chelate rings.[26-27,56] In rare cases the guanine derivatives disrupt and open the chelate ring.[57] We found that the chelate rings in the new complexes open relatively easily but that this process is not facilitated in the presence of guanine derivatives.

3.2 Experimental Section

Starting Materials. Methanesulfonamide ($MeSO_2NH_2$), *p*-tolylsulfonamide ($TolSO_2NH_2$), 2,3,5-collidine, 6-methyl-2-pyridinemethanol, tetraethylammonium chloride ($[Et_4N]Cl$), and K_2PtCl_4 were used as received from Aldrich. *cis*-$Pt(DMSO)_2Cl_2$,[58] aqueous $[Re(CO)_3(H_2O)_3]OTf$ (OTf = trifluoromethanesulfonate),[59] 2-(chloromethyl)-6-methylpyridine,[60] and 2-(chloromethyl)-3,5-dimethylpyridine[61] were prepared by known methods.

NMR Measurements. ^1H NMR spectra were recorded on a 400 MHz or on an Avance-III Prodigy 500 MHz Bruker spectrometer. Peak positions are relative to TMS or solvent residual peak with TMS as reference. All NMR data were processed with TopSpin and MestReNova software. A presaturation pulse to suppress the water peak was employed when necessary.

Mass Spectrometric Measurements. High resolution mass spectra were recorded on an Agilent 6210 ESI TOF LCMS mass spectrometer.

X-ray Data Collection and Structure Determination. Diffraction data were collected on a Bruker Kappa Apex-II DUO CCD diffractometer with Mo Kα radiation (λ = 0.71073 Å), equipped with an Oxford Cryosystems Cryostream. All X-ray structures were determined by direct methods and difference Fourier techniques and refined by full-matrix least-squares by using *SHELXL2014*[62] with H-atoms in idealized positions.

General Synthesis of Ligands. A solution of the desired 2-chloromethyl pyridine derivative (~6 mmol), K_2CO_3 (~1.7 g, 12 mmol), and the appropriate sulfonamide (~2.5 mmol) in acetonitrile (95 mL) was heated at reflux under nitrogen for 18 h. After removal of acetonitrile under reduced pressure, the residue was dissolved in water (45 mL) and the solution extracted with CH_2Cl_2 (3 x 45 mL). The organic layers were combined, washed with saturated aqueous sodium chloride solution, dried over sodium sulfate, and taken to dryness under reduced pressure. The residue was dissolved in ethyl acetate:hexane (80:20) and purified by chromatography on a silica column with the same eluent. Fractions were collected and spotted on TLC plates by using the same eluent. The cleanest fractions, as assessed by ^{1}H NMR spectroscopy, were combined and taken to dryness by rotary evaporation to afford the desired ligand in sufficient purity to use in the synthesis of the corresponding Pt(II) complex.

***N*(SO$_2$Me)3,3′,5,5′-Me$_4$dpa (1).** The general ligand synthesis described above carried out with 2-(chloromethyl)-3,5-dimethylpyridine (0.98 g, 6.2 mmol) and $MeSO_2NH_2$ (0.23 g, 2.4 mmol) produced an orange residue, which was purified by using column chromatography to afford *N*(SO$_2$Me)3,3′,5,5′-Me$_4$dpa as a white solid (0.54 g, 67% yield). ^{1}H NMR signals (ppm) in $CDCl_3$: 8.19 (s, 2H, H6/6′), 7.23 (s, 1H, H4/4′), 4.60 (s, 4H, CH_2), 3.15 (s, 3H, CH_3), 2.28 (s, 6H, CH_3), 2.21 (s, 6H, CH_3). ^{1}H NMR signals (ppm) in DMSO-d_6: 8.17 (s, 2H, H6/6′), 7.33 (s, 2H, H4/4′),

4.45 (s, 4H, CH_2), 3.13 (s, 3H, CH_3), 2.23 (s, 6H, CH_3), 2.12 (s, 6H, CH_3). ESI-MS (*m/z*): $[M + H]^+$ = 334.1596. Calcd for $[M + H]^+$ = 334.1584.

***N*(SO$_2$Tol)3,3′,5,5′-Me$_4$dpa (2).** The general ligand synthesis with 2-(chloromethyl)-3,5-dimethylpyridine (1.04 g, 6.6 mmol) and $TolSO_2NH_2$ (0.46 g, 2.6 mmol) yielded an orange residue, which was purified by using column chromatography to afford *N*(SO_2Tol)3,3′,5,5′-Me_4dpa as a pale yellow solid (0.88 g, 79% yield). ^{1}H NMR signals (ppm) in $CDCl_3$: 7.98 (s, 2H, H6/6′), 7.70 (d, *J* = 8.1 Hz, 2H, H*2*/*6*), 7.26 (masked by the solvent peak, 2H, H*3*/*5*), 7.07 (s, 2H, H4/4′), 4.48 (s, 4H, CH_2), 2.43 (s, 3H, CH_3), 2.25 (s, 6H, CH_3), 2.19 (s, 6H, CH_3). ^{1}H NMR signals (ppm) in DMSO-d_6: 7.94 (s, 2H, H6/6′), 7.62 (d, *J* = 7.8 Hz, 2H, H*2*/*6*), 7.32 (d, *J* = 7.9 Hz, 2H, H*3*/*5*), 7.21 (s, 2H, H4/4′), 4.41 (s, 4H, CH_2), 2.39 (s, 3H, CH_3), 2.16 (s, 6H, CH_3), 2.13 (s, 6H, CH_3). ESI-MS (*m/z*): $[M + H]^+$ = 410.1876. Calcd for $[M + H]^+$ = 410.1897.

***N*(SO$_2$Me)6,6′-Me$_2$dpa) (3).** The general ligand synthesis with 2-(chloromethyl)-6-methylpyridine (0.90 g, 6.4 mmol) and $MeSO_2NH_2$ (0.24 g, 2.5 mmol) yielded an orange residue, which was purified by using column chromatography to afford *N*(SO_2Me)6,6′-Me_2dpa as a colorless oil (0.68 g, 88% yield). ^{1}H NMR signals (ppm) in $CDCl_3$: 7.55 (t, *J* = 7.7 Hz, 2H, H4/4′), 7.18 (d, *J* = 7.7 Hz, 2H, H5/5′), 7.05 (d, *J* = 7.7 Hz, 2H, H3/3′), 4.54 (s, 4H, CH_2), 3.15 (s, 3H, CH_3), 2.51 (s, 6H, CH3). ^{1}H NMR signals (ppm) in DMSO-d_6: 7.63 (t, *J* = 7.7 Hz, 2H, H4/4′), 7.12 (d, *J* = 7.8 Hz, 4H, H3/3′ and H5/5′), 4.42 (s, 4H, CH_2), 3.14 (s, 3H, CH_3), 2.41 (s, 6H, CH_3). ESI-MS (*m/z*): $[M + H]^+$ = 306.1269. Calcd for $[M + H]^+$ = 306.1271.

***N*(SO$_2$Tol)6,6′-Me$_2$dpa (4).** The general ligand synthesis with 2-(chloromethyl)-6-methylpyridine (1.00 g, 7.1 mmol) and $TolSO_2NH_2$ (0.58 g, 3.4 mmol) yielded an orange residue, which was purified by using column chromatography to afford *N*(SO_2Tol)6,6′-Me_2dpa as a yellow

oil (1.14 g, 89% yield). ^{1}H NMR signals (ppm) in $CDCl_3$: 7.71 (d, *J* = 8.1 Hz, 2H, H*2*/*6*), 7.43 (t, *J* = 7.7 Hz, 2H, H4/4′), 7.24 (d, *J* = 8.1 Hz, 2H, H*3*/*5*), 7.14 (d, *J* = 7.8 Hz, 2H, H3/3′), 6.92 (d, *J* = 7.7 Hz, 2H, H5/5′), 4.56 (s, 4H, CH_2), 2.42 (s, 3H, CH_3), 2.37 (s, 6H, CH_3). ^{1}H NMR signals (ppm) in DMSO-d_6: 7.67 (d, *J* = 8.2 Hz, 2H, H*2*/*6*), 7.53 (t, *J* = 7.7 Hz, 2H, H4/4′), 7.33 (d, *J* = 8.0 Hz, 2H, H*3*/*5*), 7.04 (quasi t, 4H, H3/3′ and H5/5′), 4.43 (s, 4H, CH_2), 2.37 (s, 3H, CH_3), 2.28 (s, 6H, CH_3). ESI-MS (*m/z*): $[M + H]^+$ = 382.1591. Calcd for $[M + H]^+$ = 382.1584.

General Synthesis of Platinum Complexes. A stirred solution of the ligand (0.1 mmol) and *cis*-Pt(DMSO)$_2$Cl$_2$ (0.1 mmol) in methanol (5 mL) was heated at reflux overnight (~16 h). The yellow precipitate that formed overnight was collected by filtration, washed with methanol and ether, and air-dried (Method A). X-ray quality crystals were obtained by mixing equal volumes (1 mL) of solutions of *cis*-Pt(DMSO)$_2$Cl$_2$ (12.5 mM) and the ligand (12.5 mM) in acetonitrile and allowing the mixture to stand at room temperature. Needle-like crystals were obtained within 2 days to 2 weeks (Method B). The ^{1}H NMR data are identical for the products obtained by Methods A and B.

Pt(*N*(SO$_2$Me)3,3′,5,5′-Me$_4$dpa)Cl$_2$ (5). With *N*(SO$_2$Me)3,3′,5,5′-Me$_4$dpa (**1**, 33 mg, 0.1 mmol) and *cis*-Pt(DMSO)$_2$Cl$_2$ (42 mg, 0.1 mmol), Method A afforded a pale yellow solid (26 mg, 44% yield). Yellow crystals obtained by Method B were characterized by single-crystal X-ray crystallography. ^{1}H NMR signals (ppm) in DMSO-d_6: 8.98 (s, 2H, H6/6′), 7.56 (s, 2H, H4/4′), 5.99 (d, *J* = 14.7 Hz, 2H, CH_2), 5.37 (d, *J* = 14.9 Hz, 2H, CH_2), 3.35 (s, 3H, CH_3), 2.37 (s, 6H, CH_3), 2.23 (s, 6H, CH_3). ESI-MS (*m*/*z*): $[M-H]^-$ = 597.0450. Calcd for $[M-H]^-$ = 597.0463.

Pt(*N*(SO$_2$Tol)3,3′,5,5′-Me$_4$dpa)Cl$_2$ (6). With *N*(SO$_2$Tol)3,3′,5,5′-Me$_4$dpa (**2**, 41 mg, 0.1 mmol) and *cis*-Pt(DMSO)$_2$Cl$_2$ (42 mg, 0.1 mmol), Method A afforded a pale yellow solid (25 mg,

37% yield). Yellow crystals obtained by Method B were characterized by single-crystal X-ray crystallography. ^{1}H NMR signals (ppm) in DMSO-d_6: 8.90 (s, 2H, H6/6′), 8.03 (d, J = 8.2 Hz, 2H, H2/6), 7.60 (d, J = 8.1 Hz, 2H, H3/5), 7.56 (s, 2H, H4/4′), 5.55 (d, J = 14.3 Hz, 2H, CH_2), 5.47 (d, J = 14.3 Hz, 2H, CH_2), 2.45 (s, 6H, CH_3), 2.21 (s, 6H, CH_3); the phenyl methyl signal is masked by the solvent peak. ESI-MS (m/z): $[M + H]^+$ = 676.0926. Calcd for $[M + H]^+$ = 676.0913.

[*trans*-Pt(DMSO)Cl$_2$]$_2$(*N*(SO$_2$Me)6,6′-Me$_2$dpa) (7). With *N*(SO$_2$Me)-6,6′-Me$_2$dpa (**3**, 30 mg, 0.1 mmol) and *cis*-Pt(DMSO)$_2$Cl$_2$ (42 mg, 0.1 mmol), Method A afforded a pale yellow solid (16 mg, 28% yield). ^{1}H NMR signals (ppm) in DMSO-d_6: 7.85 (t, J = 7.8 Hz, 2H, H4/4′), 7.68 (d, J = 7.9 Hz, 2H, H3/3′), 7.46 (d, J = 7.8 Hz, 2H, H5/5′), 5.55 (s, 4H, CH_2), 3.33 (s, 3H, CH_3), 3.12 (s, 6H, CH_3). ESI-MS (m/z): $[M + H]^+$ = 993.9522. Calcd for $[M + H]^+$ = 993.9569.

[*trans*-Pt(DMSO)Cl$_2$]$_2$(*N*(SO$_2$Tol)6,6′-Me$_2$dpa) (8). With *N*(SO$_2$Tol)6,6′-Me$_2$dpa (**4**, 38 mg, 0.1 mmol) and *cis*-Pt(DMSO)$_2$Cl$_2$ (42 mg, 0.1 mmol), Method A afforded a pale yellow solid (14 mg, 22% yield). Yellow needle-shaped crystals obtained by Method B were characterized by single-crystal X-ray crystallography. ^{1}H NMR signals (ppm) in DMSO-d_6: 7.91 (d, J = 8.0 Hz, 2H, H2/6), 7.76 (t, J = 7.9 Hz, 2H, H4/4′), 7.57 (d, J = 8.0 Hz, 2H, H3/3′), 7.52 (d, J = 8.0 Hz, 2H, H3/5), 7.43 (d, J = 7.9 Hz, 2H, H5/5′), 5.46 (s, 4H, CH_2), 3.11 (s, 6H, CH_3), 2.43 (s, 3H, CH_3). ESI-MS (m/z): $[M + H]^+$ = 1069.9921 Calcd for $[M + H]^+$ = 1069.9884. The solvent of the resultant clear, pale yellow filtrate (Method A) was removed under reduced pressure, leaving a residue. The ^{1}H NMR spectrum of this residue in DMSO-d_6 shows peaks for free ligand **4** and for ligand **4** bound to Pt(II) in an unsymmetric monodentate fashion.

Isolation of *trans*-[Pt(DMSO)Cl$_2$](*N*(SO$_2$Tol)6,6′-Me$_2$dpa) Crystals (8a). In a preparation that led to the isolation of the new complex detected in the residue just mentioned, an

aqueous solution of K_2PtCl_4 (0.208 g, 0.5 mmol in 10 mL) was heated to 70 °C and treated with 70 μL (1 mmol) of DMSO followed after 10 min by *N*(SO_2Tol)-6,6′-Me_2dpa (**4**, 191 mg, 0.5 mmol). The mixture was heated and stirred for 1 h at 95 °C. The yellow solid (78 mg, 15%) that precipitated was collected by filtration, washed with methanol and ether, and identified as complex **8** by its ^{1}H NMR spectrum. Yellow X-ray quality crystals of **8a** (53 mg, 15%) deposited overnight from the clear yellow filtrate. The ^{1}H NMR signals (in DMSO-d_6) of the **8a** crystals are identical to those for the complex in the residue obtained with Method A (see above). ^{1}H NMR signals (ppm) in DMSO-d_6: 7.88 (t, J = 8.0 Hz, 1H, $H4_{bound}$), 7.78 (d, J = 8.0 Hz, 2H, H2/6), 7.54 (t, J = 7.9 Hz, 1H, $H4_{dangling}$), 7.49 (d, J = 8.0 Hz, 1H, $H3_{bound}$), 7.42 (d, J = 8.0 Hz, 3H, H3/5 & $H5_{bound}$), 7.14 (d, J = 7.9 Hz, 1H, $H3_{dangling}$), 7.04 (d, J = 7.9 Hz, 1H, $H5_{dangling}$), 5.40 (s, 2H, CH_{2bound}), 4.50 (s, 2H, $CH_{2dangling}$), 3.09 (s, 3H, CH_{3bound}), 2.42 (s, 3H, CH_3), 2.27 (s, 3H, $CH_{3dangling}$). MALDI-TOF (*m*/*z*): $[M + Na]^+$ = 748.096. Calcd for $[M + Na]^+$ = 748.052.

General Synthesis of [Re(CO)$_3$(*N*(SO_2R)Me$_n$dpa)]PF_6 Complexes. Ligands **1**-**4** were employed to synthesize [Re(CO)$_3$(*N*(SO_2R)Me$_n$dpa)]PF_6 complexes according to the following general procedure: a methanol solution of the ligand (30−41 mg, 0.1 mmol in 2 mL) was treated with aqueous [Re(CO)$_3$(H_2O)$_3$]OTf (0.1 mmol in 2 mL).[59] Methanol (2─3 mL) was added to dissolve any precipitate that formed, and the clear reaction mixture was heated at reflux for 16 h. An excess of $NaPF_6$ (0.16 g, 1 mmol) was added to the cooled clear solution, and the resulting precipitate was collected on a filter, washed with water, and air-dried. A concentrated covered solution of each compound in acetone was kept at room temperature to allow the solvent to evaporate slowly and crystals to form. Two solutions produced X-ray quality crystals, and two yielded powders.

[Re(CO)$_3$(*N*(SO$_2$Me)3,3′,5,5′-Me$_4$dpa)]PF$_6$ (9). With *N*(SO$_2$Me)3,3′,5,5′-Me$_4$dpa (**1**, 33 mg 0.1 mmol), and [Re(CO)$_3$(H$_2$O)$_3$]OTf (0.1 mmol), the general preparation described above produced [Re(CO)$_3$(*N*(SO$_2$Me)3,3′,5,5′-Me$_4$dpa)]PF$_6$ as a white solid (34 mg, 42% yield) after the addition of NaPF$_6$ (~0.16 g). Slow evaporation of a concentrated solution of this compound in acetone produced yellow needle-like crystals that were characterized by single-crystal X-ray crystallography. ^{1}H NMR signals (ppm) in DMSO-d_6: 8.60 (s, 2H, H6/6′), 7.75 (s, 2H, H4/4′), 5.29 (d, J = 17.2 Hz, 2H, CH$_2$), 5.07 (d, J = 17.0 Hz, 2H, CH$_2$), 3.96 (s, 3H, CH$_3$), 2.34 (s, 6H, CH$_3$), 2.29 (s, 6H, CH$_3$).

[Re(CO)$_3$(*N*(SO$_2$Tol)3,3′,5,5′-Me$_4$dpa)]PF$_6$ (10). With *N*(SO$_2$Me)3,3′,5,5′-Me$_4$dpa (**2**, 41 mg 0.1 mmol), and [Re(CO)$_3$(H$_2$O)$_3$]OTf (0.1 mmol), the general preparation described above produced [Re(CO)$_3$(*N*(SO$_2$Tol)3,3′,5,5′-Me$_4$dpa)]PF$_6$ as a white solid (38 mg, 57% yield) after the addition of NaPF$_6$ (~0.16 g). ^{1}H NMR signals (ppm) in DMSO-d_6: 8.63 (s, 2H, H6/6′), 8.33 (d, J = 8.2 Hz, 2H, H*2*/*6*), 7.75 (d, J = 8.5 Hz, 2H, H*3*/*5*), 7.72 (s, 2H, H4/4′), 5.48 (d, J = 17.0 Hz, 2H, CH$_2$), 4.55 (d, J = 17.0 Hz, 2H, CH$_2$), 2.56 (s, 3H, CH$_3$), 2.28 (s, 6H, CH$_3$), 2.20 (s, 6H, CH$_3$). ESI-MS (*m*/*z*): [M]$^+$ = 678.1210. Calcd for [M]$^+$ = 678.1195.

[Re(CO)$_3$(*N*(SO$_2$Me)6,6′-Me$_2$dpa)]PF$_6$ (11). With *N*(SO$_2$Me)3,3′,5,5′-Me$_4$dpa (**3**, 30 mg 0.1 mmol), and [Re(CO)$_3$(H$_2$O)$_3$]OTf (0.1 mmol), the general preparation described above produced [Re(CO)$_3$(*N*(SO$_2$Me)3,3′,5,5′-Me$_4$dpa)]PF$_6$ as a white solid (25 mg, 34% yield) after the addition of NaPF$_6$ (~0.16 g). ^{1}H NMR signals (ppm) in DMSO-d_6: 8.06 (t, J = 7.7 Hz, 2H, H4/4′), 7.65 (d, J = 7.8 Hz, 2H, H3/3′), 7.47 (d, J = 7.7 Hz, 2H, H5/5′), 5.36 (d, J = 16.9 Hz, 2H, CH$_2$), 5.03 (d, J = 17.0 Hz, 2H, CH$_2$), 3.90 (s, 3H, CH$_3$), 2.88 (s, 6H, CH$_3$). ESI-MS (*m*/*z*): [M]$^+$ = 574.0583. Calcd for [M]$^+$ = 574.0569.

[Re(CO)$_3$(*N*(SO$_2$Tol)6,6′-Me$_2$dpa)]PF$_6$ (12). With *N*(SO$_2$Tol)6,6′-Me$_2$dpa (**4**, 38 mg, 0.1 mmol) and [Re(CO)$_3$(H$_2$O)$_3$]$^+$ (0.1 mmol), the general preparation described above produced [Re(CO)$_3$(*N*(SO$_2$Tol)6,6′-Me$_2$dpa)]PF$_6$ as a pale yellow solid (41 mg, 51% yield) after the addition of NaPF$_6$ (∼0.16 g). Slow evaporation of a concentrated solution of this compound in acetone produced pale yellow, needle-like crystals that were characterized by single-crystal X-ray crystallography. ^{1}H NMR signals (ppm) in DMSO-d_6: 8.21 (d, J = 8.0 Hz, 2H, H*2*/*6*), 8.02 (t, J = 7.8 Hz, 2H, H4/4′), 7.75 (d, J = 7.7 Hz, 2H, H*3*/*5*), 7.63 (d, J = 8.0 Hz, 2H, H3/3′), 7.52 (d, J = 7.6 Hz, 2H, H5/5′), 5.23 (d, J = 16.8 Hz, 2H, CH$_2$), 4.52 (d, J = 16.6 Hz, 2H, CH$_2$), 2.90 (s, 6H, CH$_3$), 2.57 (s, 3H, CH$_3$).

Solution Studies of Pt(*N*(SO$_2$Me)3,3′,5,5′-Me$_4$dpa)Cl$_2$ (5). A solution of **5** (10 mM) in DMSO-d_6 (Solution 1), at 25 °C was monitored by ^{1}H NMR spectroscopy for at least 21 d. Another 10 mM solution of **5** in DMSO-d_6 was treated with 10 molar equiv of [Et$_4$N]Cl (10 mg) after 1 d (Solution 2). In another experiment, **5** (3.6 mg) was added to a solution of [Et$_4$N]Cl (100 mM) in DMSO-d_6 to make the solution 10 mM in **5** (Solution 3). In a similar experiment, a sufficient amount of ligand **1** (1.3 mg) was added to a solution containing *cis*-Pt(DMSO)$_2$Cl$_2$ (10 mM) and [Et$_4$N]Cl (100 mM) in DMSO-d_6 to make the solution 10 mM in ligand **1** (Solution 4). Another 10 mM solution of **1** in DMSO-d_6 was treated with 1 molar equiv of *cis*-Pt(DMSO)$_2$Cl$_2$ (1.7 mg, Solution 5). Solutions 2, 3, 4, and 5 were monitored with time by ^{1}H NMR spectroscopy. Solutions of **6** (4.0 mg, 10 mM) in DMSO-d_6 or in DMF-d_7 (partially dissolved) were kept at 25 °C and monitored by ^{1}H NMR spectroscopy. Furthermore, 10 mM solutions of **7**, **8**, and Re(I) complexes, **9**–**12**, in DMSO-d_6 were kept at 25 °C and monitored over time by ^{1}H NMR spectroscopy.

3.3 Results and Discussion

Synthesis of *N*(SO$_2$R)Me$_n$dpa Derivatives and Their Pt(II) and Re(I) Complexes. Our previous synthesis of *N*(SO$_2$R)dpa[4] ligands utilized the commercially available parent ligand, *N*(H)dpa (Figure 3.2), which was coupled with the appropriate sulfonyl chloride (Route 1, Figure 3.3). However, the *N*(H)Me$_n$dpa parent ligands needed in this study, *N*(H)3,3′,5,5′-Me$_4$dpa and *N*(H)6,6′-Me$_2$dpa, are not commercially available. Thus, the new *N*(SO$_2$R)Me$_n$dpa (**1**-**4**) ligands were synthesized by a different route, in which the desired 2-chloromethyl pyridyl derivative (2 equiv) was coupled with the appropriate sulfonamide under basic conditions (Route 2, Figure 3.3). This route gave the expected ligand as the main product, and the side-products were readily removed by column chromatography. These isolated ligands were treated with *cis*-Pt(DMSO)$_2$Cl$_2$ in methanol at reflux to obtain the neutral Pt(II) complexes in this study, **5**–**8** (Figure 3.4). Using a synthesis similar to that reported for [Re(CO)$_3$(*N*(SO$_2$R)dpa)]PF$_6$,[4] we obtained [Re(CO)$_3$(*N*(SO$_2$R)Me$_n$dpa)]PF$_6$ complexes **9**–**12** (Figure 3.5).

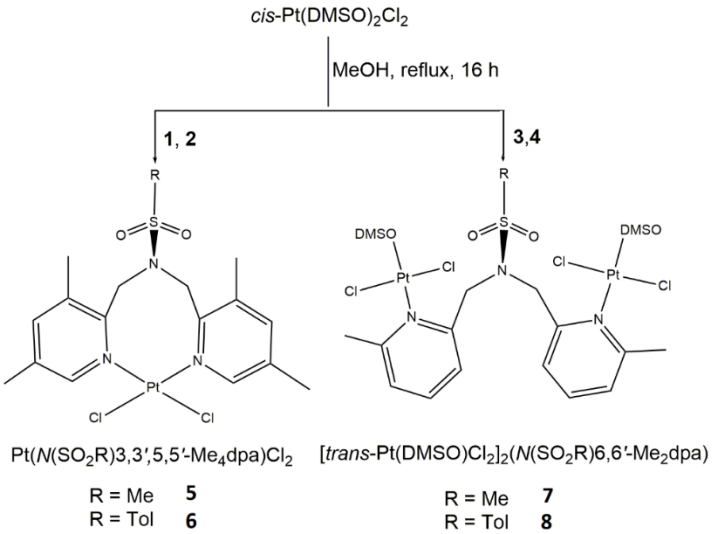

Figure 3.4. General reaction conditions for forming complexes **5**-**8**.

X-ray Structural Results. Crystal data and details of the structural refinement for Pt (**5**, **6**, **8** and **8a**) and Re (**9** and **12**) complexes are summarized in Table 3.1. The ORTEP plots **5**, **6**, **8**,

and **8a** and cations of **9** and **12** (Figures 3.6 and 3.7) show the numbering system used to describe the solid-state data. Selected bond lengths and angles are reported in Tables 3.2 and 3.3. Crystals of **6** contain two independent molecules in the asymmetric unit, only one of which (B) is shown in Figure 3.6 and used in the discussion. Structural metrics of the two halves of complex **8** are slightly different in the solid state and are reported separately in Table 3.2 as Pt1 and Pt2.

The molecular structures (Figure 3.6) and other properties of the pseudo octahedral complexes, $[Re(CO)_3(N(SO_2Me)3,3',5,5'\text{-}Me_4dpa)]PF_6$ (**9**) and $[Re(CO)_3(N(SO_2Tol)6,6'\text{-}Me_2dpa)]PF_6$ (**12**), are compared to features of the new Pt(II) complexes below. In **9** and **12**, all three nitrogen atoms of the tridentate ligands (**1** and **4**, respectively) occupy one face, and the three carbonyl ligands occupy the other face. The lengths of the Re−N(sulfonamide) bonds (Table 3.3) in both complexes are in the typical range (~2.23−2.29 Å) reported for Re−N(sp^3) bonds.[63-64] The Re−N1 and Re−N3 bond distances in **9** are in the typical range (2.14−2.18 Å) for Re−N(sp^2) bonds.[4,63,65-66] However, **12** has significantly longer Re−N1 and Re−N3 bonds [2.228(3) Å]), an observation we attribute to the steric effect of the ortho methyl groups of ligand **4**, as discussed later.

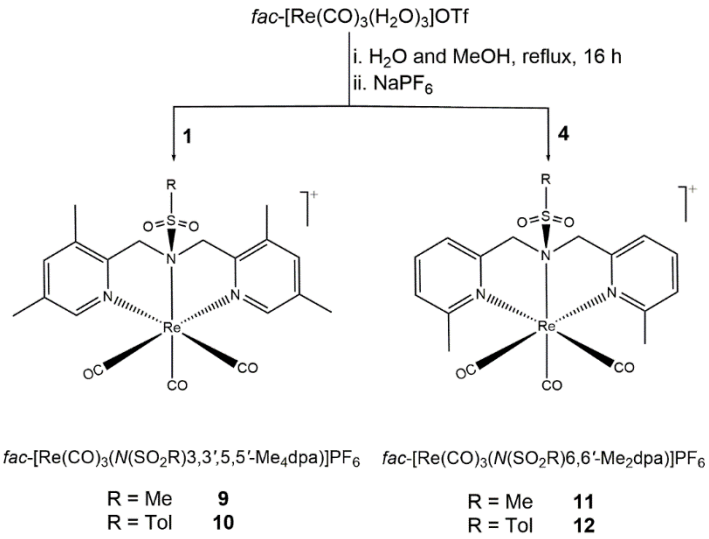

Figure 3.5. General reaction procedures for obtaining complexes **9**-**12**.

Table 3.1. Crystal Data and Structure Refinement for Pt(*N*(SO_2Me)3,3′,5,5′-Me_4dpa)Cl_2 (**5**), Pt(*N*(SO_2Tol)3,3′,5,5′-Me_4dpa)Cl_2 (**6**), [*trans*-Pt(DMSO)Cl_2]$_2$(*N*(SO_2Tol)6,6′-Me_2dpa) (**8**), [*trans*-Pt(DMSO)Cl_2](*N*(SO_2Tol)6,6′-Me_2dpa) (**8a**), [Re(CO)$_3$(*N*(SO_2Me)3,3′,5,5′-Me_4dpa)]PF_6 (**9**), and [Re(CO)$_3$(*N*(SO_2Tol)6,6′-Me_2dpa)]PF_6 (**12**)

	5	**6**	**8**	**8a**	**9**	**12**
empirical formula	$C_{17}H_{23}Cl_2N_3O_2PtS$	$C_{23}H_{27}Cl_2N_3O_2PtS$	$C_{25}H_{35}Cl_4N_3O_4Pt_2S_3$	$C_{23}H_{29}Cl_2N_3O_3PtS_2$	$C_{20}H_{23}N_3O_5ReS{\cdot}PF_6$	$C_{24}H_{23}N_3O_5ReS{\cdot}PF_6{\cdot}C_2H_3N$
fw	599.43	675.52	1069.72	725.60	748.64	837.74
crystal system	triclinic	triclinic	triclinic	monoclinic	monoclinic	triclinic
space group	*P*ī	*P*ī	*P*ī	$P2_1/n$	$P2_1/c$	*P*ī
a (Å)	9.3872(5)	9.6341(13)	11.1641(13)	13.4349(2)	18.3654(18)	7.9263(7)
b (Å)	10.7446(6)	15.4229(18)	13.1322(16)	10.4611(2)	10.1944(10)	13.2608(12)
c (Å)	11.0369(6)	17.847(2)	13.7223(16)	20.4190(4)	13.5371(13)	14.6563(12)
α (deg)	85.528(3)	66.561(5)	68.349(7)	90	90	90.652(5)
β (deg)	84.236(3)	82.411(7)	70.784(7)	108.118(1)	105.056(5)	91.950(5)
γ (deg)	79.345(3)	80.900(5)	68.683(7)	90	90	106.425(5)
V (Å^3)	1086.47(10)	2395.3(5)	1697.2(4)	2727.48(9)	2447.5(4)	1476.4(2)
T (K)	110	105	99	102	111	100
Z	2	4	2	4	4	2
ρ_{calc} (g/m^3)	1.832	1.873	2.093	1.767	2.032	1.884
abs coeff (mm^{-1})	6.82	6.19	8.77	5.52	5.20	4.32

(Table 3.1. continued)

	5	**6**	**8**	**8a**	**9**	**12**
$2\theta_{max}$ (°)	78.4	61.0	66.6	80.6	52.8	61.0
R[F2>2σ(F2)]	0.025	0.028	0.062	0.020	0.022	0.031
Rw	0.068	0.060	0.180	0.047	0.046	0.079
res. dens. (e Å^{-3})	2.85, -1.45	0.92, -1.16	7.91, -4.42	1.51, -1.30	0.97, -0.63	2.74, -2.08
data/parameters	12704/240	14452/587	12716/377	17149/312	4987/339	8815/401

[a] $R = (\sum||F_o| - |F_c||)/\sum|F_o|$. [b] $Rw = [\sum[w(F_o^2 - F_c^2)^2]/\sum[w(F_o^2)^2]]^{1/2}$, in which $w = 1/[\sigma^2(F_o^2) + (dP)^2 + (eP)]$ and $P = (F_o^2 + 2F_c^2)/3$.

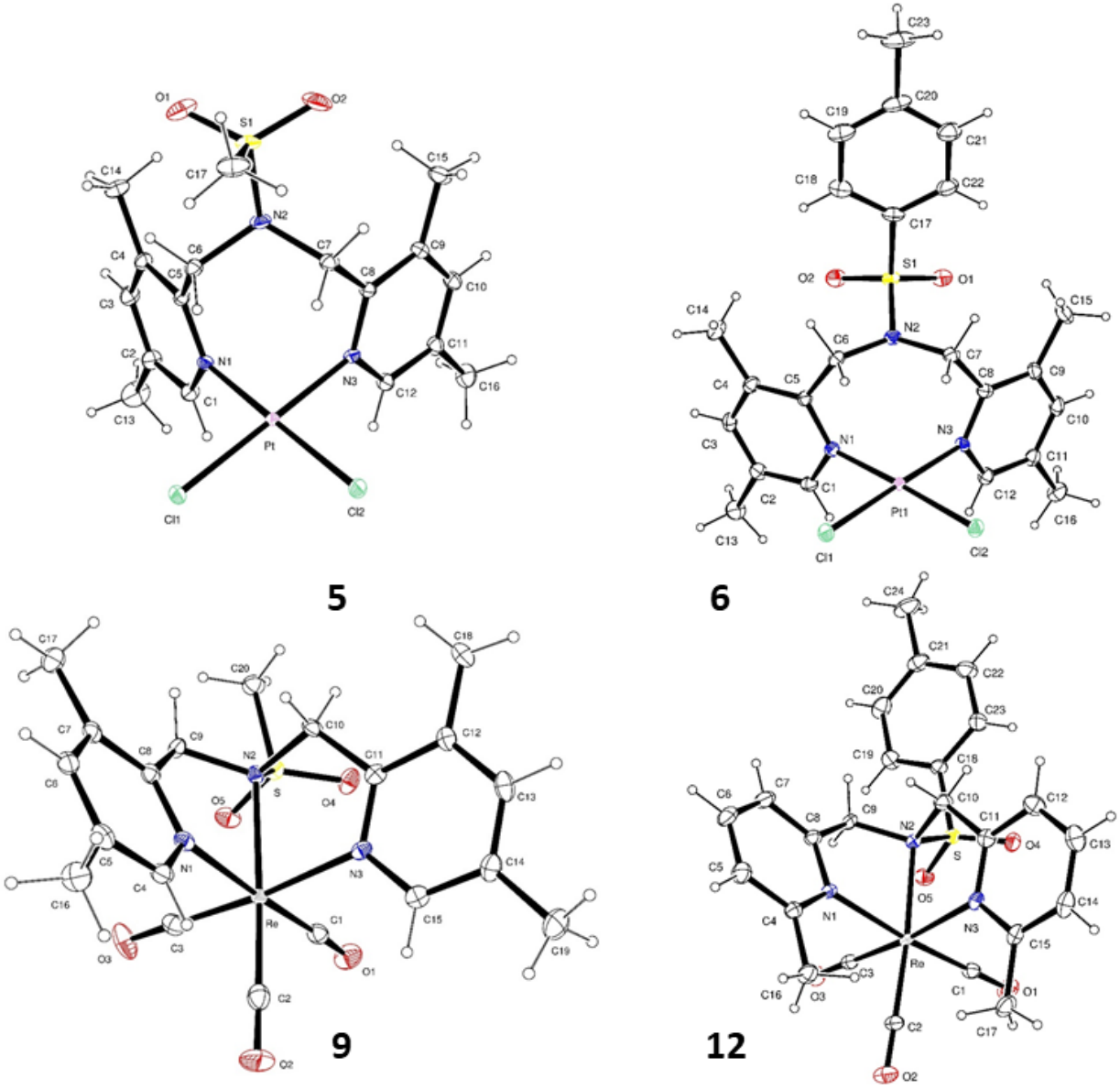

Figure 3.6. ORTEP plots of complexes Pt(*N*(SO_2Me)3,3′,5,5′-Me_4dpa)Cl_2 (**5**) and Pt(*N*(SO_2Tol)3,3′,5,5′-Me_4dpa)Cl_2 (**6**) and cations of [Re(CO)$_3$(*N*(SO_2Me)3,3′,5,5′-Me_4dpa)]PF_6 (**9**) and [Re(CO)$_3$(*N*(SO_2Tol)6,6′-Me_2dpa)]PF_6 (**12**). Thermal ellipsoids are drawn with 50% probability.

In contrast to the findings with the [Re(CO)$_3$(*N*(SO_2R)Me_ndpa)]PF_6 complexes **9**–**12**, molecular structures of the pseudo square planar Pt(II) complexes of ligands **1**, **2** and **4** reveal that the sulfonamide N does not form a Pt−N bond in any of the complexes (**5**, **6**, **8** and **8a**, Figures 3.6 and 3.7). The only Pt−N bonds found involve a pyridyl group, and all Pt−N bonds have lengths (Table 3.2) falling in the range typically reported for Pt−N(sp^2) bonds (1.99−2.08 Å).[27,67] The

bidentate coordination mode in Pt(*N*(SO_2R)3,3′,5,5′-Me_4dpa)Cl_2 complexes (**5**, R = Me and **6**, R = Tol, Figure 3.6) creates a relatively large and uncommon 8-membered chelate ring. The *N*(SO_2R)6,6′-Me_2dpa ligands, **3** and **4**, do not bind to Pt(II) as chelate ligands, and the complexes formed are discussed later.

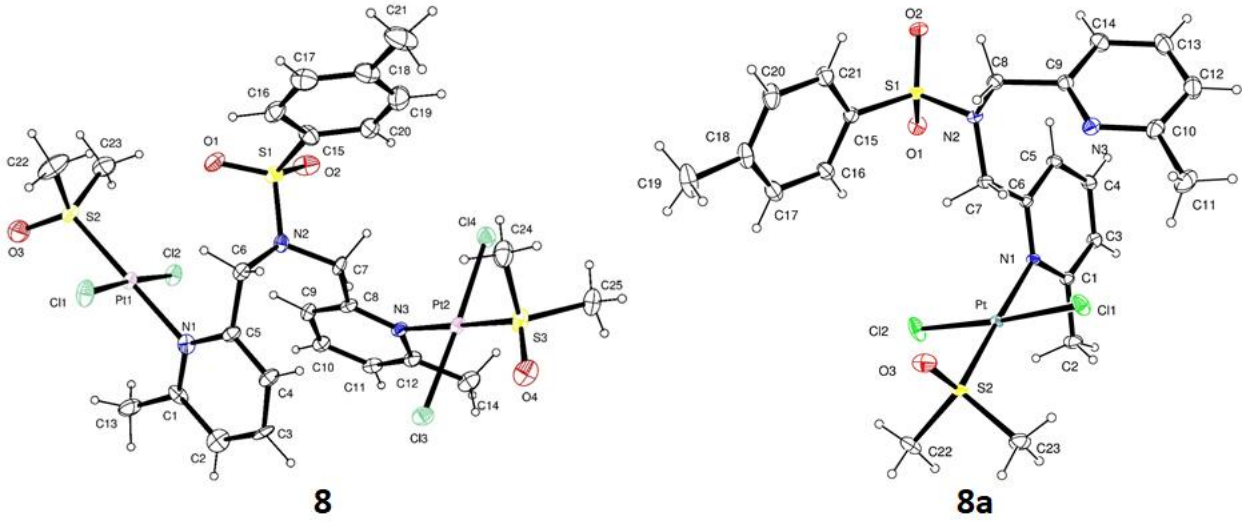

Figure 3.7. ORTEP plots of complexes [*trans*-Pt(DMSO)Cl_2]$_2$(*N*(SO_2Tol)6,6′-Me_2dpa) (**8**) and [*trans*-Pt(DMSO)Cl_2](*N*(SO_2Tol)6,6′-Me_2dpa) (**8a**). Thermal ellipsoids are drawn with 50% probability.

Structural Features Arising from the Different Chelate Binding Modes of Re(I) and Pt(II) Complexes. The angles around the sulfonamide N in the Re(I) complexes, **9** and **12**, are close to tetrahedral values (Table 3.3), indicating that the sulfonamide N hybridization changed from sp^2 to sp^3. When a tertiary sulfonamide N is bound to Re(I)[4-5] or to other metals [e.g., Mn(I), Cu(II), Ni(II), Co(II)],[1,18-19,68-69] the angles around the sulfonamide N atom are consistent with sp^3 hybridization. In contrast, the angles around the tertiary sulfonamide N in **5** and **6** (Table 3.2) are closer to 120° than to 109.5° (tetrahedral geometry), indicating that sp^2 hybridization for the sulfonamide N atom is retained.

Table 3.2. Selected Bond Distances (Å) and Angles (deg) for Pt(*N*(SO_2Me)3,3′,5,5′-Me_4dpa)Cl_2 (**5**), Pt(*N*(SO_2Tol)3,3′,5,5′-Me_4dpa)Cl_2 (**6**), [*trans*-Pt(DMSO)Cl_2]$_2$(*N*(SO_2Tol)6,6′-Me_2dpa) (**8**), and [*trans*-Pt(DMSO)Cl_2](*N*(SO_2Tol)6,6′-Me_2dpa) (**8a**)

	5	**6** (B)	**8**		**8a**
			Pt1	Pt2	
Pt–N1	2.023(2)	2.027(3)	2.062(9)	-	2.0757(9)
Pt−N2[a]	3.693(2)	3.317(3)	3.744(8)	4.51(1)	4.5556(9)
Pt–N3	2.031(2)	2.032(3)	-	2.066(8)	-
Pt–Cl1/3	2.2939(6)	2.2888(8)	2.303(2)	2.297(2)	2.2922(3)
Pt–Cl2/4	2.2990(6)	2.3009(8)	2.304(2)	2.320(3)	2.3030(3)
S1–O1	1.436(3)	1.430(3)	1.429(8)		1.4358(10)
S1–O2	1.435(3)	1.434(3)	1.431(7)		1.4327(9)
N2–S1	1.6565(19)	1.630(3)	1.642(8)		1.6390(10)
Pt–S2/3	-	-	2.217(3)	2.219(3)	2.2218(3)
N1–Pt–N3	87.98(8)	95.21(10)	-		-
S1–N2–C6	113.77(17)	118.10(2)	116.0(6)		116.85(8)
S1–N2–C7	113.83(17)	117.0(2)	118.9(6)		118.66(7)
C6–N2–C7	114.78(17)	121.30(2)	115.3(7)		116.15(9)
N1–Pt–Cl2/4	176.99(6)	176.62(8)	89.4(2)	-	89.70(3)
N1−Pt−Cl1/3	89.51(6)	86.18(8)	86.9(2)	-	87.15(3)
N3–Pt–Cl1/3	175.88(6)	178.51(7)	-	86.2(2)	-
N3−Pt−Cl2/4	90.22(6)	86.92(8)	-	89.4(2)	-
Cl1/3–Pt–Cl2/4	92.15(2)	90.66(3)	176.05(9)	175.57(9)	175.68(12)
dihedral angle[b]	77.18, 82.61	86.47, 87.17	75.13	82.91	85.23
Pt−N−centroid	174.82, 174.23	169.84, 166.56	173.49	179.52	174.16
N1−N3[a]	2.816(3)	2.998(4)	5.15(1)		4.632(1)

[a]Non-bonded distance between the two atoms. [b]Angle between the coordination plane (defined by the Pt, N1, N3, and two Cl atoms) and the pyridyl ring planes.

Table 3.3. Selected Bond Distances (Å) and Angles (deg) for [Re(CO)$_3$(*N*(SO$_2$Me)3,3′,5,5′-Me$_4$dpa)]PF$_6$ (**9**), and [Re(CO)$_3$(*N*(SO$_2$Tol)6,6′-Me$_2$dpa)]PF$_6$ (**12**)

	9	**12**
Re–N1	2.180(3)	2.228(3)
Re–N2	2.253(3)	2.263(3)
Re–N3	2.176(3)	2.228(3)
Re–C1	1.926(4)	1.933(3)
Re–C2	1.899(4)	1.917(3)
Re–C3	1.919(3)	1.919(3)
S1–O4	1.431(2)	1.428(3)
S1–O5	1.425(2)	1.428(3)
N2–S1	1.749(3)	1.752(3)
N1–Re–N2	74.21(10)	74.38(10)
N1–Re–N3	89.37(9)	90.49(10)
N2–Re–N3	77.26(9)	77.19(10)
S1–N2–C9	111.34(19)	111.2(2)
S1–N2–C10	110.4(2)	110.9(2)
C9–N2–C10	109.9(2)	109.0(2)
Re–N2–S1	109.34(13)	111.31(13)
Re–N2–C9	105.51(18)	104.27(18)
Re–N2–C10	110.26(18)	109.93(19)
N1–Re–C2	96.13(13)	100.28(12)
N1–Re–C3	90.02(12)	87.33(12)
N3–Re–C2	98.31(12)	103.07(13)
N3–Re–C1	91.59(12)	90.49(10)
dihedral angle[a]	74.23, 77.72	72.18, 79.53
Re−N−centroid	173.88, 173.92	171.33, 171.64
N1−N3[b]	3.063(4)	3.164(4)

[a]Angle between the coordination plane (defined by the Re, N1, N3, O1 and O3 atoms) and the pyridyl ring planes. [b]Non-bonded distance between the two atoms.

The N−S bond distances are generally longer (1.73−1.78 Å)[1,4,18-19,68-69] in metal complexes with an N-coordinated tertiary sulfonamide than in complexes with an uncoordinated sulfonamide N (1.62−1.64 Å).[1,4,68,70] Accordingly, the N−S bond distances in the Pt(II) complexes reported here are shorter than those for Re(I) complexes (Tables 3.2 and 3.3). Shorter N−S bond distances in an uncoordinated sulfonamide group indicate a considerable amount of double-bond character of the N−S bond owing to the delocalization of the lone pair of the N atom.[1,4,71]

Coordination geometry could be another factor leading to the different chelate ligand binding modes in the new Pt(II) and Re(I) complexes. The *N*(SO_2R)dpa-type ligands (including **1**-**4**) act as tridentate chelators in the pseudo octahedral compounds, **9**-**12**, as well as in the known complexes, (*fac*-[Re(CO)$_3$(*N*(SO_2R)dpa)]$^+$ and *fac*-[Mn(CO)$_3$(*N*(SO_2R)dpa)]$^+$).[4,18-19] In these complexes, the metal atom and the three donor N atoms (sulfonamide N and the two N atoms of the adjacent pyridyl rings) do not define a common plane: the three N-donor atoms are facially coordinated. Similarly, in almost all of the metal complexes in which the metal is bound to a tertiary sulfonamide nitrogen, the three N-donor atoms occupy the face of an octahedron or have a similar arrangement in complexes with other geometries (such as distorted trigonal bipyramidal or square pyramidal).[4,18,72] In square-planar Pt(II) complexes, the central donor atom of a tridentate ligand forming two 5-membered chelate rings must be able to accommodate the meridional coordination mode. A clear case in which a tertiary sulfonamide group anchors two chelate rings having a meridional disposition has been reported for a square planar Cu(II) complex of a derivative of cyclam (a cyclic tetradentate macrocyclic N-donor ligand with alternating 5- and 6-membered chelate rings).[72] One of the four donor nitrogens in the derivative bears a tosyl group. The angles and other parameters involving the sulfonamide N are normal for a coordinated sulfonamide. Even in this case with 5- and 6-membered chelate rings anchored by the sulfonamide

N, the complex is distorted relative to the complex of the parent cyclam lacking the tosyl group. In the complex having the tosyl group, the Cu(II) atom deviates by ~0.2 Å from the planes defined either by all four ligating N atoms or by any three ligating N atoms. However, in the cyclam complex, the Cu(II) atom lies in all such planes (deviation ~0.002 Å). We believe that our analysis of this reported data makes a strong case that there is a steric requirement that the N of a tertiary sulfonamide group with two adjacent 5-membered chelate rings must anchor a facially coordinated rather than a meridionally coordinated tridentate ligand. Hence, ligands **1** and **2** coordinate bidentately in Pt(II) complexes **5** and **6**, respectively.

Comparison of Structural Features of the New Pt(*N*(SO_2R)3,3′,5,5′-Me_4dpa)Cl_2 Complexes with Other Bifunctional Pt(II) Complexes. The 8-membered chelate ring in the Pt(*N*(SO_2R)Me_ndpa)Cl_2 complexes is a rare and hence interesting feature. Indeed, only limited types of Pt(II) complexes containing 8-membered chelate rings have molecular structures reported in the Cambridge Crystallographic Data Centre (CCDC). Most examples have very closely related bidentate ligand derivatives with Pt(II) bound to the pyridyl N of a fused bicyclic 7-azaindo-1-yl group.[45-46,49] Only one Pt(II) complex contains a linear ligand terminated with two simple aromatic rings (pyridyl). Other complexes commonly have macrocyclic N-donor (mostly sp^3) ligands bound in a bidentate mode.[47-48] We found that there are only three Pt(II) complexes of 8-membered chelate rings containing two aromatic ring nitrogens (pyridyl/imidazolyl) and two halides as the other ligating atoms listed in the CCDC data base;[48-50] in contrast, there are seven, seventeen and one hundred eight for 7-, 6-, and 5-membered chelate rings, respectively.[28-44] Data for fifty-three complexes (all of the complexes containing 8-, 7- and 6-membered chelate rings, plus twenty-six randomly chosen complexes of 5-membered chelate rings) were utilized in the following structural comparisons with the structural data for **5** and **6**.

In bifunctional Pt(II) complexes with two cis aromatic planar N-donor rings (one bidentate or two monodentate), the tilting of each ring can be gauged by the dihedral angle between the plane of the aromatic ring (defined by the C and N atoms in the ring) and the coordination plane (defined by Pt and the four ligating atoms). If the dihedral angle is close to 90°, the aromatic ring is described as not being tilted. As the angle decreases, the ring is said to become more tilted. The two pyridyl rings in **5** and **6** are only slightly tilted, with the dihedral angles ranging from 77° to 87° (Table 3.2); thus, the 8-membered ring allows the pyridyl rings to be oriented roughly perpendicular to the coordination plane. In contrast, other known bifunctional Pt(II) complexes with a bidentate ligand terminated by pyridyl or imidazolyl rings [and the remaining coordination site(s) occupied by halide(s)] and forming 5-, 6-, or 7-membered chelate rings[28-44] have relatively smaller average dihedral angles (Figure 3.8). However, the three known Pt(II) complexes with 8-membered chelate rings[48-50] used in the plot have high dihedral angles (73−89°), values close to

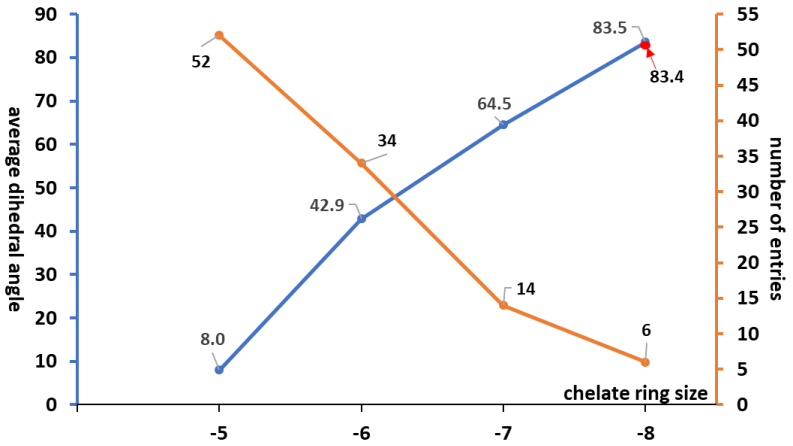

Figure 3.8. Relationship between the average dihedral angle (blue line, left axis, degrees) and the chelate ring size plotted for the reported molecular structures of bifunctional platinum(II) complexes with linear bidentate ligands terminated by pyridyl or imidazolyl donor rings (the remaining two coordination sites are occupied by halide ligands). The orange line shows the number of donor rings utilized for each chelate ring size. The red dot shows the average (83.4°) of the dihedral angles for 5 and 6. Note: All published data in this figure and in Figure 3.9 are from the Cambridge Crystallographic Data Centre, ConQuest 1.19. Of the 108 structures available for complexes with a 5-membered chelate ring, data from 26 randomly selected structures were used to prepare the plot.

the dihedral angles observed in the complexes reported here (Figure 3.8). Furthermore, the dihedral angles of the known bifunctional Pt(II) complexes increase almost linearly with increasing chelate ring size (Figure 3.8). Therefore, the low degree of tilting in **5** and **6** reflects the structural freedom allowed by the relatively large 8-membered chelate ring.

The N1−Pt−N3 bite angle of **5** (87.98°) is at the high end of the range (78° to 91°) in reports for Pt complexes with mono- or bidentately coordinated ligands terminated by pyridyl or imidazolyl rings.[28-55] Known Pt complexes containing 8-membered chelate rings have higher bite angles (average 89.5°) than the average bite angle values of the Pt complexes containing smaller chelate rings (Figure 3.9).[28-50] In fact, the bite angles of the complexes with 8-membered chelate rings are quite close to the corresponding angles observed in monodentate complexes (average 89.4°).[51-55] We attribute this finding to the greater spatial freedom provided by the large chelate ring; this freedom allows the rings to be located in the same relative position as monodentate ligands. Complex **6** has a high bite angle (95.21°) but this may be a solid-state effect because the solution behavior of **6** is close to that of **5**, see below.

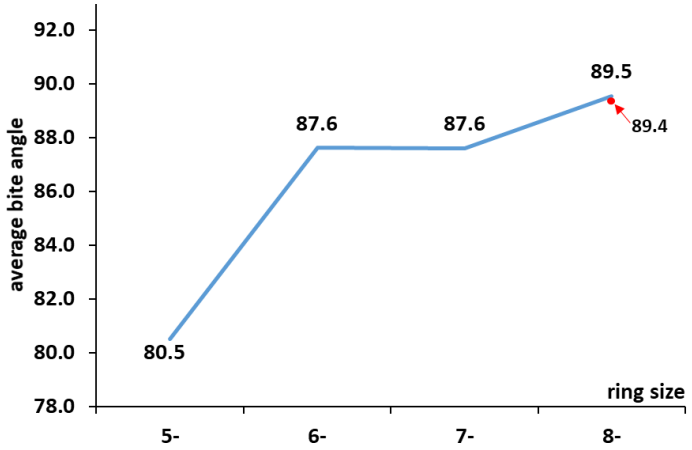

Figure 3.9. Relationship of the average N−Pt−N bite angle (degrees, from reported molecular structures) to the chelate ring size of bifunctional Pt(II) complexes of bidentate ligands terminated by pyridyl or imidazolyl donor rings (with the remaining coordination sites occupied by halide ligands). Note: of the 108 structures available for complexes with a 5-membered chelate ring, data from 26 randomly selected structures were used to prepare the plot. The average (89.4°) of the bite angles for 8 cis bifunctional Pt(II) complexes of monodentately bound pyridyl or imidazolyl rings is shown by the red dot in the figure for comparison.

In an ideal situation, the lone pair of the N atom in the ring of an aromatic N donor ligand is positioned directly toward the Pt(II) center to allow excellent overlap of bonding orbitals, thereby creating a strong bond. The angle between the N-donor aromatic ring plane and the Pt atom is a good structural parameter for assessing how close the Pt is to being in this plane. This angle can be defined as Pt−N−centroid angle (N = N1 or N3, centroid = aromatic ring center). When this angle is ~180°, the Pt atom lies in the plane of the aromatic ring. The Pt−N−centroid angle ranges from 164−180° for known Pt(II) complexes of imidazolyl or pyridyl ligands bound monodentately, bidentately, or tridentately;[27-57,73-80] for **5** this angle is >174° (Table 3.2). This finding is another indication that the large chelate rings permit the pyridine rings to adopt a location for binding with the same freedom as that of monodentate ligands (Supporting Information).

NMR Spectroscopy. All of the complexes (in DMSO-d_6) and ligands (in $CDCl_3$ and DMSO-d_6) reported here were characterized by ^{1}H NMR spectroscopy. In freshly prepared DMSO-d_6 solutions, all of the new complexes gave one set of signals, consistent with the presence of one time-averaged symmetrical complex and agreeing with the solid-state molecular structure, when it was available. The atom-numbering scheme in Figure 3.2 was used for NMR data. Signals were assigned by analyzing their chemical shifts, splitting pattern, integration, and data from ^{1}H-^{1}H ROESY NMR experiments (the ROESY spectra of selected complexes are presented in Supporting Information). ^{1}H NMR data and assignments appear in the Experimental Section; see also Table 3.4 for selected data.

Effects of Coordination Binding Mode on the Methylene ^{1}H NMR Signals of 1 to 4. Inversion at the sulfonamide N of ligands **1** to **4** leads to time averaging and makes the methylene protons magnetically equivalent, and the methylene ^{1}H NMR signal is a singlet. When the ligand is coordinated bidentately (as in the Pt(II) complexes **5** and **6**) or tridentately (as in the Re(I)

complexes **9**−**12**), the methylene protons are no longer made equivalent by a time-averaging process. The protons projecting toward and away from the Cl or CO ligands are designated as *endo*-CH and *exo*-CH protons, respectively (Figure 3.10). The *endo*-CH and *exo*-CH protons in the complexes produce either an AB pattern or two doublets in ^{1}H NMR spectra (Figure 3.11 and Supporting Information). Similar methylene group NMR features have been reported for Pd(II),[70] Pt(II),[26-27,56] and Re(I)[4-5] complexes. Whereas an AB pattern or two doublets for the methylene signals is a good indication that the bound ligand is symmetrical, the observation of an AB pattern or two doublets cannot be used to distinguish between a bidentate or tridentate coordination mode. The assignment of the AB features/doublets as *endo*-CH or *exo*-CH for **5** and **6** (explained in Supporting Information) can be found in Figure 3.11 and in Table 3.4. The ^{1}H NMR assignments of the methylene signals of $[Re(CO)_3(N(SO_2R)Me_ndpa)]PF_6$ (**9**−**12**, Table 3.4) were based on ROESY spectra, and the approach to the assignments followed the rationale used for **5**, **6**, and for the previously reported $[Re(CO)_3(N(SO_2R)dpa)]PF_6$ complexes.[4]

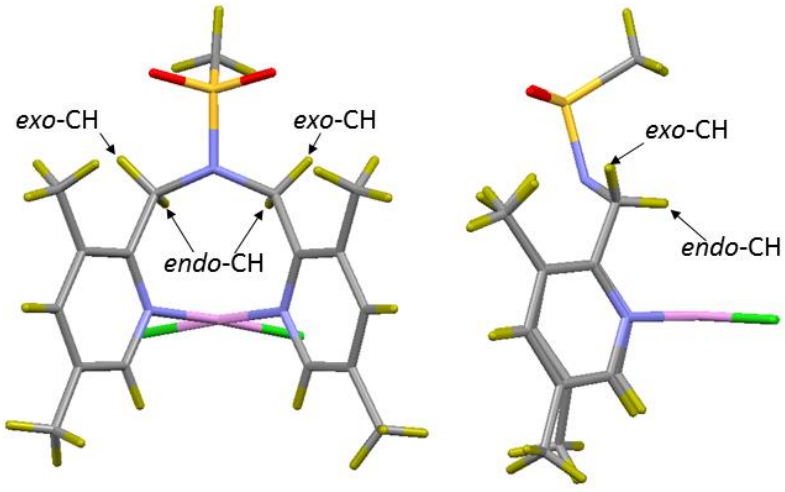

Figure 3.10. Designation of the methylene *endo*-CH and *exo*-CH protons, illustrated for the structure of Pt(*N*(SO$_2$Me)3,3′,5,5′-Me$_4$dpa)Cl$_2$ (**5**).

Table 3.4. Selected ^{1}H NMR Chemical Shifts for the *N*(SO_2R)Me_ndpa Free Ligands (**1**-**4**) and for Their Pt(II) (**5**-**8a**) and Re(I) (**9**-**12**) Complexes (ppm, DMSO-d_6, 25 °C)

complex/ ligand	H6/6′	H5/5′	H4/4′	H3/3′	CH_2	6/6′-Me	5/5′-Me	3/3′-Me	SO_2Me
1	8.17	-	7.33	-	4.45	-	2.12	2.23	3.13
5	8.98	-	7.56	-	5.99[a], 5.37[b]	-	2.23	2.37	3.35
9	8.60	-	7.75	-	5.29[a], 5.07[b]	-	2.29	2.34	3.96
2	7.94	-	7.21	-	4.41	-	2.13	2.16	-
6	8.90	-	7.56	-	5.55[b], 5.47[a]	-	2.21	2.45	-
10	8.63	-	7.72	-	5.48[a], 4.55[b]	-	2.20	2.28	-
3	-	7.12	7.63	7.12	4.42	2.41	-	-	3.14
7	-	7.46	7.85	7.68	5.55	3.12	-	-	3.33
7a	-	7.49[c], 7.16[d]	7.97[c], 7.60[d]	7.57[c], 7.18[d]	5.44[c], 4.52[d]	3.23[c], 2.44[d]	-	-	3.22
11	-	7.47	8.06	7.65	5.36[a], 5.03[b]	2.88	-	-	3.90
4	-	7.04	7.53	7.04	4.43	2.28	-	-	-
8	-	7.43	7.76	7.57	5.46	3.11	-	-	-
8a	-	7.42[c], 7.04[d]	7.88[c], 7.54[d]	7.49[c], 7.14[d]	5.40[c], 4.50[d]	3.09[c], 2.27[d]	-	-	-
12	-	7.52	8.02	7.63	5.23[a], 4.52[b]	2.90	-	-	-

[a]*endo*-CH. [b]*exo*-CH. [c]Bound. [d]Dangling.

From the NMR data for **5** and **9**−**12** and for the previously reported [Re(CO)$_3$(*N*(SO$_2$R)dpa)]PF$_6$,[4] [Pt(*N*(H)dpa)]Cl,[26] and [Pt(*N*(H)6,6′-Me$_2$dpa)]Cl[56-57] complexes, the *endo*-CH signal is normally clearly downfield of the *exo*-CH signal for both Pt(II) and Re(I) complexes. The only exception is the *endo*-CH signal (5.47 ppm) of **6**, which is slightly upfield of the *exo*-CH signal (5.55 ppm) at 25 °C. These signals appear in an overlapped AB pattern, and the assignments were aided by a study of temperature dependence of the chemical shifts (Supporting Information).

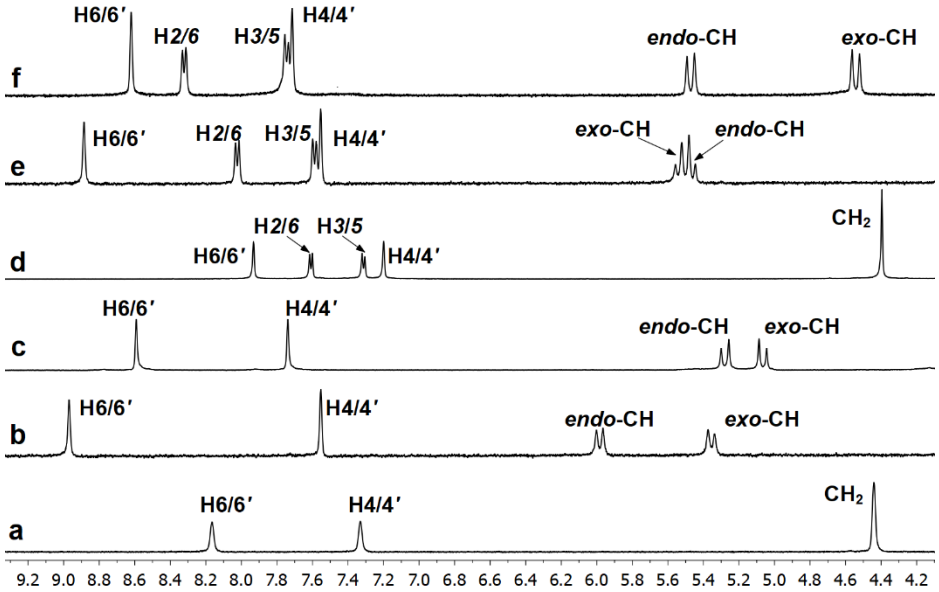

Figure 3.11. Selected region of ^{1}H NMR spectra in DMSO-d_6 at 25 °C (shifts in ppm) of (a) *N*(SO$_2$Me)3,3′,5,5′-Me$_4$dpa (**1**); (b) Pt(*N*(SO$_2$Me)3,3′,5,5′-Me$_4$dpa)Cl$_2$ (**5**); (c) [Re(CO)$_3$(*N*(SO$_2$Me)3,3′,5,5′-Me$_4$dpa)]PF$_6$ (**9**); (d) *N*(SO$_2$Tol)3,3′,5,5′-Me$_4$dpa (**2**); (e) Pt(*N*(SO$_2$Tol)3,3′,5,5′-Me$_4$dpa)Cl$_2$ (**6**); and (f) Re(CO)$_3$(*N*(SO$_2$Tol)3,3′,5,5′-Me$_4$dpa)]PF$_6$ (**10**).

The structures of [*trans*-Pt(DMSO)Cl$_2$]$_2$(*N*(SO$_2$Tol)6,6′-Me$_2$dpa) (**8**) and [*trans*-Pt(DMSO)Cl$_2$](*N*(SO$_2$Tol)6,6′-Me$_2$dpa) (**8a**) (Figure 3.7) and the NMR data for complexes **7**, **7a**, **8**, and **8a** establish that, unlike **1** and **2**, the *N*(SO$_2$R)6,6′-Me$_2$dpa ligands (**3**, R = Me and **4**, R = Tol) coordinate monodentately (not bidentately) to the Pt(II) center to form binuclear or mononuclear complexes. ^{1}H NMR spectra (Figure 3.12) obtained for fresh solutions of the X-ray

quality crystals of **8** or of **8a** in DMSO-d_6 are consistent with symmetric binuclear and unsymmetric mononuclear complexes, respectively. Also, the signal corresponding to the methylene protons is a singlet (Figure 3.12), indicating that ligand **4** coordinates monodentately to Pt(II) (Figure 3.7). The methylene signal remains a singlet, as occurs in the free ligands, because inversion at the sulfonamide N (N2) is not inhibited when the ligand is bound monodentately. Similar NMR features were observed for **7** (Table 3.4, Figure 3.12), thus confirming that ligand **3** (*N*(SO_2Me)6,6′-Me_2dpa) forms a binuclear complex similar to **8**.

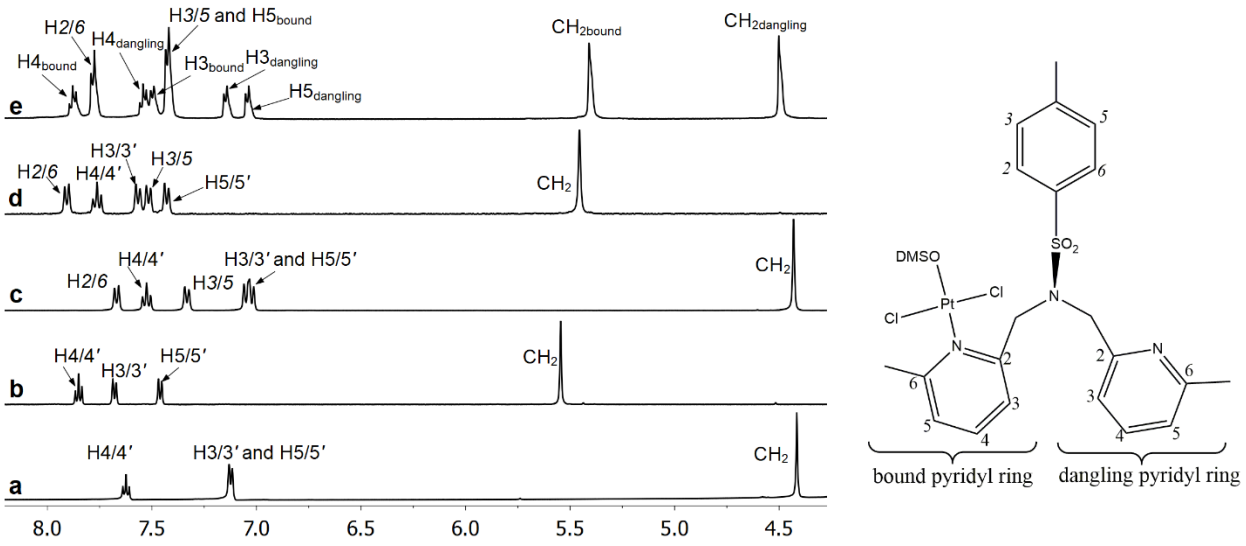

Figure 3.12. Selected region of ^{1}H NMR spectra in DMSO-d_6 at 25 °C (shifts in ppm) of (a) *N*(SO_2Me)6,6′-Me_2dpa (**3**), (b) [*trans*-Pt(DMSO)Cl_2]$_2$(*N*(SO_2Me)6,6′-Me_2dpa) (**7**), (c) *N*(SO_2Tol)6,6′-Me_2dpa (**4**), (d) [*trans*-Pt(DMSO)Cl_2]$_2$(*N*(SO_2Tol)6,6′-Me_2dpa) (**8**) and (e) [*trans*-Pt(DMSO)Cl_2](*N*(SO_2Tol)6,6′-Me_2dpa) (**8a**). Line drawing of **8a** shown on the right.

The methylene singlets at 4.42 ppm in **3** and 4.43 ppm in **4** have shifted downfield upon Pt(II) metal binding to 5.55 ppm in **7** and to 5.46 ppm in **8** (Figure 3.12). Furthermore, in the mononuclear Pt(II) compound (**8a**) with ligand **4** bound monodentately and unsymmetrically (Figure 3.7), the methylene protons produce two singlets (Figure 3.12). From the characteristic shift, the more downfield singlet (5.40 ppm) is assigned to CH_{2bound} (the methylene group attached to the bound pyridyl ring; see Figure 3.12 for atom designations). The other **8a** singlet at 4.50 ppm

has a shift close to that of the free ligand methylene signal (4.42 ppm) and thus is assigned to $CH_{2dangling}$. Even though the compound **7a** was not isolated, it is undoubtedly the analog of **8a**, from the methylene singlets at 5.44 (CH_{2bound}) and 4.52 ppm ($CH_{2dangling}$).

Other ^{1}H NMR Signal Assignments for Pt and Re Complexes. The ^{1}H NMR assignments of [Re(CO)$_3$(*N*(SO$_2$R)Me$_n$dpa)]PF$_6$ (**9**−**12**) were based on ROESY spectra (Supporting Information) and arguments similar to those used for the previously reported [Re(CO)$_3$(*N*(SO$_2$R)dpa)]PF$_6$ complexes;[4] this assignment approach is also illustrated next for the Pt(II) chelate complexes, **5** and **6**.

The observation of one set of ^{1}H NMR signals within 10 min of dissolution of Pt(*N*(SO$_2$Me)3,3′,5,5′-Me$_4$dpa)Cl$_2$ (**5**, 10 mM) in DMSO-d_6 (Figure 3.11) indicates that **5** dissolves as one species. The signals are consistent with a symmetrical complex, such as the dichloro complex. For example, there is one aromatic singlet at 8.98 ppm with a shift and intensity of two protons consistent with assignment of the peak to H6/6′ of **5**. This assignment is confirmed by an NOE cross-peak to one of the two pyridyl ring methyl singlets (at 2.23 ppm, integrating to 6 protons) in a ROESY spectrum of **5** in DMSO-d_6 (Supporting Information). This pyridyl ring methyl singlet can be assigned to 5/5′-Me because it is the only methyl group near the H6/6′ protons, and thus the other pyridyl ring methyl singlet (2.37 ppm) can be assigned to the 3/3′-Me. The more upfield aromatic singlet at 7.56 ppm has NOE cross-peaks to both 3/3′-Me and 5/5′-Me singlets and thus can be assigned to the H4/4′ protons. The ^{1}H NMR signals for Pt(*N*(SO$_2$Tol)3,3′,5,5′-Me$_4$dpa)Cl$_2$ (**6**) likewise occur as one set, indicating that fresh solutions contain the symmetrical dichloro complex. The ^{1}H NMR signals for **6** were assigned as for **5**, by using a ROESY spectrum of **6** in DMSO-d_6 (Supporting Information). (The *p*-tolyl group numbering is *italicized* to prevent confusion with the pyridyl ring numbering, Figure 3.2.) The

H2/6 signal was identified as the doublet at 8.03 ppm from an NOE cross-peak to the methylene AB feature.

Assignments of the methylene signals of **7**, **8**, **7a,** and **8a** in DMSO-d_6 were discussed above. Other signals were assigned by using ROESY spectra (Supporting Information). All spectral features of fresh solutions are consistent with a single complex that has the molecular structure expected from the solid-state data (Figure 3.7). The only triplet in the ^{1}H NMR spectrum of **7** is assigned to the H4/4′ protons (Figure 3.12). Singlets at 3.12, 3.33 and 5.55 ppm are respectively assigned to the 6/6′-Me, the sulfonamide methyl (SO_2Me), and the methylene groups, based on the integration (6, 3, and 4 protons, respectively). In the ROESY spectrum of **7** (Supporting Information), the more upfield (7.46 ppm) of the two aromatic doublets has NOE cross-peaks to the 6/6′-Me signal and the H4/4′ signal and can thus be assigned to H5/5′. The other aromatic doublet (7.68 ppm) is therefore assigned to H3/3′, an assignment further supported by the observed NOE cross-peaks from this signal to the H4/4′, the SO_2Me, and the methylene signals. The ^{1}H NMR ROESY spectrum of **8** (Supporting Information) was used for assignments in a similar way as for **7**.

The atom-numbering scheme for **8a** shown in Figure 3.12 is used to discuss the NMR data. In the ROESY spectrum of **8a** (Supporting Information), a doublet at 7.14 ppm shows NOE cross-peaks to the two methylene singlets (the NOE cross-peak to the $CH_{2dangling}$ is stronger than the NOE peak to the CH_{2bound}) and is assigned to $H3_{dangling}$. This doublet has an NOE cross-peak to the triplet at 7.54 ppm, which can be assigned to $H4_{dangling}$, because only the H4 protons are close to the H3 protons and can produce triplet peaks. Therefore, the other triplet in the spectrum (at 7.88 ppm) can be assigned to $H4_{bound}$. The $H4_{dangling}$ peak has an NOE cross-peak to the doublet at 7.04 ppm, which can be assigned to $H5_{dangling}$, the only other proton near the $H4_{dangling}$ proton. This doublet

($H5_{dangling}$) has an NOE cross-peak to a singlet at 2.27 ppm (integrating to 3 protons), which can be assigned to 6-$Me_{dangling}$. There are two more singlets with similar integrations in the aliphatic region at 3.09 and 2.41 ppm. The singlet at 3.09 ppm can be assigned to 6-Me_{bound}, because it has a similar shift to the 6/6′-Me singlet of **8**. Therefore, the other singlet at 2.41 ppm can be assigned to the tolyl Me group. The $H4_{bound}$ triplet has two NOE cross-peaks to two doublets at 7.49 and 7.42 ppm. The doublet at 7.49 ppm (integrating to one proton) has an NOE cross-peak to the CH_{2bound} singlet, thus can be assigned to $H3_{bound}$. The doublet at 7.42 ppm integrates for three protons, indicating that it consists of overlapping aromatic signals. This doublet has NOE cross-peaks to the 6-Me_{bound} and to the tolyl-Me signals, indicating that the doublet is a combination of the $H5_{bound}$ and H*3/5* signals. Furthermore, this doublet has another NOE cross-peak to a doublet at 7.78 ppm (with an integration of 2 protons), which can be assigned to H*2/6* in the tolyl group.

Because all of the ^{1}H NMR peaks of **7a** have chemical shifts similar to those of **8a** and are consistent with the unsymmetrically bound ligand **3** (Table 3.4), the **7a** signals were assigned as for **8a**. As an example, two triplets corresponding to the H4/4′ protons in **7a** are observed at 7.97 (for $H4_{bound}$) and at 7.60 ppm (for $H4_{dangling}$). Note that because of rapid inversion at the sulfonamide N in the dangling group, **7a** and **8a** have time-averaged symmetry.

Solution Studies of ^{1}H NMR Spectral Features and Robustness of Pt(II) and Re(I) Complexes of *N*(SO_2R)3,3′,5,5′-Me_4dpa Ligands 1 and 2. All of the corresponding ^{1}H NMR signals of ligands **1** and **2** are shifted downfield in Pt(*N*(SO_2R)3,3′,5,5′-Me_4dpa)Cl_2 (**5** and **6**) and [$Re(CO)_3$(*N*(SO_2R)3,3′,5,5′-Me_4dpa)]PF_6 (**9** and **10**) (Table 3.4). The ^{1}H NMR spectra of the complexes **5** and **9** of ligand **1** (having R = Me) are less complicated than the spectra of the complexes **6** and **10** of ligand **2** (having R = Tol). Hence, the data for **5** and **9** are utilized here for comparison. For example, the H6/6′ singlet of the free ligand **1** shifted downfield by 0.79 ppm

upon formation of Pt(*N*(SO_2Me)3,3′,5,5′-Me_4dpa)Cl_2 (**5**) and by 0.41 ppm upon formation of [Re(CO)$_3$(*N*(SO_2Me)3,3′,5,5′-Me_4dpa)]PF_6 (**9**). The greater downfield shift of the H6/6′ singlet of **5** compared to the shift of **9** is a result of the greater electron-withdrawing inductive effect of Pt(II) when compared to Re(I).[4] The *J* coupling constants (15−17 Hz) of the methylene doublets are similar for the Pt(II) and Re(I) complexes. Regardless of the coordination mode, the chemical shifts of the methylene proton signals for a given carrier ligand are more downfield when bound to Pt(II) than when bound to Re(I) (Table 3.4). For example, the chemical shifts of the *endo*-CH and *exo*-CH signals are at 5.99 and 5.37 ppm in **5** at 5.29 and 5.07 ppm in **9**.

The downfield shift change of the sulfonamide methyl (SO_2Me) singlet observed for ligand **1** upon metal coordination is 0.83 ppm for [Re(CO)$_3$(*N*(SO_2Me)3,3′,5,5′-Me_4dpa)]PF_6 (**9**) and 0.22 ppm for Pt(*N*(SO_2Me)3,3′,5,5′-Me_4dpa)Cl_2 (**5**). This difference can be attributed to the inductive effect acting through the direct Re−N(sulfonamide) bond in **9**, compared to the transmission of the inductive effect of Pt(II) through several bonds in **5**. This SO_2Me signal is thus diagnostic of sulfonamide metal binding. Although complexes of ligand **2** have more complicated NMR spectra owing to the Tol group, the observations noted for ligand **1** complexes apply also to ligand **2** complexes. These results show that the pyridyl groups of ligands **1** and **2** can adopt a position very favorable for bonding to Pt(II) and that such interactions lead to good electron donation from the pyridyl groups to Pt(II) in complexes **5** and **6**.

^{1}H NMR spectra of 10 mM solutions of [Re(CO)$_3$(*N*(SO_2Me)3,3′,5,5′-Me_4dpa)]PF_6 (**9**) and [Re(CO)$_3$(*N*(SO_2Tol)3,3′,5,5′-Me_4dpa)]PF_6 (**10**) in DMSO-d_6 show no change even after more than 3 years, indicating that the Re(I) complexes of ligands **1** and **2** are very robust. The Pt(II) complexes Pt(*N*(SO_2R)3,3′,5,5′-Me_4dpa)Cl_2 (**5** and **6**) of these ligands in DMSO-d_6, however, are much less robust. We examined the solution chemistry of the R = Me complex **5** in more detail

because **5** has fewer and simpler NMR signals than **6**. One hour after "Solution 1" [Pt(*N*(SO_2Me)3,3′,5,5′-Me_4dpa)Cl_2 (**5**), 10 mM in DMSO-d_6] was prepared, its spectrum showed, in addition to the peaks for **5**, a small but detectable new set of ^{1}H NMR peaks; these new peaks gradually increased with time (Figure 3.13). The intensity of the H6/6′ singlet of **5** at 8.98 ppm gradually decreased. The presence of two new equally intense singlets arising at 9.17 and 8.76 ppm indicates that the new product contains geometrically inequivalent pyridyl groups, both still bound to Pt(II). These new aromatic H6 and H6′ signals are consistent with formation of the solvolysis product, [Pt(*N*(SO_2Me)3,3′,5,5′-Me_4dpa)(DMSO-d_6)Cl]$^+$ (**5**$_{sol}$). Unlike the H6/6′ protons, the H4/4′ protons of **5**$_{sol}$ appear as one overlapped signal (7.74 ppm) with an intensity twice that of the H6 or H6′ signals. The H4/4′ protons are located farther from the Pt(II) center than are the H6/6′ protons, accounting for the presence of an overlapped H4/4′ signal. A different solution (Solution 2) but otherwise identical to Solution 1 was allowed to sit for one day and then 10 molar equiv of [Et_4N]Cl was added. The **5**$_{sol}$ peaks converted within 4 h almost completely to signals of the original dichloro complex **5** (Supporting Information).

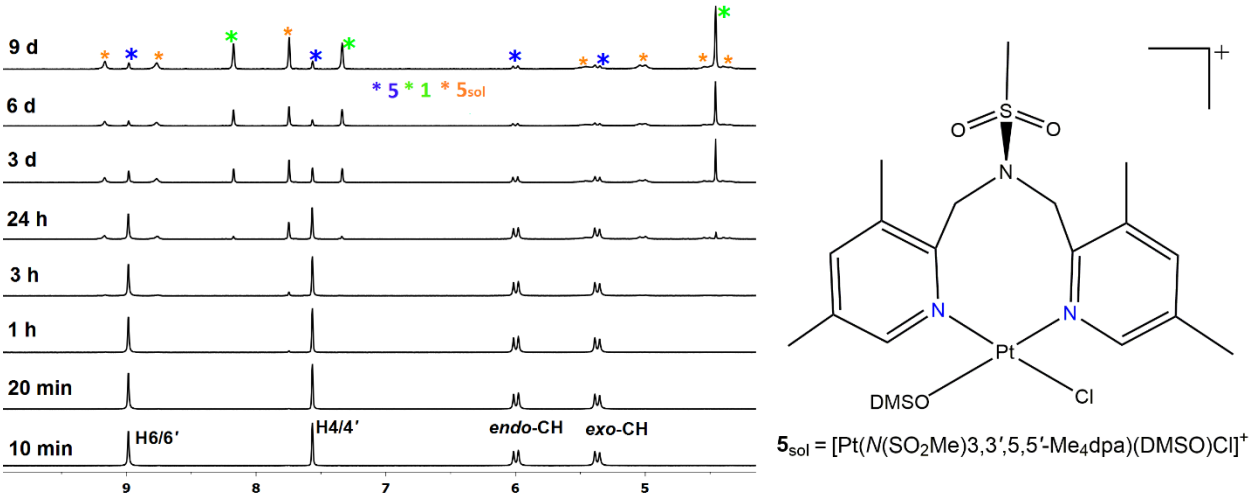

Figure 3.13. Selected region of ^{1}H NMR spectra of Solution 1 (Pt(*N*(SO_2Me)3,3′,5,5′-Me_4dpa)Cl_2 (**5**) in DMSO-d_6, 10 mM, 25 °C, shifts in ppm). Spectra at various times after dissolution of **5** reveal its solvolysis to form [Pt(*N*(SO_2Me)3,3′,5,5′-Me_4dpa)(DMSO)Cl]$^+$ (**5**$_{sol}$, shown in line drawing on the right) and free ligand **1**. The top trace at 9 d records the equilibrated solution.

This result further confirms that the new set of signals arises from [Pt(*N*(SO_2Me)3,3′,5,5′-Me_4dpa)(DMSO-d_6)Cl]$^+$ (**5**$_{sol}$). This conclusion is supported by the absence of the **5**$_{sol}$ signals when solid **5** (10 mM) is dissolved in a DMSO-d_6 solution containing 100 mM [Et_4N]Cl (Solution 3). Other reported examples of mono-solvolysis in DMSO-d_6 of Pt(II) dichloro complexes include complexes with a bidentate pyridyl ligand (Pt(bis(pyridine-2-yl)amine)Cl_2),[43] a bidentate ethylenediamine (Pt(en)Cl_2),[81] or a bidentate ligand bearing a deprotonated sulfonamide group (Pt(DNSH-dienH)Cl_2).[10]

The changes over time in the species arising in solutions of **5** are revealing. In addition to the appearance of **5**$_{sol}$ NMR signals in Solution 1 as just described, signals of the free *N*(SO_2Me)3,3′,5,5′-Me_4dpa (**1**) ligand became detectable 4 h after **5** was dissolved in DMSO-d_6 (Figure 3.13). At 24 h, the ratio of **5**:**5**$_{sol}$:**1** was 59:34:7 (Figure 3.14). At 9 d, the major species was **5**$_{sol}$ (**5**:**5**$_{sol}$:**1** = 12:46:42); this is the equilibrium composition, as no further change in the ratio was detected even after 21 d. As discussed below, this finding indicates that the large chelate ring formed by ligand **1** in **5** leads to dissociation of the chelate even though the pyridyl rings interact favorably with Pt(II).

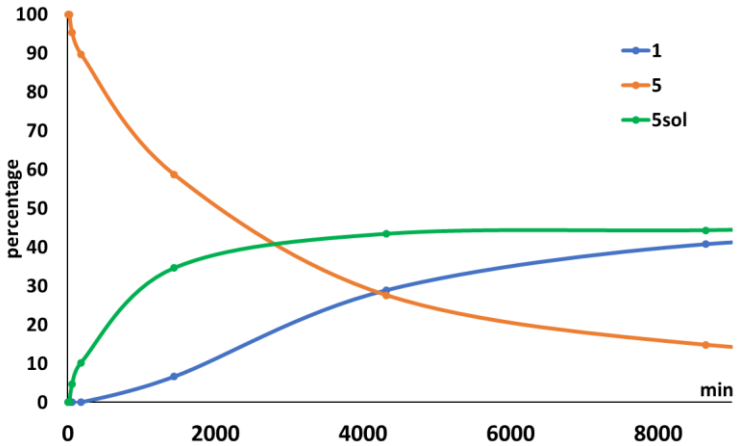

Figure 3.14. Percent distribution of Pt(*N*(SO_2Me)3,3′,5,5′-Me_4dpa)Cl_2 (**5**, orange), [Pt(*N*(SO_2Me)3,3′,5,5′-Me_4dpa)(DMSO)Cl]$^+$ (**5**$_{sol}$, green), and free *N*(SO_2Me)3,3′,5,5′-Me_4dpa (**1**, blue) in Solution 1 (10 mM solution of **5** in DMSO-d_6) at 25 °C plotted versus time. Percent distribution values were calculated by using integrations of H4/4′ signals of each species.

Solution 2, which was created from a one-day-old 10 mM solution of **5** in DMSO-d_6 with NMR signals indicating **5**:**5**$_{sol}$:**1** = 54:38:8, was also followed with time. When 10 molar equiv of [Et$_4$N]Cl was added to this solution, the abundance of **5** increased (to 66%) and that of **5**$_{sol}$ decreased (to 20%) during the first hour; thereafter the abundance of **5** began to decline (Supporting Information). By 24 h, almost no **5**$_{sol}$ remained, while 42% of **5** remained. The decrease of **5** continued until the only NMR signals present were those for free **1** (~12 days). Solution 3 was made by dissolving 3.6 mg of solid **5** (10 mM) in a 100 mM [Et$_4$N]Cl solution. At 1 h, the amount of **5**$_{sol}$ in Solution 3 was only 1%. For this solution, a maximum amount of 3% of **5**$_{sol}$ was detected in the spectrum recorded at 8 h, and by 24 h this amount had decreased again to 1%. (In contrast, the abundance of **5**$_{sol}$ reached 5% and 35% at 1 h and 24 h after the preparation of Solution 1 of **5**, having no added [Et$_4$N]Cl). In Solution 3, the **5**$_{sol}$ peaks were no longer detectable by 3 d. Furthermore, ^{1}H NMR peaks of free ligand **1** were first detected in the spectrum of Solution 3 recorded after 4 h, and these increased until 100% free **1** was present by ~12 days (Figure 3.15). Collectively this evidence indicates that the chloride ions facilitate ligand **1** dissociation from **5** or **5**$_{sol}$.

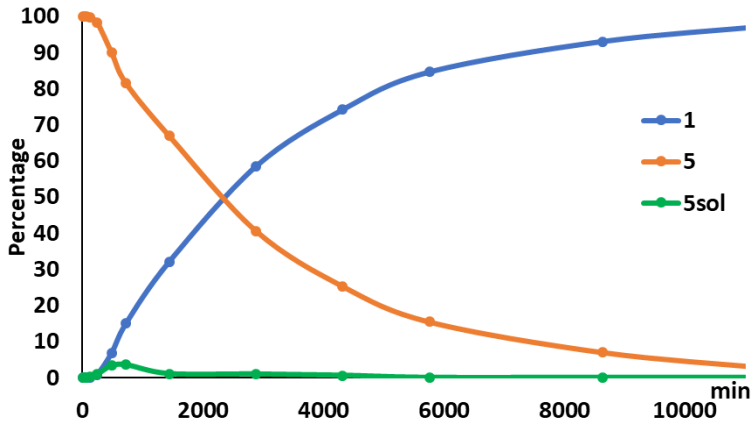

Figure 3.15. Percent distribution of Pt(*N*(SO$_2$Me)3,3′,5,5′-Me$_4$dpa)Cl$_2$ (**5**, orange), [Pt(*N*(SO$_2$Me)3,3′,5,5′-Me$_4$dpa)(DMSO)Cl]$^+$ (**5**$_{sol}$, green), and free *N*(SO$_2$Me)3,3′,5,5′-Me$_4$dpa (**1**, blue) in Solution 3 [a mixture of **5** (3.6 mg, 1 molar equiv) added to a 100 mM solution of [Et$_4$N]Cl in DMSO-d_6] at 25 °C plotted versus time. Percent distribution values were calculated by using integrations of H4/4′ signals of each species.

In another experiment, a freshly prepared 10 mM solution of ligand **1** was made by addition of 1.3 mg of **1** to 600 μL of a *cis*-Pt(DMSO)$_2$Cl$_2$ (10 mM) and [Et$_4$N]Cl (100 mM) solution in DMSO-d_6. This "Solution 4" showed no NMR signals for **5** or **5**$_{sol}$ even after 4 days, indicating that a high chloride ion concentration prevents **1** from coordinating to Pt(II). In contrast, when only ligand **1** and *cis*-Pt(DMSO)$_2$Cl$_2$ were mixed together in a 1:1 ratio (Solution 5, 10 mM) in DMSO-d_6, NMR signals for **5**$_{sol}$ were detectable in a spectrum recorded after 1 h. By 24 h after mixing, the **5**:**5**$_{sol}$:**1** distribution was = 3:38:59, indicating that ligand **1** can coordinate to Pt(II) in the absence of an excess of competing chloride ions and that at 10 mM its affinity for Pt(II) is comparable to that of the DMSO-d_6 solvent (the solvent molecule concentration is 14 M).

NMR evidence for solvolysis and ligand dissociation over time as found for **5** in DMSO-d_6 solution was also observed for Pt(*N*(SO$_2$Tol)3,3′,5,5′-Me$_4$dpa)Cl$_2$ (**6**). Spectra recorded for a DMSO-d_6 solution of **6** (10 mM) show signals for **6**$_{sol}$ and **2** for the first time in 1 h and 4 h after dissolving, respectively. The equilibrated composition of this solution observed by 9 days (**6**:**6**$_{sol}$:**2** = 17:51:32) is similar to the composition of 10 mM solution of **5**, indicating that the dangling group has minimal influence on the robustness of these complexes. In contrast to the results in DMSO-d_6, **5** and **6** show no sign of solvolysis or chelate ligand dissociation even after 7 d in DMF-d_7. Thus, **5** and **6** are rather robust in DMF-d_7, although both are much less soluble in DMF-d_7 than in DMSO-d_6.

Complexes **5** and **6**, with a relatively large 8-membered chelate ring, exhibit low robustness in solution when compared to the known robust Pt(II) complexes of related ligands that have 5-membered,[26-28,57] 6-membered[33,43] or 7-membered[55] chelate rings. However, the Pt−N−centroid angles of **5** are similar to the values of other bifunctional Pt(II) complexes of monodentate pyridyl ligands, which can adopt optimal metrics not limited by the chelate ring (Supporting Information).

These structural metrics as well as the greater downfield shifting of NMR signals noted above indicate that **5** has enthalpically favorable pyridyl-Pt bonding interactions; however, the unfavorable entropy component of an 8-membered chelate ring and possibly strain within the large chelate ring itself decrease the robustness of **5** and **6** in DMSO-d_6. The relatively high robustness of **9** and **10** versus **5** and **6** can be attributed to a third bond, the Re−N(sulfonamide) bond, present in **9** and **10**, which allows tridentate coordination to an octahedral face.

The reactivity of Pt(*N*(SO_2Me)3,3′,5,5′-Me_4dpa)Cl_2 (**5**) with simple **G** derivatives, 9-MeG or Guo, was assessed at 25 °C. Because **5** is stable in DMF-d_7, a 1:2.5 molar equiv mixture of **5** (5 mM) and Guo in DMF-d_7 (solution was cloudy because of poor solubility) was monitored by ^{1}H NMR spectroscopy. No reaction was detected even after 4 days. In DMSO-d_6, **5** (10 mM) was treated with 2.5 molar equiv of 9-MeG or Guo. For both solutions, new ^{1}H NMR peaks for $\mathbf{5}_{sol}$ and for free **1** were first detectable after ~1 h and ~4 h, respectively. These results are very similar to those observed in the absence of added 9-MeG or Guo. Several new peaks consistent with the formation of **G** adducts were observed only at later times. However, even at 24 h the integration of these new peaks indicated a very low amount of **G** adduct formation as compared to reactions forming $\mathbf{5}_{sol}$ and free ligand **1**. In addition, three reaction mixtures of **5** in DMSO-d_6 solutions (10 mM) with 2.5 molar equiv of ligands known to bind Pt(II) (1-methylimidazole, 5,5′-Me_2bpy or Me_4dt)[28,44,82] were studied. During the first few hours, all three solutions exhibited new ^{1}H NMR peaks for $\mathbf{5}_{sol}$ and for free **1**, which appeared over a time course similar to that found for solutions of **5**. These results in DMF-d_7 and DMSO-d_6 indicate that **G** derivatives and other ligands do not promote chelate ring opening in **5**. In contrast, 9-EtG (2.5 equiv) immediately promoted chelate ring opening of the tridentate ligand in [Pt(*N*(H)6,6′-Me_2dpa)Cl]Cl (10 mM in a 64:36

D_2O/DMSO-d_6 mixture, pH ≈ 4, 25 °C).[57] The carrier ligand is bidentate in the adduct, [Pt(*N*(H)6,6′-Me_2dpa)(9-EtG)$_2$]$^{2+}$, indicating that 9-EtG facilitates chelate ring opening.[57]

Solution Studies of ^{1}H NMR Spectral Features and Robustness of Pt(II) and Re(I) Complexes of *N*(SO$_2$R)6,6′-Me$_2$dpa Ligands 3 and 4. All of the corresponding ^{1}H NMR signals of ligands **3** and **4** are shifted downfield in [*trans*-Pt(DMSO)Cl$_2$]$_2$(*N*(SO_2R)6,6′-Me_2dpa) (**7** and **8**) and [Re(CO)$_3$(*N*(SO_2R)6,6′-Me_2dpa)]PF_6 (**11** and **12**) (Table 3.4). The ^{1}H NMR spectra of the complexes **7** and **11** of ligand **3** (having R = Me) are less complicated than those of **8** and **12** of ligand **4** (having R = Tol). Hence, the data for **7** and **11** are utilized here for comparison.

As mentioned, [Re(CO)$_3$(*N*(SO_2R)3,3′,5,5′-Me_4dpa)]PF_6 (**9** and **10**) are much more robust in DMSO-d_6 than the Pt(II) complexes of the same ligands **1** and **2**. However, a ^{1}H NMR spectrum of a 10 mM solution of [Re(CO)$_3$(*N*(SO_2Me)6,6′-Me_2dpa)]PF_6 (**11**) in DMSO-d_6 recorded after 8 d shows signals for free ligand **3** (9%, with no other signals except for the tridentately bound or free ligand signals). Similarly, a 12-days-old, 10 mM solution of [Re(CO)$_3$(*N*(SO_2Tol)6,6′-Me_2dpa)]PF_6 (**12**) in DMSO-d_6 also shows 16% of free ligand **4**. Furthermore, the ~3-years-old solutions of **11** and **12** show signals for the corresponding free ligand only.

Ligand dissociation from an octahedral Re(I) complex ordinarily occurs via a dissociative mechanism. In chelate complexes such as the [Re(CO)$_3$(*N*(SO_2R)Me_ndpa)]PF_6 complexes, a terminal Re−N(sp^2) bond is expected to be the first Re−N bond to start chelate ligand dissociation. This first step would be followed by solvent addition. Unlike the Re(I) complexes **11** and **12**, **9** and **10** do not show ligand dissociation, indicating that the carrier-ligand Re–N bonds are stronger in **9** and **10** than in **11** and **12**. This conclusion is further supported by the normal Re−N bond distances observed for **9** (~2.18 Å; the typical Re−N(sp^2) bond distance range is 2.14−2.18 Å).[4,63,65-66] In contrast, complex **12**, which has long terminal Re−N bonds (~2.23 Å, Table 3.3),

undergoes ligand dissociation, indicating that the Re−N bonds are weak and likely to break. A molecular structure of $[Re(CO)_3(N(H)6,6'\text{-}Me_2dpa)]PF_6$ obtained by our group (unpublished) also shows relatively long terminal Re−N(sp^2) bonds (2.23 Å). Furthermore, the molecular structures of $[Re(CO)_3(N(H)6,6'\text{-}Me_2dpa)]PF_6$ and **12** overlap well when superimposed through Re and the three ligating N atoms, indicating that the structural features of the two complexes are similar. Also, the Re−N−centroid angles of the molecular structures of **9** (~174°) and **12** (~171°) are not very different from those angles for $[Re(CO)_3(N(H)6,6'\text{-}Me_2dpa)]PF_6$ (169° and 173° for the two rings), indicating that the long terminal Re−N(sp^2) bonds are not a result of the orientation of the pyridyl rings or the structural effects of the sulfonamide group. Therefore, we believe that the steric repulsion between the carbonyl ligands and the 6/6′ Me groups in **3** and **4** weaken the Re−N(sp^2) bonds, thereby facilitating the release of ligands **3** and **4** from complexes **11** and **12**.

The ^{1}H NMR spectrum of a 1-day-old solution of $[trans\text{-}Pt(DMSO)Cl_2]_2(N(SO_2Tol)6,6'\text{-}Me_2dpa)$ (**8**) in DMSO-d_6 (10 mM) shows new peaks corresponding to the mononuclear species $[trans\text{-}Pt(DMSO)Cl_2](N(SO_2Tol)6,6'\text{-}Me_2dpa)$ (**8a**). Peaks corresponding to the free ligand **4** were first observed after 5 days. The peaks of **8a** and **4** grew with time; by 18 d, the composition of the **8**:**8a**:**4** mixture was 37:56:7 (based on methylene signal integrations). Furthermore, a ^{1}H NMR spectrum recorded for another ~3-year-old solution of **8** shows signals chiefly for the free ligand (~90%). Similarly, spectra recorded for a 10 mM solution of $[trans\text{-}Pt(DMSO)Cl_2]_2(N(SO_2Me)6,6'\text{-}Me_2dpa)$ (**7**) in DMSO-d_6 also show that new peaks start appearing in 24 h. The chemical shifts of these new peaks (Table 3.4) indicate that they belong to the corresponding mononuclear species, **7a**, as discussed above. In addition to the **7a** signals, this 10 mM solution of **7** showed signals of the free ligand **3** for the first time in a spectrum recorded 5 d after dissolution. The new peaks for **7a** and **3** grew with time, and the change in composition

of the solution of **7** with time was similar to observations for **8** (e.g., by 18 d, **7**:**7a**:**3** = 42:50:8 vs **8**:**8a**:**4** = 37:56:7). Also, an ~3-year-old solution of **7** showed peaks for only free ligand **3**.

Under the same conditions, free ligand **1** or **2** appeared more quickly in DMSO-d_6 solutions of Pt(II) complexes of these bidentate ligands than the free ligand **3** or **4** appeared from solutions of Pt(II) complexes of these monodentate ligands. As an example, by 9 d, the composition of the 10 mM solution of **7**, [*trans*-Pt(DMSO)Cl_2]$_2$(*N*(SO_2Me)6,6′-Me_2dpa), mentioned above was **7**:**7a**:**3** = 60:37:3. In contrast, at a similar point in elapsed time (9 d), the 10 mM solution of Pt(*N*(SO_2Me)3,3′,5,5′-Me_4dpa)Cl_2 (**5**) in DMSO-d_6 exhibited a composition of **5**:**5**$_{sol}$:**1** = 12:46:42. The ligand dissociation of the square planar Pt(II) complexes is initiated by the associative axial attack of a DMSO molecule. As shown in Figure 3.16, we believe that, in **7** and **8**, a steric block created by the 6/6′ methyl groups and the rest of the dangling ligand near the coordination sphere impedes the axial approach of the solvent molecule. In contrast, ligands **1** and **2** in complexes **5** and **6** cannot move freely **(**bound bidentately) and do not contain any methyl groups near the axial attack site; thus, the solvent can approach the Pt(II) axial position more easily in **5** and **6** than in **7** and **8**.

The partial (~40%) ligand release process for complexes **5** and **6** (bidentately bound ligand) reached completion in less time than the essentially complete (>90%) ligand release process for **7** and **8** (monodentately bound ligand). This result indicates that the bidentate coordination of the ligands **1** and **2** leads to more thermodynamically stable complexes than does the monodentate coordination of ligands **3** and **4**, as might be expected. However, the reasons for the slower release of ligands **3** and **4** are not so obvious. The Pt−N bond distances for **8** (2.062(9) and 2.066(8) Å) and for **8a** (2.0757(9) Å) are not statistically different from these distances for **5** (2.023(2) and 2.031(2) Å) and for **6** (2.027(3) and 2.032(3) Å). Although the differences ranging from 0.03 to

0.05 Å are not all statistically justified, there are enough consistent reports of Pt(II) structures to suggest that having a monodentate pyridine substituted at both the 2 and the 6 positions with groups having CH_2Y (Y various groups such as OH) will increase the Pt−N bond distance by ~0.02 to ~0.03 Å, and having a trans DMSO ligand will add a further ~0.01 to ~0.02 Å.[83-86] Therefore, it is likely that the known trans influence of the DMSO ligand[87-88] and the steric effect of the 2,6 substituents weaken the Pt−N bond, leading to the more complete release of ligands **3** and **4**, as compared to ligands **1** and **2**.

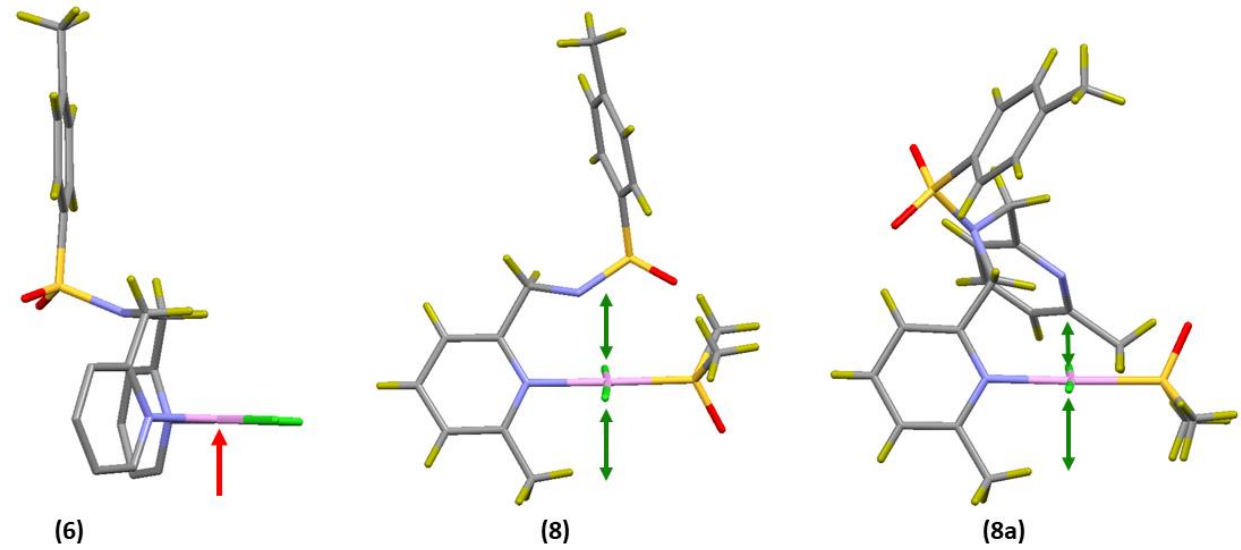

Figure 3.16. Possible role of the pyridine ring substituents in impeding axial solvent attack from the axial direction shown for Pt(*N*(SO_2Tol)3,3′,5,5′-Me_4dpa)Cl_2 (**6**), for [*trans*-Pt(DMSO)Cl_2]$_2$(*N*(SO_2Tol)6,6′-Me_2dpa) (**8**), and for [*trans*-Pt(DMSO)Cl_2](*N*(SO_2Tol)6,6′-Me_2dpa) (**8a**). The axial attack (red arrow) is less sterically impeded for **6**, with no substituents projecting toward the bottom axial approach pathway, as compared to axial attack (green double arrows) for **8** and **8a**, both with substituents projecting toward the two axial approach pathways. One-half of the carrier ligand in **8** is removed for clarity.

Possible Causes for the Absence of Bidentate Coordination to Pt(II) by *N*(SO_2R)6,6′-Me_2dpa ligands (3 and 4). No evidence was found for bidentate coordination to the Pt(II)Cl_2 core by *N*(SO_2R)6,6′-Me_2dpa ligands (**3**, R = Me and **4**, R = Tol). In contrast, no direct evidence was found for monodentate coordination to the Pt(II)Cl_2 core by *N*(SO_2Me)3,3′,5,5′-Me_4dpa ligands **1**

and **2** (**1**, R = Me and **2**, R = Tol). Because [t*rans*-Pt(DMSO)Cl_2](*N*(SO_2Tol)6,6′-Me_2dpa) (**8a**) was structurally characterized (Figure 3.7), we focus on studies with the *N*(SO_2Tol)6,6′-Me_2dpa ligand (**4**). Ligand **4** did not coordinate bidentately to Pt(II) but instead formed the binuclear compound (**8**) even under favorable conditions, such as longer reaction time of **4** with *cis*-Pt(DMSO)Cl_2 under reflux in MeOH or heating a dilute methanol solution of **8a** (3.6 mg/5 ml, 1 mM) at reflux overnight. Furthermore, a 5 mM solution of **8a** in DMF-d_7 was heated at 50 °C for several days, and the solution was monitored by ^{1}H NMR spectroscopy at 24-h intervals. These spectra showed no change, indicating that the absence of bidentate coordination does not depend on the solvent.

In the preceding section, we compared the release of all these bidentate ligands and monodentate ligands from Pt(II) in DMSO-d_6 solution. It is noteworthy that we did not detect any buildup of monodentate intermediates as complexes **5** and **6** with bidentate ligands released free ligands **1** and **2**, respectively. NMR spectra showed that ligands **1** and **2** were either free or coordinated in a bidentate mode. This finding means that the dangling pyridyl ring of the undetectably small amount of monodentate intermediates (**5a** and **6a**), with only one pyridyl ring bound (the analogs of **7a** and **8a**) rapidly added to Pt(II), creating the 8-membered chelate ring present in **5** and **6**.

Solutions of **8a** in DMSO-d_6 gave no NMR spectral evidence for any bidentate chelate complex. If chelation were favorable, these DMSO-d_6 conditions should have allowed such chelate ring closure because closure occurs readily in analogous intermediates having ligands **1** and **2**. Factors that could inhibit or prevent ring closure in **7a** and **8a** most likely involve the 2,6-substituents of the bound pyridyl ring. These 2,6-substituents might prevent this bound ring from tilting sufficiently to allow the dangling pyridyl ring to approach the axial attack site on Pt(II).

Also, these substituents could offer a steric barrier to axial attack. Finally, the 2,6-substituents on the attacking dangling pyridyl ring itself would create very high steric hindrance to Pt–N bond formation. Only five structures of complexes containing two 2,6-substituted pyridyl ligands bound to the same Pt(II) center are in the CCDC data base, indicating that steric hindrance makes it difficult for two 2,6-substituted pyridyl ligands to coordinate to the same Pt(II). Only one such complex has the two 2,6-substituted pyridyl ligands in cis positions, and in this case the pyridyl rings form part of a macrocycle.[48] The 2,6-substituted pyridyl ligands in the other four complexes are in trans positions.[89-90] In fact Kong et al. stated that it is almost impossible to form Pt(2,6-lutidine)$_2$Cl$_2$ complexes.[91]

Furthermore, the two 2-methyl groups in *cis*-Pt(2-picoline)$_2$Cl$_2$ are anti to each other,[52] minimizing the steric repulsion between the two syn 2-methyl groups. In contrast, if the *N*(SO$_2$R)6,6′-Me$_2$dpa ligands coordinated bidentately to Pt(II), as in **5** and **6,** the 6/6′ methyl groups would be syn; the resulting sterically unfavorable proximity of the 6/6′ methyl groups would make bidentate coordination of **3** and **4** thermodynamically unlikely. Thus, we believe that both thermodynamic and kinetic factors make bidentate coordination of *N*(SO$_2$R)6,6′-Me$_2$dpa ligands to Pt(II) unfavorable.

3.4 Conclusions

The *N*(SO$_2$R)Me$_n$dpa ligands investigated here bind tridentately to the *fac*-[Re(I)(CO)$_3$]$^+$ core in the [Re(CO)$_3$(*N*(SO$_2$R)Me$_n$dpa)]PF$_6$ complexes but bind in diverse modes to the *cis*-Pt(II)Cl$_2$ core. The two types of ligands, *N*(SO$_2$R)3,3′,5,5′-Me$_4$dpa and *N*(SO$_2$R)6,6′-Me$_2$dpa, bind bidentately and monodentately to Pt(II), respectively. We suggest that these differences in ligand binding modes arise mainly from electronic factors involving the central sulfonamide donor and from steric factors involving the 6/6′ methyl groups of the terminal pyridyl N-donors.

Because of the steric preferences of the central tertiary sulfonamide donor, we propose that tridentate coordination by the new carrier ligands requires a facial rather than a meridional binding geometry. Therefore, ligands **1** to **4** all bind readily and facially to Re(I) in *fac*-[Re(CO)$_3$(*N*(SO$_2$R)Me$_n$dpa)]PF$_6$ complexes. In cases we can find in which ligands having a tertiary sulfonamide donor bind meridionally, one of the adjacent chelate rings is 6-membered and one is 5-membered (see, for example, a Cu complex).[72] Thus, we conclude that ligands such as *N*(SO$_2$R)3,3′,5,5′-Me$_4$dpa (**1** and **2**), which would have two adjacent 5-membered chelate rings if bound tridentately, cannot bind tridentately to Pt(II) and must instead adopt the bidentate mode.

The [Re(CO)$_3$(*N*(SO$_2$R)3,3′,5,5′-Me$_4$dpa)]PF$_6$ complexes (**9** and **10**) formed by the two *N*(SO$_2$R)3,3′,5,5′-Me$_4$dpa ligands, in which two protons are present at the 6/6′ positions instead of the two methyl groups, are stable indefinitely in DMSO-d_6. These complexes have relatively short Re–N bond lengths. In contrast, longer Re–N bond lengths to the pyridyl N are found for [Re(CO)$_3$(*N*(SO$_2$R)6,6′-Me$_2$dpa)]PF$_6$ complexes (**11** and **12**) and the analog, [Re(CO)$_3$(*N*(H)6,6′-Me$_2$dpa)]PF$_6$. The longer bonds are a result of the steric repulsion between the 6/6′ methyl groups of coordinated tridentate ligands and the CO ligands in these complexes. However, only **11** and **12** release tridentate ligand with time in DMSO-d_6. Thus, both the steric repulsions involving the 6/6′ methyl groups and the poor donor ability of the central sulfonamide of coordinated *N*(SO$_2$R)6,6′-Me$_2$dpa tridentate ligands in **11** and **12** contribute to release of the tridentate ligand in DMSO-d_6.

The Pt(*N*(SO$_2$R)3,3′,5,5′-Me$_4$dpa)Cl$_2$ complexes (**5** and **6**) of the bidentately bound ligands (**1** and **2**) have an unusually large 8-membered chelate ring. These complexes release free ligand, and eventually an equilibrium is established. The process occurs more rapidly than the release of free ligands from the [t*rans*-Pt(DMSO)Cl$_2$]$_2$(*N*(SO$_2$R)6,6′-Me$_2$dpa) complexes (**7** and **8**) of monodentately bound ligands (**3** and **4**). The monodentate coordination mode is caused by steric

hindrance of the 6/6′ methyl groups in *N*(SO_2R)6,6′-Me_2dpa (**3** and **4**). However, the 6/6′ methyl groups and the dangling part of the ligand act as barriers to the axial attack by solvent, accounting for the slower release of monodentately bound ligands **3** and **4** from **7** and **8** [*trans*-(Pt(DMSO)Cl_2]$_2$(*N*(SO_2R)6,6′-Me_2dpa)) than release of the bidentately bound ligands **1** and **2** from **5** and **6** (Pt(*N*(SO_2R)3,3′,5,5′-Me_4dpa)Cl_2). Because there is no buildup of the monodentate intermediate during the ligand release process, we do not know whether the trans ligand in the intermediate is chloride or DMSO. However, **7a** and **8a** have DMSO in the trans position, and DMSO has a larger trans effect than chloride.[87-88] Thus, the slower release of ligands **3** and **4** from **7a** and **8a** is clearly steric in nature; the steric effect undoubtedly involves the inhibition of axial attack of solvent DMSO.

3.5 References

1. Veltze, S.; Egdal, R. K.; Johansson, F. B.; Bond, A. D.; McKenzie, C. J. *Dalton Trans.* **2009,** (47), 10495-10504.

2. Lu, G.; Hillier, S. M.; Maresca, K. P.; Zimmerman, C. N.; Eckelman, W. C.; Joyal, J. L.; Babich, J. W. *J. Med. Chem.* **2013,** *56*, 510-520.

3. Langdon-Jones, E. E.; Symonds, N. O.; Yates, S. E.; Hayes, A. J.; Lloyd, D.; Williams, R.; Coles, S. J.; Horton, P. N.; Pope, S. J. A. *Inorg. Chem.* **2014,** *53* (7), 3788-3797.

4. Perera, T.; Abhayawardhana, P.; Marzilli, P. A.; Fronczek, F. R.; Marzilli, L. G. *Inorg. Chem.* **2013,** *52*, 2412−2421.

5. Abhayawardhana, P. L.; Marzilli, P. A.; Fronczek, F. R.; Marzilli, L. G. *Inorg. Chem.* **2014,** *53*, 1144-1155.

6. Bartholoma, M.; Valliant, J.; Maresca, K. P.; Babichc, J.; Zubieta, J. *Chem. Commun.* **2009,** *5*, 493-512.

7. Maresca, K. P.; Marquis, J. C.; Hillier, S. M.; Lu, G.; Femia, F. J.; Zimmerman, C. N.; Eckelman, W. C.; Joyal, J. L.; Babich, J. W. *Bioconjug. Chem.* **2010,** *21* (6), 1032-1042.

8. Maresca, K. P.; Kronauge, J. F.; Zubieta, J.; Babich, J. W. *Inorg. Chem. Commun.* **2007,** *10* (12), 1409-1412.

9. Zhu, J.; Zhao, Y.; Zhu, Y.; Wu, Z.; Lin, M.; He, W.; Wang, Y.; Chen, G.; Dong, L.; Zhang, J.; Lu, Y.; Guo, Z. *Chem. Eur. J.* **2009,** *15* (21), 5245-5253.

10. Christoforou, A. M.; Marzilli, P. A.; Marzilli, L. G. *Inorg. Chem.* **2006,** *45*, 6771-6781.

11. Olivova, R.; Kasparkova, J.; Vrana, O.; Vojtiskova, M.; Suchankova, T.; Novakova, O.; He, W.; Guo, Z.; Brabec, V. *Mol. Pharm.* **2011,** *8* (6), 2368-2378.

12. Zhao, Y.; He, W.; Shi, P.; Zhu, J.; Qiu, L.; Lin, L.; Guo, Z. *Dalton Trans.* **2006,** (22), 2617-2619.

13. Wu, S.; Zhu, C.; Zhang, C.; Yu, Z.; He, W.; He, Y.; Li, Y.; Wang, J.; Guo, Z. *Inorg. Chem.* **2011,** *50* (23), 11847-11849.

14. Ndinguri, M. W.; Fronczek, F. R.; Marzilli, P. A.; Crowe, W. E.; Hammer, R. P.; Marzilli, L. G. *Inorg. Chim. Acta* **2010,** *363* (8), 1796-1804.

15. van der Schilden, K.; Garcìa, F.; Kooijman, H.; Spek, A. L.; Haasnoot, J. G.; Reedijk, J. *Angew. Chem., Int. Ed.* **2004,** *43* (42), 5668-5670.

16. Reedijk, J. *Pure Appl. Chem.* **2011,** *83* (9), 1709-1719.

17. Damian, M. S.; Hedman, H. K.; Elmroth, S. K. C.; Diederichsen, U. *Eur. J. Org. Chem.* **2010,** *2010* (32), 6161-6170.

18. Reddy, U. G.; Axthelm, J.; Hoffmann, P.; Taye, N.; Gläser, S.; Görls, H.; Hopkins, S. L.; Plass, W.; Neugebauer, U.; Bonnet, S.; Schiller, A. *J. Am. Chem. Soc.* **2017,** *139* (14), 4991-4994.

19. Reddy G, U.; Liu, J.; Hoffmann, P.; Steinmetzer, J.; Gorls, H.; Kupfer, S.; Askes, S. H. C.; Neugebauer, U.; Grafe, S.; Schiller, A. *Chem. Sci.* **2017,** *8* (9), 6555-6560.

20. Park, G. Y.; Wilson, J. J.; Song, Y.; Lippard, S. J. *Proc. Natl. Acad. Sci. U.S.A.* **2012,** *109* (30), 11987-11992.

21. Saad, J. S.; Natile, G.; Marzilli, L. G. *J. Am. Chem. Soc.* **2009,** *131*, 12314-12324.

22. Johnstone, T. C.; Wilson, J. J.; Lippard, S. J. *Inorg. Chem.* **2013,** *52* (21), 12234-12249.

23. Zhu, G.; Myint, M.; Ang, W. H.; Song, L.; Lippard, S. J. *Cancer Res.* **2012,** *72* (3), 790-800.

24. Lovejoy, K. S.; Todd, R. C.; Zhang, S.; McCormick, M. S.; D'Aquino, J. A.; Reardon, J. T.; Sancar, A.; Giacomini, K. M.; Lippard, S. J. *Proc. Natl. Acad. Sci.* **2008,** *105* (26), 8902-8907.

25. Wang, Z.; Yu, H.; Gou, S.; Chen, F.; Fang, L. *Inorg. Chem.* **2016,** *55* (9), 4519-4528.

26. Andrepont, C.; Marzilli, P. A.; Marzilli, L. G. *Inorg. Chem.* **2012,** *51* (21), 11961-11970.

27. Ranasinghe, K.; Marzilli, P. A.; Pakhomova, S.; Marzilli, L. G. *Inorg. Chem.* **2017,** *56* (14), 8462-8477.

28. Bhattacharyya, D.; Marzilli, P. A.; Marzilli, L. G. *Inorg. Chem.* **2005,** *44* (21), 7644-7651.

29. Tu, C.; Wu, X.; Liu, Q.; Wang, X.; Xu, Q.; Guo, Z. *Inorg. Chim. Acta* **2004,** *357* (1), 95-102.

30. Rauterkus, M. J.; Fakih, S.; Mock, C.; Puscasu, I.; Krebs, B. *Inorg. Chim. Acta* **2003,** *350*, 355-365.

31. Kelly, M. E.; Gómez-Ruiz, S.; Steinborn, D.; Wagner, C.; Schmidt, H. *Transition Met. Chem.* **2008,** *33* (6), 721-727.

32. Bulak, E.; Leboschka, M.; Schwederski, B.; Sarper, O.; Varnali, T.; Fiedler, J.; Lissner, F.; Schleid, T.; Kaim, W. *Inorg. Chem.* **2007,** *46* (14), 5562-5566.

33. Bloemink, M. J.; Engelking, H.; Karentzopoulos, S.; Krebs, B.; Reedijk, J. *Inorg. Chem.* **1996,** *35* (3), 619-627.

34. Maheshwari, V.; Bhattacharyya, D.; Fronczek, F. R.; Marzilli, P. A.; Marzilli, L. G. *Inorg. Chem.* **2006,** *45*, 7182-7190.

35. McFarlane, A.; Lusty, J. R.; Fiol, J. J.; Terrón, A.; Molins, E.; Miravitlles, C.; Moreno, V. *Zeitschrift für Naturforschung B* **1994,** *49* (6), 844.

36. Safa, M.; Jennings, M. C.; Puddephatt, R. J. *Organometallics* **2012,** *31* (9), 3539-3550.

37. Tabatabaei Rezaei, S. J.; Amani, V.; Nabid, M. R.; Safari, N.; Niknejad, H. *Polym. Chem.* **2015,** *6* (15), 2844-2853.

38. Grzesiak, A. L.; Matzger, A. J. *Inorg. Chem.* **2007,** *46* (2), 453-457.

39. Canty, A. J.; Gardiner, M. G.; Jones, R. C.; Sharma, M. *Aust. J. Chem.* **2011,** *64* (10), 1355-1359.

40. Andrade-Lopez, N.; Alvarado-Rodriguez, J. G.; Gonzalez-Montiel, S.; Paez-Hernandez, M. E.; Galan-Vidal, C. A.; Jimenez-Perez, A. *Arkivoc* **2008,** *9* (5), 43-45.

41. Bulak, E.; Varnali, T.; Schwederski, B.; Sarkar, B.; Hartenbach, I.; Fiedler, J.; Kaim, W. *Dalton Trans.* **2011,** *40* (12), 2757-2763.

42. Casas, J. S.; Castineiras, A.; Parajo, Y.; Sordo, J.; Varela, J. M. *Acta Crystallogr. Sec. C* **1998,** *54* (12), 1777-1779.

43. Roy, S.; Westmaas, J. A.; Buda, F.; Reedijk, J. *J. Inorg. Biochem.* **2009,** *103* (9), 1278-1287.

44. Maheshwari, V.; Marzilli, P. A.; Marzilli, L. G. *Inorg. Chem.* **2008,** *47* (20), 9303-9313.

45. Song, D.; Wang, S. *Organometallics* **2003,** *22* (11), 2187-2189.

46. Zhao, S.-B.; Liu, G.-h.; Song, D.; Wang, S. *Dalton Trans.* **2008,** (48), 6953-6965.

47. Davies, M. S.; Fenton, R. R.; Huq, F.; Ling, E. C. H.; Hambley, T. W. *Aust. J. Chem.* **2000,** *53* (6), 451-456.

48. Moriguchi, T.; Kitamura, S.; Sakata, K.; Tsuge, A. *Polyhedron* **2001,** *20* (18), 2315-2320.

49. Zhao, S.-B.; Wang, R.-Y.; Wang, S. *Organometallics* **2009,** *28* (8), 2572-2582.

50. Yang, Y.; Lu, C.; Wang, H.; Liu, X. *Dalton Trans.* **2016,** *45* (25), 10289-10296.

51. Sakai, K.; Yokoyama, Y.; Masaoka, S. *Acta Crystallogr. Sect. E* **2007,** *63* (1), m97-m99.

52. Tessier, C.; Rochon, F. D. *Inorg. Chim. Acta* **1999,** *295* (1), 25-38.

53. Colamarino, P.; Orioli, P. L. *Dalton Trans.* **1975,** (16-17), 1656-1659.

54. Graves, B. J.; Hodgson, D. J.; Van Kralingen, C. G.; Reedijk, J. *Inorg. Chem.* **1978,** *17* (11), 3007-3011.

55. Marcelis, A. T. M.; Veer, J. L. V. D.; Zwetsloot, J. C. M.; Reedijk, J. *Inorg. Chim. Acta* **1983,** *78*, 195-203.

56. Andrepont, C.; Marzilli, P. A.; Pakhomova, S.; Marzilli, L. G. *J. Inorg. Biochem.* **2015,** *153*, 219-230.

57. Andrepont, C.; Pakhomova, S.; Marzilli, P. A.; Marzilli, L. G. *Inorg. Chem.* **2015,** *54*, 4895-4908.

58. Price., J. H.; Williamson, A. N.; Robert, F. S.; Bradford, B. W. *Inorg. Chem.* **1972,** *11*, 1280-1284.

59. He, H.; Lipowska, M.; Xu, X.; Taylor, A. T.; Carlone, M.; Marzilli, L. G. *Inorg. Chem.* **2005,** *44*, 5437–5446.

60. Komatsu, K.; Kikuchi, K.; Kojima, H.; Urano, Y.; Nagano, T. *J.Am.Chem.Soc.* **2005,** *127*, 10197-10204.

61. Stock, N. S.; Bain, G.; Zunic, J.; Li, Y.; Ziff, J.; Roppe, J.; Santini, A.; Darlington, J.; Prodanovich, P.; King, C. D.; Baccei, C.; Lee, C.; Rng, H.; Chapman, C.; Broadhead, A.; Lorrain, D.; Correa, L.; Hutchinson, J. H.; Evans, J. F.; Prasit, P. *J. Med. Chem.* **2011,** *54*, 8013-8029.

62. Sheldrick, G. *Acta Crystallogr. Sect. A* **2008,** *64* (1), 112-122.

63. Perera, T.; Marzilli, P. A.; Fronczek, F. R.; Marzilli, L. G. *Inorg. Chem.* **2010,** *49*, 5560-5572.

64. Christoforou, A. M.; Marzilli, P. A.; Fronczek, F. R.; Marzilli, L. G. *Inorg. Chem.* **2007,** *46* (26), 11173-11182.

65. Perera, T.; Fronczek, F. R.; Marzilli, P. A.; Marzilli, L. G. *Inorg. Chem.* **2010,** *49*, 7035-7045.

66. Christoforou, A. M.; Fronczek, F. R.; Marzilli, P. A.; Marzilli, L. G. *Inorg. Chem.* **2007,** *46* (17), 6942-6949.

67. Lewis, N. A.; Pakhomova, S.; Marzilli, P. A.; Marzilli, L. G. *Inorg. Chem.* **2017,** *56* (16), 9781-9793.

68. Lee, W.-Z.; Tseng, H.-S.; Kuo, T.-S. *Dalton Trans.* **2007,** (24), 2563-2570.

69. Seidler-Egdal, R. K.; Johansson, F. B.; Veltze, S.; Skou, E. M.; Bond, A. D.; McKenzie, C. J. *Dalton Trans.* **2011,** *40* (13), 3336-3345.

70. Canovese, L.; Visentin, F.; Chessa, G.; Uguagliati, P.; Levi, C.; Dolmella, A.; Bandoli, G. *Organometallics* **2006,** *25*, 5355-5365.

71. Calligaris, M.; Carugo, O.; Crippa, G.; Santis, G. D.; Casa, M.; Fabbrizzi, L.; Poggi, A.; Seghi, B. *Inorg. Chem.* **1990,** *29*, 2964-2970.

72. Kim, S.; Minier, M. A.; Loas, A.; Becker, S.; Wang, F.; Lippard, S. J. *J. Am. Chem. Soc.* **2016,** *138* (6), 1804-1807.

73. Seubert, K.; Böhme, D.; Kösters, J.; Shen, W.-Z.; Freisinger, E.; Müller, J. *Z. Anorg. Allg. Chem.* **2012,** *638* (11), 1761-1767.

74. Lonnon, D. G.; Craig, D. C.; Colbran, S. B. *J. Chem. Soc., Dalton Trans.* **2006,** (31), 3785-3797.

75. Lo, W. K. C.; Huff, G. S.; Preston, D.; McMorran, D. A.; Giles, G. I.; Gordon, K. C.; Crowley, J. D. *Inorg. Chem.* **2015,** *54* (14), 6671-6673.

76. Yuan, Z.; Shen, X.; Huang, J. *RSC Adv.* **2015,** *5* (14), 10521-10528.

77. Zhang, R.; Liang, Z.; Han, A.; Wu, H.; Du, P.; Lai, W.; Cao, R. *CrystEngComm* **2014,** *16* (25), 5531-5542.

78. Petrović, B.; Bugarčić, Ž. D.; Dees, A.; Ivanović-Burmazović, I.; Heinemann, F. W.; Puchta, R.; Steinmann, S. N.; Corminboeuf, C.; van Eldik, R. *Inorg. Chem.* **2012,** *51* (3), 1516-1529.

79. Ha, K. *Z. Kristallogr., New Cryst. Struct.* **2011,** *226* (1), 55-56.

80. Imler, G. H.; Lu, Z.; Kistler, K. A.; Carroll, P. J.; Wayland, B. B.; Zdilla, M. J. *Inorg. Chem.* **2012,** *51* (19), 10122-10128.

81. Kerrison, S. J. S.; Sadler, P. J. *Inorg. Chim. Acta* **1985,** *104* (3), 197-201.

82. van Kralingen, G.; Reedijk, J. *Inorg. Chim. Acta* **1978,** *30* (0), 171-177.

83. Klein, A.; Elmas, S.; Butsch, K. *Eur. J. Inorg. Chem.* **2009,** *2009* (15), 2271-2281.

84. Grabner, S.; Bukovec, P. *Acta Chim. Slov.* **2015,** *62* (2), 5.

85. Rochon, F. D.; Fakhfakh, M. *Inorg. Chim. Acta* **2009,** *362* (5), 1455-1466.

86. Bostrom, D.; Strandberg, R.; Noren, B.; Oskarsson, A. *Acta Cryst. C* **1991,** *47* (10), 2101-2104.

87. Kukushkin, Y. N. *Russ. Chem. Rev.* **1974,** *43* (10), 805.

88. Manojlovic-Muir, L. J.; Muir, K. W. *Inorg. Chim. Acta* **1974,** *10*, 47-49.

89. Zeits, P. D.; Rachiero, G. P.; Hampel, F.; Reibenspies, J. H.; Gladysz, J. A. *Organometallics* **2012,** *31* (7), 2854-2877.

90. D., F.; Bensimon, C.; Beauchamp, A. L. *Can. J. Chem.* **1996,** *74* (11), 2121-2130.

91. Kong, P. C.; Rochon, F. D. *Can. J. Chem.* **1978,** *56* (4), 441-445.

CHAPTER 4. NNN-TRIDENTATE LIGANDS WITH TERMINAL IMIDAZOLYL RING AND CENTRAL SULFONAMIDE N-DONORS COORDINATED TO *fac*-$[Re(I)(CO)_3]^+$ AND $Pt(II)Cl_2$ "CORES". DYNAMIC PROPERTIES OF THE 8-MEMBERED CHELATE RING IN THE PT(II) COMPLEXES AND IN THEIR ADDUCTS FORMED WITH MONODENTATE N-DONOR AROMATIC HETEROCYCLIC LIGANDS

4.1 Introduction

Identification of new linking strategies useful in modifying chelating ligands is crucial in developing new metal-mediated diagnostic or therapeutic drug molecules; new properties can be introduced to the drug molecules by linking groups such as fluorophores.[1-15] A linear symmetrical tridentate ligand with an easily functionalizable central donor is a good framework to study and develop such new linking chemistries (Figure 4.1). Over the last few years our group was particularly interested in studying new bioconjugation possibilities involving a N−S linker within a similar framework (Figure 4.1). These studies have shown that *N*(SO_2R)dpa[6,16] and *N*(SO_2R)dien[7] type ligands in which the central *N*-donor atom is part of a tertiary sulfonamide group function as a new class of tridentate ligands; these ligands were derived from the parent ligands *N*(H)dpa (2-dipicolylamine) and dien (diethylenetriamine), respectively.

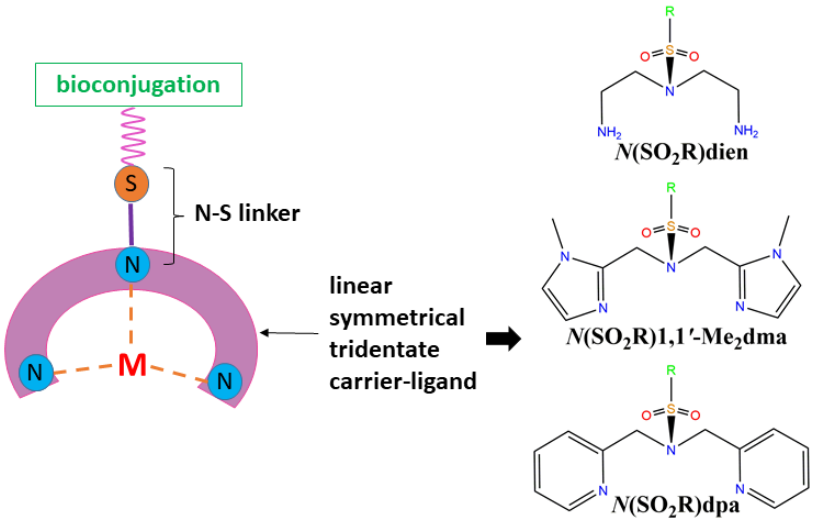

Figure 4.1. *Left*: Schematic representation of a linear symmetrical tridentate carrier-ligand bound to a metal ion (M). *Right*: Sulfonamide group containing parent ligands studied by Marzilli Group (R = Me, Tol, etc.). The *N*(SO_2R)1,1′-Me_2dma-type ligands are employed in this study.

Use of non-radioactive Re(I) complexes as models in developing new ligand systems for ^{99m}Tc diagnostic agents and $^{186/188}$Re(I) therapeutic agents is common.[17-21] Therefore, the *N*(SO_2R)dpa and *N*(SO_2R)dien ligands were utilized to synthesize a number of Re(I) complexes (*fac*-[Re(CO)$_3$(*N*(SO_2R)dpa)]$^+$ and *fac*-[Re(CO)$_3$(*N*(SO_2R)dien)]$^+$, R = Me, Tol, etc.) and their relevance to the development of ^{99m}Tc radiopharmaceutical agents was discussed.[6-7] These complexes are the first examples to have a normal metal-to-N(sulfonamide) bond length when any metal is bound to a noncyclic linear tridentate ligand through a sulfonamide N-donor.[6-7]

Furthermore, in order to introduce the N−S linker in ligands employed in Pt chemistry, *N*(SO_2R)Me$_n$dpa-type ligands (*N*(SO_2R)dpa derivatives with methyl groups replacing some of the pyridyl ring protons; *N*(SO_2R)3,3′,5,5′-Me$_4$dpa and *N*(SO_2R)6,6′-Me$_2$dpa, R = Me and Tol) were utilized to synthesize Pt(II) complexes.[16] These ligands coordinated to Pt center either bidentately (to form Pt(*N*(SO_2R)3,3′,5,5′-Me$_4$dpa)Cl$_2$) or monodentately (to form [*trans*-Pt(DMSO)Cl$_2$]$_2$(*N*(SO_2R)6,6′-Me$_2$dpa).[16] The sulfonamide nitrogen was not coordinated to the Pt(II) center in any of these complexes. Thus, the bidentate *N*(SO_2R)3,3′,5,5′-Me$_4$dpa ligand forms an unusually large 8-membered chelate ring. The *N*(SO_2R)6,6′-Me$_2$dpa ligand binds monodentately because the 6,6′-methyl groups inhibit chelate ring formation.[16] We concluded that the reason the tertiary sulfonamide N did not bind to Pt(II) was because such a donor group cannot anchor two adjacent 5-membered chelate rings in a meridional geometry.

A key feature to be evaluated in Pt(II) complexes designed for biological applications is the ability to form adducts with biological molecules (such as guanine derivatives used to test propensity for reactivity toward G residues in DNA, a feature correlating with Pt drug anticancer activity). Unfortunately, none of the Pt complexes mentioned above were robust in DMSO-d_6 and the Pt(*N*(SO_2R)3,3′,5,5′-Me$_4$dpa)Cl$_2$ complexes did not exhibit any useful reactivity towards

biomolecules such as guanine derivatives.[16] Based on an extensive NMR and X-ray structural analysis, we hypothesized that the main reason for the low robustness and poor biomolecule reactivity of the Pt(*N*(SO_2R)3,3′,5,5′-Me_4dpa)Cl_2 complexes is the bulk of the 6-membered pyridyl donor groups of the carrier-ligands, *N*(SO_2R)Me_ndpa. There was no evidence that the steric effect of this ring lacking a substituent in the Pt(*N*(SO_2R)3,3′,5,5′-Me_4dpa)Cl_2 complexes prevents the binding of the tertiary sulfonamide N, but this possibility cannot be ruled out.

In this study, we designed *N*(SO_2R)1,1′-Me_2dma ligands (Figure 4.1) with smaller 5-membered imidazolyl rings (compared to 6-membered pyridyl rings in *N*(SO_2R)dpa and *N*(SO_2R)Me_ndpa ligands); these new carrier ligands (R = Me and Tol, Figure 4.2) are derivatives of the parent ligand, *N*(H)1,1′-Me_2dma (bis(1-methyl-2-methylimidazolyl)amine). As observed for the *N*(SO_2R)3,3′,5,5′-Me_4dpa ligands, the *N*(SO_2R)1,1′-Me_2dma ligands coordinate tridentately in *fac*-[Re$(CO)_3$(*N*(SO_2R)1,1′-Me_2dma)]ClO_4 and bidentately in Pt(*N*(SO_2R)1,1′-Me_2dma)Cl_2 complexes (Figure 4.2). All of the *fac*-[Re$(CO)_3$(chelate)]Y (Y = ClO_4 or PF_6) complexes discussed below have facial geometry, and thus from this point onward we omit the *fac*-designation when discussing specific compounds.

In addition to the characterization of the new carrier ligands and their metal complexes by ^{1}H NMR spectroscopy and single-crystal X-ray crystallography or mass spectrometry, we studied the dynamic properties of the Pt(*N*(SO_2R)1,1′-Me_2dma)Cl_2 complexes. EXSY cross-peaks between the two ^{1}H NMR signals of the methylene groups in DMF reveal that the 8-membered chelate ring undergoes dynamic motion involving rotation around the Pt–N bond. This process was not observed for the Pt(*N*(SO_2R)3,3′,5,5′-Me_4dpa)Cl_2 complexes, consistent with a steric effect of the larger terminal 6-membered pyridyl rings.

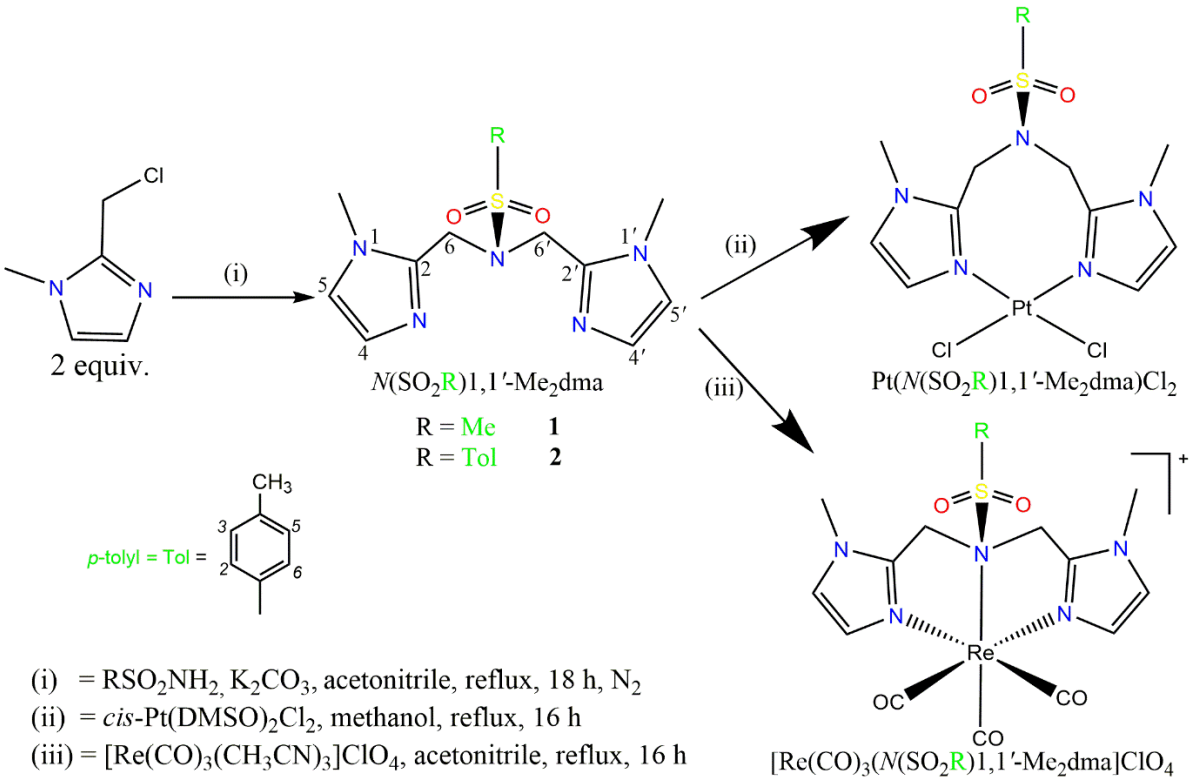

Figure 4.2. General reaction route for forming *N*(SO$_2$R)1,1′-Me$_2$dma ligands: *N*,*N*-di(1-methyl-2-methylimidazolyl)methanesulfonamide, *N*(SO$_2$Me)1,1′-Me$_2$dma (**1**) and *N*,*N*-di(1-methyl-2-methylimidazolyl)-*p*-tolylsulfonamide, *N*(SO$_2$Tol)1,1′-Me$_2$dma (**2**) and their [Re(CO)$_3$(*N*(SO$_2$R)1,1′-Me$_2$dma)]ClO$_4$ (**3**, R = Me and **4**, R = Tol) and Pt(*N*(SO$_2$R)1,1′-Me$_2$dma)Cl$_2$ (**5**, R = Me and **6**, R = Tol) complexes. The numbering scheme shown here is employed in the NMR discussion. Note that the *p*-tolyl group numbering is *italicized* to prevent confusion with the imidazolyl ring numbering.

Finally, we describe the use of ^{1}H NMR spectroscopy and in some cases X-ray crystallography to examine adducts formed by the Pt(*N*(SO$_2$R)1,1′-Me$_2$dma)Cl$_2$ complexes with small N-donor ligands (such as 4-picoline) and guanine derivatives (**G**) such as guanosine and 9-methylguanine. The substitution of the chloride ligands by biomolecules is important for biological applications of platinum(II) agents. In a previous study, we have shown that **G** readily form monoadducts in solutions with the monofunctional [Pt(*N*(R)1,1′-Me$_2$dma)Cl]$^+$ cation in which the *N*(H)1,1′-Me$_2$dma parent ligand and its methyl derivative, *N*(Me)1,1′-Me$_2$dma, are bound tridentately to Pt(II).[22] Furthermore, similar monofunctional platinum(II) complexes of *N*(H)dpa and its derivatives, [Pt(*N*(H)dpa)Cl]Cl,[23] [Pt(*N*(H)6-Medpa)Cl]Cl[24] and [Pt(*N*(H)6,6′-

Me_2dpa)Cl]Cl,[25] also form **G** monoadducts in solution. As mentioned, the Pt(*N*(SO_2R)3,3′,5,5′-Me_4dpa)Cl_2 complexes did not exhibit useful reactivity towards guanine derivatives or other N-donor ligands.[16] In the current study, we find that the Pt(*N*(SO_2R)1,1′-Me_2dma)Cl_2 complexes do form mono adducts ([Pt(*N*(SO_2R)1,1′-Me_2dma)**G**Cl]$^+$) in the presence of an excess of **G** (**G** = 9-MeG and Guo). Thus, reducing the size of the terminal rings does facilitate reaction. Indeed, the Pt(*N*(SO_2R)1,1′-Me_2dma)Cl_2 complexes also form bis adducts with monodentate pyridyl ligands (4-picoline, 4-dimethylaminopyridine, and 3,5-lutidine). ^{1}H NMR spectral and X-ray structural results of these bis complexes exhibit the existence of two bis conformers, Bis1 and Bis2 in which the SO_2R group is projecting towards and away from the coordination sphere, respectively. Because the sulfonamide group is not coordinated to the Pt(II) center, the 8-membered ring of the Pt(*N*(SO_2R)1,1′-Me_2dma)Cl_2 complexes and their adducts has a degree of dynamic freedom; the imidazolyl rings can rotate around the Pt–N bond and inversion can occur at the N(sulfonamide) atom. We believe that the observed monofunctional behavior of the Pt(*N*(SO_2R)1,1′-Me_2dma)Cl_2 complexes is due to a combination of the steric bulk of the chelate ligand and the guanine base, which is bulkier than the added monodentate pyridyl ligands. The monodentate pyridyl ligands are small enough to form bis adducts but the two bound cis monodentate pyridyl ligands decrease the dynamic motion of the 8-membered ring.

4.2 Experimental Section

Starting Materials. Methanesulfonamide ($MeSO_2NH_2$), *p*-tolylsulfonamide ($TolSO_2NH_2$), 1-methyl-2-imidazolecarboxaldehyde, tetraethylammonium chloride ([Et_4N]Cl), guanosine (Guo), 9-methylguanine (9-MeG), 4-methylpyridine (4-pic), 3,5-lutidine (3,5-lut) and 4-dimethylaminopyridine (DMAP) were used as received from Aldrich. *cis*-Pt(DMSO)$_2Cl_2$,[26]

$[Re(CO)_3(CH_3CN)_3]ClO_4$,[27] and 2-(chloromethyl)-1-methylimidazole hydrochloride[28] were prepared by known methods.

NMR Measurements. ^1H NMR spectra were recorded on a 400 MHz or on an Avance-III Prodigy 500 MHz Bruker spectrometer. Peak positions are relative to TMS or solvent residual peak with TMS as reference. All NMR data were processed with TopSpin and MestReNova software. A presaturation pulse to suppress the water peak was employed when necessary.

Mass Spectrometric Measurements. High resolution mass spectra were recorded on an Agilent 6210 ESI TOF LCMS mass spectrometer.

X-ray Data Collection and Structure Determination. Diffraction data were collected on a Bruker Kappa Apex-II DUO CCD diffractometer with Mo Kα radiation (λ = 0.71073 Å), equipped with an Oxford Cryosystems Cryostream. All X-ray structures were determined by direct methods and difference Fourier techniques and refined by full-matrix least-squares by using *SHELXL2014*[29] with H-atoms in idealized positions.

***N*(SO$_2$Me)1,1′-Me$_2$dma) (1).** A solution of 2-(chloromethyl)-1-methylimidazole hydrochloride (1.00 g, 5.98 mmol), K_2CO_3 (~1.7 g, 12 mmol), and $MeSO_2NH_2$ (0.23 g, 2.4 mmol) in acetonitrile (95 mL) was heated at reflux under nitrogen for 18 h. The brown residue obtained after the removal of acetonitrile under reduced pressure was dissolved in water (45 mL) and the solution was extracted with CH_2Cl_2 (3 x 45 mL). The organic layers were combined, washed with saturated aqueous sodium chloride solution, dried over sodium sulfate, and taken to dryness under reduced pressure. The residue was dissolved in a solvent mixture of acetone:5.0 M NH_4OH (90:10) and purified by chromatography on a silica column with the same eluent. Fractions were collected and spotted on TLC plates by using the same eluent. The cleanest fractions, as assessed by ^1H NMR spectroscopy, were combined and taken to dryness by rotary evaporation to afford

N(SO_2Me)1,1′-Me_2dma as a pale yellow oil (0.55 g, 82% yield). ^{1}H NMR signals (ppm) in $CDCl_3$: 6.98 (2H, H5/5′), 6.86 (2H, H4/4′), 4.52 (s, 4H, CH_2), 3.70 (s, 6H, CH3), 2.97 (s, 3H, CH_3). ^{1}H NMR signals (ppm) in DMSO-d_6: 7.12 (2H, H5/5′), 6.86 (2H, H4/4′), 4.40 (s, 4H, CH_2), 3.61 (s, 6H, CH3), 3.05 (s, 3H, CH_3). ESI-MS (*m/z*): $[M + H]^+$ = 284.1171. Calcd for $[M + H]^+$ = 284.1176.

***N*(SO$_2$Tol)1,1′-Me$_2$dma) (2).** A similar procedure as for ligand **1** with 2-(chloromethyl)-1-methylimidazole hydrochloride (1.00 g, 5.98 mmol), K_2CO_3 (~1.7 g, 12 mmol), and $TolSO_2NH_2$ (0.41 g, 2.4 mmol) afforded a brown residue, which was purified by using a solvent mixture of acetone:5.0 M NH_4OH (90:10) to afford *N*(SO_2Tol)1,1′-Me_2dma as a white solid (0.15 g, 20% yield). ^{1}H NMR signals (ppm) in $CDCl_3$: 7.62 (d, *J* = 7.3 Hz, 2H, H*2*/*6*), 7.30 (d, *J* = 8.2 Hz, 2H, H*3*/*5*), 6.87 (2H, H5/5′), 6.75 (2H, H4/4′), 4.43 (s, 4H, CH_2), 3.60 (s, 6H, CH_3), 2.43 (s, 3H, CH_3). ^{1}H NMR signals (ppm) in DMSO-d_6: 7.56 (d, *J* = 8.3 Hz, 2H, H*2*/*6*), 7.34 (d, *J* = 8.1 Hz, 2H, H*3*/*5*), 7.01 (2H, H5/5′), 6.70 (2H, H4/4′), 4.30 (s, 4H, CH_2), 3.54 (s, 6H, CH_3), 2.38 (s, 3H, CH_3). ESI-MS (*m/z*): $[M + H]^+$ = 360.1499. Calcd for $[M + H]^+$ = 360.1489.

[Re(CO)$_3$(*N*(SO$_2$Me)1,1′-Me$_2$dma)]ClO$_4$ (3). A solution of *N*(SO_2Me)1,1′-Me_2dma (**1**, 28 mg, 0.1 mmol) and $[Re(CO)_3(CH_3CN)_3]ClO_4$ (49 mg, 0.1 mmol) in acetonitrile (5 mL) was heated at reflux overnight (~16 h). The resultant clear pale-yellow solution was kept at room temperature to allow the solvent to evaporate slowly to produce white X-ray quality crystals overnight (34 mg, 52% yield). ^{1}H NMR signals (ppm) in DMSO-d_6: 7.34 (d, *J* = 1.5 Hz, 2H, H5/5′), 7.13 (d, *J* = 1.5 Hz, 2H, H4/4′), 5.20 (d, *J* = 16.5 Hz, 2H, CH_2), 4.98 (d, *J* = 16.4 Hz, 2H, CH_2), 3.85 (s, 3H, CH_3), 3.66 (s, 6H, CH_3).

[Re(CO)$_3$(*N*(SO$_2$Tol)1,1′-Me$_2$dma)]ClO$_4$ (4). A solution of *N*(SO_2Tol)1,1′-Me_2dma (**2**, 36 mg, 0.1 mmol) and $[Re(CO)_3(CH_3CN)_3]ClO_4$ (49 mg, 0.1 mmol) in acetonitrile (5 mL) was

heated at reflux overnight (~16 h). The resultant clear pale-yellow solution was kept at room temperature to allow the solvent to evaporate slowly to produce white crystalline solid overnight (55 mg, 76% yield). ^{1}H NMR signals (ppm) in DMSO-d_6: 8.19 (d, J = 8.1 Hz, 2H, H*2*/*6*), 7.74 (d, J = 8.2 Hz, 2H, H*3*/*5*), 7.29 (s, 2H, H5/5′), 7.13 (s, 2H, H4/4′), 5.40 (d, J = 16.2 Hz, 2H, CH_2), 4.44 (d, J = 16.5 Hz, 2H, CH_2), 3.54 (s, 6H, CH_3), 2.56 (s, 3H, CH_3). ESI-MS (*m/z*): $[M]^+$ = 630.0825. Calcd for $[M]^+$ = 630.0815.

Pt(*N*(SO$_2$Me)1,1′-Me$_2$dma)Cl$_2$ (5). A solution of *N*(SO$_2$Me)1,1′-Me$_2$dma (**1**, 28 mg, 0.1 mmol) and *cis*-Pt(DMSO)$_2$Cl$_2$ (42 mg, 0.1 mmol) in methanol (5 mL) was heated at reflux overnight (~16 h) to afford a pale yellow solid, which was collected by filtration, washed with methanol and ether, and air-dried (17 mg, 36% yield). X-ray quality crystals were obtained by mixing equal volumes (1 mL) of *cis*-Pt(DMSO)$_2$Cl$_2$ (12.5 mM) and *N*(SO$_2$Me)-1,1′-Me$_2$dma (12.5 mM) in acetonitrile and allowing the mixture to stand at room temperature. Yellow crystals collected within 2 days were characterized by single-crystal X-ray crystallography. The ^{1}H NMR data for the solid and the crystals are identical. ^{1}H NMR signals (ppm) in DMSO-d_6: 7.20 (2H, H5/5′), 7.10 (2H, H4/4′), 5.25 (d, J = 17.6 Hz, 2H, CH_2), 5.13 (d, J = 17.8 Hz, 2H, CH_2), 3.72 (s, 6H, CH_3), 3.28 (s, 3H, CH_3). ^{1}H NMR signals (ppm) in DMF-d_7: 7.28 (2H, H5/5′), 7.18 (2H, H4/4′), 5.47 (d, J = 16.5 Hz, 2H, CH_2), 5.29 (d, J = 16.3 Hz, 2H, CH_2), 3.87 (s, 6H, CH_3), 3.41 (s, 3H, CH_3).

Pt(*N*(SO$_2$Tol)1,1′-Me$_2$dma)Cl$_2$ (6). A similar procedure as for complex **5** with *N*(SO$_2$Tol)1,1′-Me$_2$dma (**2**, 36 mg, 0.1 mmol) and *cis*-Pt(DMSO)$_2$Cl$_2$ (42 mg, 0.1 mmol) afforded a pale yellow solid (20 mg, 32% yield). X-ray quality crystals were obtained by mixing equal volumes (1 mL) of *cis*-Pt(DMSO)$_2$Cl$_2$ (12.5 mM) and *N*(SO$_2$Tol)-1,1′-Me$_2$dma (12.5 mM) in acetonitrile and allowing the mixture to stand at room temperature. Yellow crystals obtained within

4 days were characterized by single-crystal X-ray crystallography. The ^{1}H NMR data for the solid and the crystals are identical. ^{1}H NMR signals (ppm) in DMSO-d_6: 7.97 (d, J = 7.9 Hz, 2H, H*2*/*6*), 7.58 (d, J = 8.0 Hz, 2H, H*3*/*5*), 7.22 (s, 2H, H5/5′), 7.10 (s, 2H, H4/4′), 5.30 (d, J = 16.1 Hz, 2H, CH_2), 4.77 (d, J = 15.7 Hz, 2H, CH_2), 3.79 (s, 6H, CH_3); the phenyl methyl signal is masked by the solvent peak. ^{1}H NMR signals (ppm) in DMF-d_7: 8.10 (d, J = 8.1 Hz, 2H, H*2*/*6*), 7.63 (d, J = 8.1 Hz, 2H, H*3*/*5*), 7.31 (2H, H5/5′), 7.18 (2H, H4/4′), 5.40 (d, J = 15.7 Hz, 2H, CH_2), 5.08 (d, J = 15.6 Hz, 2H, CH_2), 3.97 (s, 6H, CH_3), 2.52 (s, 3H, CH_3).

Reactions of Pt(*N*(SO$_2$R)1,1′-Me$_2$dma)Cl$_2$ (5, R = Me and 6, R = Tol) with N-donor Monodentate Ligands (DMAP, 4-pic, and 3,5-lutidine). A 20 mM solution of DMAP in DMSO-d_6 (0.9 mg in 600 µl) was treated with 1.6 mg of **5** (5 mM) and the solutions were monitored by ^{1}H NMR spectroscopy. Another 1 day-old 5 mM solution of **5** in DMSO-d_6 was treated with 4 molar equiv of DMAP (0.9 mg, 20 mM) and the solution was monitored by ^{1}H NMR spectroscopy. Further, a 20 mM solution of DMAP in DMSO-d_6 was treated with 1.9 mg of Pt(*N*(SO$_2$Tol)1,1′-Me$_2$dma)Cl$_2$ (**6**, 5mM) and the solution was monitored by ^{1}H NMR spectroscopy. Isolation of [Pt(*N*(SO$_2$R)1,1′-Me$_2$dma)(N-donor)$_2$](PF$_6$)$_2$-type solids/X-ray quality crystals (N-donor = 4-pic and 3,5-lut) was performed as follows.

Isolation of [Pt(*N*(SO$_2$R)1,1′-Me$_2$dma)(4-pic)$_2$](PF$_6$)$_2$ Complexes (7, R = Me and 8, R = Tol). A suspension of 3 mg of **5** in 150 µl of 4-pic was heated at 60 °C and a clear pale-yellow solution was obtained overnight. Then the solution was treated with 3.7 mg of Na_2PF_6 (4 molar equiv) dissolved in 1 ml of H_2O. The resultant milky white mixture was heated for ~5 min until became clear with two layers (a pale yellow 4-pic layer at the bottom and the aqueous layer at the top). X-ray quality white crystals of **7**, [Pt(*N*(SO$_2$Me)1,1′-Me$_2$dma)(4-pic)$_2$](PF$_6$)$_2$, were collected by allowing the clear solution to stand at room temperature for 2 days. ^{1}H NMR signals (ppm) in

DMSO-d_6 Bis1: 8.79 (d, J = 6.0 Hz, 4H, H2/6$_{4\text{-pic}}$), 7.44 (d, J = 6.0 Hz, 4H, H3/5$_{4\text{-pic}}$), 7.32 (s, 2H, H5/5′), 7.16 (s, 2H, H4/4′), 4.95 (s, 4H, CH_2), 3.64 (s, 6H, CH_3), 3.46 (s, 3H, CH_3), 2.36 (s, 6H, CH_3). Bis2: 8.93 (d, J = 5.9 Hz, 4H, H2/6$_{4\text{-pic}}$), 7.50 (d, J = 6.0 Hz, 4H, H3/5$_{4\text{-pic}}$), 7.32 (s, 2H, H5/5′), 7.37 (s, 2H, H4/4′), 5.54 (d, J = 16.4 Hz, 2H, CH_2), 5.20 (d, J = 16.4 Hz, 2H, CH_2), 3.73 (s, 6H, CH_3), 2.36 (s, 6H, CH_3), the sulfonamide methyl signal is masked by the HOD peak. From a similar experiment performed using **6** produced pale-orange color X-ray quality crystals of [Pt(*N*(SO_2Tol)1,1′-Me_2dma)(4-pic)$_2$](PF_6)$_2$·Me_2CO (**8**) (One drop of acetone is added to the final solution to aid the crystallization). ^{1}H NMR signals (ppm) in DMSO-d_6 Bis1: 8.87 (d, J = 5.7 Hz, 4H, H2/6$_{4\text{-pic}}$), 8.09 (d, J = 8.1 Hz, 2H, H*2*/*6*), 7.64 (m, 2H, H*3*/*5*), 7.49 (d, J = 6.0 Hz, 4H, H3/5$_{4\text{-pic}}$), 7.33 (s, 2H, H5/5′), 7.21 (s, 2H, H4/4′), 4.84 (s, 4H, CH_2), 3.60 (s, 6H, CH_3), the phenyl methyl signal is masked by the solvent peak, 2.38 (s, 6H, CH_3). Bis2: 8.87 (s, 4H, H2/6$_{4\text{-pic}}$), 8.03 (d, J = 8.0 Hz, 2H, H*2*/*6*), 7.64 (m, 2H, H*3*/*5*), 7.45 (d, J = 6.3 Hz, 4H, H3/5$_{4\text{-pic}}$), 7.33 (s, 2H, H5/5′), 7.37 (s, 2H, H4/4′), 5.35 (d, J = 16.3 Hz, 2H, CH_2), 5.20 (d, J = 16.4 Hz, 2H, CH_2), 3.84 (s, 6H, CH_3), the phenyl methyl signal is masked by the solvent peak, 2.34 (s, 6H, CH_3).

Isolation of [Pt(*N*(SO_2R)1,1′-Me_2dma)(3,5-lut)$_2$](PF_6)$_2$ Complexes (9, R = Me and 10, R = Tol). A suspension of 3 mg of **5** in 150 µl of 3,5-lutidine was heated at 80 °C. A white solid has deposited overnight, which was filtered and treated with 1 ml of aqueous solution of Na_2PF_6 (4 molar equiv, 3.7 mg). Another 1 ml of acetone was added to the resultant milky white mixture. The resultant clear colorless solution was kept at room temperature to allow the solvent to evaporate slowly. A white crystalline solid of **9**, [Pt(*N*(SO_2Me)1,1′-Me_2dma)(3,5-lut)$_2$](PF_6)$_2$ was obtained overnight. ^{1}H NMR signals (ppm) in DMSO-d_6 Bis1: 8.77 (s, 4H, H2/6$_{3,5\text{-lut}}$), 7.67 (s, 2H, H4$_{3,5\text{-lut}}$), 7.32 (s, 2H, H5/5′), 7.15 (s, 2H, H4/4′), 4.95 (s, 4H, CH_2), 3.64 (s, 6H, CH_3), 3.49 (s, 3H, CH_3), 2.24 (s, 12H, CH_3). Bis2: 8.87 (s, 4H, H2/6$_{3,5\text{-lut}}$), 7.67 (s, 2H, H4$_{3,5\text{-lut}}$), 7.32 (s, 2H, H5/5′),

7.41 (s, 2H, H4/4′), 5.50 (d, *J* = 16.1 Hz, 2H, CH_2), 5.23 (d, *J* = 16.1 Hz, 2H, CH_2), 3.74 (s, 6H, CH_3), 3.35 (s, 3H, CH_3), 2.29 (s, 12H, CH_3). ESI-MS (*m/z*): $[M]^{2+}$ = 346.1106. Calcd for $[M]^{2+}$ = 346.1105. A similar experiment performed using **6** produced white color X-ray quality crystals of [Pt(*N*(SO_2Tol)1,1′-Me_2dma)(3,5-lut)$_2$](PF_6)$_2$·2Me_2CO (**10**). ^{1}H NMR signals (ppm) in DMSO-d_6 Bis1: 8.87 (s, 4H, H2/6$_{3,5\text{-lut}}$), 8.13 (d, *J* = 7.8 Hz, 2H, H*2*/*6*), 7.71 (s, 2H, H4$_{3,5\text{-lut}}$), 7.66 (bs, 2H, H*3*/*5*), 7.32 (s, 2H, H5/5′), 7.20 (s, 2H, H4/4′), 4.76 (s, 4H, CH_2), 3.59 (s, 6H, CH_3), the phenyl methyl signal is masked by the solvent peak, 2.28 (s, 12H, CH_3). Bis2: 8.83 (s, 4H, H2/6$_{3,5\text{-lut}}$), 8.04 (d, *J* = 8.0 Hz, 2H, H*2*/*6*), 7.66 (bs, 2H, H*3*/*5*), 7.66 (bs, 2H, H4$_{3,5\text{-lut}}$), 7.33 (s, 2H, H5/5′), 7.41 (s, 2H, H4/4′), 5.33 (d, *J* = 16.3 Hz, 2H, CH_2), 5.21 (d, *J* = 16.4 Hz, 2H, CH_2), 3.85 (s, 6H, CH_3), the phenyl methyl signal is masked by the solvent peak, 2.24 (s, 12H, CH_3).

G Adduct Formation with Pt(*N*(SO_2R)1,1′-Me_2dma)Cl_2 (5 and 6). Two 25 mM solutions of 9-MeG and Guo were treated separately with 1.6 mg of **5** in DMSO-d_6 to make each solution 5 mM in complex **5**. The solutions were maintained at 25 °C and monitored by ^{1}H NMR spectroscopy until there was no change in the bound vs free H8 signal intensity. Another 50 mM solution of 9-MeG was treated with 1.6 mg of **5** (5 mM) in DMSO-d_6. In another experiment, a 1-day old 5 mM solution of **5** in DMSO-d_6 was treated with 5 molar equiv of 9-MeG (2.5 mg, 25 mM). Another 25 mM solution of 9-MeG was treated with 1.6 mg of **5** (5 mM) in DMF-d_7. The solutions were maintained at 25 °C and monitored by ^{1}H NMR spectroscopy. Two 25 mM solutions of 9-MeG and Guo) were treated with 1.9 mg of **6** in DMSO-d_6 to make each solution 5 mM in complex **6** and the solutions were monitored with time by ^{1}H NMR spectroscopy.

4.3 Results and Discussion

Synthesis of *N*(SO_2R)1,1′-Me_2dma Derivatives and Their Re(I) and Pt(II) Complexes. The *N*(SO_2R)1,1′-Me_2dma ligands (**1** and **2**) were synthesized by coupling the appropriate

sulfonamide compound with two equiv of 2-(chloromethyl)-1-methylimidazole under basic conditions (Figure 4.2), a similar synthetic route to that used in the synthesis of the analogous ligands containing pyridyl rings ($N(SO_2R)Me_ndpa$).[16] However, the purification of the new ligands was more difficult and required more polar eluents (see Experimental Section) compared to the $N(SO_2R)Me_ndpa$[16] ligands, perhaps owing to the higher hydrophilicity of the new ligands than the latter ligands. Using a slightly modified method reported in literature[30] we obtained $[Re(CO)_3(N(SO_2R)1,1'\text{-}Me_2dma)]ClO_4$ complexes **3** and **4** by using $[Re(CO)_3(CH_3CN)_3]ClO_4$ as the metal precursor (Figure 4.2). The $Pt(N(SO_2R)1,1'\text{-}Me_2dma)Cl_2$ complexes (**5** and **6**) were synthesized by employing a similar procedure as used in the synthesis of $Pt(N(SO_2R)Me_ndpa)Cl_2$ complexes (using *cis*-$Pt(DMSO)_2Cl_2$ in methanol to react with the ligands at reflux), which produced the neutral Pt(II) complexes (**5** and **6**) in good yield. Even after several years, no evidence for chelate ligand dissociation was found in DMSO-d_6 (complexes **3**–**6**) or in DMF-d_7 (complexes **5** and **6**) indicating that the ligands **1** and **2** can form robust $[Re(CO)_3(N(SO_2R)1,1'\text{-}Me_2dma)]ClO_4$ and $Pt(N(SO_2R)1,1'\text{-}Me_2dma)Cl_2$ complexes.

Structural Results. Crystal data and details of the structural refinement for all complexes are summarized in Table 4.1. Selected bond lengths and angles are reported in Tables 4.2 and 4.3. The ORTEP plots of **5** and **6** and cations of **3**, **7**, **8**, and **10** (Figures 4.3 and 4.4) show the numbering system used to describe the solid-state data.

The molecular structures of $[Re(CO)_3(N(SO_2Me)1,1'\text{-}Me_2dma)]^+$ (**3**) and $Pt(N(SO_2R)1,1'\text{-}Me_2dma)Cl_2$ (**5**, R = Me and **6**, R = Tol) complexes (Figure 4.3) confirm that the new imidazolyl ligands (**1** and **2**) coordinate tridentately to the *fac*-$[Re(I)(CO)_3]^+$ core and bidentately to the $Pt(II)Cl_2$ core. In $[Re(CO)_3(N(SO_2Me)1,1'\text{-}Me_2dma)]ClO_4$ (**3**), all three nitrogen atoms of the tridentate ligand occupy one face, and the three carbonyl ligands occupy the other face. In the Pt

Table 4.1. Crystal Data and Structure Refinement for [Re(CO)$_3$(*N*(SO$_2$Me)1,1′-Me$_2$dma)]ClO$_4$ (**3**), Pt(*N*(SO$_2$Me)1,1′-Me$_2$dma)Cl$_2$ (**5**), Pt(*N*(SO$_2$Tol)1,1′-Me$_2$dma)Cl$_2$ (**6**), [Pt(*N*(SO$_2$Me)1,1′-Me$_2$dma)(4-pic)$_2$](PF$_6$)$_2$ (**7**), [Pt(*N*(SO$_2$Tol)1,1′-Me$_2$dma)(4-pic)$_2$](PF$_6$)$_2$ (**8**), and [Pt(*N*(SO$_2$Tol)1,1′-Me$_2$dma)(3,5-lut)$_2$](PF$_6$)$_2$ (**10**)

	3	**5**	**6**	**7**	**8**	**10**
formula	$C_{14}H_{17}N_5O_5ReS\cdot ClO_4$	$C_{11}H_{17}Cl_2N_5O_2PtS$	$C_{17}H_{21}Cl_2N_5O_2PtS$	$C_{23}H_{31}N_7O_2PtS\cdot 2(PF_6)$	$C_{29}H_{35}N_7O_2PtS\cdot 2(PF_6)\cdot Me_2CO$	$C_{31}H_{39}N_7O_2PtS\cdot 2(PF_6)\cdot 2Me_2CO$
fw	653.03	549.34	625.44	954.64	1088.81	1174.93
crystal system	monoclinic	orthorhombic	triclinic	triclinic	triclinic	monoclinic
space group	*C*2/*c*	*Pnma*	*P*ī	*P*ī	*P*ī	P2$_1$/*n*
a (Å)	18.9064(3)	9.1464(9)	9.2992(3)	10.5913(9)	10.4923(2)	9.8237(10)
b (Å)	10.3460(2)	15.1789(17)	9.7727(4)	11.3539(9)	13.6072(4)	8.9302(9)
c (Å)	22.1733(4)	12.055(1)	12.2223(6)	15.9287(14)	15.1738(4)	53.291(6)
α (deg)	90	90	112.967(3)	71.804(6)	75.610(2)	90
β (deg)	100.861(1)	90	91.062(3)	85.583(6)	89.200(2)	90.185(5)
γ (deg)	90	90	94.381(3)	62.623(5)	77.032(5)	90
V (Å^3)	4259.53(13)	1673.6 (3)	1018.29(8)	1610.8 (2)	2042.88 (9)	4675.0(8)
T (K)	105	90	90	90	90	150
Z	8	4	2	2	2	4
ρ_{calc} (g/m^3)	2.037	2.180	2.040	1.968	1.770	1.669

(Table 4.1. continued)

	3	**5**	**6**	**7**	**8**	**10**
abs coeff (mm^{-1})	5.99	8.84	7.28	4.63	3.66	7.52
$2\theta_{max}$ (°)	95.2	51.4	54.2	61.2	66.6	136.8
R[F2>2σ(F2)]	0.028	0.032	0.029	0.040	0.037	0.039
Rw	0.057	0.062	0.101	0.080	0.086	0.090
res. dens. (e $Å^{-3}$)	3.37, -2.30	1.84, -1.00	2.95, -1.94	2.34, -1.47	2.50, -2.06	0.82, -1.22
data/parameters	19874/283	1659/108	4005/256	9846/438	15504/567	32022/663

[a] $R = (\sum||F_o| - |F_c||)/\sum|F_o|$. [b] $Rw = [\sum[w(F_o^2 - F_c^2)^2]/\sum[w(F_o^2)^2]]^{1/2}$, in which $w = 1/[\sigma^2(F_o^2) + (dP)^2 + (eP)]$ and $P = (F_o^2 + 2F_c^2)/3$.

complexes **5** and **6**, two cis coordination positions are occupied by the imidazolyl nitrogen atoms creating a large 8-membered chelate ring. The remaining coordination positions are occupied by two Cl atoms. As discussed in our previous work of the analogous ligands containing pyridyl rings, *N*(SO_2R)Me_ndpa,[16] we believe that the different coordination modes exhibited by the new ligands in Pt(*N*(SO_2R)1,1′-Me_2dma)Cl_2 and [Re($CO)_3$(*N*(SO_2R)1,1′-Me_2dma)]ClO_4 complexes could be mainly due to steric restraints as a tertiary sulfonamide N with two adjacent 5-membered chelate rings must anchor a facially coordinated rather than a meridionally coordinated ligand.

Table 4.2. Selected Bond Distances (Å) and Angles (deg) for [Re($CO)_3$(*N*(SO_2Me)1,1′-Me_2dma)]ClO_4 (**3**)

Bonds		Angles	
Re–N1	2.1493(11)	N1–Re–N2	75.29(4)
Re–N2	2.3706(10)	N1–Re–N3	83.59(4)
Re–N3	2.1536(10)	N2–Re–N3	75.45(4)
Re–C1	1.9040(14)	S1–N2–C9	108.16(7)
Re–C2	1.9233(13)	S1–N2–C10	108.69(7)
Re–C3	1.9274(13)	C9–N2–C10	111.39(9)
S1–O4	1.4315(10)	Re–N2–S1	110.62(5)
S1–O5	1.4328(11)	Re–N2–C9	109.45(8)
N2–S1	1.7477(10)	Re–N2–C10	108.54(7)
N1−N3[a]	2.868(2)	N1–Re–C2	95.11(5)
		N1–Re–C3	93.51(5)
		N3–Re–C2	97.76(5)
		N3–Re–C1	93.93(5)
		dihedral angle[b]	87.67, 82.29
		Re−N−centroid	170.65, 171.28

[a]Non-bonded distance between the two atoms. [b]Angle between the coordination plane (defined by the Re, N1, N3, O1 and O3 atoms) and the pyridyl ring planes.

Table 4.3. Selected Bond Distances (Å) and Angles (deg) for Pt(*N*(SO_2Me)1,1′-Me_2dma)Cl_2 (**5**), Pt(*N*(SO_2Tol)1,1′-Me_2dma)Cl_2 (**6**), [Pt(*N*(SO_2Me)1,1′-Me_2dma)(4-pic)$_2$](PF_6)$_2$ (**7**), [Pt(*N*(SO_2Tol)1,1′-Me_2dma)(4-pic)$_2$](PF_6)$_2$ (**8**) and [Pt(*N*(SO_2Tol)1,1′-Me_2dma)(3,5-lut)$_2$](PF_6)$_2$ (**10**)

	5	**6**	**7**	**8**	**10**
Pt–N1	2.004(5)	2.020(6)	2.002(3)	2.011(3)	2.015(4)
N2−Pt[a]	3.912	3.765(5)	3.050(4)	3.083(3)	3.0840(4)
Pt–N3	2.004(5)	2.027(6)	2.004(3)	2.023(2)	2.016(4)
Pt–Cl1/N6	2.3051(15)	2.313(2)	2.018(3)	2.022(2)	2.017(4)
Pt–Cl2/N7	2.3051(15)	2.2925(16)	2.021(3)	2.014(3)	2.017(4)
S1–O1	1.425(5)	1.434(6)	1.424(3)	1.423(3)	1.428(4)
S1–O2	1.425(5)	1.433(6)	1.436(3)	1.428(3)	1.430(4)
N2–S1	1.641(7)	1.641(7)	1.626(3)	1.641(3)	1.649(4)
S1−Pt[a]	5.532	5.343(2)	3.726(1)	3.7266(8)	3.877(2)
N1–Pt–N3	88.8 (3)	93.2 (2)	90.60 (13)	91.49(10)	89.00(14)
S1–N2–C4	116.3 (4)	116.9 (4)	119.6 (3)	118.0(2)	117.3(3)
S1–N2–C5	116.3 (4)	119.3 (5)	117.3 (3)	118.4(2)	117.0(3)

(Table 4.3 continued)

	5	**6**	**7**	**8**	**10**
C4–N2–C5	114.7 (7)	118.5 (6)	118.8 (3)	117.8(3)	117.1(4)
N1–Pt–Cl2/N7	177.87 (15)	176.52 (19)	176.98 (14)	176.62(10)	177.86(16)
N1−Pt−Cl1/N6	89.56(14)	88.3(2)	90.75(13)	88.83(11)	91.61(14)
N3–Pt–Cl1/N6	177.87 (15)	178.36 (15)	178.23 (14)	178.48(10)	178.44(16)
N3−Pt−Cl2/N7	89.56(14)	87.31(15)	91.58(14)	89.63(11)	91.59(15)
Cl1/N6–Pt–Cl2/N7	92.07 (8)	91.10 (7)	87.11 (14)	89.97(11)	87.75(15)
dihedral angle[b]	74.85	66.61, 71.56	84.96, 54.19	72.39, 57.69	84.99, 57.88
Pt− N−centroid	176.87	167.81, 173.67	176.66, 176.82	175.44, 174.19	177.72, 175.63
N1−N3[a]	2.805(6)	2.941(8)	2.847(5)	2.890(3)	2.825(5)

[a]Non-bonded distance between the two atoms. [b]Angle between the coordination plane (defined by the Pt, N1, N3, and two Cl atoms) and the imidazolyl ring planes.

The length of the Re−N(sulfonamide) bond (Table 4.2) in **3** (2.3706(10) Å) is longer than the typical range (2.23−2.29 Å) reported for Re−N(sp^3) bonds,[31-32] while the Re−N1 and Re−N3 bond distances of **3** (2.1493(11) and 2.1536(10) Å) are in the typical range (2.14−2.18 Å) for Re−N(sp^2) bonds.[6,31,33-34] As discussed in the previous work of $[Re(CO)_3(N(SO_2R)Me_ndpa)]^+$ and $Pt(N(SO_2R)Me_ndpa)Cl_2$ complexes,[16] the structural features such as the angles around the sulfonamide N and the N−S bond lengths of the $Pt(N(SO_2R)1,1'\text{-}Me_2dma)Cl_2$ complexes (**5** and **6**) are consistent with the uncoordinated tertiary sulfonamide group, while these structural features of **3** ($[Re(CO)_3(N(SO_2Me)1,1'\text{-}Me_2dma)]ClO_4$) are consistent with the coordinated NSO_2Me group (Tables 4.2 and 4.3). Similarly, the structural metrics of the molecular structures of **7** = $[Pt(N(SO_2Me)1,1'\text{-}Me_2dma)(4\text{-pic})_2](PF_6)_2$, **8** = $[Pt(N(SO_2Tol)1,1'\text{-}Me_2dma)(4\text{-pic})_2](PF_6)_2$, and **10** = $[Pt(N(SO_2Tol)1,1'\text{-}Me_2dma)(3,5\text{-lut})_2](PF_6)_2$ are also consistent with the uncoordinated sulfonamide group (Table 4.3).

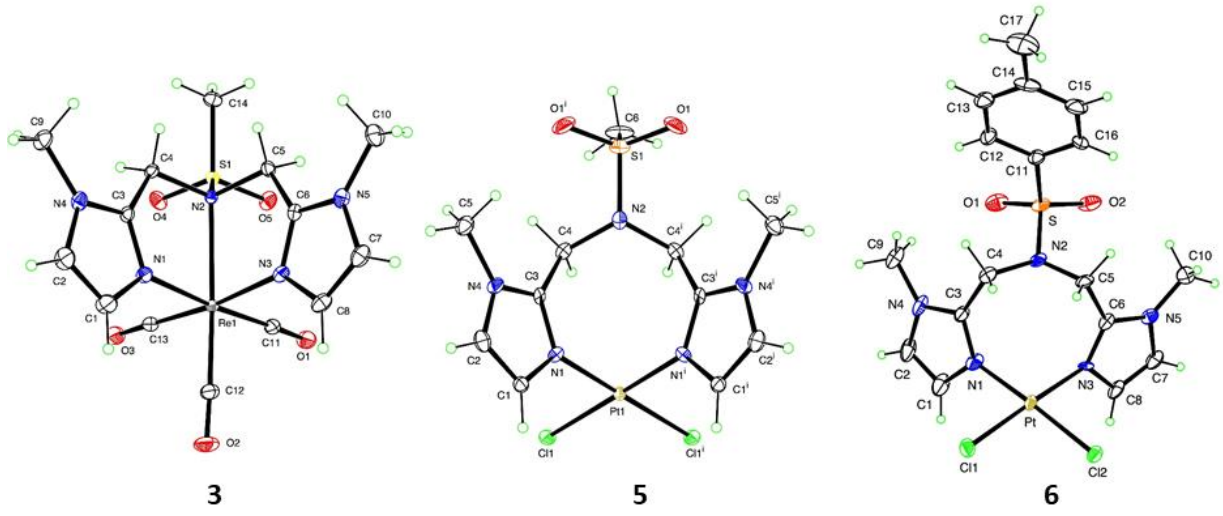

Figure 4.3. ORTEP plots of complexes $[Re(CO)_3(N(SO_2Me)1,1'\text{-}Me_2dma)]ClO_4$ (**3**), $Pt(N(SO_2Me)1,1'\text{-}Me_2dma)Cl_2$ (**5**), and $Pt(N(SO_2Me)1,1'\text{-}Me_2dma)Cl_2$ (**6**). Thermal ellipsoids are drawn with 50% probability.

The Pt−N(1) and Pt−N(3) bond lengths (Table 4.3) in all the Pt complexes (**5**, **6**, **7**, **8**, and **10**) are in the range typically reported for Pt−N(sp^2) bonds (1.99−2.08 Å).[16,22,24-25,35] The N1−Pt−N3 bite angles (~90°, Table 4.3) of these complexes are comparable to the angles of the reported platinum complexes containing relatively large uncommon 8-membered chelate rings (average 89.5°).[16,36-38] The dihedral angles (defined as the angle between the coordination plane and the imidazolyl ring planes) of **5** and **6** (67-75°, Table 4.3) are not as large as the dihedral angles of the reported platinum complexes containing 8-membered chelate rings (average value ~83°),[16,36-38] but significantly larger than the values reported for complexes of smaller chelating ligands (<65° for platinum(II) complexes of 5-, 6- and 7-membered chelate rings).[16] In order to understand the special structural features of relatively rare square planar Pt(II) complexes containing 8-membered chelate rings, in a previous work we have analyzed more than fifty molecular structures of *cis* Pt(II) complexes containing two aromatic ring nitrogens (pyridyl/imidazolyl) and two halides as the ligating atoms (data obtained from the CCDC data base).[16] The study indicated that the certain structural features such as the dihedral angles and the N1−Pt−N3 bite angles of the complexes differ based on the chelate ring size; the dihedral angles of the studied complexes increase almost linearly with the increasing chelate ring size. Also, the N1−Pt−N3 bite angles increase with the increasing ring size. These structural features in **5** and **6** follow the trends we found in our previous analysis of structural features of chelate in platinum complexes, including the few containing relatively large 8-membered chelate rings.[16]

[Pt(*N*(SO_2R)1,1′-Me_2dma)(N-donor)$_2$](PF_6)$_2$ crystalline solids (**7** = [Pt(*N*(SO_2Me)1,1′-Me_2dma)(4-pic)$_2$](PF_6)$_2$, **8** = [Pt(*N*(SO_2Tol)1,1′-Me_2dma)(4-pic)$_2$](PF_6)$_2$, and **10** = [Pt(*N*(SO_2Tol)1,1′-Me_2dma)(3,5-lut)$_2$](PF_6)$_2$) were isolated by treating **5** and **6** (Pt(*N*(SO_2R)1,1′-Me_2dma)Cl_2) with the N-donor ligand. The molecular structures of **7**, **8** and **10** (Figure 4.4) confirm

that the chelate ligand in **5** and **6** are not displaced by the high temperature conditions (60 °C or 80 °C). In contrast, 40% of the bound chelate ligand dissociated within 9 days when Pt(*N*(SO_2R)3,3′,5,5′-Me_4dpa)Cl_2 complexes were dissolved in DMSO-d_6 at room temperature.[16]

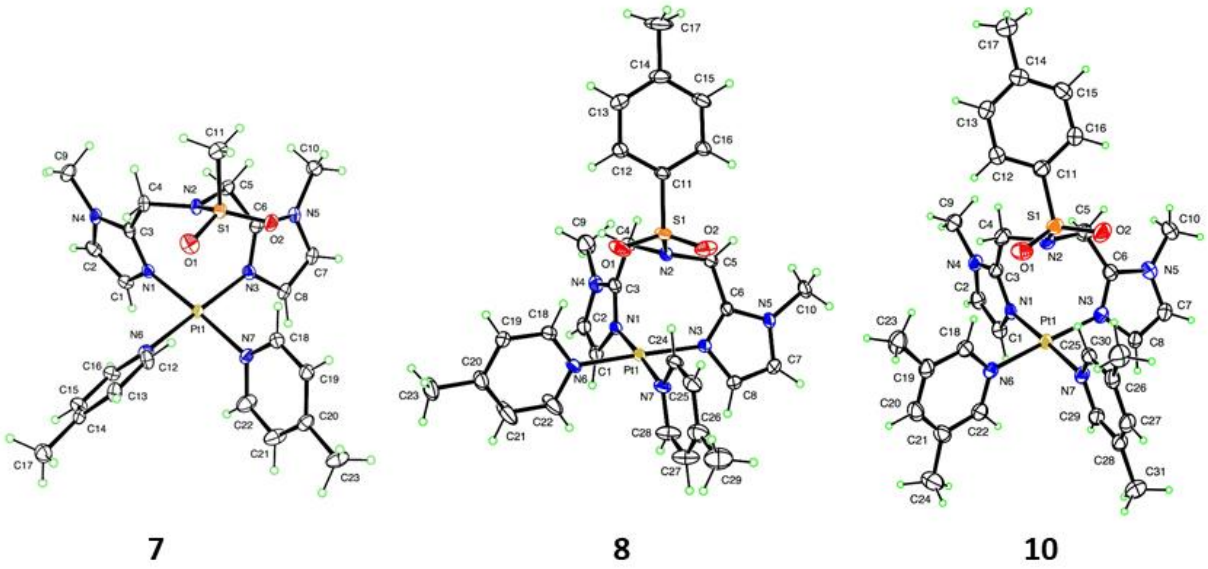

Figure 4.4. ORTEP plots of complexes [Pt(*N*(SO_2Me)1,1′-Me_2dma)(4-pic)$_2$](PF_6)$_2$ (**7**), [Pt(*N*(SO_2Tol)1,1′-Me_2dma)(4-pic)$_2$](PF_6)$_2$·Me_2CO (**8**), and [Pt(*N*(SO_2Tol)1,1′-Me_2dma)(3,5-lut)$_2$](PF_6)$_2$·2Me_2CO (**10**). Thermal ellipsoids are drawn with 50% probability.

The location of the sulfonamide group is the main structural difference between the chelate ligands in the dichloro complexes, **5** and **6**, and the chelate ligands in [Pt(*N*(SO_2R)1,1′-Me_2dma)(N-donor)$_2$](PF_6)$_2$ (**7**, **8** and **10**, Figure 4.4). In order to explain the difference in location of the sulfonamide group in the two types of complexes, a new plane (plane A) is defined as follows: Plane A is perpendicular to the coordination plane and goes through the two N atoms of the imidazolyl rings of the carrier ligand (Figure 4.5). In **5** and **6** and in the previously reported Pt(*N*(SO_2R)Me_ndpa)Cl_2 complexes (R = Me or Tol), the sulfonamide group and the rest of the carrier ligand are almost completely on the same side of Plane A as the sulfonamide group, which projects out from the coordination sphere (chelate ligand conformation SO_2R-out). In contrast, in **7**, **8**, and **10**, most of the carrier ligand is on the opposite side of Plane A as the sulfonamide group,

which projects toward the coordination sphere (chelate ligand conformation SO_2R-in). Furthermore, the reported molecular structures of *fac*-[$Re(CO)_3$(chelate)]Y complexes of the similar sulfonamide-incorporated tridentate ligands[6-7,16] and of [$Re(CO)_3$(*N*(SO_2Me)1,1′-Me_2dma)]ClO_4 (**3**, Figure 4.3) show that the chelate ligand conformation is "SO_2R-in" to allow formation of the Re–N(sulfonamide bond). The observation of the sulfonamide group in two different locations in different molecular structures of Pt(II) complexes indicates that a bidentate chelate ligand with the sulfonamide group uncoordinated to Pt(II) center has enough dynamic freedom to exchange between SO_2R-in and SO_2R-out conformations. ^{1}H NMR data discussed below also provide evidence for the inversion of the SO_2R group at the N(sulfonamide) atom and/or the rotation around the Pt–N bond in the Pt(II) complexes studied here.

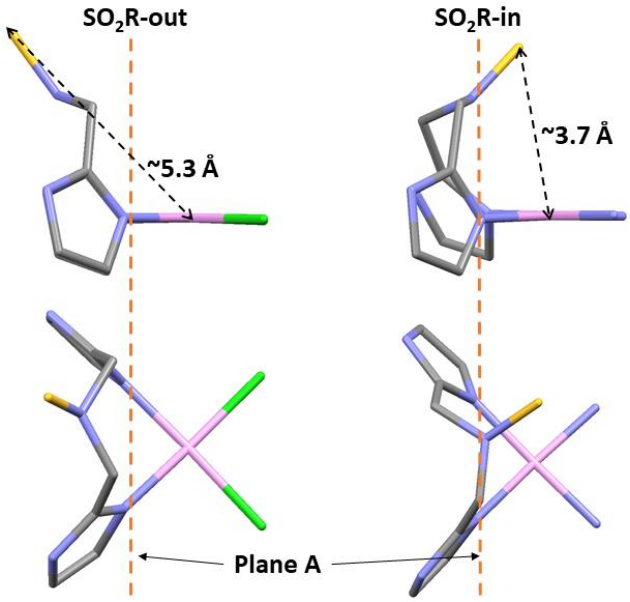

Figure 4.5. Line drawings of Pt(*N*(SO_2Me)1,1′-Me_2dma)Cl_2 (**5**, left) and [Pt(*N*(SO_2Me)1,1′-Me_2dma)(4-pic)$_2$]$(PF_6)_2$ (**7**, right) showing the location of the sulfonamide group in each complex. Plane A is indicated as an orange broken-line. The 1/1′-Me groups, hydrogen atoms in **5** and **7** and 4-pic rings in **7** are hidden for clarity.

NMR Spectroscopy. The ligands, **1** and **2** (in $CDCl_3$ and DMSO-d_6) and their Re and Pt complexes, **3**–**10** (in DMSO-d_6 and/or in DMF-d_7) reported here were characterized by ^{1}H NMR spectroscopy. Using the atom-numbering scheme in Figure 4.2, we assigned the proton signals of

the complexes by analyzing the chemical shift, splitting pattern, integration and data from ^{1}H-^{1}H ROESY NMR experiments as discussed below. ^{1}H NMR data and assignments are presented in the Experimental Section; see also Tables 4.4 and 4.5.

^{1}H NMR Assignments of [Re(CO)$_3$(*N*(SO$_2$R)1,1′-Me$_2$dma)]ClO$_4$ Complexes (3, R = Me and 4, R = Tol) and Pt(*N*(SO$_2$R)1,1′-Me$_2$dma)Cl$_2$ (5, R = Me and 6, R = Tol). The ^{1}H NMR spectra recorded in DMSO-d_6 (and also in DMF-d_7 for **5** and **6**) show that all the aromatic signals of the free ligands **1** and **2** upon metal coordination to form **3**–**6** were shifted downfield, a result caused by the inductive effect of the Pt(II) or Re(I) metal center (Figure 4.6). The [Re(CO)$_3$(*N*(SO$_2$R)1,1′-Me$_2$dma)]ClO$_4$ complexes (**3** and **4**) in DMSO-d_6 do not show any change in the spectra with time. The ^{1}H NMR assignments of **3** and **4** were based on their ROESY spectra recorded in DMSO-d_6 (a selected region of the ROESY spectrum of **3** is presented in Supporting Information) and arguments similar to those used for the previously reported [Re(CO)$_3$(*N*(SO$_2$R)Me$_n$dpa)]PF$_6$[16] and [Re(CO)$_3$(*N*(SO$_2$R)dpa)]PF$_6$[6] complexes.

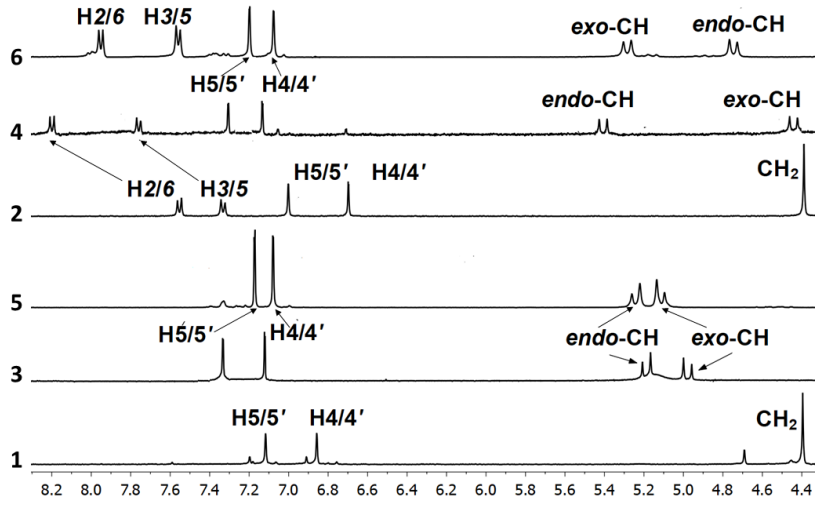

Figure 4.6. Selected region of ^{1}H NMR spectra in DMSO-d_6 at 25 °C (shifts in ppm) of *N*(SO$_2$Me)1,1′-Me$_2$dma (**1**), [Re(CO)$_3$(*N*(SO$_2$Me)1,1′-Me$_2$dma)]ClO$_4$ (**3**), Pt(*N*(SO$_2$Me)1,1′-Me$_2$dma)Cl$_2$ (**5**), *N*(SO$_2$Tol)1,1′-Me$_2$dma (**2**), [Re(CO)$_3$(*N*(SO$_2$Tol)1,1′-Me$_2$dma)]ClO$_4$ (**4**), and Pt(*N*(SO$_2$Tol)1,1′-Me$_2$dma)Cl$_2$ (**6**).

Table 4.4. Selected ^{1}H NMR Chemical Shifts for the *N*(SO_2R)1,1′-Me_2dma Free Ligands (**1** and **2**) and for Their Re(I) (**3** and **4**) and Pt(II) (**5** and **6**) Complexes (ppm, DMSO-d_6, 25 °C). ^{1}H NMR Chemical Shifts of the Platinum Complexes in DMF-d_7 also Presented within Brackets

	H5/5′	H4/4′	CH_2	1/1′-Me	SO_2Me	SO_2Tol		
						H*2/6*	H*3/5*	Me
1	7.12	6.86	4.40	3.61	3.05	-	-	-
3	7.34	7.13	5.20[a], 4.98[b]	3.85	3.66	-	-	-
5	7.20 (7.28)	7.10 (7.18)	5.25 (5.47)[a], 5.13 (5.29)[b]	3.72 (3.87)	3.28 (3.41)	-	-	-
2	7.01	6.70	4.30	3.54	-	7.56	7.34	2.38
4	7.29	7.13	5.40[a], 4.44[b]	3.54	-	8.19	7.74	2.56
6	7.22 (7.31)	7.10 (7.18)	5.30 (5.40)[a], 4.77 (5.08)[b]	3.79 (3.97)	-	7.97 (8.10)	7.58 (7.63)	2.50[c] (2.52)

[a]*Endo*-CH. [b]*Exo*-CH. [c]Signal is masked by the solvent peak.

Table 4.5. Selected ^{1}H NMR Chemical Shifts for the [Pt(*N*(SO_2R)1,1′-Me_2dma)(N-donor)$_2$]$^{2+}$ Adducts or Complexes (R = Me or Tol, N-Donor = DMAP, 4-pic or 3,5-lut) (ppm, DMSO-d_6, 25 °C)

	N-donor	SO_2R	H2/6$_{DMAP/4\text{-}pic/3,5\text{-}lut}$		H5/5′		H4/4′		CH_2		1/1′-Me		Bis1:Bis2
			Bis1	Bis2	Bis1	Bis2	Bis1	Bis2	Bis1	Bis2	Bis1	Bis2	
	DMAP[a]	Me	8.23	8.52	7.31	7.28	7.13	7.42	4.91	5.80, 5.17	3.65	3.75	2.19:1
	DMAP[a]	Tol	8.33	8.40	7.33	7.31	7.19	7.44	4.82	5.46, 5.18	3.62	3.84	1.38:1
7	4-pic	Me	8.79	8.93	7.32	7.32	7.16	7.37	4.95	5.54, 5.20	3.64	3.73	2.54:1
8	4-pic	Tol	8.87	8.87	7.33	7.33	7.21	7.37	4.84[b]	5.35, 5.20	3.60	3.84	1.23:1
9	3,5-lut	Me	8.77	8.87	7.32	7.32	7.15	7.41	4.95[b]	5.50, 5.23	3.64	3.74	2.55:1
10	3,5-lut	Tol	8.87	8.83	7.32	7.33	7.20	7.41	4.76[b]	5.33, 5.21	3.59	3.85	1.27:1

[a]Spectra are recorded for a solution with excess of DMAP. [b]Very broad.

Our experience is that $PtLCl_2$ complexes in DMSO-d_6 change and also form adducts with added ligands but $PtLCl_2$ complexes usually do not change or from adducts in DMF-d_7**.** The ^{1}H NMR spectra recorded for freshly prepared DMSO-d_6 solutions of X-ray quality crystals of **5** and **6** are consistent with symmetrical Pt(*N*(SO_2R)1,1′-Me_2dma)Cl_2 complexes, as found in the solid. However, within the first 10 min of dissolution of **5** or **6** in DMSO-d_6, a new set of minor signals (denoted as $\mathbf{5}_m$ or $\mathbf{6}_m$, discussed later) start to appear. In contrast, the spectra recorded for **5** or **6** in DMF-d_7 do not change or produce new signals with time but are similar to the major set of **5** or **6** signals, respectively, in DMSO-d_6.

NMR spectra recorded in DMF-d_7 were used in assigning the signals of **5** (R = Me) and **6** (R = Tol). Both complexes have two apparent ^{1}H NMR singlets in the aromatic region, as expected for the H4/4′ and H5/5′ protons. As discussed previously for [Pt(*N*(R)1,1′-Me_2dma)Cl]Cl complexes (R = H and Me),[22] owing to the nearby quadrupolar nitrogens, these signals appear as singlets rather than doublets. In the ^{1}H-^{1}H ROESY spectrum of **5** (Figure 4.7), a strong NOE cross-peak from the 1/1′-Me signal at 3.87 ppm (assigned based on integration) to the more downfield (7.28 ppm) of two aromatic singlets allows the signal to be assigned to H5/5′. The other aromatic peak (7.18 ppm) thus can be assigned to H4/4′, an assignment supported by the absence of any NOE cross-peaks from this signal to any other peaks except to the H5/5′ signal. The methylene protons of **5** show an AB pattern in the ^{1}H NMR spectrum, an observation reported for many similar compounds and extensively discussed in our previous work.[22-25] The inequivalent methylene protons in the complex **5** (also in **6**) project toward and away from the Cl ligands and are designated as *endo*-CH and *exo*-CH protons, respectively (Figure 4.8). In the ROESY spectrum of **5**, the more upfield AB signal (5.29 ppm) showed a strong cross-peak to the 1/1′-Me signal, thus assigning it to the *exo*-CH (Figure 4.7). In the molecular structure of **5**, the 1/1′-Me protons are

closer to the *exo*-CH protons (2.97 Å) than the *endo*-CH protons (4.23 Å). The downfield AB peak (5.47 ppm) is thus assigned to the *endo*-CH.

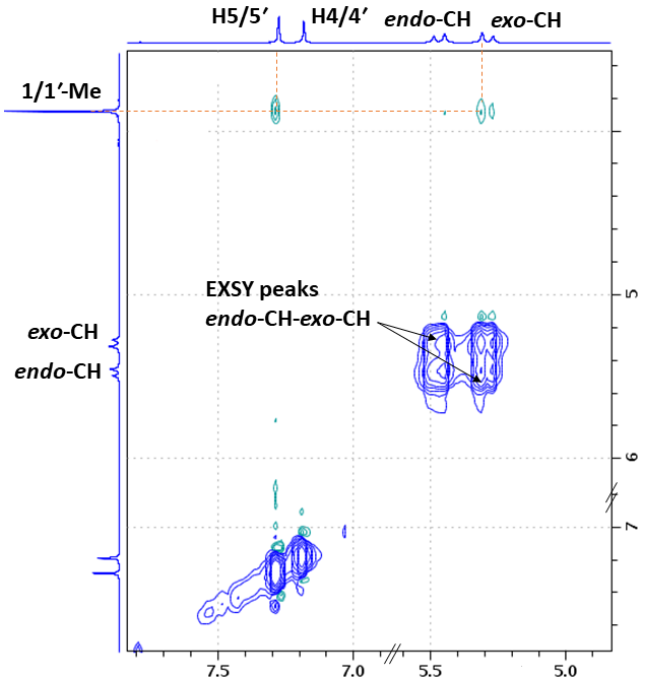

Figure 4.7. ^{1}H-^{1}H ROESY spectrum (selected region) of Pt(*N*(SO_2Me)1,1′-Me_2dma)Cl_2 (**5**) (25 °C, 10 mM, DMF-d_7, shifts in ppm).

The carrier-ligand signals including the methylene signals (two doublets instead of an AB signal) of the complex **6** were assigned in a similar manner as for **5** except for the Tol (*p*-tolyl) signals (8.10, 7.63 and 2.52 ppm). Between the two aromatic doublets corresponding to the Tol group, the more upfield doublet (8.10 ppm) was assigned to H*3*/*5* because it showed an NOE cross-peak to the tolyl methyl signal at 2.52 ppm in a ROESY spectrum of **6** in DMF-d_7 (Supporting Information). Therefore, the other doublet at 8.10 ppm was assigned to the H*2*/*6* protons.

Furthermore, the ROESY spectra of **5** and **6** in DMF-d_7 recorded at RT (25 °C), have EXSY cross-peaks between the *endo* and *exo*-CH signals (Figure 4.7 and Supporting Information). These cross-peaks indicate that the *endo*- and *exo*-CH protons are made magnetically equivalent by a dynamic process. At high T, these two doublets merge into a broad singlet, indicating that this

dynamic process becomes faster at high T. We suggest that a similar dynamic process as observed within Bis1 conformer (see below) in the [Pt(*N*(SO_2R)1,1′-Me_2dma)(N-donor)$_2$]$^{2+}$-type complexes takes place in the symmetrical Pt(*N*(SO_2R)1,1′-Me_2dma)Cl_2 dichloro complexes, **5** and **6**. In contrast, the ROESY spectrum of the [Re(CO)$_3$(*N*(SO_2Me)1,1′-Me_2dma)]ClO_4 (**3**, Supporting Information) or of other reported Pt(II) complexes of analogous ligands such as [Pt(*N*(R)1,1′-Me_2dma)Cl]Cl,[22] [Pt(*N*(H)dpa)Cl]Cl,[23] [Pt(*N*(H)6-Medpa)Cl]Cl,[24] and [Pt(*N*(H)6,6′-Me_2dpa)]Cl,[25] do not show any EXSY cross-peaks (but show NOE cross-peaks) between the methylene doublets. In these complexes, the ligands are bound tridentately. Therefore, the inversion of the central N atom and also the rotation of the pyridyl/imidazoyl rings are restricted; thus, a dynamic process making the *endo*- and *exo*-CH protons magnetically equivalent is unlikely to occur. However, the Pt(*N*(SO_2R)3,3′,5,5′-Me_4dpa)Cl_2 (R = Me or Tol) complexes in which the ligands are bound bidentately also do not show any EXSY cross-peaks (but show NOE cross-peaks) between the methylene doublets, indicating that a process in which a methylene proton's position changes between the *endo*- and *exo*-CH positions is not fast enough to give cross-peaks.

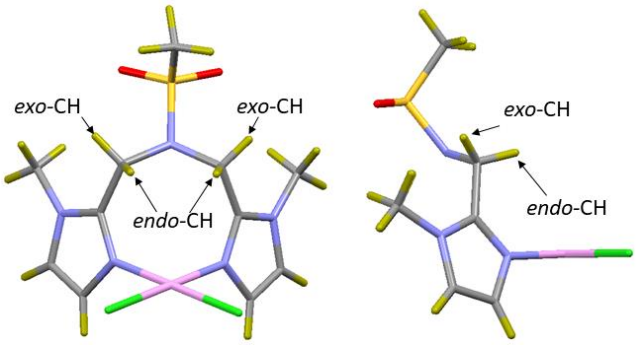

Figure 4.8. Designation of the *endo*-CH and *exo*-CH methylene protons illustrated for the structure of Pt(*N*(SO_2Me)1,1′-Me_2dma)Cl_2 (**5**).

The Pt(*N*(SO_2R)1,1′-Me_2dma)Cl_2 complexes (**5** and **6**) dissolved in DMSO-d_6 (10 mM) do not show any free ligand signals even in years-old solutions (~3 years), indicating that the imidazolyl ligands **1** and **2** remain robustly bound to Pt(II). In contrast, the analogous pyridyl

complexes, Pt(*N*(SO_2R)3,3′,5,5′-Me_4dpa)Cl_2 (R = Me or Tol), in DMSO-d_6 eventually (within a 9 d period) released the free ligand until only 60% of the ligand remained bound.[16] The relatively high robustness of the chelate in Pt(*N*(SO_2R)1,1′-Me_2dma)Cl_2 (**5** and **6**) compared to Pt(*N*(SO_2R)3,3′,5,5′-Me_4dpa)Cl_2 could be explained by the less steric hindrance in the coordination sphere of **5** and **6** as imidazole rings are smaller than the pyridyl rings and also by the higher basicity of the imidazolyl N donors (pKa (DMSO) = 6.26) than the pyridyl N donors (pKa (DMSO) = 3.4).[39]

After **5** (Pt(*N*(SO_2Me)1,1′-Me_2dma)Cl_2, 10 mM) was dissolved in DMSO-d_6, the new signals, $\mathbf{5}_m$, gradually increased for ~7 h. The results for a 10 mM solution of **6** (Pt(*N*(SO_2Tol)1,1′-Me_2dma)Cl_2) in DMSO-d_6 were similar. Interestingly, the formation of these species ($\mathbf{5}_m$ or $\mathbf{6}_m$) giving the initial minor set of signals did not affect the yield of products in the adduct formation reactions; the solutions of **5** and **6** in DMSO-d_6 readily react with different **G** derivatives (9-MeG and Guo) and with other N-donor ligands (DMAP, 4-pic and 3,5-lut) to produce expected mono or bis products (confirmed based on the NMR and X-ray structural data). Thus, the species, $\mathbf{5}_m$ or $\mathbf{6}_m$, will not be further discussed.

Reactions of Pt(*N*(SO_2R)1,1′-Me_2dma)Cl_2 Complexes (5 and 6) with DMAP, 4-pic, and 3,5-lut. A spectrum of the reaction mixture of Pt(*N*(SO_2Me)1,1′-Me_2dma)Cl_2 (**5**, 5 mM) and 4 molar equiv of DMAP (20 mM) in DMSO-d_6 recorded about 1 h after mixing contained a new set of peaks for the mono adduct, [Pt(*N*(SO_2Me)1,1′-Me_2dma)(DMAP)Cl]$^+$, in addition to the **5** and $\mathbf{5}_m$ peaks (Figure 4.9). A spectrum recorded about 7 h after mixing had peaks for a mono adduct (deduced from the integration of the bound DMAP signals and the carrier-ligand aromatic signals) along with another two new sets of peaks (in 2 to 1 ratio), but no peaks for $\mathbf{5}_m$ or **5**. The mono adduct signals disappeared in 9 d, leaving only the two sets of peaks having a ~2:1

abundance ratio (Figure 4.9). Each of these two sets of peaks are consistent with a symmetric compound and have integrations between the bound DMAP signals and the carrier-ligand aromatic signals indicating that each is a bis adduct, [Pt(*N*(SO_2Me)1,1′-Me_2dma)(DMAP)$_2$]$^{2+}$. These two sets of peaks are denoted as Bis1 (more abundant species) and Bis2 (Figure 4.9). (Very similar results were obtained when a 1 day-old 5 mM solution of **5** containing more **5**$_m$ than fresh solutions was treated with 4 molar equiv of DMAP). Similarly, a solution of Pt(*N*(SO_2Tol)1,1′-Me_2dma)Cl_2 (**6**, 5mM) and DMAP (20 mM) in DMSO-d_6 at ~9 d gave similar results as found for **5** but with a slightly different final Bis1:Bis2 ratio of a ~1.4:1 (Table 4.5 and Supporting Information).

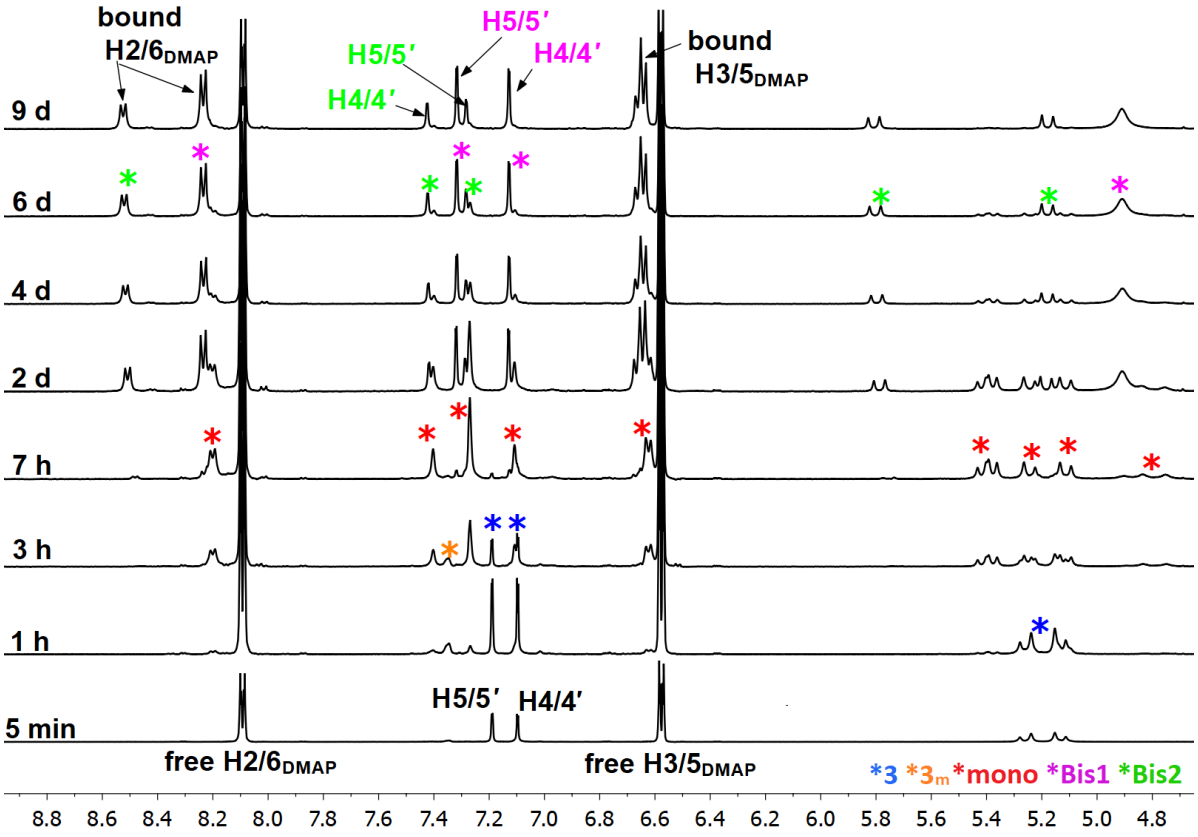

Figure 4.9. Selected region of ^{1}H NMR spectra showing the formation of mono (red) and bis adducts (Bis1-purple and Bis2-green) of **5** with DMAP at various time points after 1.6 mg of Pt(*N*(SO_2Me)1,1′-Me_2dma)Cl_2 (**5**, blue) was dissolved in a 20 mM solution of DMAP in DMSO-d_6 (25 °C, shifts in ppm).

A ROESY spectrum of the final solution of the reaction between **5** and DMAP (in DMSO-d_6 at 25 °C) shows EXSY peaks between Bis1 and Bis2, indicating that the two sets of peaks are for two conformers of the same bis adduct (Figure 4.10). This finding prompted us to prepare and isolate crystals of such a bis adduct. As described in the Experimental Section, we used liquid N-donor ligands (4-pic and 3,5-lut; this method is not suitable to use with DMAP because it is a solid at RT) to prepare [Pt(*N*(SO_2R)1,1′-Me_2dma)(N-donor)$_2$](PF_6)$_2$. The molecular structures of the resultant X-ray quality crystals (**7**, **8**, and **10**) show cis configuration in each bis complex (Figure 4.4) and ^{1}H NMR spectra of each isolated complex **7**−**9** (solid or crystals) recorded immediately after dissolving in DMSO-d_6 show two sets of peaks similar to what is observed for the bis adducts of **5** and **6** with DMAP (Figure 4.11). Furthermore, as observed for the [Pt(*N*(SO_2Me)1,1′-Me_2dma)(DMAP)$_2$]$^{2+}$ adduct, ROESY spectra recorded at 25 °C for all the isolated bis complexes (in DMSO-d_6 or DMF-d_7) show EXSY cross-peaks between Bis1 and Bis2. The ^{1}H NMR shifts of the corresponding signals of **7**−**9** are similar and are listed in Table 4.5 (selected regions of the ROESY spectra of the complexes are presented in Supporting Information).

Structural and Spectral Assignment Strategy for [Pt(*N*(SO_2R)1,1′-Me_2dma)(N-donor)$_2$]$^{2+}$ Conformers. As mentioned in the Structural Section, the location of the sulfonamide group with respect to Plane A in the molecular structures of the [Pt(*N*(SO_2R)1,1′-Me_2dma)(N-donor)$_2$]$^{2+}$ complexes **7**, **8**, and **10** (SO_2R-in, Pt−S distance is <3.8 Å) is different from the location of the sulfonamide group in the molecular structures of the dichloro Pt(*N*(SO_2R)1,1′-Me_2dma)Cl_2 complexes **5** and **6** (SO_2R-out, Pt−S distance is >5.3 Å) (Figure 4.5). This observation suggests that dynamic motion of the chelate ring occurs such that there is interchange between the SO_2R-in and SO_2R-out conformers in Pt(*N*(SO_2R)1,1′-Me_2dma)Cl_2 and [Pt(*N*(SO_2R)1,1′-Me_2dma)(N-donor)$_2$]$^{2+}$-type complexes. If this conformer interchange is slow enough on the NMR time scale,

two sets of peaks can be observed corresponding to the two conformers, which is the case for the [Pt(*N*(SO_2R)1,1′-Me_2dma)(N-donor)$_2$]$^{2+}$complexes/adducts analyzed in this study. Therefore, we suggest that the two conformers (Bis1 and Bis2) detected in the ^{1}H NMR studies for [Pt(*N*(SO_2R)1,1′-Me_2dma)(N-donor)$_2$]$^{2+}$ are likely to be to the two conformers, SO_2R-in and SO_2R-out. Below, we use 2D NMR data to assign the two sets of ^{1}H NMR signals to each conformer.

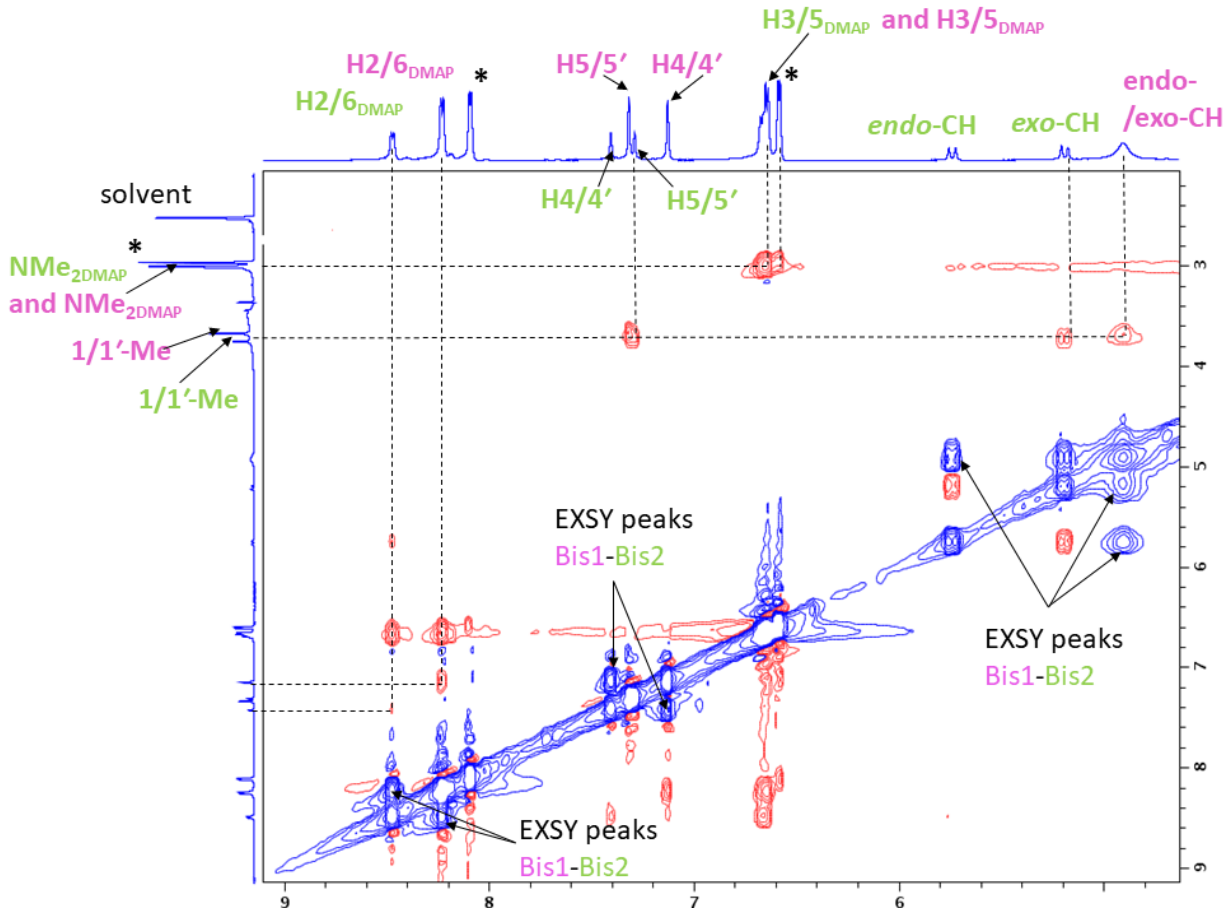

Figure 4.10. ^{1}H-^{1}H ROESY spectrum (selected region) of the [Pt(*N*(SO_2Me)1,1′-Me_2dma)(DMAP)$_2$]$^{2+}$ bis adducts, Bis1 (purple) and Bis2 (green) at 25 °C in DMSO-d_6 (shifts in ppm). *Indicates the free DMAP signals.

NOE cross-peaks from the SO_2R group signals to signals of the carrier-ligand or the bound N-donor can be analyzed to indicate whether the location of the sulfonamide group for a given set of signals is most consistent with the Bis1 or Bis2 conformer. This task could be difficult for

SO_2Me adducts because SO_2Me signals appear near the HOD peak. However, the SO_2Me singlet of Bis1 (3.49 ppm) of [Pt(*N*(SO_2Me)1,1′-Me_2dma)(3,5-lut)$_2$](PF_6)$_2$ (**9**) is well resolved from the HOD peak and has an NOE cross-peak to the H2/6$_{3,5\text{-lut}}$ singlet (8.77 ppm) of the Bis1 conformer (Figure C.4). No such NOE cross-peak is observed for the Bis2 conformer. This information indicates that Bis1 has the SO_2R-in conformation, because the SO_2Me group is closer to the bound 3,5-lut ligands in the SO_2R-in conformer than in the SO_2R-out conformer (Figure 4.5). Therefore, Bis2 can be assign to the SO_2R-out conformer. Furthermore, in the ROESY spectra of [Pt(*N*(SO_2Tol)1,1′-Me_2dma)(N-donor)$_2$](PF_6)$_2$ (**8** and **10**), the H*2/6* doublets of the Tol group of Bis1 are connected to the H2/6 signals of the N-donor (4-pic and 3,5-lut) through NOE cross-peaks (Figures C.5 and C.6). In contrast, the Bis2 signals do not show such NOE cross-peaks. In order to relate this information with structural data, we superimposed the molecular structure of [Pt(*N*(SO_2Tol)1,1′-Me_2dma)Cl_2 (**6**) with its corresponding bis complexes [Pt(*N*(SO_2Tol)1,1′-Me_2dma)(N-donor)$_2$](PF_6)$_2$ (**8** and **10**) through Pt, N1, and N2 atoms and then the non-bonded distances between the H*2/6* protons of the Tol group and the H2/6 protons of the N-donor were measured (Figures C.7). In both cases, the shortest non-bonded distances between the H*2/6* protons of the Tol group and the H2/6 protons of the N-donor measured (Figures C.7) in the SO_2R-in conformer (~ 4.0 Å) is shorter than these distances in the SO_2R-out conformer (~ 6.6 Å), supporting the above conclusion.

The ^{1}H NMR signals for the methylene protons of the Bis2 conformer in all of the [Pt(*N*(SO_2R)1,1′-Me_2dma)(N-donor)$_2$]$^{2+}$complexes/adducts are sharp doublets which are connected to each other through NOE cross-peaks. The more upfield methylene doublet of each complex is assigned to *exo*-CH, as this doublet exhibited an NOE cross-peak to the 1/1′-Me singlet (Figure 4.10 and Supporting Information). Therefore, the downfield doublet of the Bis2 conformer

in each complex is assigned to *endo*-CH; no or relatively very weak NOE cross-peak can be observed between this doublet and the 1/1′-Me singlet. In the ROESY spectra of all the [Pt(*N*(SO_2R)1,1′-Me_2dma)(N-donor)$_2$]$^{2+}$complexes/adducts, the *endo*-CH signal of the Bis2 conformer is connected to the H2/6 doublet of the N-donor (DMAP, 4-pic, and 3,5-lut) through a sharp NOE cross-peak.

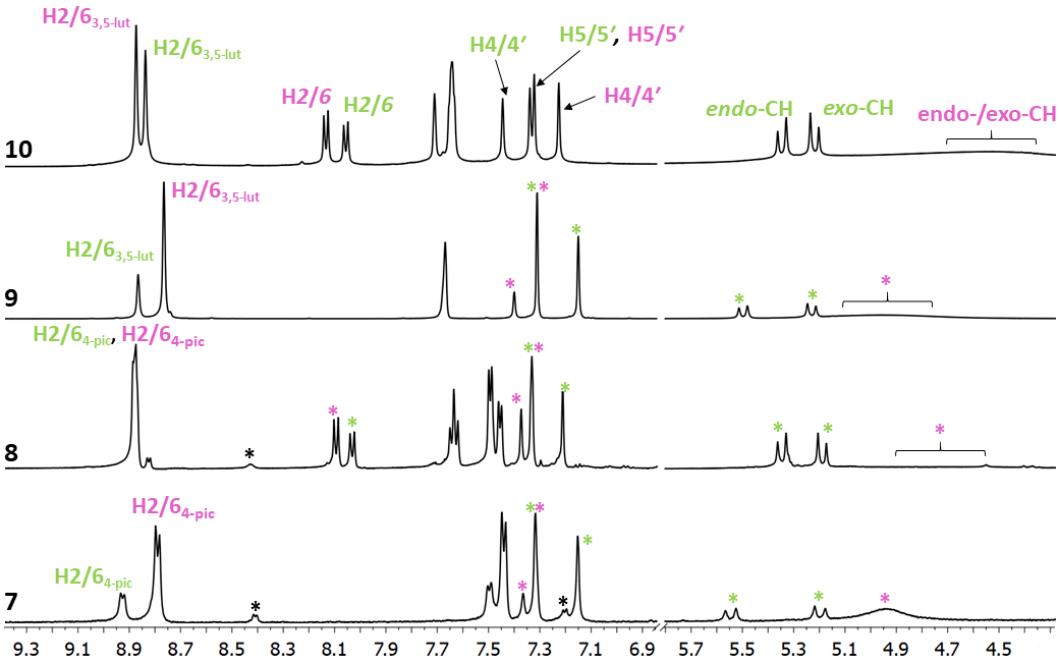

Figure 4.11. Selected region of ^{1}H NMR spectra in DMSO-d_6 at 25 °C (shifts in ppm) of the [Pt(*N*(SO_2R)1,1′-Me_2dma)(N-donor)$_2$](PF_6)$_2$ bis complexes (Bis1-purple and Bis2-green), [Pt(*N*(SO_2Me)1,1′-Me_2dma)(4-pic)$_2$](PF_6)$_2$ (**7**), [Pt(*N*(SO_2Tol)1,1′-Me_2dma)(4-pic)$_2$](PF_6)$_2$ (**8**), [Pt(*N*(SO_2Me)1,1′-Me_2dma)(3,5-lut)$_2$](PF_6)$_2$ (**9**), and [Pt(*N*(SO_2Tol)1,1′-Me_2dma)(3,5-lut)$_2$](PF_6)$_2$ (**10**). *Free 4-pic as an impurity.

In contrast, no such NOE cross-peak is observed between the broad Bis1 methylene signal and the N-donor H2/6. This observation indicates that the *endo*-CH protons in the Bis2 conformer is relatively closer to the N-donor aromatic ring than the *endo*-CH protons of the Bis1 conformer. In superimposed molecular structures of [Pt(*N*(SO_2R)1,1′-Me_2dma)Cl_2 (**5** or **6**) with their corresponding bis complexes [Pt(*N*(SO_2R)1,1′-Me_2dma)(N-donor)$_2$](PF_6)$_2$ (**7**, **8**, or **10**) through Pt, N1, and N2 atoms, the non-bonded distances between the *endo*-CH and the H2/6 protons of the N-

donor were measured; the overlay of [Pt(*N*(SO_2Tol)1,1′-Me_2dma)Cl_2 (**6**) and [Pt(*N*(SO_2Tol)1,1′-Me_2dma)(4-pic)$_2$](PF_6)$_2$ (**8**) along with the measured non-bonded distances are shown in Figure 4.12. In all the cases, the non-bonded distances between the *endo*-CH and the H2/6 protons in the SO_2R-out conformer are shorter by at least 0.1 Å than these distances in the SO_2R-in conformer, supporting the above conclusion that made through NMR data stating that the *endo*-CH protons in the Bis2 conformer is relatively closer to the N-donor aromatic ring than the *endo*-CH protons of the Bis1 conformer.

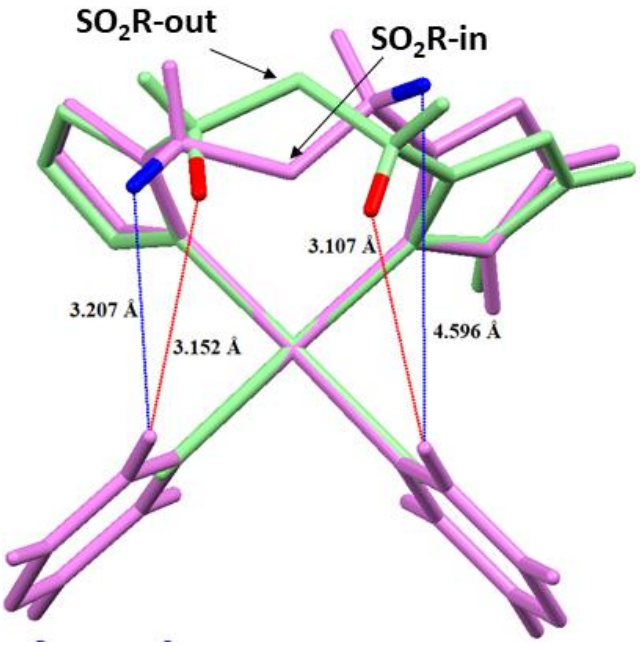

Figure 4.12. Overlap of the stick drawings of [Pt(*N*(SO_2Tol)1,1′-Me_2dma)Cl_2 (**6**, green) and [Pt(*N*(SO_2Tol)1,1′-Me_2dma)(4-pic)$_2$]$^{2+}$ (**8**, purple) by superimposing the Pt, N1, and N2 atoms. The non-bonded distances between the *endo*-CH and the H2/6$_{4\text{-pic}}$ protons were measured by using Mercury CSD 3.10.1 software. For clarity, some of the hydrogens, methyl groups and the SO_2Tol group of the sulfonamides are hidden.

For all the bis complexes/adducts, the chemical shifts of H4/4′ signals of Bis1 are relatively upfield by ~0.2 ppm than the chemical shifts of the H4/4′ signals of Bis2 (Table 4.5). Whereas, the chemical shifts of the H5/5′ signals are similar for both conformers. As an example, the H4/4′ shifts for Bis1 and Bis2 in [Pt(*N*(SO_2Me)1,1′-Me_2dma)(4-pic)$_2$](PF_6)$_2$ (**7**) is 7.21 and 7.37 ppm,

respectively, while the H5/5′ shift for both conformers is 7.32 ppm. This observation suggests that the H4/4′ protons might be affected differently by the anisotropic aromatic rings of the monodentate N-donors in each conformer resulting in different shifts as mentioned above; in the Bis1 conformer, the N-donor aromatic ring anisotropy experienced by the H4/4′ protons could be higher relative to the anisotropic effect experienced by the H4/4′ protons in the Bis2 conformer. All the molecular structures containing SO_2R-in conformation (**3**, **7**, **8**, and **10**), the carrier-ligand is distorted when compared to the molecular structures of the SO_2R-out conformation (**5** and **6**). In the former complexes, one of the imidazolyl rings (dihedral angle ~55°) is significantly more canted than the other ring (72-85°), whereas in **5** and **6**, the molecular structures are relatively more symmetrical and both imidazolyl rings have similar dihedral angles (67-75°, Table 4.3). Because of the low dihedral angle, the H4/4′ protons of the highly canted imidazolyl ring in each of **7**, **8** and **10** complexes are closer to the nearby bound N-donor group ($H_{4/4'}-N_{4\text{-pic}/3,5\text{-lut}}$ non-bonded distance ~3.1 Å) than the H4/4′ protons in the less canted imidazolyl ring in the same complex ($H_{4/4'}-N_{4\text{-pic}/3,5\text{-lut}}$ non-bonded distance ~3.5 Å). Therefore, we suggest that due to the distorted carrier-ligand in Bis1 (SO_2R-in), the H4/4′ protons could be projecting towards the N-donor aromatic rings, thus the H4/4′ signals of Bis1 could have upfield chemical shifts compared to the H4/4′ signals of Bis2 (SO_2R-out).

The conformational interchanging processes are greatly affected by temperature. Thus, to further understand the processes involved in the conformer interchange in [Pt(*N*(SO_2R)1,1′-Me_2dma)(N-donor)$_2$]$^{2+}$-type complexes, we collected NMR data at different temperatures by utilizing a solution of [Pt(*N*(SO_2Me)1,1′-Me_2dma)(4-pic)$_2$](PF_6)$_2$ (**7**) in DMF-d_7 (freezing point -60 °C). At RT, the two methylene doublets observed for Bis2 are connected through NOE cross-peaks (Figure C.8), showing that the *endo*- and *exo*-CH protons of Bis2 do not interchange. Even

at high T such as 50 °C and low T such as -13 °C, these peaks remain sharp doublets (Figure C.9), showing there are no dynamic processes involved within the Bis2 conformer (in contrast, NMR data discussed below suggest that there is another dynamic process involved within Bis1 other than the Bis1-Bis2 interchange). Each of the methylene doublets of Bis2 has EXSY peaks with the broad methylene peak of Bis1 at RT, indicating the Bis1 and Bis2 methylene protons interchange with each other through a relatively fast process on the NMR time scale. However, in the ROESY spectrum recorded at low temperature (-13 °C, Figure C.10), no EXSY peaks were observed between the methylene signals of Bis1 and Bis2, indicating that at this T, the interchange between Bis1 and Bis2 is relatively very slow or does not occur.

The broadness of the methylene signal of Bis1 conformer [Pt(*N*(SO_2Me)1,1′-Me_2dma)(4-pic)$_2$](PF_6)$_2$ (**7**) in DMF-d_7 at RT (5.33 ppm) suggests that all four methylene signals of Bis1 either have similar chemical shifts or they interchange with each other very rapidly on the NMR time scale. At high T such as 50 °C, we observed that the methylene signal for Bis1 become sharper than the peak at RT (Supporting Information). However, in the ^{1}H NMR spectra recorded at low T (0 and -13 °C), the Bis1 methylene signal eventually resolve in to two signals (at -13 °C, Bis1 methylene protons produce two broad peaks at 5.04 and 5.62 ppm, Supporting Information). The ROESY spectrum of this solution at -13 °C shows EXSY cross-peaks between these two peaks. All these data indicate that within the Bis1 conformer, another rapid methylene proton interchange process takes place. This interchange is a faster-dynamic process relative to the Bis1-Bis2 conversion process at RT, but this process slows down at low T to produce two peaks connected through EXSY peaks (Supporting Information). The distortion of the carrier-ligand in SO_2R-in conformer shown in **7**, **8**, and **10** suggests that this fast interchange process within the Bis1 conformer could be a result of the inversion of the sulfonamide group.

As discussed in the structural section, the central sulfonamide N is not bound, hence the imidazolyl groups have freedom to rotate around the Pt−N bonds and the sulfonamide group has some degree of freedom to invert at the N(sulfonamide) atom. Therefore, it is conceivable that the observation of two different conformers for the $[Pt(N(SO_2R)1,1'\text{-}Me_2dma)(DMAP)_2]^{2+}$ adduct is a result of a combination of the rotation of the imidazolyl rings and the inversion at N of the central sulfonamide group.

Formation of the $[Pt(N(SO_2R)1,1'\text{-}Me_2dma)(\text{N-donor})_2]^{2+}$-type complexes through the reaction of **5** and **6** with simple N-donors indicates that the $Pt(N(SO_2R)1,1'\text{-}Me_2dma)Cl_2$ complexes are capable of acting as bifunctional platinum agents to form bis adducts with N-donors, an important functionality relevant to biological applications because platinum anticancer agents form adducts with guanine bases in DNA. As a preliminary step of evaluating the reactivity of the $Pt(N(SO_2R)1,1'\text{-}Me_2dma)Cl_2$ complexes towards biological molecules, we treated **5** and **6** with two different guanine derivatives, 9-MeG and Guo.

Reactions of $Pt(N(SO_2Me)1,1'\text{-}Me_2dma)Cl_2$ (5) with G (G = 9-MeG and Guo). A ^1H NMR spectra of the reaction mixture of $Pt(N(SO_2Me)1,1'\text{-}Me_2dma)Cl_2$ (**5**, 5 mM) and 2.5 molar equiv of 9-MeG in DMSO-d_6 lead to growth of a new set of signals with time until the reaction was completed at 19 h (Figure 4.13). The new signals remained unchanged even after 14 d, indicating that the adduct formed is stable.

In the ^1H NMR spectrum of the adduct solution has a new broad H8 singlet at 8.60 ppm characteristic of Pt(II)-bound 9-MeG[40] because it is shifted downfield from the free H8 signal at 7.62 ppm (Table 4.6). Also, a new NH peak (11.35 ppm), which is shifted downfield from the free NH signal by 0.8 ppm, is observed. A new NH_2 peak detected at 7.01 ppm is downfield shifted by 0.54 ppm from the free NH_2 signal. In addition to these peaks, four sharp doublets can be seen in

the aromatic region; these should be signals of the carrier-ligand protons of the new **G** adduct because they are the only other aromatic protons in the formed adduct (Figure 4.13). The integration values of the four doublets and the bound H8 signal are roughly the same, which indicates that the reaction produced a mono **G** adduct, [Pt(*N*(SO_2Me)1,1′-Me_2dma)(9-MeG)Cl]$^+$.

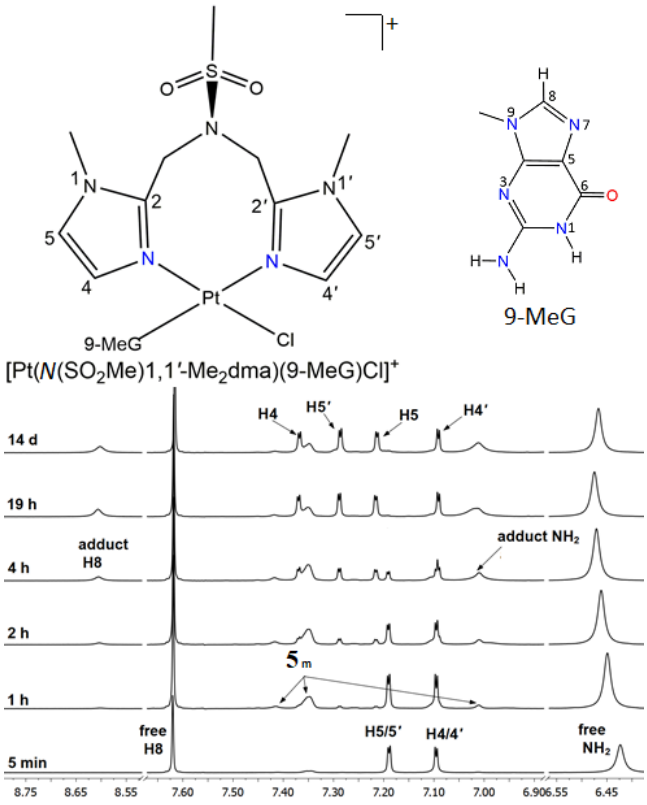

Figure 4.13. Line drawings of [Pt(*N*(SO_2Me)1,1′-Me_2dma)(9-MeG)Cl]$^+$ and 9-MeG (top) and selected region of the ^{1}H NMR spectra (bottom, 25 °C, DMSO-d_6, shifts in ppm) of the reaction mixture forming the adduct recorded 5 min, 1 h, 2 h, 4 h, 19 h, and 14 d after addition of 1.6 mg of solid **5** in to a 25 mM solution of 9-MeG.

In order to conveniently assign the proton signals of the [Pt(*N*(SO_2Me)1,1′-Me_2dma)(9-MeG)Cl]$^+$ adduct, the 9-MeG and the imidazolyl ring with non-prime numbers are drawn on the same side of the coordination plane, as shown in Figure 4.13. In a ROESY spectrum of the final reaction mixture (Figure 4.14), an NOE cross-peak between the bound H8 signal and the most downfield-shifted doublet (7.37 ppm) allows the signal to be assigned to the H4 proton (Table 4.7). This H4 signal has an NOE cross-peak to the doublet at 7.21 ppm, allowing that signal to be

assigned to H5. Two imidazolyl Me signals can be seen at 3.79 and 3.68 ppm (identified by integration); the more upfield singlet at 3.68 ppm has an NOE cross-peak with the H5 signal and thus can be assigned to 1-Me. The other aliphatic Me singlet at 3.79 ppm has an NOE cross-peak with another aromatic doublet at 7.28 ppm, therefore each signal can be assigned to 1-Me′ and H5′. The remaining doublet is assigned to H4′ (7.09 ppm), which is further supported by an NOE cross peak between this peak and the H5′ signal.

Table 4.6. Selected ^{1}H NMR Data (ppm) for the **G** Ligand in [Pt(*N*(SO_2R)1,1′-Me_2dma)**G**Cl]$^{+}$ Adducts (ppm, DMSO-d_6, 25 °C). Non-prime Numbering Signals are for the Protons of the Imidazolyl Ring Closest to the Bound **G** (See Figure 4.10)

R		H8		NH_2		NH	
		free	adduct	free	adduct	free	adduct
Me	9-MeG	7.62	8.60	6.47	7.01	10.56	11.35
Me	Guo	7.93	8.92, 8.90	6.49	7.01	10.66	11.39
Tol	9-MeG	7.61	8.59	6.41	6.93	10.50	11.19
Tol	Guo	7.90	8.91, 8.88	6.44	6.95	10.62	11.25

Observing only one H8 signal for the [Pt(*N*(SO_2Me)1,1′-Me_2dma)(9-MeG)Cl]$^{+}$ adduct indicates that the rotation of the guanine derivative is not highly impeded in the new adduct. As discussed in our previous papers, the metal-bound-**G** molecules can rotate around the Pt−N7(**G**) bond.[22-23] If the in plane bulk of the carrier-ligand is high enough to restrict this rotation of the bound **G** base on the NMR time scale, two or more H8 signals should be observed corresponding to different rotamers of the adduct.[22-23] However, the broadness of the H8 peak (instead of the expected sharp peak for H8) of the [Pt(*N*(SO_2Me)1,1′-Me_2dma)(9-MeG)Cl]$^{+}$ adduct suggests that possibly the chemical shifts of the resulting rotamers perhaps have similar chemical shifts. The adduct formation of the Pt(*N*(SO_2Me)1,1′-Me_2dma)Cl_2 (**5**) complex is significantly faster (~19 h to complete the reaction) than its analog compound, [Pt(*N*(Me)1,1′-Me_2dma)Cl]Cl (the reaction

completion time with 9-EtG is 10 d).[22] The less steric hindrance created by the low canted aromatic rings (dihedral angle ~75°) in the bifunctional coordination sphere of the new complex compared to the monofunctional coordination sphere of the [Pt(*N*(Me)1,1′-Me_2dma)Cl]Cl complex (dihedral angle ~12°)[22] might be the reason for the significantly different reaction times.

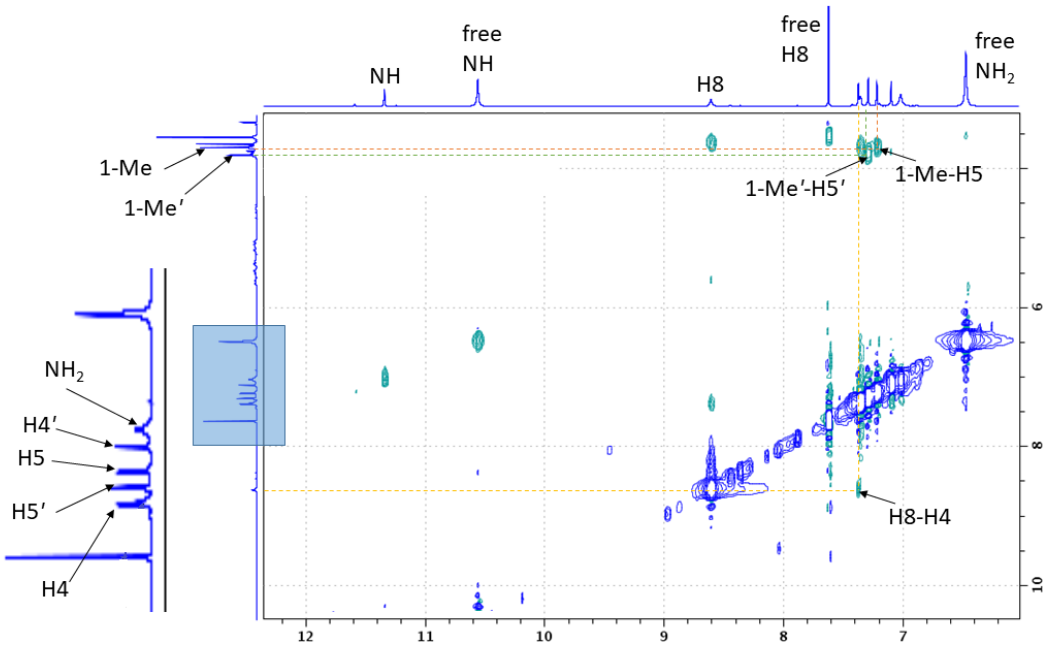

Figure 4.14. ^{1}H-^{1}H ROESY spectrum (selected region) of the [Pt(*N*(SO_2Me)1,1′-Me_2dma)(9-MeG)Cl]$^+$ adduct (25 °C, DMSO-d_6, shifts in ppm).

Similar results were obtained when a 12.5 mM solution of Guo (2.5 molar equiv) in DMSO-d_6 was treated with 1.6 mg of Pt(*N*(SO_2Me)1,1′-Me_2dma)Cl_2 (**5**, 5 mM). An ^{1}H NMR spectrum taken 10 min after the mixing showed signals of $\mathbf{5}_m$ (Figure 4.15). In a spectrum recorded about 5 h after mixing showed clearly detectable peaks for the new adduct, [Pt(*N*(SO_2Me)1,1′-Me_2dma)(Guo)Cl]$^+$ (in addition to $\mathbf{5}_m$ peaks). The reaction was completed during the first 24 h period as indicated by the ratio between the adduct peaks and the $\mathbf{5}_m$ peaks being constant (4:1, calculated based on the integrations of carrier-ligand aromatic protons). The proton signals of the [Pt(*N*(SO_2Me)1,1′-Me_2dma)(Guo)Cl]$^+$ adduct were assigned in a similar way as for the 9-MeG adduct, by using a ROESY spectrum of the reaction mixture (Tables 4.6 and 4.7 and Supporting

Information). Among the four doublets corresponding to the imidazolyl aromatic protons, the two peaks of H4 (7.40 ppm) and H5 (7.24 ppm) are broad, which may be because of quadrupolar N atoms in the nearby guanine base. In contrast, the H4′ (7.08 ppm) and H5′ (7.30 ppm) peaks corresponding to the carrier ligand side close to the bound chloride ion were sharp doublets. In contrast to the broad one H8 peak observed for the 9-MeG adduct ([Pt(*N*(SO_2Me)1,1′-Me_2dma)(9-MeG)Cl]$^+$), the Guo adduct of **5** shows two closely associated signals at 8.92 and 8.90 ppm as the adduct now contain a chiral center (Figure 4.12 and Table 4.6). In order to investigate if the reaction would consume all of the complex (**5** or $\mathbf{5}_m$) molecules with the presence of a high concentration of **G**, another experiment was performed by mixing Guo (100 mM) and **5** (10 mM) in a 10:1 ratio (in DMSO-d_6). The reaction was completed during the first 24 h and the integration shows the same ratio of adduct:$\mathbf{5}_m$ = ~4:1 as of the reaction mentioned above with a reaction mixture of 2.5:1 (12.5 mM Guo and 5 mM **5**).

Table 4.7. Selected ^{1}H NMR Data (ppm) for the *N*(SO_2R)1,1′-Me_2dma Carrier Ligands in [Pt(*N*(SO_2R)1,1′-Me_2dma)**G**Cl]$^+$ and in Pt(*N*(SO_2R)1,1′-Me_2dma)Cl_2 (ppm, DMSO-d_6, 25 °C). Non-prime Numbering Signals are for the Protons of the Imidazolyl Ring Closest to the Bound **G** (See Figure 4.10)

		H4/4′		H5/5′		1/1′-Me		SO_2Me
R		H4	H4′	H5	H5′	1-Me	1′-Me	
Me	Cl[a]		7.10		7.20		3.72	3.28
Me	9-MeG	7.37	7.09	7.21	7.28	3.68	3.79	3.31[c]
Me	Cl[b]		7.10		7.19		3.72	3.28
Me	Guo	7.40	7.08	7.25	7.30	3.68	3.79	3.31[c]
Tol	Cl[a]		7.10		7.21		3.79	-
Tol	9-MeG	7.38	7.10	7.23	7.31	3.75	3.88	-
Tol	Cl[b]		7.09		7.20		3.79	-
Tol	Guo	7.41	7.10	7.27	7.32	3.64	3.76	-

[a]Signals are recorded for a solution with excess of 9-MeG. [b]Signals are recorded for a solution with excess of Guo. [a]Signal is masked by a free **G** signal.

The results for the reactions of Pt(*N*(SO_2Me)1,1′-Me_2dma)Cl_2 (**5**) with 9-MeG and Guo reveal a contrastingly high reactivity compared to its dpa analog, Pt(*N*(SO_2Me)3,3′,5,5′-Me_4dpa)Cl_2.[16] The Pt(*N*(SO_2Me)3,3′,5,5′-Me_4dpa)Cl_2 complex, does not show any prominent reaction with either 9-MeG or Guo.[16] Instead, the complex get attacked by the solvent (DMSO) to produce a monosolvolysis product and eventually 40% of the chelate ligand get dissociated. The relative high robustness of **5** than of its analogous dpa complexes, Pt(*N*(SO_2R)3,3′,5,5′-Me_4dpa)Cl_2,[16] could be due to the less steric hindrance in the coordination sphere due to the small size and the high basicity of the imidazolyl rings relative to the pyridyl rings.

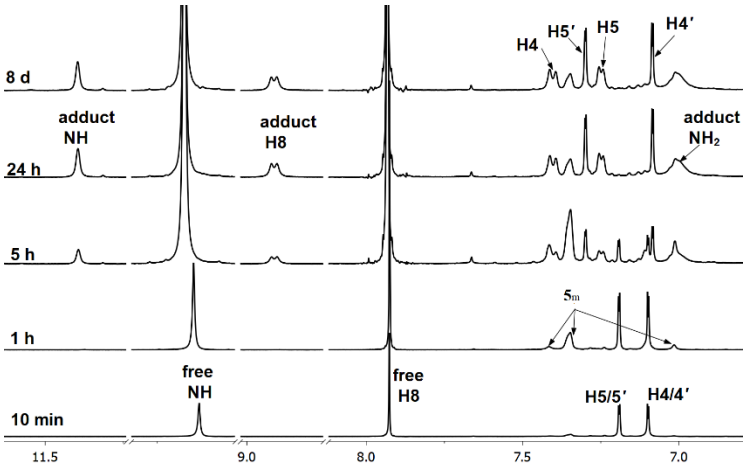

Figure 4.15. Selected region of the ^{1}H NMR spectra (bottom, 25 °C, DMSO-d_6, shifts in ppm) of the reaction mixture forming the [Pt(*N*(SO_2Me)1,1′-Me_2dma)(Guo)Cl]$^+$ adduct recorded 10 min, 1 h, 5 h, 24 h, and 8 d after addition of 1.6 mg of solid **5** in to a 25 mM solution of Guo.

Reactions of Pt(*N*(SO_2Tol)1,1′-Me_2dma)Cl_2 (6) with G (G = 9-MeG and Guo). As observed for Pt(*N*(SO_2Me)1,1′-Me_2dma)Cl_2 (**5**), the Pt(*N*(SO_2Tol)1,1′-Me_2dma)Cl_2 (**6**, 5 mM) complex also produces mono **G** adducts, [Pt(*N*(SO_2Tol)1,1′-Me_2dma)**G**Cl]$^+$, when treated with 2.5 molar equiv of **G** in DMSO-d_6 (Supporting Information). The adduct yields and the reaction completion times of the formation of each **G** adduct (**G** = 9-MeG and Guo) of **6** is similar to the corresponding adduct formed with **5**; the reactions between **6** and 9-MeG and Guo were finished by ~19 h (100% yield) and ~24 h (80% yield), respectively. Furthermore, the chemical shifts of

the carrier ligand and the **G** in each [Pt(*N*(SO_2Tol)1,1′-Me_2dma)**G**Cl]$^+$ mono adduct is similar to its corresponding [Pt(*N*(SO_2Me)1,1′-Me_2dma)**G**Cl]$^+$ adduct (Tables 4.6 and 4.7), indicating that the effect of the dangling R group on the chemical properties of the **G** adducts is minimal.

4.4 Conclusions

The *N*(SO_2R)Me_ndpa ligands investigated here bind tridentately to the *fac*-[Re(I)$(CO)_3$]$^+$ core in the [Re$(CO)_3$(*N*(Even though the *N*(R)1,1′-Me_2dma type ligands (R = H or Me) bind tridentately to Pt(II), the *N*(SO_2R)1,1′-Me_2dma ligands show bidentate coordination. In contrast, *N*(SO_2R)1,1′-Me_2dma ligands coordinate tridentately to *fac*-[Re$(CO)_3$]$^+$ core. The different binding modes exhibited by the *N*(SO_2R)1,1′-Me_2dma ligands with Pt(II) and Re(I) can be attributed to the steric factors of the terminal imidazolyl rings and the electronic factors of the central sulfonamide donor. Regardless of the different binding modes, both Pt(*N*(SO_2R)1,1′-Me_2dma)Cl_2 and [Re$(CO)_3$(*N*(SO_2R)1,1′-Me_2dma)]ClO_4 complexes are robust and do not show any ligand dissociation in solution (DMSO-d_6), indicating that the sulfonamide-incorporated imidazolyl ligands, *N*(SO_2R)1,1′-Me_2dma, are better N-donor ligands than their dpa analogs, *N*(SO_2R)3,3′,5,5′-Me_4dpa. Chloride ligands of the Pt(*N*(SO_2R)1,1′-Me_2dma)Cl_2 complexes were easily replaced by simple N-donor ligands such as DMAP, 4-picoline, and 3,5-lutidine to produce bis adducts. Furthermore, Pt(*N*(SO_2R)1,1′-Me_2dma)Cl_2 react with **G** to form stable mono adducts, [Pt(*N*(SO_2R)1,1′-Me_2dma)(**G**)Cl]$^+$ (**G** = 9-MeG and Guo) in DMSO-d_6, indicating that the new imidazolyl based complexes are robust and reactive enough to employ in further studies to evaluate if they possess any actual anticancer properties. Furthermore, NMR spectral data for the Pt(*N*(SO_2R)1,1′-Me_2dma)Cl_2 and [Pt(*N*(SO_2R)1,1′-Me_2dma)(N-donor)$_2$]$^{2+}$-type complexes provide evidence for dynamic motion involving the 8-membered chelate ring. From the X-ray structural results it is reasonable to conclude that the dynamic motion involves the rotation of the

imidazolyl rings around the Pt–N bond and the inversion of the SO_2R group at the sulfonamide N atom leading to SO_2R-in and SO_2R-out conformations evident in solid-state structures.

4.5 References

1. Langdon-Jones, E. E.; Symonds, N. O.; Yates, S. E.; Hayes, A. J.; Lloyd, D.; Williams, R.; Coles, S. J.; Horton, P. N.; Pope, S. J. A. *Inorg. Chem.* **2014,** *53* (7), 3788-3797.

2. Christoforou, A. M.; Marzilli, P. A.; Marzilli, L. G. *Inorg. Chem.* **2006,** *45*, 6771-6781.

3. Wu, S.; Zhu, C.; Zhang, C.; Yu, Z.; He, W.; He, Y.; Li, Y.; Wang, J.; Guo, Z. *Inorg. Chem.* **2011,** *50* (23), 11847-11849.

4. Veltze, S.; Egdal, R. K.; Johansson, F. B.; Bond, A. D.; McKenzie, C. J. *Dalton Trans.* **2009,** (47), 10495-10504.

5. Lu, G.; Hillier, S. M.; Maresca, K. P.; Zimmerman, C. N.; Eckelman, W. C.; Joyal, J. L.; Babich, J. W. *J. Med. Chem.* **2013,** *56*, 510-520.

6. Perera, T.; Abhayawardhana, P.; Marzilli, P. A.; Fronczek, F. R.; Marzilli, L. G. *Inorg. Chem.* **2013,** *52*, 2412−2421.

7. Abhayawardhana, P. L.; Marzilli, P. A.; Fronczek, F. R.; Marzilli, L. G. *Inorg. Chem.* **2014,** *53*, 1144-1155.

8. Bartholoma, M.; Valliant, J.; Maresca, K. P.; Babichc, J.; Zubieta, J. *Chem. Commun.* **2009,** *5*, 493-512.

9. Maresca, K. P.; Marquis, J. C.; Hillier, S. M.; Lu, G.; Femia, F. J.; Zimmerman, C. N.; Eckelman, W. C.; Joyal, J. L.; Babich, J. W. *Bioconjug. Chem.* **2010,** *21* (6), 1032-1042.

10. Maresca, K. P.; Kronauge, J. F.; Zubieta, J.; Babich, J. W. *Inorg. Chem. Commun.* **2007,** *10* (12), 1409-1412.

11. Zhu, J.; Zhao, Y.; Zhu, Y.; Wu, Z.; Lin, M.; He, W.; Wang, Y.; Chen, G.; Dong, L.; Zhang, J.; Lu, Y.; Guo, Z. *Chem. Eur. J.* **2009,** *15* (21), 5245-5253.

12. Olivova, R.; Kasparkova, J.; Vrana, O.; Vojtiskova, M.; Suchankova, T.; Novakova, O.; He, W.; Guo, Z.; Brabec, V. *Mol. Pharm.* **2011,** *8* (6), 2368-2378.

13. Zhao, Y.; He, W.; Shi, P.; Zhu, J.; Qiu, L.; Lin, L.; Guo, Z. *Dalton Trans.* **2006,** (22), 2617-2619.

14. Ndinguri, M. W.; Fronczek, F. R.; Marzilli, P. A.; Crowe, W. E.; Hammer, R. P.; Marzilli, L. G. *Inorg. Chim. Acta* **2010,** *363* (8), 1796-1804.

15. van der Schilden, K.; Garcìa, F.; Kooijman, H.; Spek, A. L.; Haasnoot, J. G.; Reedijk, J. *Angew. Chem., Int. Ed.* **2004,** *43* (42), 5668-5670.

16. Ranasinghe, K.; Marzilli, P. A.; Pakhomova, S.; Marzilli, L. G.

17. Desbouis., D.; Struthers, H.; Spiwok, V.; Ster, T. K.; Schibli, R. *J. Med. Chem.* **2008,** *51*, 6689–6698.

18. Paulo, A.; Morais, G. R.; Santos, I. In *Advances in Organometallic Chemistry and Catalysis*, Pombeiro, A. J., Ed. 2014.

19. Schibli, R.; Schubiger, A. P. *Eur. J. Nucl. Med. Mol. Imaging* **2002,** *29* (11), 1529-1542.

20. Abram, U.; Alberto, R. *J. Braz. Chem. Soc.* **2006,** *17*, 1486−1500.

21. Kyprianidou, P.; Tsoukalas, C.; Chiotellis, A.; Papagiannopoulou, D.; Raptopoulou, C. P.; Terzis, A.; Pelecanou, M.; Papadopoulos, M.; Pirmettis, I. *Inorg. Chim. Acta* **2011,** *370* (1), 236-242.

22. Ranasinghe, K.; Marzilli, P. A.; Pakhomova, S.; Marzilli, L. G. *Inorg. Chem.* **2017,** *56* (14), 8462-8477.

23. Andrepont, C.; Marzilli, P. A.; Marzilli, L. G. *Inorg. Chem.* **2012,** *51* (21), 11961-11970.

24. Andrepont, C.; Marzilli, P. A.; Pakhomova, S.; Marzilli, L. G. *J. Inorg. Biochem.* **2015,** *153*, 219-230.

25. Andrepont, C.; Pakhomova, S.; Marzilli, P. A.; Marzilli, L. G. *Inorg. Chem.* **2015,** *54*, 4895-4908.

26. Price., J. H.; Williamson, A. N.; Robert, F. S.; Bradford, B. W. *Inorg. Chem.* **1972,** *11*, 1280-1284.

27. Edwards, D. A.; Marshalsea, J. *J. Organomet. Chem.* **1977,** *131* (1), 73-91.

28. Gautier, F.-M.; Jones, S.; Martin, S. J. *Org. Biomol. Chem.* **2009,** *7* (2), 229-231.

29. Sheldrick, G. *Acta Crystallogr. Sect. A* **2008,** *64* (1), 112-122.

30. Abhayawardhana, P.; Marzilli, P. A.; Perera, T.; Fronczek, F. R.; Marzilli, L. G. *Inorg. Chem.* **2012,** *51* (13), 7271-7283.

31. Perera, T.; Marzilli, P. A.; Fronczek, F. R.; Marzilli, L. G. *Inorg. Chem.* **2010,** *49*, 5560-5572.

32. Christoforou, A. M.; Marzilli, P. A.; Fronczek, F. R.; Marzilli, L. G. *Inorg. Chem.* **2007,** *46* (26), 11173-11182.

33. Perera, T.; Fronczek, F. R.; Marzilli, P. A.; Marzilli, L. G. *Inorg. Chem.* **2010,** *49*, 7035-7045.

34. Christoforou, A. M.; Fronczek, F. R.; Marzilli, P. A.; Marzilli, L. G. *Inorg. Chem.* **2007,** *46* (17), 6942-6949.

35. Lewis, N. A.; Pakhomova, S.; Marzilli, P. A.; Marzilli, L. G. *Inorg. Chem.* **2017,** *56* (16), 9781-9793.

36. Yang, Y.; Lu, C.; Wang, H.; Liu, X. *Dalton Trans.* **2016,** *45* (25), 10289-10296.

37. Moriguchi, T.; Kitamura, S.; Sakata, K.; Tsuge, A. *Polyhedron* **2001,** *20* (18), 2315-2320.

38. Zhao, S.-B.; Wang, R.-Y.; Wang, S. *Organometallics* **2009,** *28* (8), 2572-2582.

39. Izutsu, K., *Acid-Base Dissociation Constants in Dipolar Aprotic Solvents; IUPAC Chemical Data Series No. 35*. Blackwell Scientific: Oxford, 1990.

40. Marcelis, A. T. M.; Veer, J. L. V. D.; Zwetsloot, J. C. M.; Reedijk, J. *Inorg. Chim. Acta* **1983,** *78*, 195-203.

CHAPTER 5. CONCLUSIONS

This dissertation research contributes to the understanding of fundamental chemistry of Pt(II) and Re(I) complexes of linear tridentate ligands terminated with aromatic N-donor groups; this chemistry is relevant to biological/biomedical applications. A series of new ligands terminated with either two pyridyl rings or two imidazolyl rings were utilized in preparing the new Pt(II) and Re(I) complexes. Furthermore, the basic ligand framework of the tridentate ligands terminated by aromatic rings was utilized to explore new bioconjugation possibilities with a N−S linker by making the central nitrogen atom part of a tertiary sulfonamide group.

The [Pt(*N*(R)1,1′-Me_2dma)Cl]Cl complexes were used to prepare several Pt(*N*(R)1,1′-Me_2dma)**G** mono adducts (**G** = unlinked guanine or hypoxanthine derivatives), which were analyzed by using NMR spectroscopy to evaluate the chemical properties of the adducts relevant to anticancer activity. The observation of two sharp **G** H8 NMR signals (corresponding to a syn/anti rotamer mixture) indicates that these carrier-ligands are bulky enough to impede the free rotation of the bound **G** molecules. Anticancer-active monofunctional platinum(II) complexes have bulky carrier-ligands that cause DNA adducts to be distorted. Therefore, the [Pt(*N*(R)1,1′-Me_2dma)Cl]Cl complexes could be a good starting point to further analyze the relationship between the ligand steric bulk and the anticancer properties of the monofunctional Pt(II) complexes.

The *N*(SO_2R)1,1′-Me_2dma and *N*(SO_2R)Me_ndpa ligands were utilized to develop a new conjugation approach through a N−S link. Such new linking strategies are useful in introducing biological properties (such as enhanced targeting ability, fluorescence, and high anticancer activity) to metal complexes. The new *N*(SO_2R)1,1′-Me_2dma and *N*(SO_2R)Me_ndpa ligand frameworks demonstrate the derivatization flexibility of the central N−S linker and form

isomerically pure highly robust *fac*-Re[$(CO)_3L]^+$ type complexes. These new complexes provide useful insights in the development of ^{99m}Tc and ^{187}Re radiopharmaceuticals.

The *N*(SO_2R)1,1′-Me_2dma and *N*(SO_2R)Me_ndpa ligands were also utilized to investigate whether the normally highly favorable Pt−N bond could also be formed by a sulfonamide N-donor present in a tridentate ligand terminated by aromatic rings. This study shows that the sulfonamide N atom in the *N*(SO_2R)1,1′-Me_2dma and *N*(SO_2R)Me_ndpa ligands does not coordinate to the Pt(II) center; as a consequence the ligands usually form Pt(*N*(SO_2R)1,1′-Me_2dma)Cl_2 or Pt(*N*(SO_2R)Me_ndpa)Cl_2 complexes with a bidentate coordination mode and an unusually large 8-membered chelate ring; these complexes are the very first examples of Pt(II) complexes of sulfonamide-incorporated linear ligands having 8-membered chelate rings. Both Pt(*N*(SO_2R)1,1′-Me_2dma)Cl_2 and Pt(*N*(SO_2R)Me_ndpa)Cl_2 type complexes exhibit interesting and unusual chemical properties that are relevant to understanding the fundamental chemistry of this new class of Pt(II) compounds.

APPENDIX A. SUPPLEMENTARY MATERIAL FOR CHAPTER 2

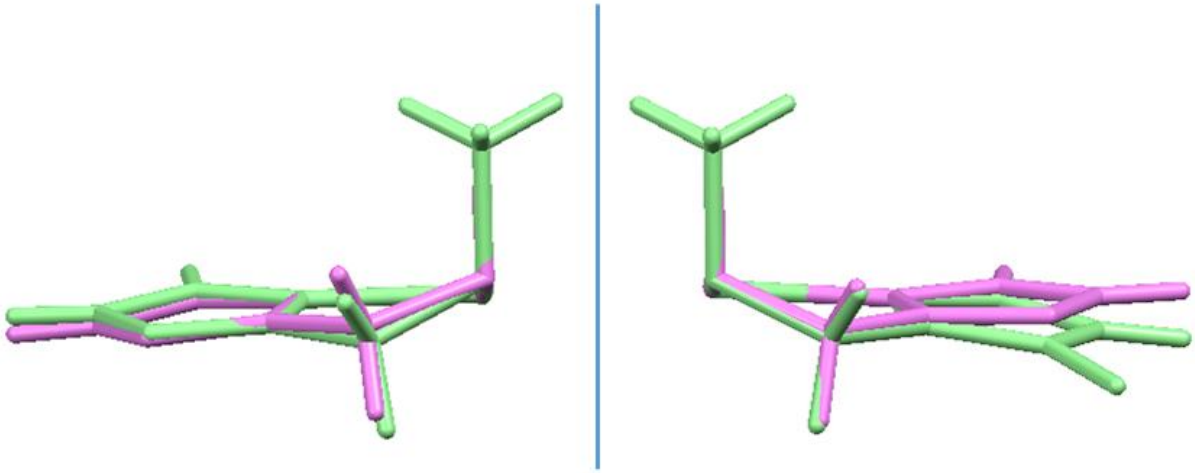

Figure A.1. Tilting of the imidazolyl rings in the [Pt(*N*(R)1,1′-Me_2dma)Cl]BF_4 cations (overlay of **3b** (R = H, pink) and **4b** (R = Me, green) by superimposing the Pt, N2, and N3 atoms (*left*) and Pt, N2, and N1 atoms (*right*) viewed along the coordination plane. In order to display the tilting clearly, only parts of one chelate ring are shown in each half of the figure, and the N-Me group on each imidazolyl ring is hidden. The figure shows that the methylene groups are farther on the other side of the coordination plane from the NH or NMe group in the R = Me cation.

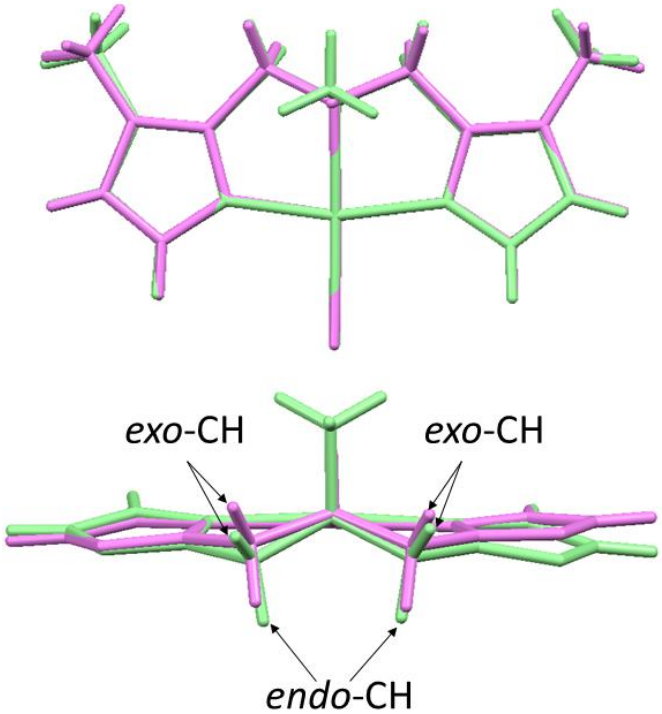

Figure A.2. Overlay of the [Pt(*N*(R)1,1′-Me_2dma)Cl]BF_4 cations, **3b** (R = H, pink) and **4b** (R = Me, green) by superimposing the Pt, Cl, N1, N2, and N3 atoms, viewed from the top (*top*) and along the coordination plane (*bottom*), where the *endo*-CH and the *exo*-CH protons are designated. For clarity, the N-Me groups of the imidazolyl rings are hidden in the bottom structure.

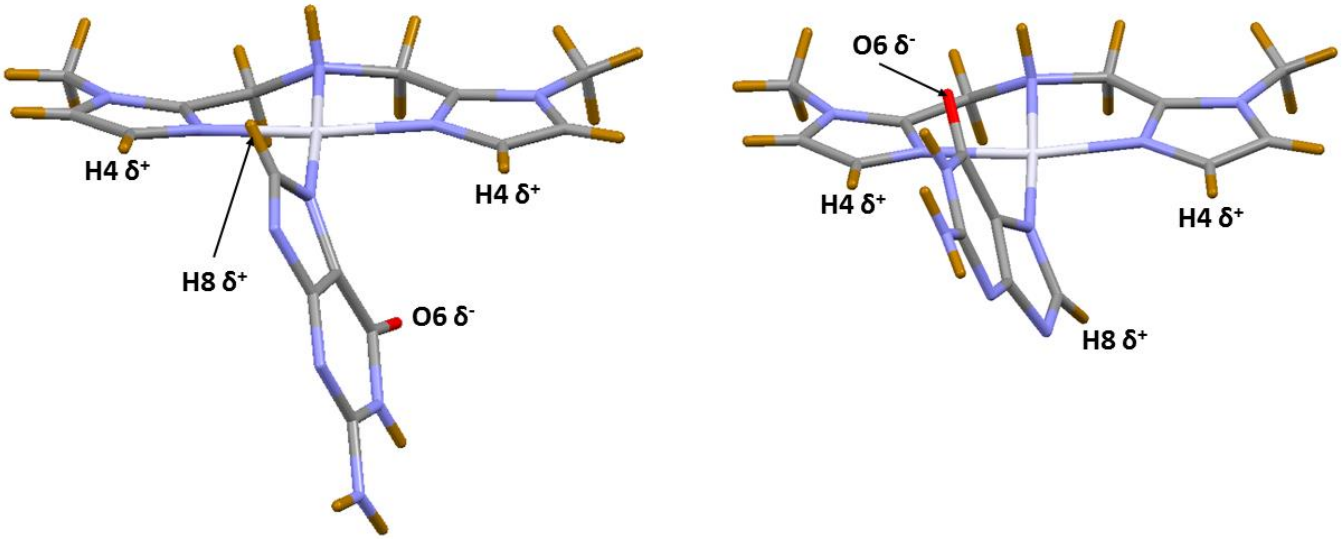

Figure A.3. Models of the anti (*left*) and syn (*right*) rotamers of the Pt(*N*(H)1,1′-Me$_2$dma)(3′-GMP) adduct based on the molecular structure of **5** as described in the main text. The ribose and phosphate groups are hidden in order to display the models clearly.

Structural Features of the 3′-GMPH Ligand. Bond lengths and angles for the guanine rings are in the normal range found for nucleotides, e.g., 5′-GMP[70-71] and 3′-GMP.[64] The nucleotide conformation in **5** is anti, i.e., antiperiplanar (the C12─N6─C1′─O2 torsion angle around the N6─C1′ glycosidic bond is –164.9°).[178] The 5′-GMP has the anti conformation in all of the structurally characterized bis adducts of 5′-GMP[69-72] referred to in the main text discussion. The pucker of the ribose sugar group in **5** is C2′-*endo* (S pucker), as indicated by the 0.157 Å displacement in the C5′ direction of the C2′ atom from the plane defined by the C1′, C4′ and O2 atoms and by the pseudo-rotation phase angle *P* ~177°.[179] The ribose S puckering is retained in solution, as indicated by the H1′ and H2′ coupling constant of 4.8 Hz.[180-181] Most of the platinum **G** adducts described in the literature have ribose groups with similar S puckering.[66,70,181] Two of the terminal P─O bonds in **5** have lengths (P─O5, 1.492(9) Å, and P─O7, 1.471(8) Å) that are shorter than the P─O6 bond (1.574(9) Å), which is comparable in length to the P─OH bonds (1.536(1)–1.598(5) Å) of the bis complexes of 5′-GMP referenced above.[69-72] Thus, O6 in **5** is protonated, although an H atom at O6 is not visible in the electron density map.

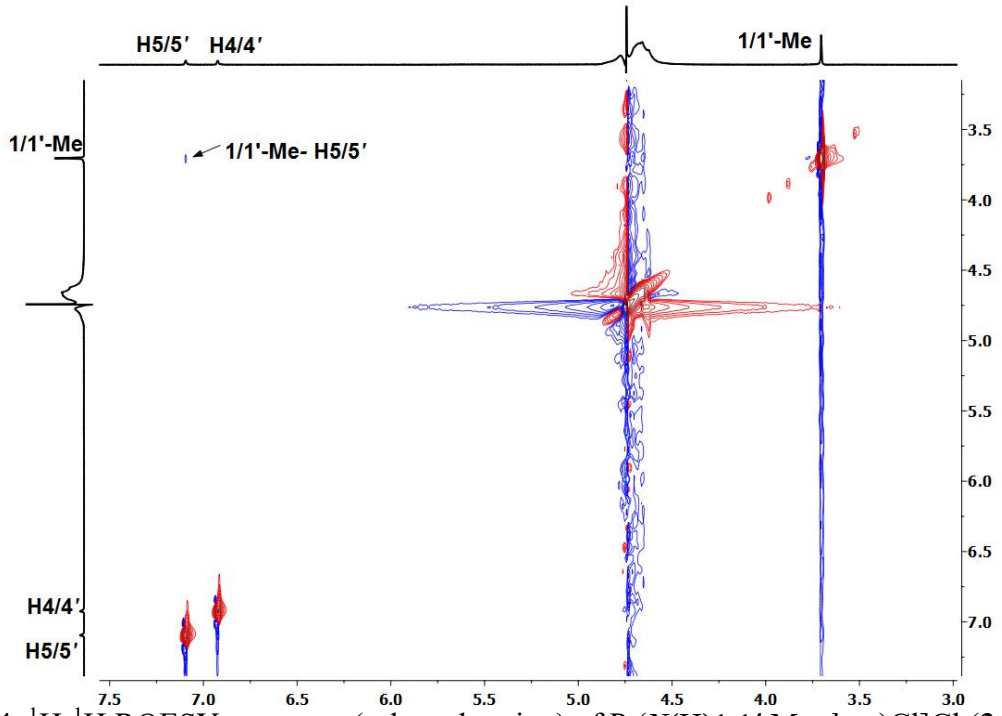

Figure A.4. ^{1}H-^{1}H ROESY spectrum (selected region) of Pt(*N*(H)1,1′-Me$_2$dma)Cl]Cl (**3a**) (25 °C, D$_2$O, pH 6, shifts in ppm).

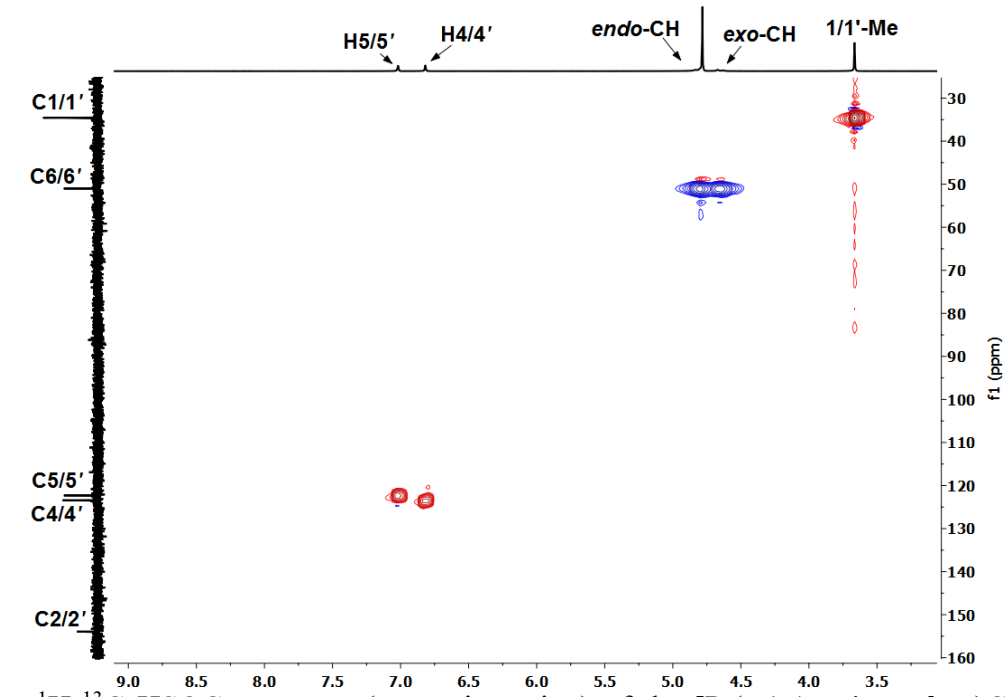

Figure A.5. ^{1}H-^{13}C HSQC spectrum (aromatic region) of the [Pt(*N*(H)1,1′-Me$_2$dma)Cl]Cl (**3a**) complex (25 °C, D$_2$O, pH 6, shifts in ppm).

NMR Assignments for [Pt(*N*(Me)1,1′-Me$_2$dma)Cl]Cl (4a). As discussed in the main text, **4a** has downfield ^{1}H NMR signals for the H4/4′ and H5/5′ aromatic protons. In the ROESY spectrum in D_2O for **4a** (Figure A.6), a strong NOE cross-peak from the 1/1′-Me signal at 3.78 ppm assigns the most downfield signal (7.19 ppm) to H5/5′. The other aromatic peak (7.05 ppm) can thus be assigned to H4/4′, an assignment supported by the NOE cross-peak to the H5/5′ signal and by the absence of any other cross-peak. By the reasoning used in the main text, the upfield and downfield methylene signals of **4a** were assigned to the *exo*-CH and *endo*-CH signals, respectively. Assignments of the ^{13}C NMR signals for **4a** were made through an HSQC experiment (Figure A.7). ^{13}C NMR signals for the C4/4′, C5/5′, and C1/1′ were assigned with the aid of cross-peaks (in ppm) involving the H4/4′ (7.05−124.3), H5/5′ (7.20−122.6), Me-1/1′ (3.78−34.7) and N-Me (3.14−52.73) signals, respectively. Cross-peaks from the *endo*-CH and *exo*-CH signals assign the ^{13}C NMR signal at 61.95 ppm to C6/6′. The signal at 152.87 ppm, the only ^{13}C NMR signal with no HSQC cross-peak, is assigned to C2/2′.

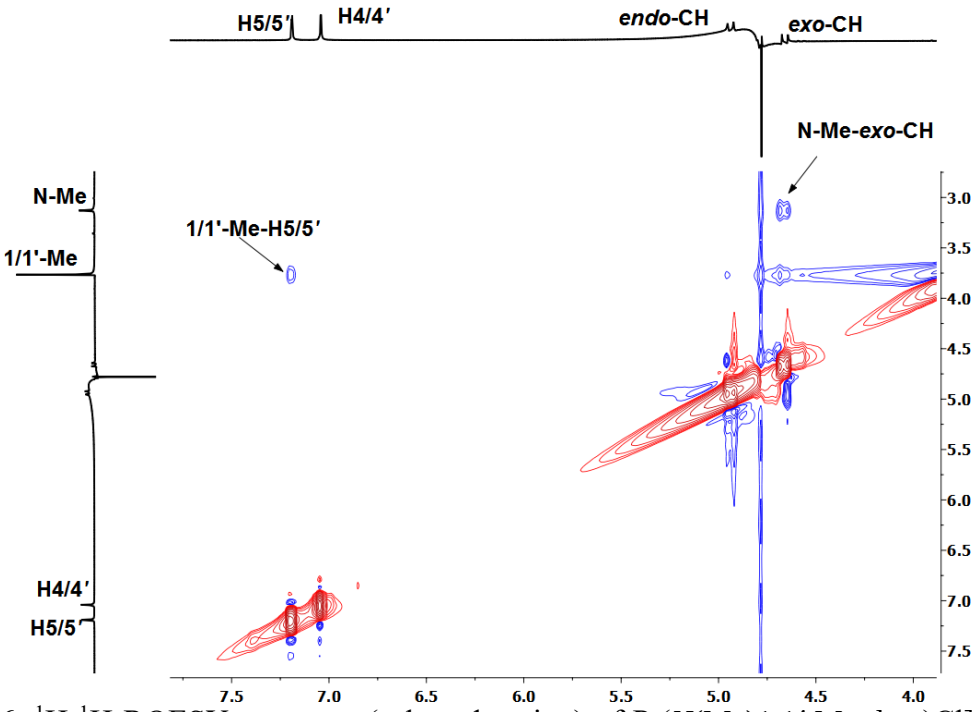

Figure A.6. ^{1}H-^{1}H ROESY spectrum (selected region) of Pt(*N*(Me)1,1′-Me$_2$dma)Cl]Cl (**4a**) (25 °C, D_2O, pH 6, shifts in ppm).

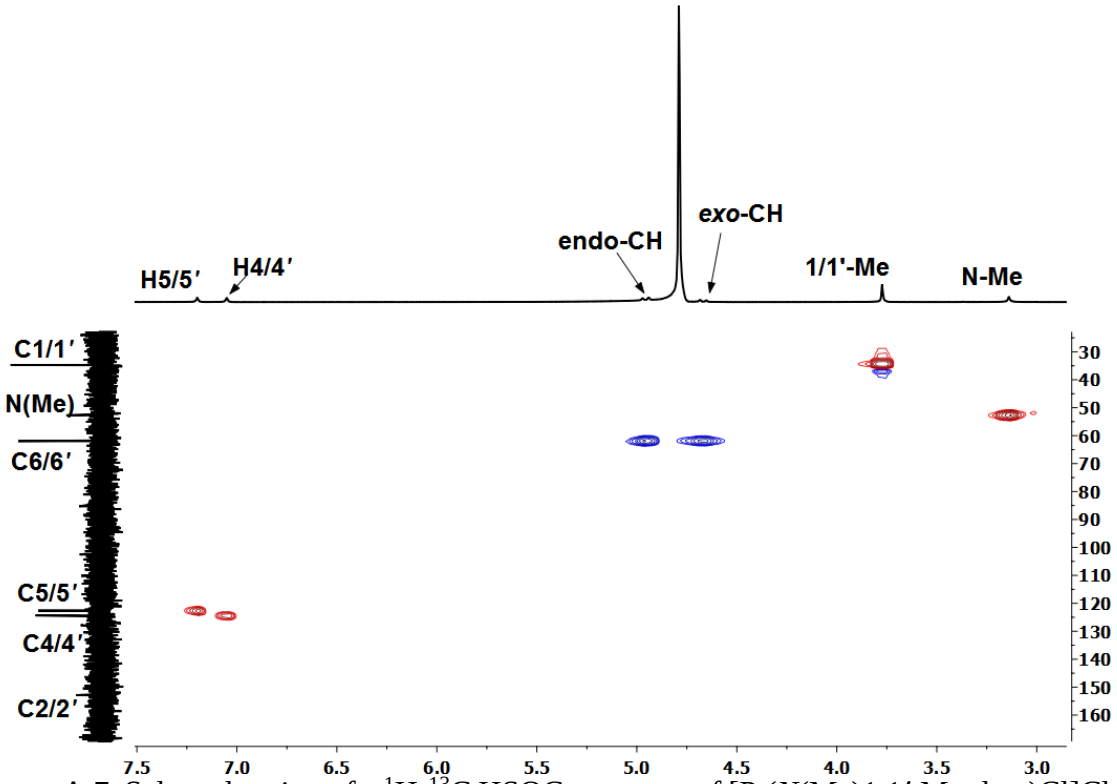

Figure A.7. Selected region of a ^{1}H-^{13}C HSQC spectrum of [Pt(*N*(Me)1,1′-Me_2dma)Cl]Cl (**4a**) (25 °C, D_2O, pH 6, shifts in ppm).

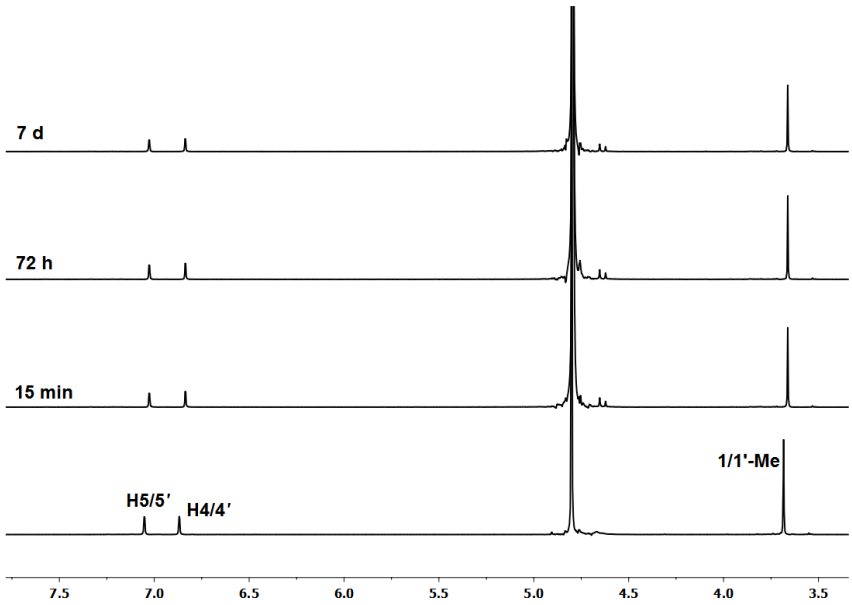

Figure A.8. ^{1}H NMR spectra of a 10 mM solution (600 μL) of [Pt(*N*(H)1,1′-Me_2dma)Cl]Cl (**3a**) (25 °C, D_2O, shifts in ppm) at pH 7 before (*bottom*), and after adding 10 μL of concentrated HCl (final $[H^+]$ = 0.2 M) at 15 min, 72 h and 7 d.

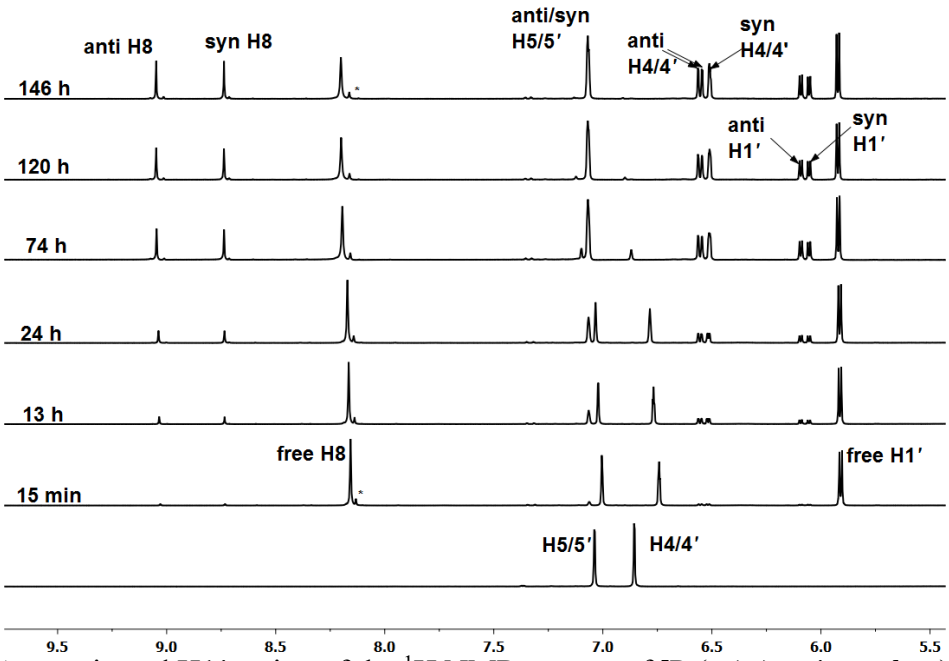

Figure A.9. Aromatic and H1′ region of the ^{1}H NMR spectra of [Pt(*N*(H)1,1′-Me$_2$dma)Cl]$^+$ (10 mM, *bottom*) and of the reaction mixture with 5′-GTP (1:2.5 molar ratio, 25 °C, D_2O, pH 4.0, shifts in ppm). Peaks labeled as * are from 5′-GDP present as an impurity.

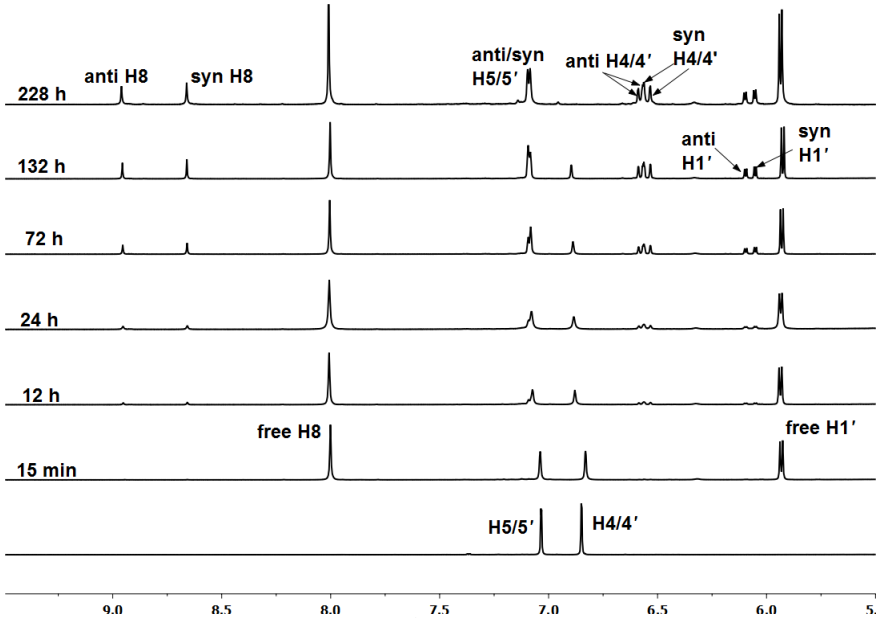

Figure A.10. Aromatic and H1′ region of the ^{1}H NMR spectra of [Pt(*N*(H)1,1′-Me$_2$dma)Cl]$^+$ (10 mM, *bottom*) and of the reaction mixture with 3′-GMP (1:2.5 molar ratio, 25 °C, D_2O, pH 4.0, shifts in ppm).

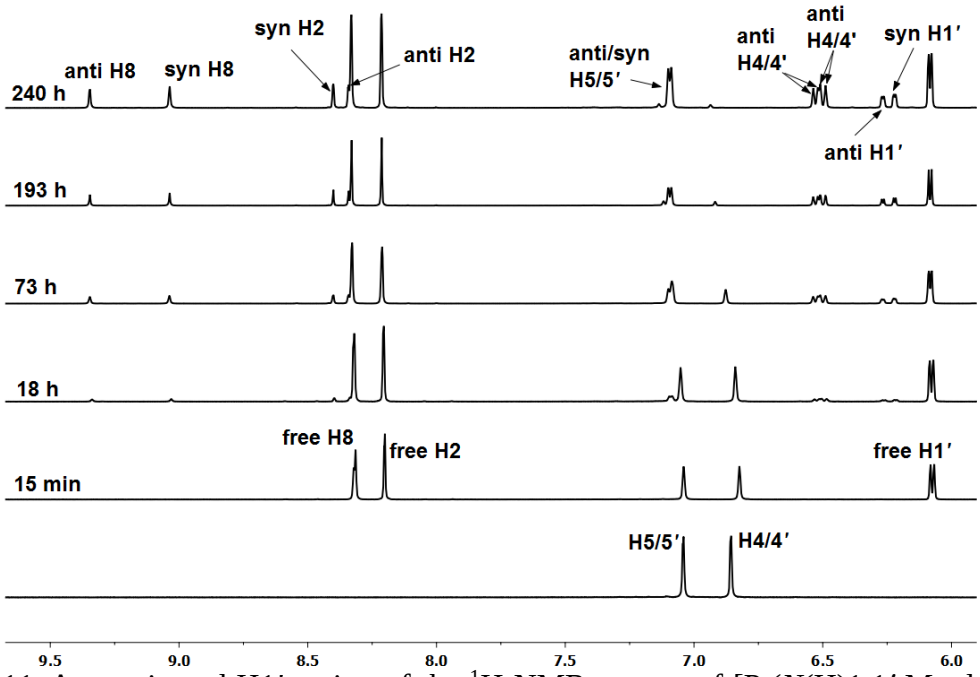

Figure A.11. Aromatic and H1′ region of the ^{1}H NMR spectra of [Pt(*N*(H)1,1′-Me$_2$dma)Cl]$^+$ (10 mM, *bottom*) and of the reaction mixture with Ino (1:2.5 molar ratio, 25 °C, D_2O, pH 4.0, shifts in ppm).

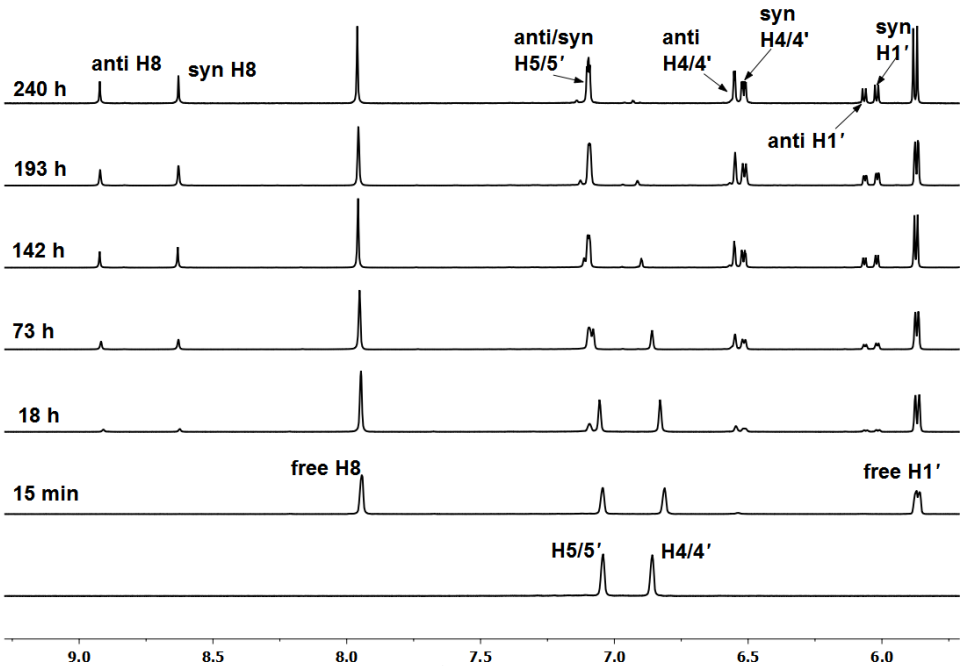

Figure A.12. Aromatic and H1′ region of the ^{1}H NMR spectra of [Pt(*N*(H)1,1′-Me$_2$dma)Cl]$^+$ (10 mM, *bottom*) and of the reaction mixture with 1-MeGuo (1:2.5 molar ratio, 25 °C, D_2O, pH 4.0, shifts in ppm).

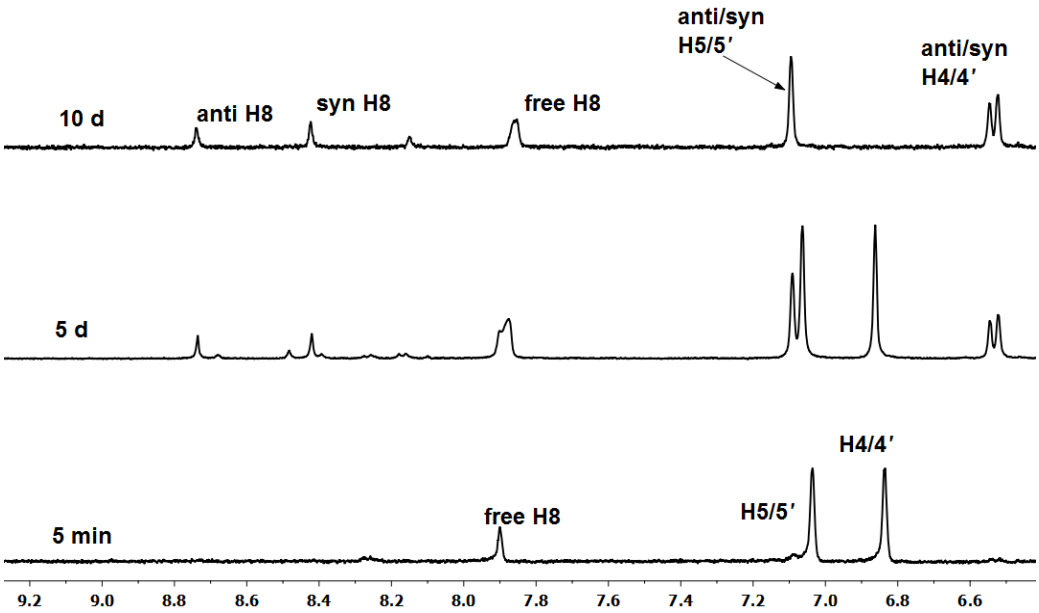

Figure A.13. Aromatic and H1′ region of the ^{1}H NMR spectra of [Pt(*N*(H)1,1′-Me$_2$dma)Cl]$^+$ (10 mM, *bottom*) and of the reaction mixture with 9-EtG (1:2.5 molar ratio, 25 °C, D$_2$O, pH 4.0, shifts in ppm). Note that 9-EtG is only partially soluble in D$_2$O.

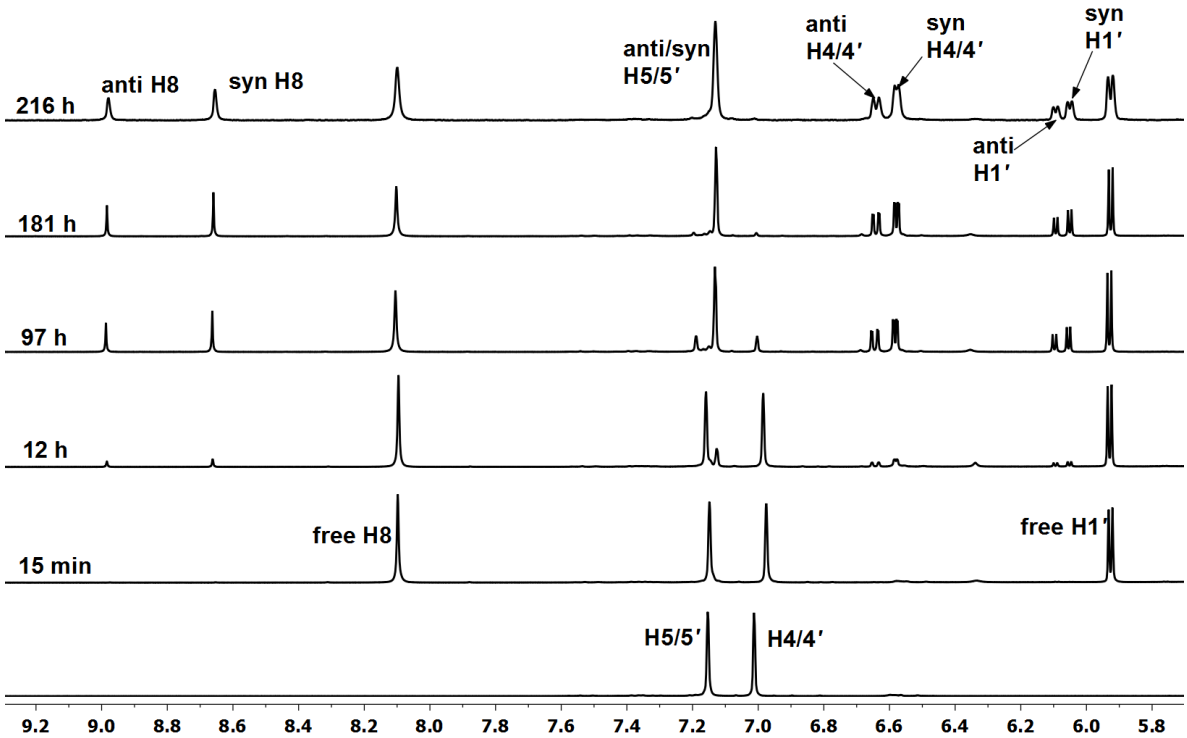

Figure A.14. Aromatic and H1′ region of the ^{1}H NMR spectra (25 °C, D$_2$O, pH 4) of [Pt(*N*(Me)1,1′-Me$_2$dma)Cl]$^+$(10 mM, bottom) and of the reaction mixture forming Pt(*N*(Me)1,1′-Me$_2$dma)(5′-GMP) 15 min, 12 h, 97 h, 181 h and 216 h after adding 2.5 molar equiv of 5′-GMP (shifts in ppm).

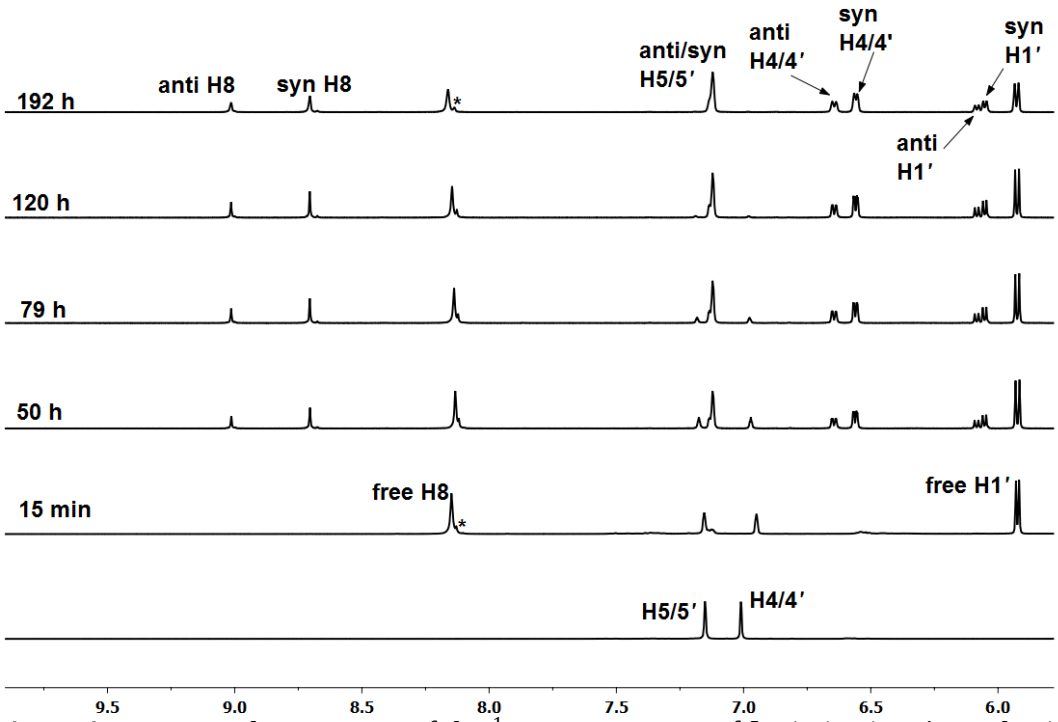

Figure A.15. Aromatic and H1′ region of the ^{1}H NMR spectra of [Pt(*N*(Me)1,1′-Me$_2$dma)Cl]$^+$ (10 mM, *bottom*) and of the reaction mixture with 5′-GTP (1:2.5 molar ratio, 25 °C, D_2O, pH 4.0, shifts in ppm). Peaks labeled as * are from 5′-GDP present as an impurity.

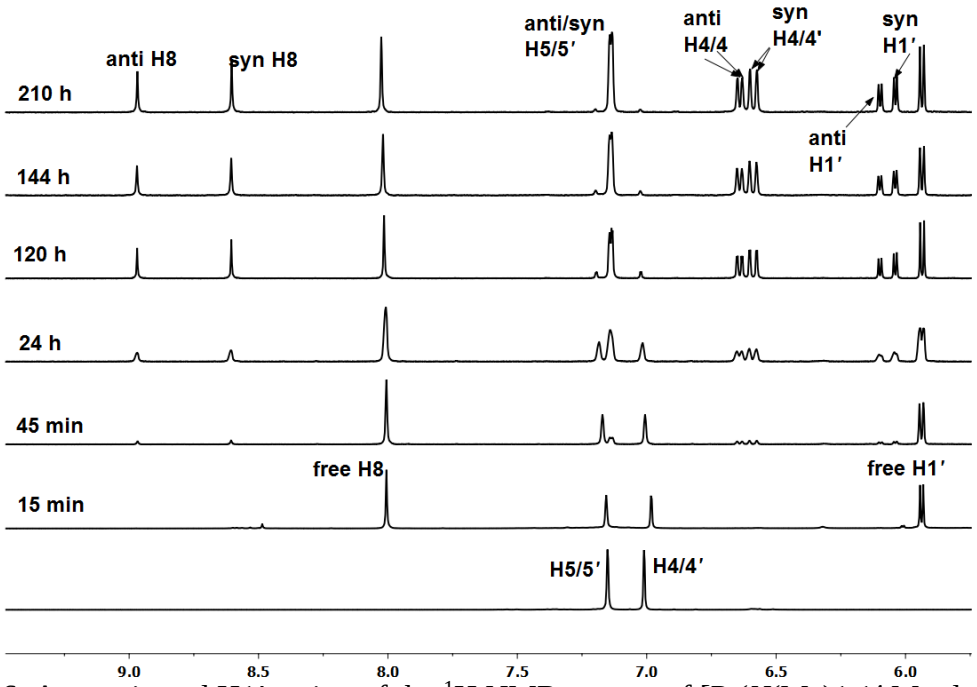

Figure A.16. Aromatic and H1′ region of the ^{1}H NMR spectra of [Pt(*N*(Me)1,1′-Me$_2$dma)Cl]$^+$ (10 mM, *bottom*) and of the reaction mixture with 3′-GMP (1:2.5 molar ratio, 25 °C, D_2O, pH 4.0, shifts in ppm).

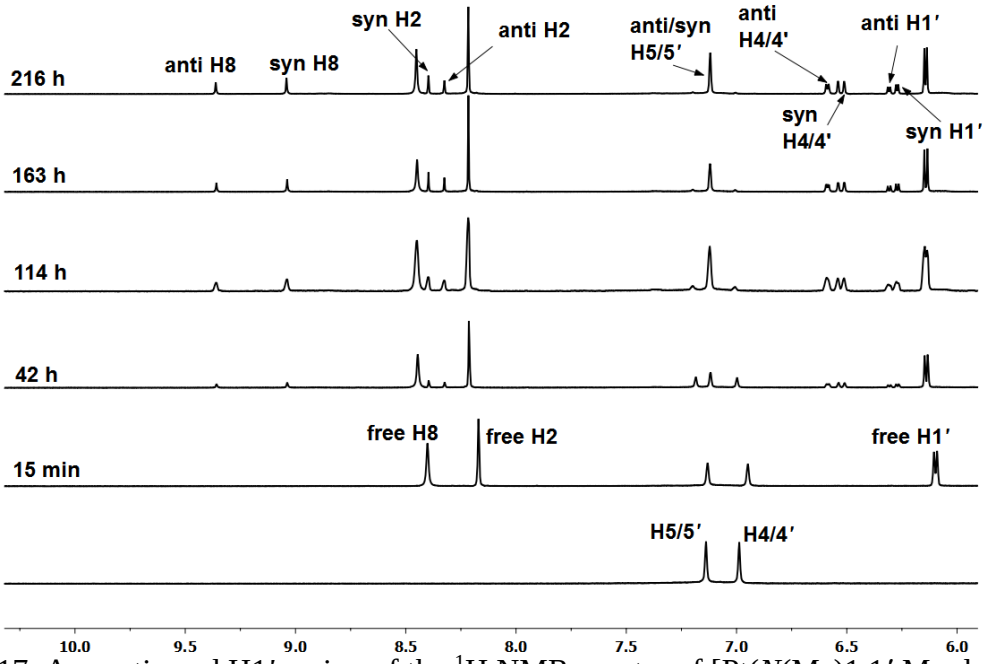

Figure A.17. Aromatic and H1′ region of the ^{1}H NMR spectra of [Pt(*N*(Me)1,1′-Me$_2$dma)Cl]$^{+}$ (10 mM, *bottom*) and of the reaction mixture with 5′-IMP (1:2.5 molar ratio, 25 °C, D_2O, pH 4.0, shifts in ppm).

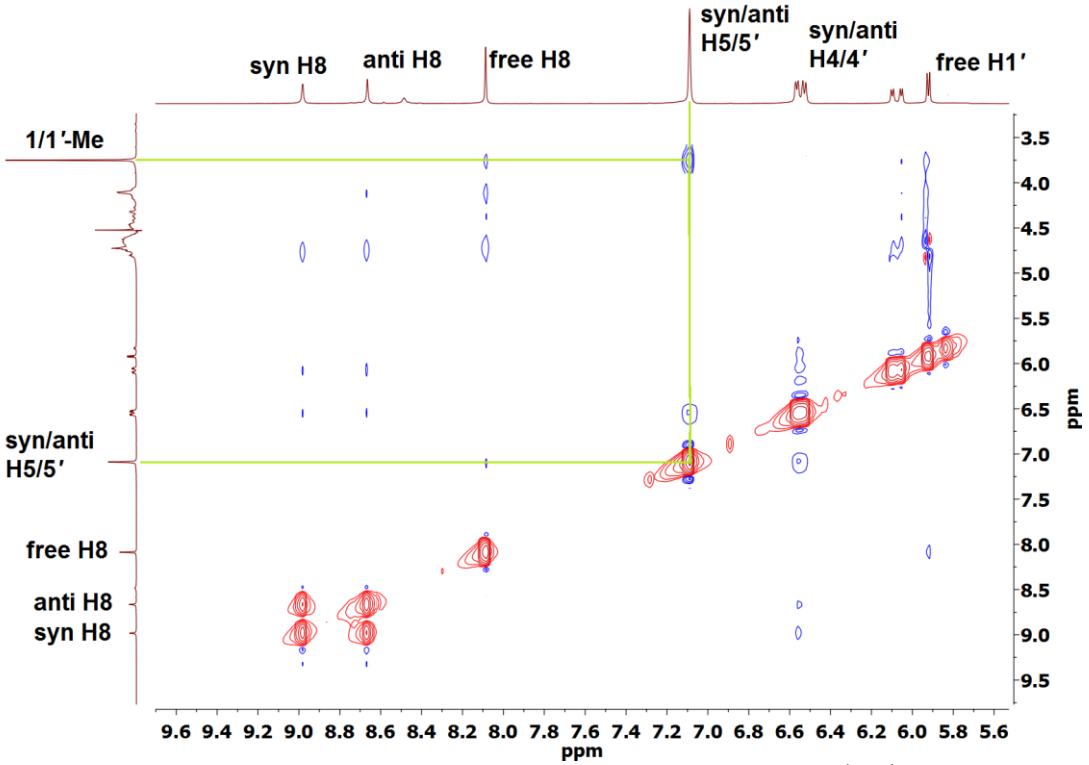

Figure A.18. 1,1′-Me-to-H5/5′ NOE cross-peak (traced in green) in the ^{1}H-^{1}H ROESY spectrum of the Pt(*N*(H)1,1′-Me$_2$dma)(5′-GMP) adduct (25 °C, D_2O, pH 4, shifts in ppm).

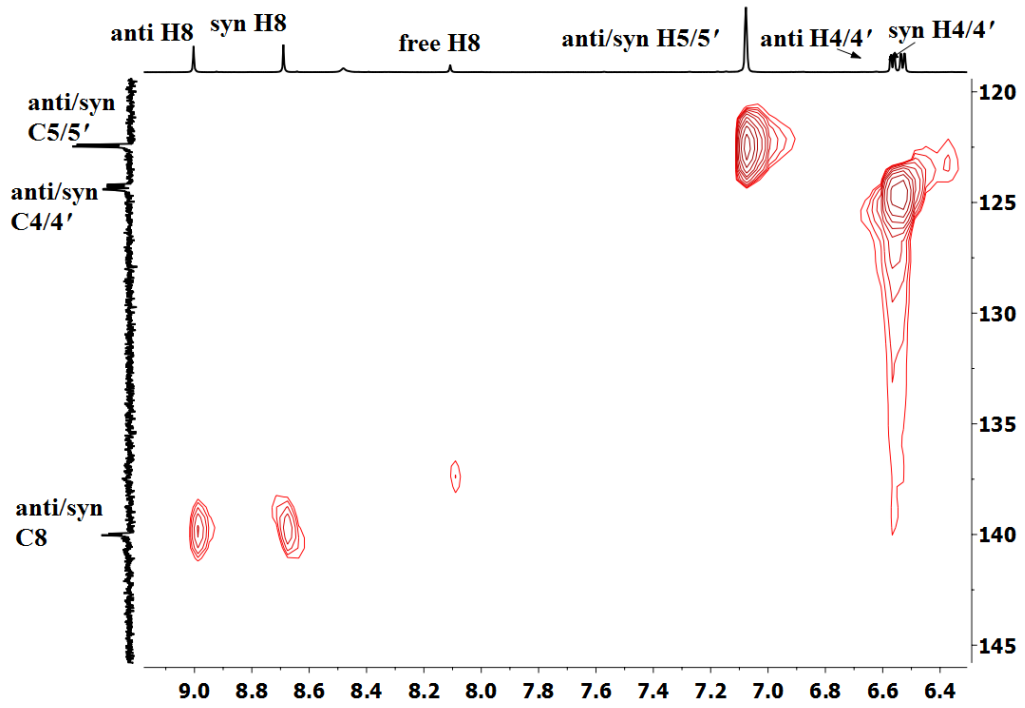

Figure A.19. ^{1}H-^{13}C HSQC spectrum (aromatic region) of the Pt(*N*(H)1,1′-Me$_2$dma)(5'-GMP) adduct (25 °C, D$_2$O, pH 4, shifts in ppm).

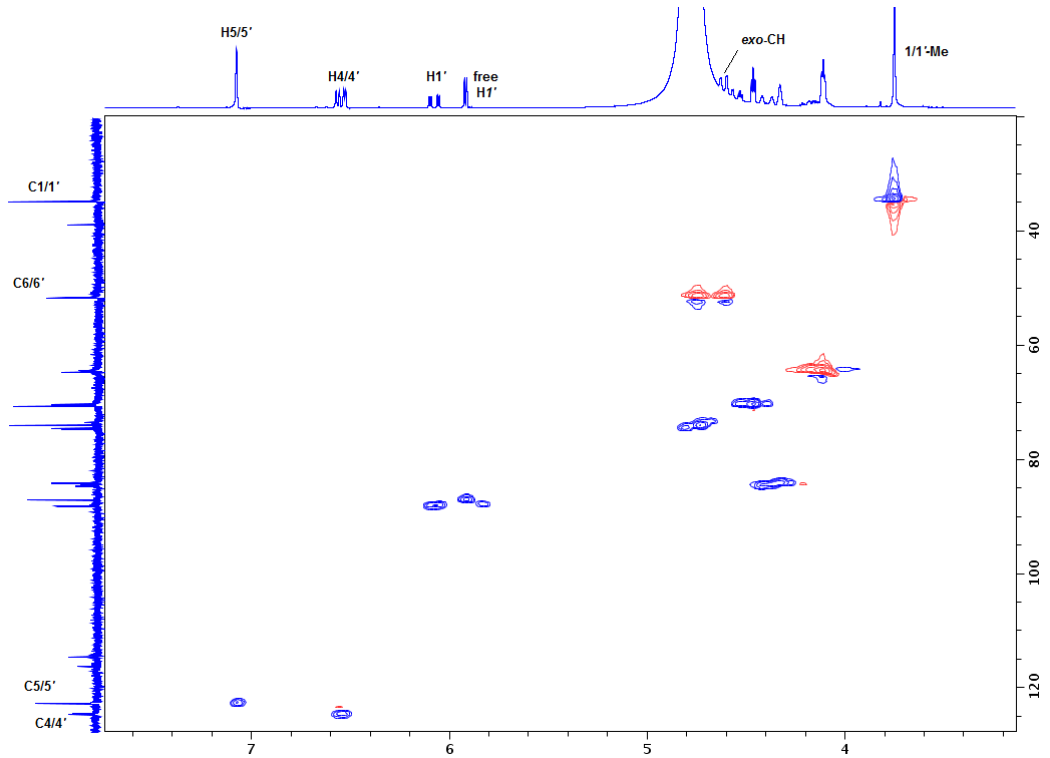

Figure A.20. ^{1}H-^{13}C HSQC spectrum (selected region) of the Pt(*N*(H)1,1′-Me$_2$dma)(5'-GMP) adduct (25 °C, D$_2$O, pH 4, shifts in ppm).

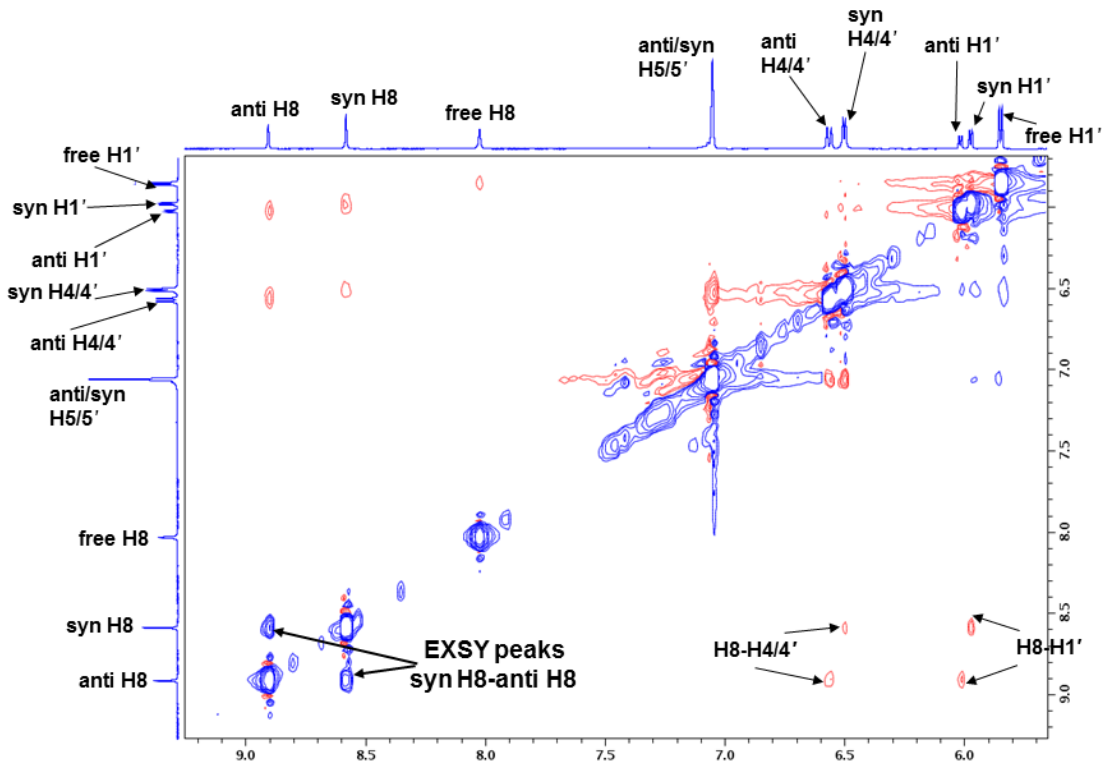

Figure A.21. A selected region of the ^{1}H-^{1}H ROESY spectrum of the Pt(*N*(Me)1,1′-Me$_2$dma)(5′-GMP) adduct (25 °C, D_2O, pH 4, shifts in ppm).

Table A.1. ^{1}H NMR Shifts (ppm) for the *N*(H)1,1′-Me$_2$dma Carrier Ligands in Pt(*N*(H)1,1′-Me$_2$dma)**G** Adducts and in [Pt(*N*(H)1,1′-Me$_2$dma)Cl]Cl in 65:35 D$_2$O:DMSO-d_6 (pH 4.0) at 25 °C. (Data[5] for [Pt(*N*(H)dpa)(Cl)]Cl and Pt(*N*(H)dpa)**G** Are Included for Comparison.)

Complex	H4/4′ or H6/6′		H5/5′	Me-1/1′	*N*(Me)
	syn	anti			
[Pt(*N*(H)1,1′-Me$_2$dma)Cl]Cl[a]	6.80		7.02	3.56	-
Pt(*N*(H)1,1′-Me$_2$dma)(5′-GMP)[a]	6.41, 6.39	6.44	6.96[b]	3.57	-
Pt(*N*(H)1,1′-Me$_2$dma)(5′-GTP)[a]	6.39, 6.37	6.42	6.97[b]	3.57	-
[Pt(*N*(H)dpa)(Cl)]Cl	8.61		7.34	-	-
Pt(*N*(H)dpa)(5′-GMP)	7.51, 7.44	7.57	7.21	-	-
Pt(*N*(H)dpa)(5′-GTP)	7.49, 7.43	7.57	7.23	-	-

[a]*endo* and *exo*-H6/6′ are masked by the solvent peak. [b]syn and anti signals are overlapped.

Table A.2. Selected ^{1}H NMR Shifts (ppm) for **G** in Pt(*N*(H)1,1′-Me$_2$dma)**G** Adducts 65:35 D$_2$O:DMSO-d_6 (pH 4.0) at 25 °C. (Data for Pt(*N*(H)dpa)**G**[5] Are Included for Comparison.)

Complex	H8 free	H8 syn	H8 anti	H1′ free	H1′ syn	H1′ anti	syn:anti ratio	Δδ
Pt(*N*(H)1,1′-Me$_2$dma)(5′-GMP)	7.95	8.57	8.86	5.71	5.85	5.89	1.08:1	0.29
Pt(*N*(H)1,1′-Me$_2$dma)(5′-GTP)	7.98	8.61	8.91	5.71	5.85	5.90	0.95:1	0.30
Pt(*N*(H)dpa)(5′-GMP)	7.96	8.72	9.08	5.71	5.91	5.98	1.14:1	0.36
Pt(*N*(H)dpa)(5′-GTP)	7.97	8.79	9.21	5.70	5.91	5.98	0.82:1	0.42

Appendix A. References

1. Benedetti, M.; Tamasi, G.; Cini, R.; Natile, G. *Chem. -Eur. J.* **2003,** *9* (24), 6122-6132.

2. Benedetti, M.; Tamasi, G.; Cini, R.; Marzilli, L. G.; Natile, G. *Chem. -Eur. J.* **2007,** *13* (11), 3131-3142.

3. Sheldrick, W. S. *Z. Naturforsch.* **1983,** *38 b*, 16-19.

4. Saenger, W., *Principles of Nucleic Acid Structure*. Springer: Berlin, 1984.

5. Barnham, K. J.; Bauer, C. J.; Djuran, M. I.; Mazid, M. A.; Rau, T.; Sadler, P. J. *Inorg. Chem.* **1995,** *34* (11), 2826-2832.

6. Djuran, M. I.; Milinkovic, S. U.; Habtemariam, A.; Parsons, S.; Sadler, P. J. *J. Inorg. Biochem.* **2002,** *88* (3–4), 268-273.

7. Altona, C.; Sundaralingam, M. *J. Am. Chem. Soc.* **1972,** *94* (23), 8205-8212.

8. Okamoto, K.; Behnam, V.; Tan Phan Viet, M.; Polissiou, M.; Gauthier, J.-Y.; Hanessian, S.; Theophanides, T. *Inorg. Chim. Acta* **1986,** *123* (1), L3-L5.

9. Reily, M. D.; Marzilli, L. G. *J. Am. Chem. Soc.* **1986,** *108*, 8299-8300.

10. Melanson, R.; Rochon, F. D. *Acta Crystallogr., Sect. B: Struct. Sci.* **1978,** *34* (12), 3594-3598.

11. Andrepont, C.; Marzilli, P. A.; Marzilli, L. G. *Inorg. Chem.* **2012,** *51* (21), 11961-11970.

APPENDIX B. SUPPLEMENTARY MATERIAL FOR CHAPTER 3

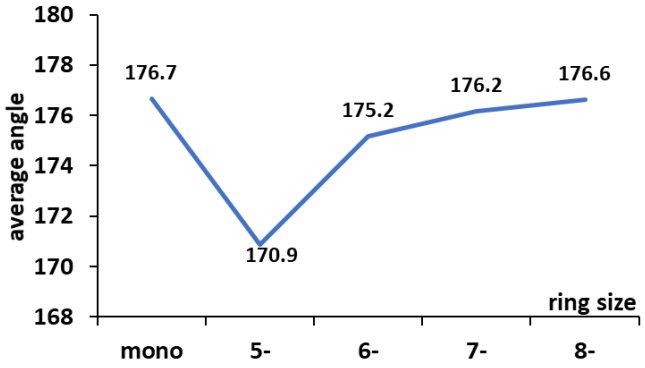

Figure B.1. Relationship between the average Pt–N–aromatic ring centroid angle and the chelate ring size of bifunctional Pt(II) complexes of linear ligands terminated by pyridyl or imidazolyl rings (with the remaining coordination sites occupied by halide). Plot is based on reported molecular structures (Cambridge Crystallographic Data Centre, ConQuest 1.19); of the 108 structures available for complexes with a 5-membered chelate ring, data from 26 randomly selected structures were used to prepare the plot. Data for bifunctional Pt(II) complexes of monodentately bound pyridyl or imidazolyl rings are also included for comparison.

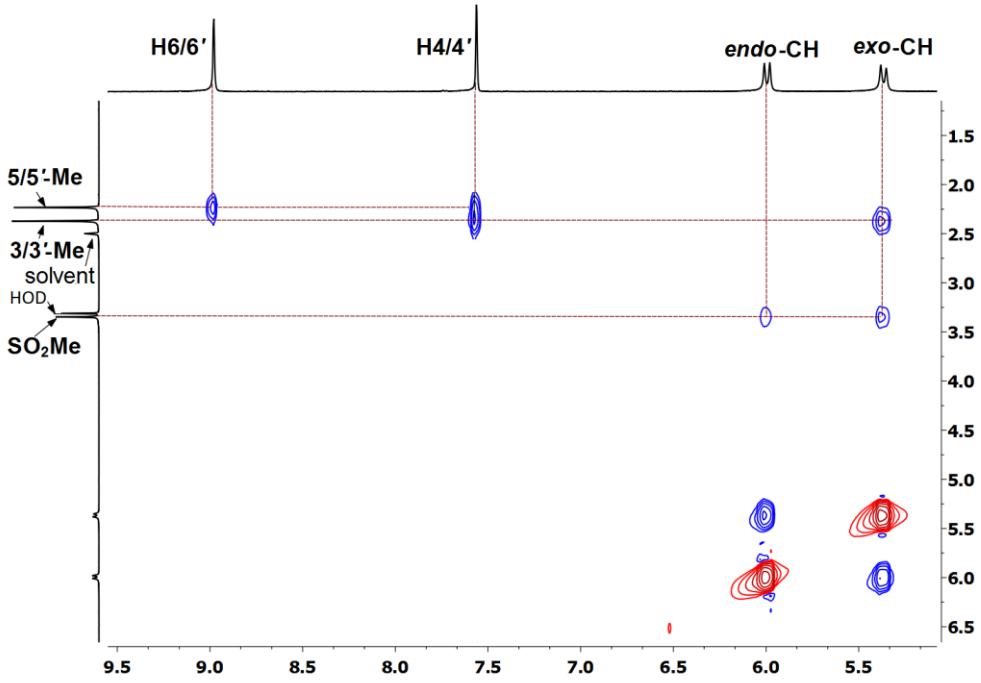

Figure B.2. ^{1}H-^{1}H ROESY spectrum (selected region) of Pt(*N*(SO_2Me)3,3′,5,5′-Me_4dpa)Cl_2 (**5**) (25 °C, 10 mM, DMSO-d_6, shifts in ppm). which is diminished when the solvent peak is suppressed.

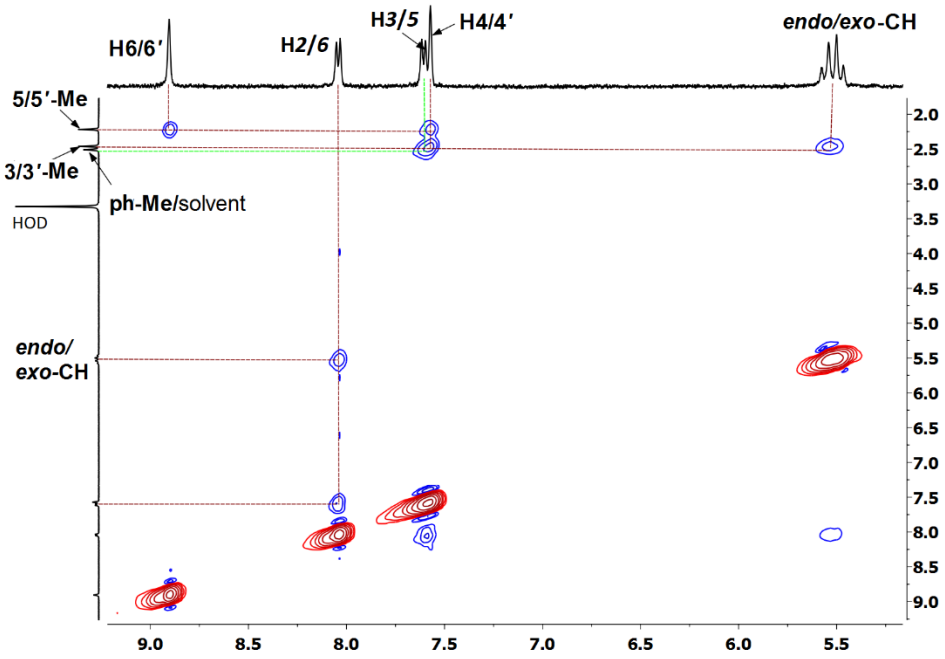

Figure B.3. ^{1}H-^{1}H ROESY spectrum (selected region) of Pt(*N*(SO_2Tol)3,3′,5,5′-Me_4dpa)Cl_2 (**6**) (25 °C, 10 mM, DMSO-d_6, shifts in ppm).

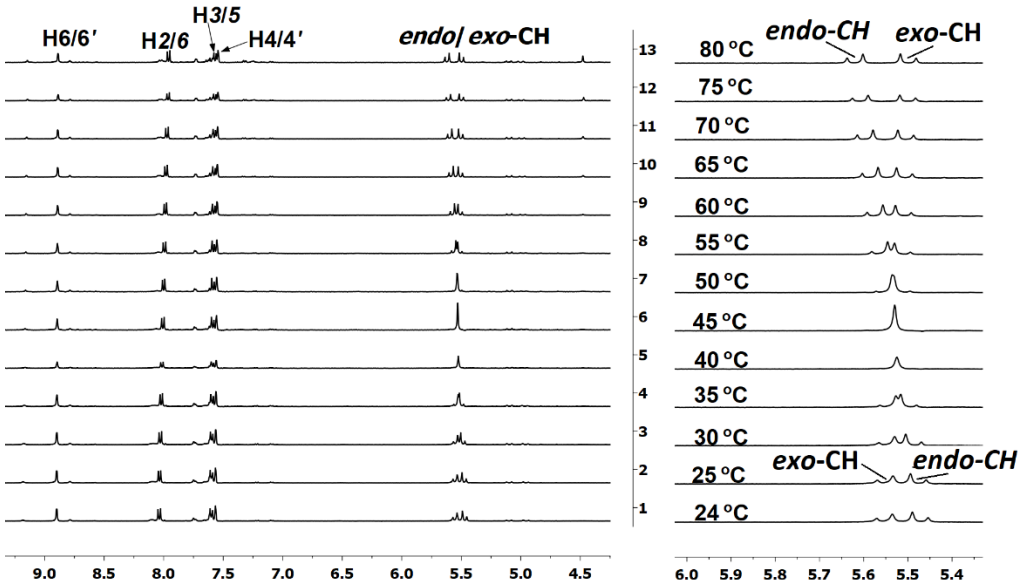

Figure B.4. Stack plot of ^{1}H NMR spectra (selected region) of Pt(*N*(SO_2Tol)3,3′,5,5′-Me_4dpa)Cl_2 (**6**) taken at different temperatures (10 mM, DMSO-d_6, shifts in ppm).

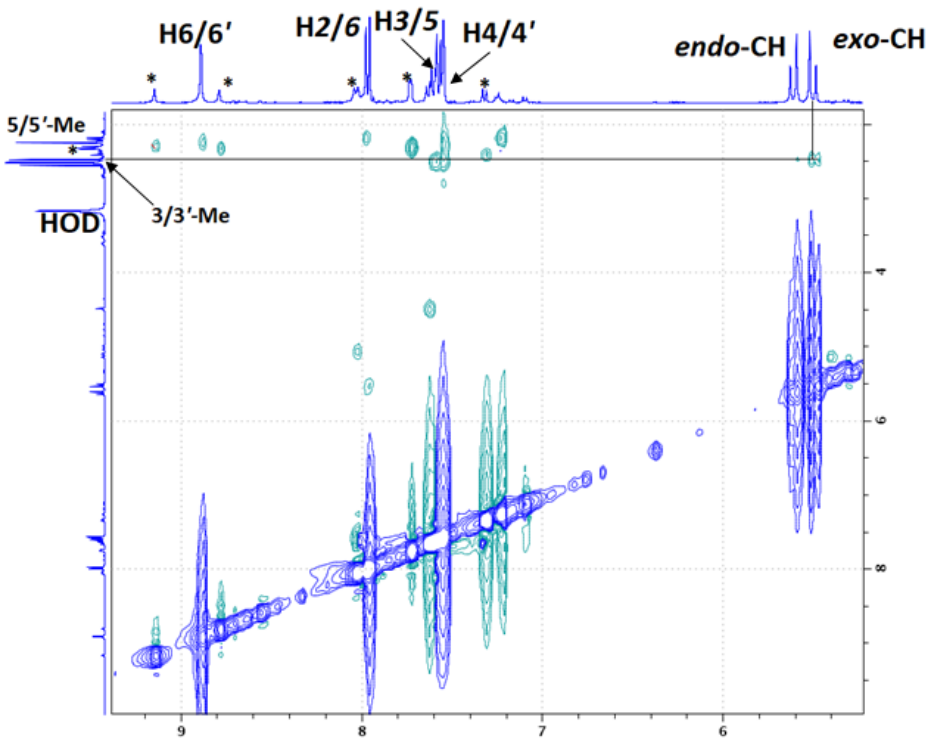

Figure B.5. ^{1}H-^{1}H ROESY spectrum (selected region) of Pt(*N*(SO_2Tol)3,3′,5,5′-Me_4dpa)Cl_2 (**6**) (75 °C, 10 mM, DMSO-d_6, shifts in ppm). *Solvolysis peaks.

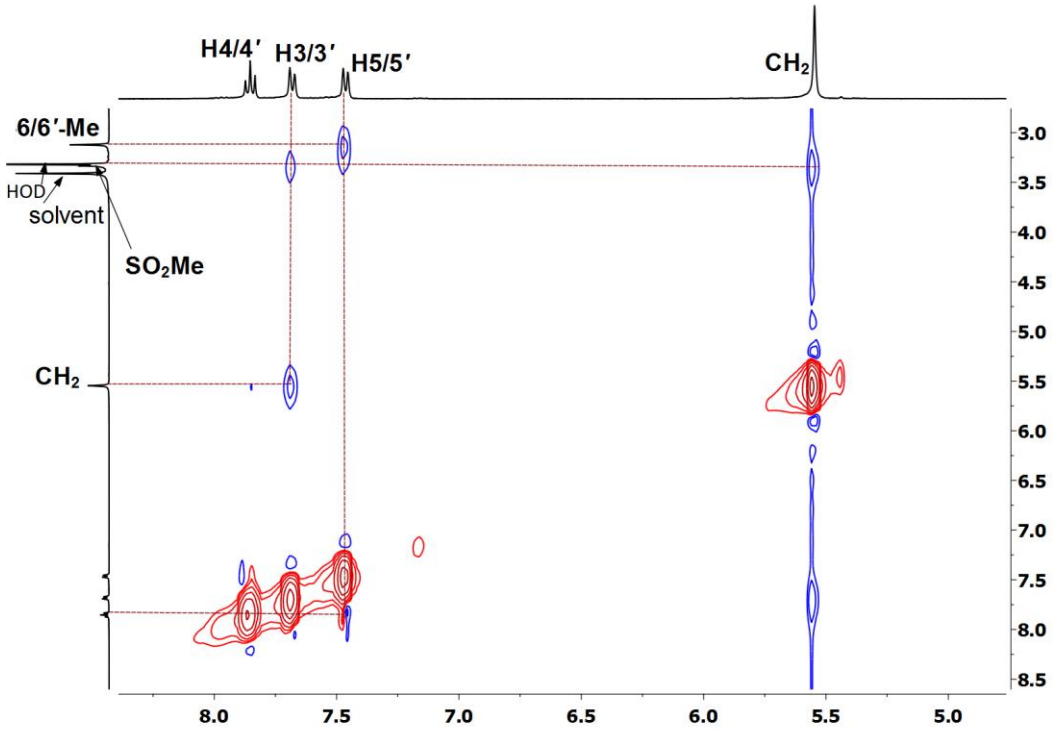

Figure B.6. ^{1}H-^{1}H ROESY spectrum (selected region) of [*trans*-Pt(DMSO)Cl_2]$_2$(*N*(SO_2Me)6,6′-Me_2dpa) (**7**) (25 °C, 10 mM, DMSO-d_6, shifts in ppm).

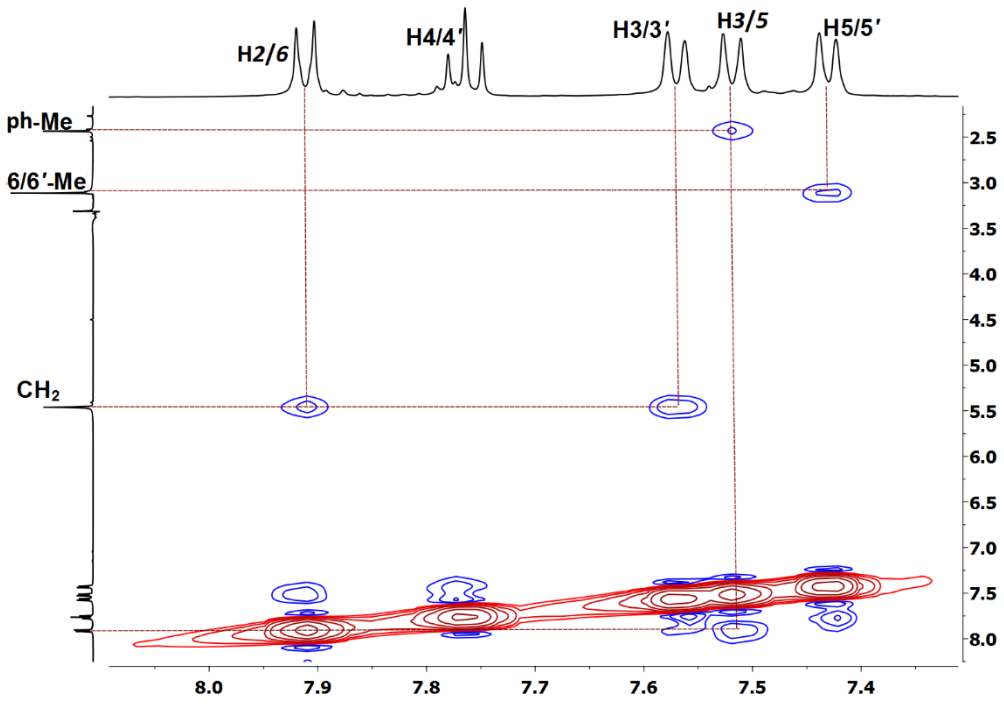

Figure B.7. ^{1}H-^{1}H ROESY spectrum (selected region) of [*trans*-Pt(DMSO)Cl$_2$]$_2$(*N*(SO$_2$Tol)6,6′-Me$_2$dpa) (**8**) (25 °C, 10 mM, DMSO-d_6, shifts in ppm).

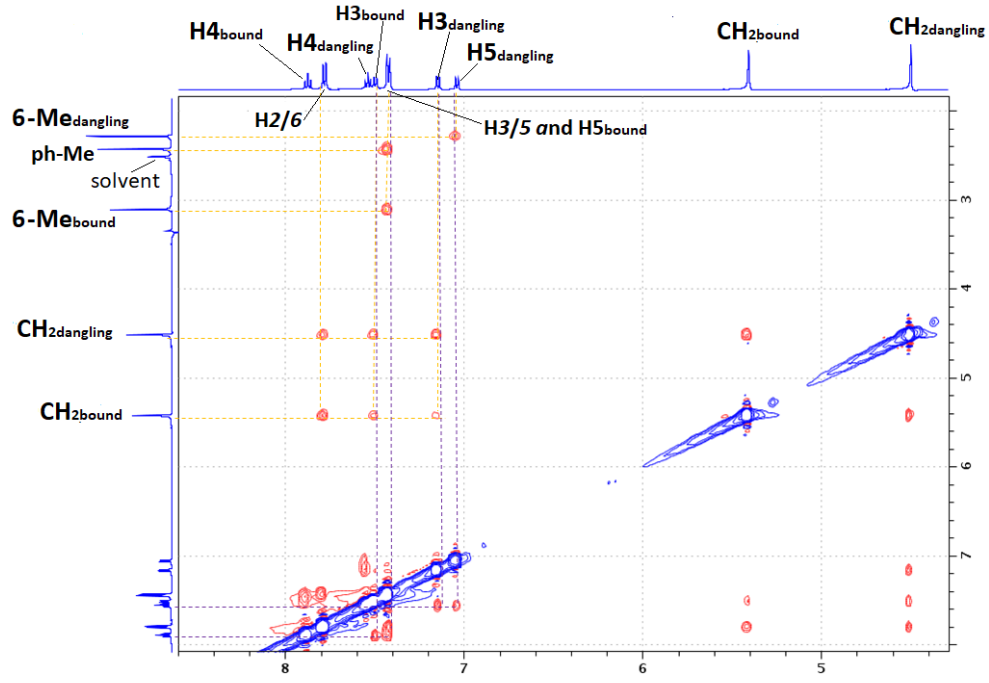

Figure B.8. ^{1}H-^{1}H ROESY spectrum (selected region) of [*trans*-Pt(DMSO)Cl$_2$](*N*(SO$_2$Tol)6,6′-Me$_2$dpa) (**8a**) (25 °C, 10 mM, DMSO-d_6, shifts in ppm).

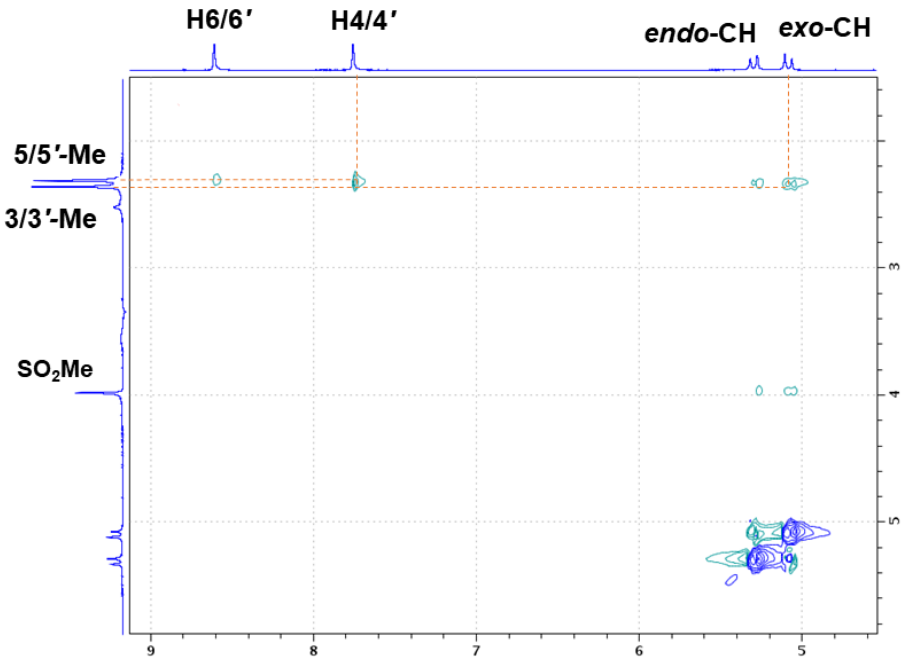

Figure B.9. ^{1}H-^{1}H ROESY spectrum (selected region) of *fac*-[Re(CO)$_3$(*N*(SO$_2$Me)3,3′,5,5′-Me$_4$dpa)]PF$_6$ (**9**) (25 °C, 10 mM, DMSO-d_6, shifts in ppm).

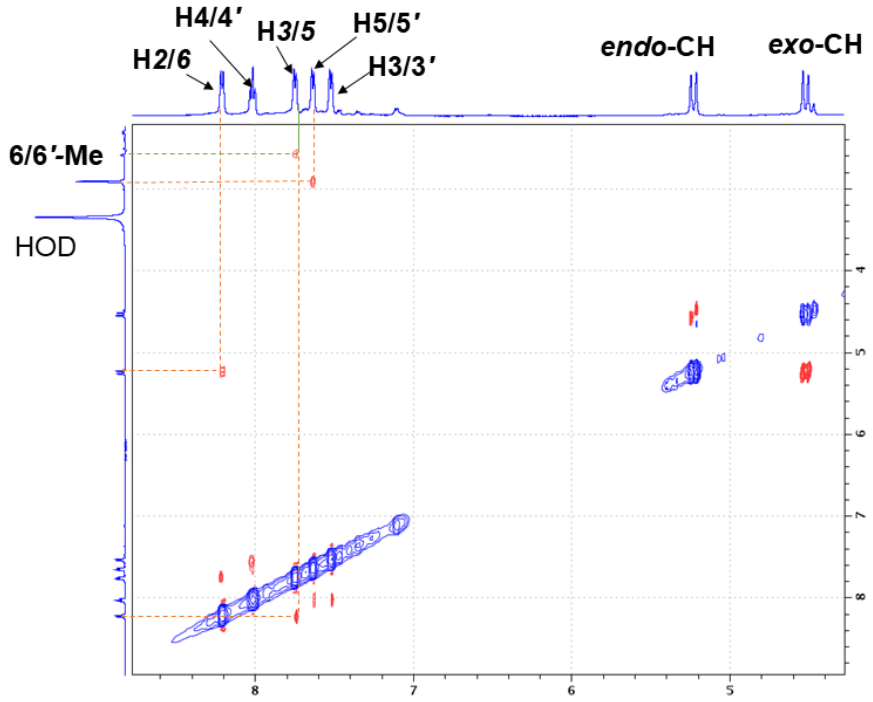

Figure B.10. ^{1}H-^{1}H ROESY spectrum (selected region) of *fac*-[Re(CO)$_3$(*N*(SO$_2$Tol)6,6′-Me$_2$dpa)]PF$_6$ (**12**) (25 °C, 10 mM, DMSO-d_6, shifts in ppm). The green line indicates the NOE cross-peak between the H*3*/*5* signal and the *p*-tolyl methyl signal, which is diminished when the solvent peak is suppressed.

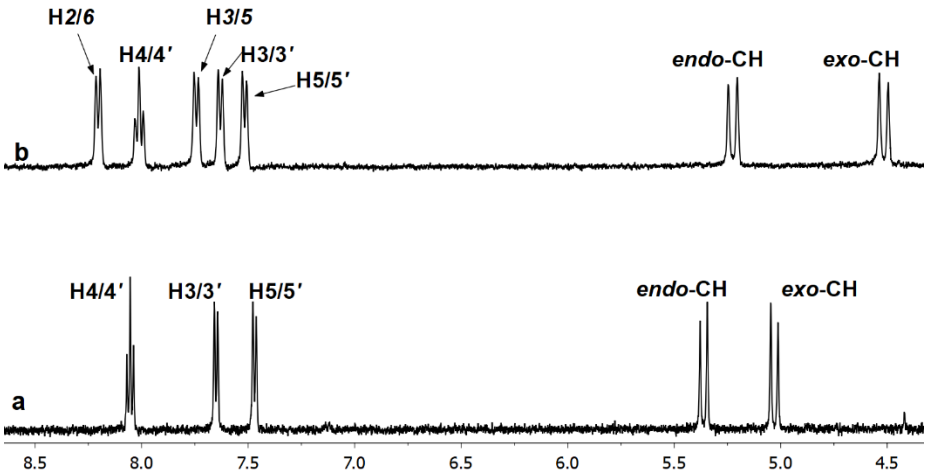

Figure B.11. Selected region of ^{1}H NMR spectra in DMSO-d_6 at 25 °C (shifts in ppm) of (a) [Re(CO)$_3$(*N*(SO$_2$Me)6,6′-Me$_2$dpa)]PF$_6$ (**11**) and (b) Re(CO)$_3$(*N*(SO$_2$Tol)6,6′-Me$_2$dpa)]PF$_6$ (**12**).

^{1}H NMR Assignments of Methylene Signals. In the ROESY Spectrum of **5** (Figure B.2), the 3/3′-Me signal has a very intense NOE cross-peak with the more upfield methylene doublet (5.37 ppm). The cross-peak allows us to assign the doublet to the *exo*-CH, owing to the spatial proximity of the *exo*-CH protons to the 3/3′-Me group (the non-bonded distances range from 2.22−2.31 Å). Therefore, the more downfield doublet (5.99 ppm) can confidently be assigned to the *endo*-CH (the non-bonded distances between the *endo*-CH and the 3/3′-Me groups range from 3.66−3.71 Å). This conclusion is further supported by a relatively stronger *exo*-CH to SO$_2$Me NOE cross-peak compared to the *endo*-CH to SO$_2$Me NOE cross-peak. In the molecular structure, the non-bonded distances between this methyl group and the *exo*-CH (2.59−2.62 Å) are smaller than the distances to the *endo*-CH (2.78−2.86 Å). This reasoning applies also to *fac*-[Re(CO)$_3$(*N*(SO$_2$R)Me$_n$dpa)]PF$_6$ complexes (**9**−**12**), and the ROESY spectra for **9** and **12** are shown in Figures S9 and S10.

The ROESY spectrum of **6** taken at 25 °C (Figure B.3) has strong NOE cross-peaks between the methylene AB signals and the 3/3′-Me and H2/6 protons. However, it is difficult to assign the AB signals to *endo*- or *exo*-CH protons because the two AB signals have very similar

shifts (separated by 0.08 ppm). Therefore, to assign the methylene signals of **6**, the temperature dependence of the shift of the methylene signals was investigated (Figure B.4). With increasing temperature, the more downfield AB signal (5.55 ppm at 25 °C) moved upfield and the other signal moved downfield (the two signals crossed between 40-50 °C). In the ROESY spectrum of **6** at 75 °C (Figure B.5), the 3/3′-Me signal has an intense NOE cross-peak with the more upfield methylene signal (5.50 ppm), a finding allowing assignment of the 5.50 ppm signal to the *exo*-CH. Therefore, the more downfield signal (5.60 ppm) can confidently be assigned to the *endo*-CH. The more upfield AB signal at 75 °C and the more downfield AB signal at 25 °C can be assigned to the *exo*-CH. Similarly, the more upfield AB signal at 25 °C can be assigned to the *endo*-CH.

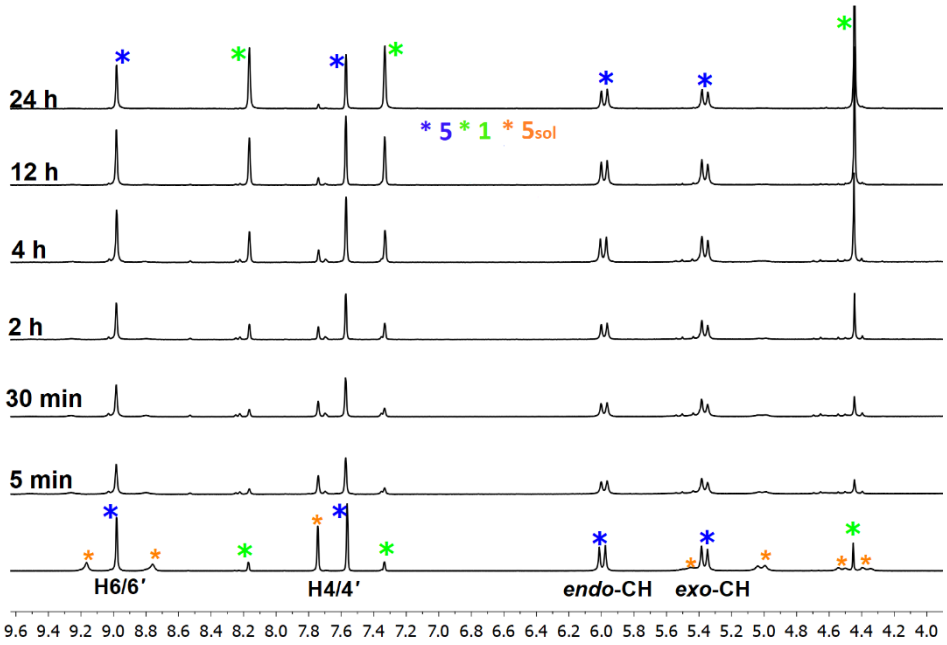

Figure B.12. Selected region of ^{1}H NMR spectra showing the reduction of $\mathbf{5}_{sol}$ peaks in a 1-day-old solution of Pt(*N*(SO_2Me)3,3′,5,5′-Me_4dpa)Cl_2 (**5**) in DMSO-d_6 (10 mM, bottom spectrum) when 10 mg (10 molar equiv) of solid [Et_4N]Cl was added (Solution 2). Spectra recorded 5 min, 30 min, 2 h, 4 h, 12 h, and 24 h after adding [Et_4N]Cl (25 °C, shifts in ppm).

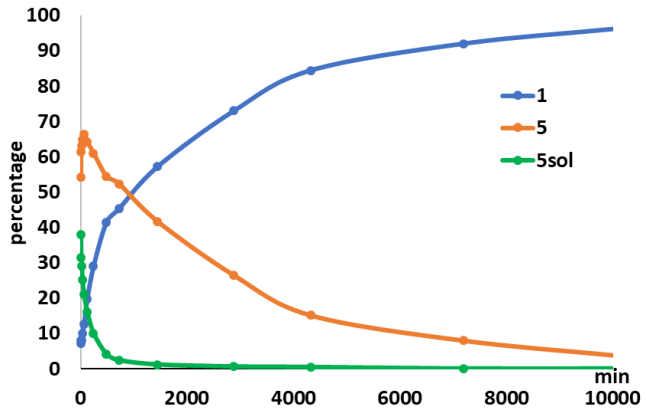

Figure B.13. Percent distribution of Pt(*N*(SO_2Me)3,3′,5,5′-Me_4dpa)Cl_2 (**5**, orange), [Pt(*N*(SO_2Me)3,3′,5,5′-Me_4dpa)(DMSO)Cl]$^+$ (**5**$_{sol}$, green), and free *N*(SO_2Me)3,3′,5,5′-Me_4dpa (**1**, blue) in Solution 2 [a mixture of [Et_4N]Cl (10 mg, 10 molar equiv) added to a 1-day-old solution of **5** (10 mM) in DMSO-d_6] at 25 °C plotted versus time. Percent distribution values were calculated by using integrations of H4/4′ signals of each species.

Table B.1. Selected ^{1}H NMR Chemical Shifts for *N*(SO_2Me)3,3′,5,5′-Me_4dpa (**1**) and *N*(SO_2Tol)3,3′,5,5′-Me_4dpa (**2**) and for Their Pt(II) Complexes (ppm, DMSO-d_6, 25 °C)

	H6/6′	H4/4′	CH_2	5/5′-Me	3/3′-Me	SO_2Me	SO_2Tol		
							H*2/6*	H*3/5*	Me
1	8.17	7.33	4.45	2.12	2.23	3.13	-	-	-
5	8.98	7.56	5.99, 5.37	2.23	2.37	3.35	-	-	-
5[a]	9.04	7.61	6.25, 5.50	2.29	2.48	3.46	-	-	-
2	7.94	7.21	4.41	2.13	2.16	-	7.62	7.32	2.39
6	8.9	7.56	5.55, 5.47	2.21	2.45	-	8.03	7.60	2.50[b]
6[a]	8.97	7.63	5.77, 5.66	2.28	2.59	-	8.12	7.65	2.52

[a]Shifts in DMF-d_7, reference peak at 8.03 ppm. [b]Signal is masked by the solvent peak (DMSO-d_6).

APPENDIX C. SUPPLEMENTARY MATERIAL FOR CHAPTER 4

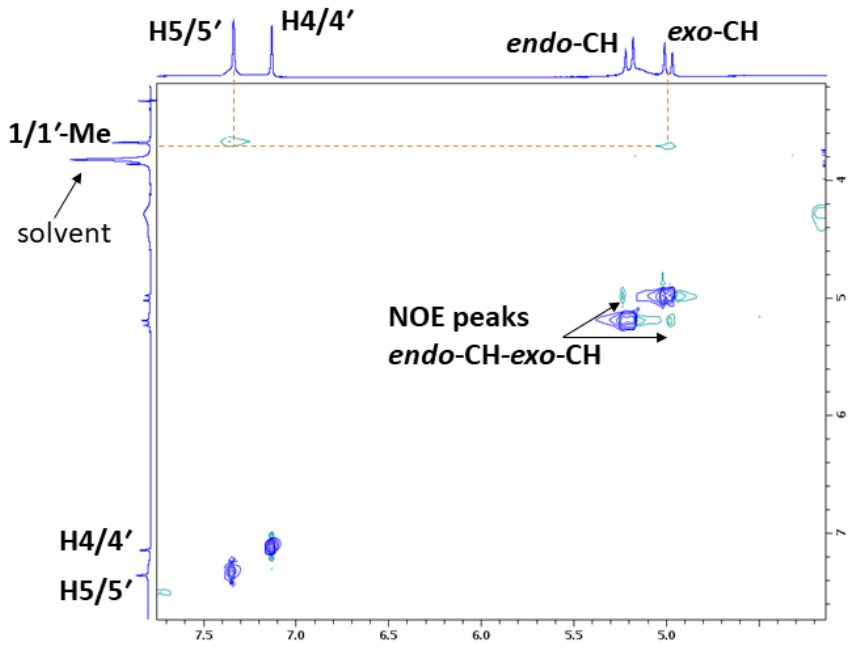

Figure C.1. ^{1}H-^{1}H ROESY spectrum (selected region) of *fac*-[Re(CO)$_3$(*N*(SO$_2$Me)1,1′-Me$_2$dma)]ClO$_4$ (**3**) (25 °C, 10 mM, DMSO-d_6, shifts in ppm).

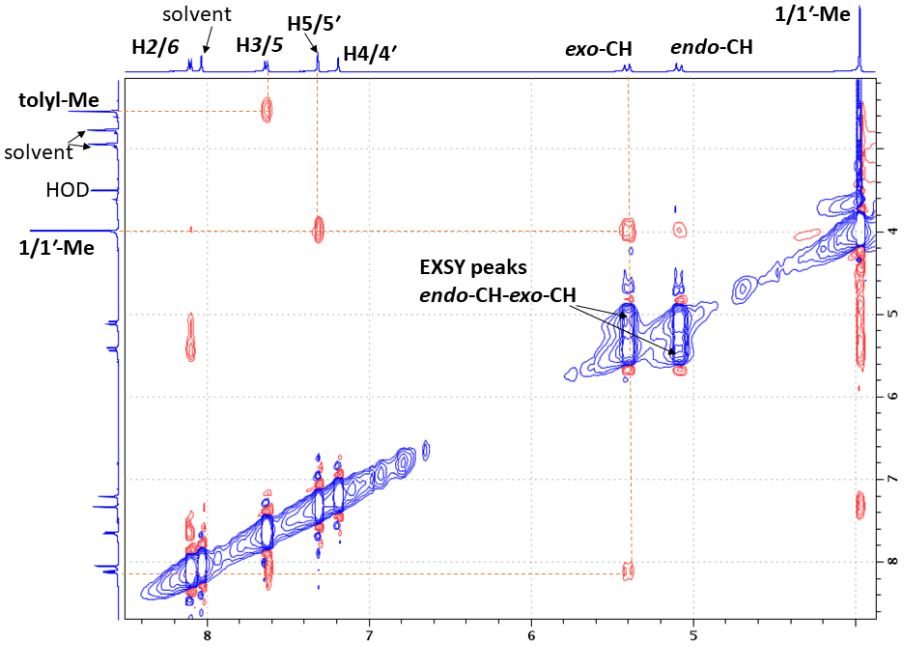

Figure C.2. ^{1}H-^{1}H ROESY spectrum (selected region) of Pt(*N*(SO$_2$Tol)1,1′-Me$_2$dma)Cl$_2$ (**6**) (25 °C, 10 mM, DMF-d_7, shifts in ppm).

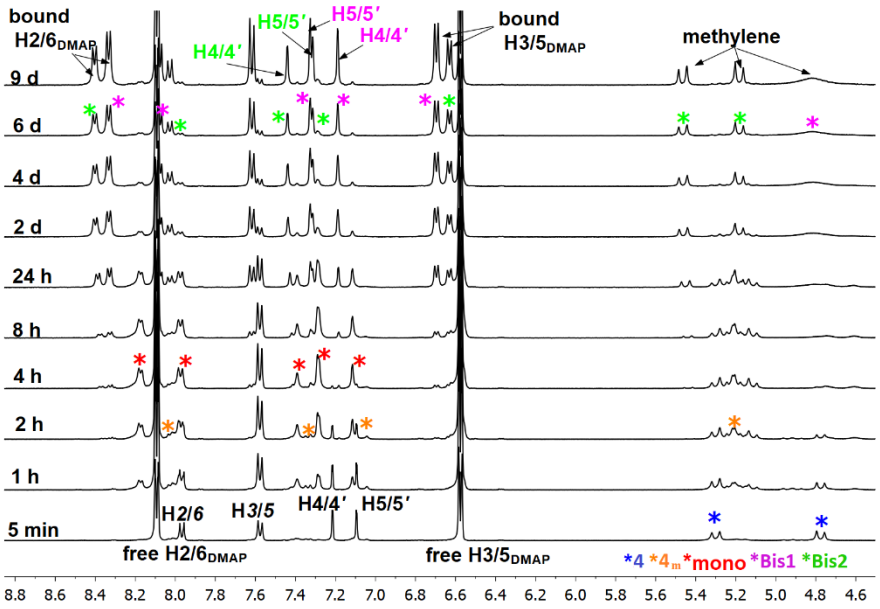

Figure C.3. Selected region of ^{1}H NMR spectra showing the formation of mono (red) and bis adducts (Bis1-purple and Bis2-green) of **6** with DMAP at various time points after 1.9 mg of Pt(*N*(SO_2Tol)1,1′-Me_2dma)Cl_2 (**6**, blue) was dissolved in a 20 mM solution of DMAP in DMSO-d_6 (25 °C, shifts in ppm).

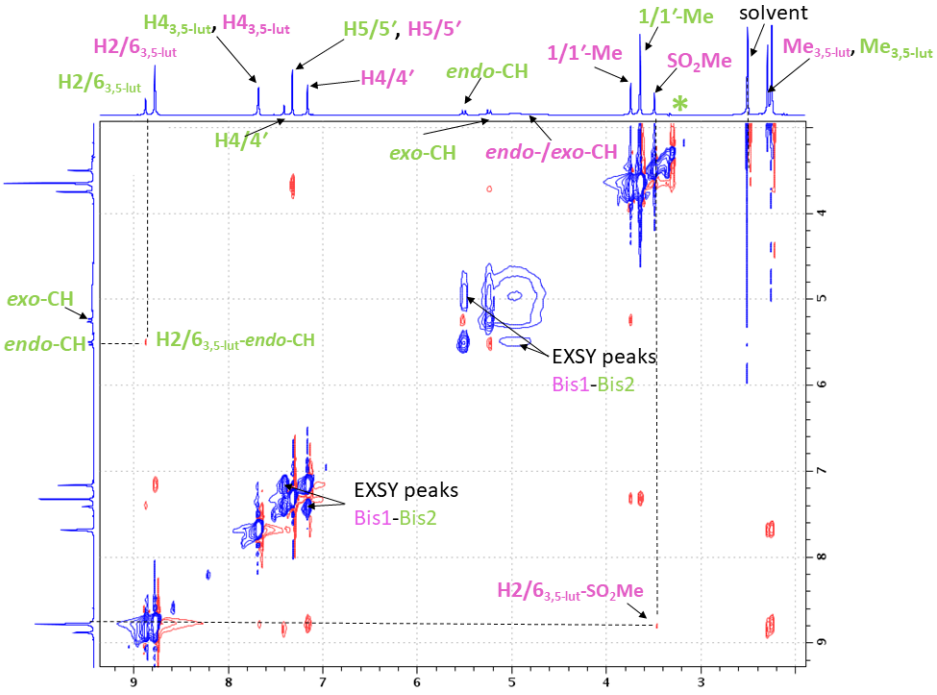

Figure C.4. ^{1}H-^{1}H ROESY spectrum (selected region) of [Pt(*N*(SO_2Me)1,1′-Me_2dma)(3,5-lut)$_2$](PF_6)$_2$ (**9**) (25 °C, 10 mM, DMSO-d_6, shifts in ppm). *SO_2Me group of Bis2 is suppressed along with the HOD peak.

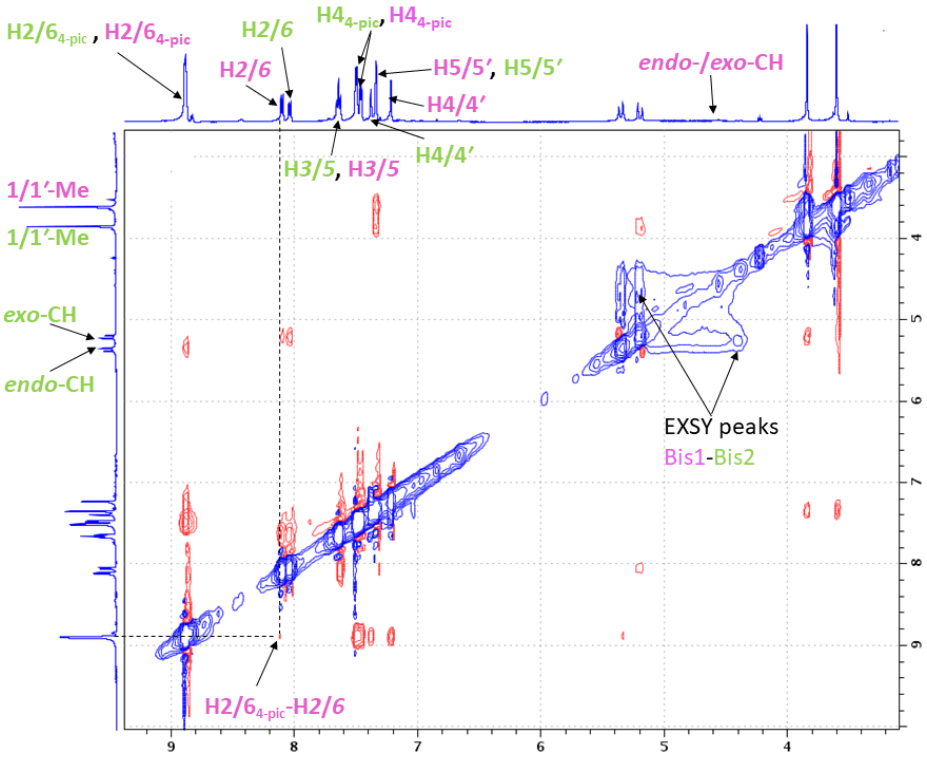

Figure C.5. ^{1}H NMR spectra (selected region) of [Pt(*N*(SO$_2$Tol)1,1′-Me$_2$dma)(4-pic)$_2$](PF$_6$)$_2$ (**8**) (25 °C, 10 mM, DMSO-d_6, shifts in ppm).

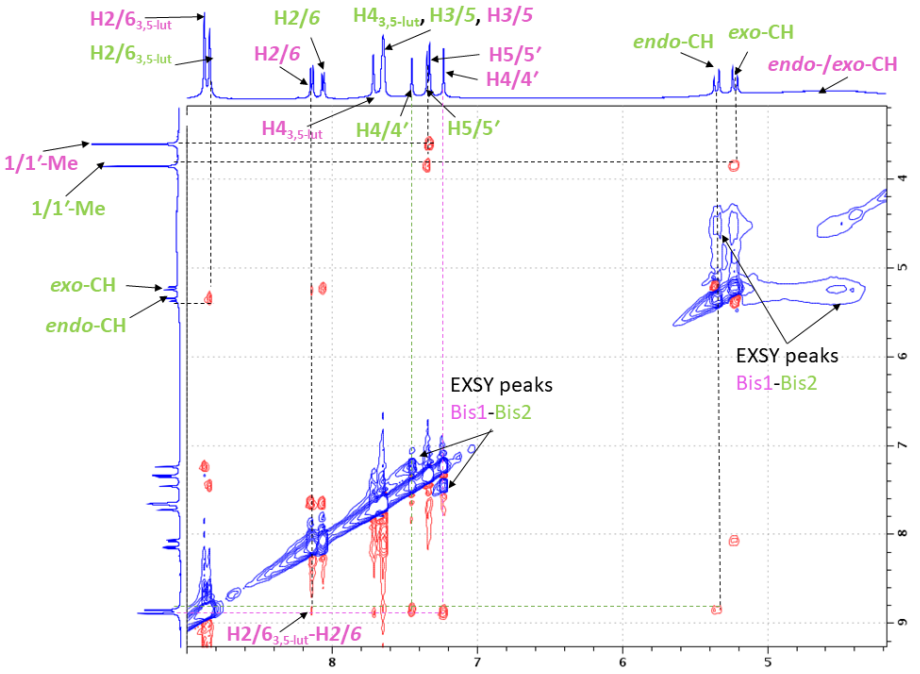

Figure C.6. ^{1}H-^{1}H ROESY spectrum (selected region) of [Pt(*N*(SO$_2$Tol)1,1′-Me$_2$dma)(3,5-lut)$_2$](PF$_6$)$_2$ (**10**) (25 °C, 10 mM, DMSO-d_6, shifts in ppm).

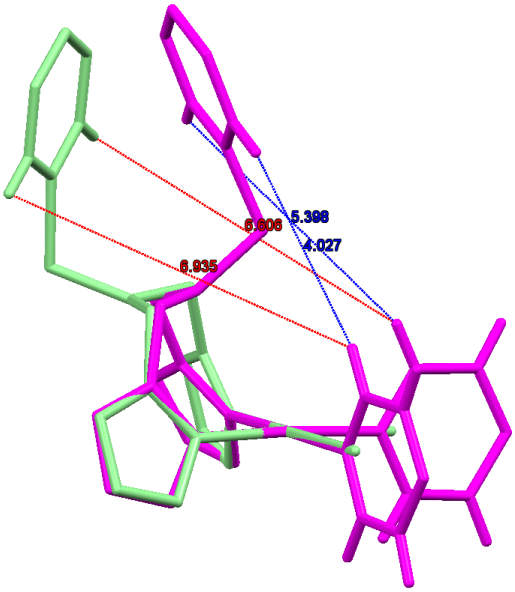

Figure C.7. Overlap of the stick drawings of [Pt(*N*(SO_2Tol)1,1′-Me_2dma)Cl_2 (**6**, green) and [Pt(*N*(SO_2Tol)1,1′-Me_2dma)(4-pic)$_2$]$^{2+}$ (**8**, purple) by superimposing the Pt, N1, and N2 atoms. The non-bonded distances (Å) between the H*2/6* protons of the Tol group and the H2/$6_{4\text{-pic}}$ protons were measured by using Mercury CSD 3.10.1 software. For clarity, some of the hydrogen atoms, oxygen atoms, and methyl groups are hidden.

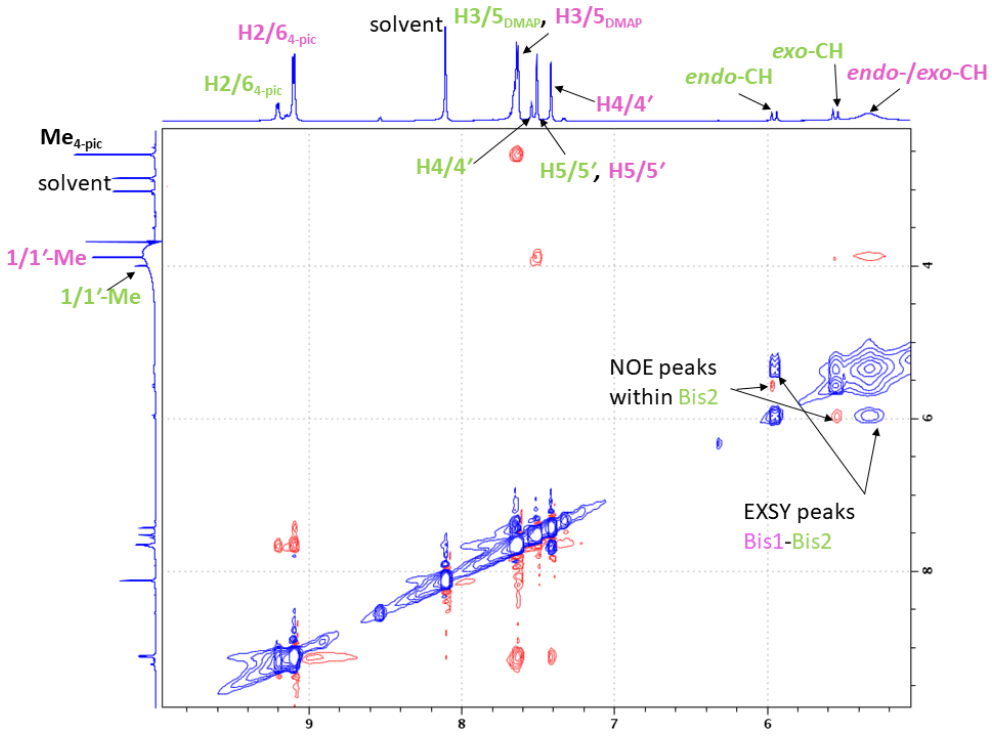

Figure C.8. ^{1}H-^{1}H ROESY spectrum (selected region) of [Pt(*N*(SO_2Me)1,1′-Me_2dma)(4-pic)$_2$](PF_6)$_2$ (**7**) (25 °C, 10 mM, DMF-d_6, shifts in ppm).

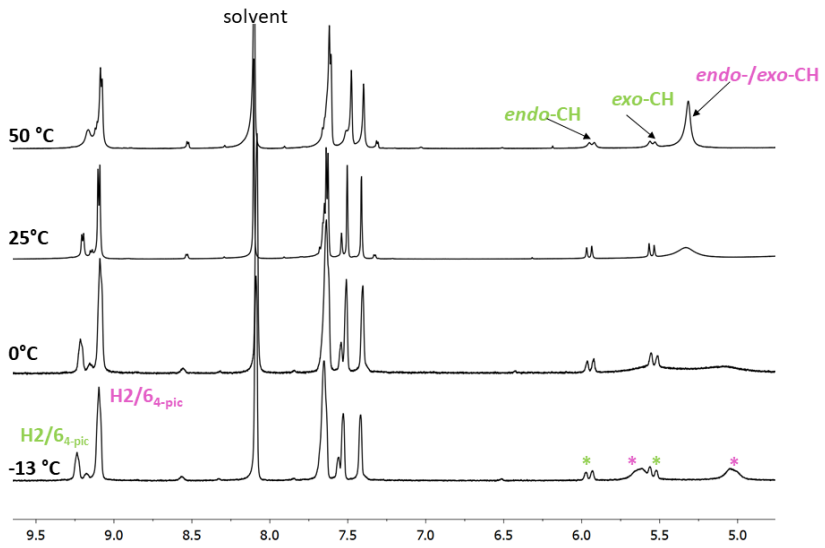

Figure C.9. ^{1}H NMR spectrum (selected region) of [Pt(*N*(SO_2Me)1,1′-Me_2dma)(4-pic)$_2$](PF_6)$_2$ (**7**, 10 mM, DMF-d_6, shifts in ppm) recorded at different temperatures, 50, 25, 0, and -13 °C.

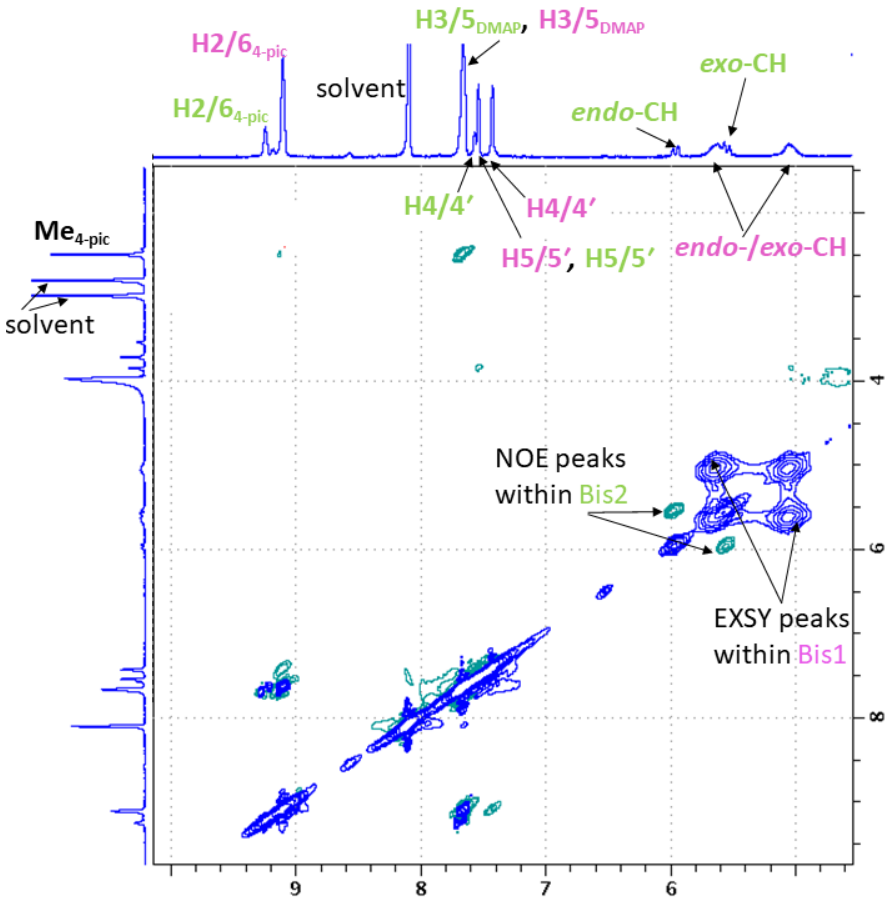

Figure C.10. ^{1}H-^{1}H ROESY spectrum (selected region) of [Pt(*N*(SO_2Me)1,1′-Me_2dma)(4-pic)$_2$](PF_6)$_2$ (**7**) (-13 °C, 10 mM, DMF-d_6, shifts in ppm).

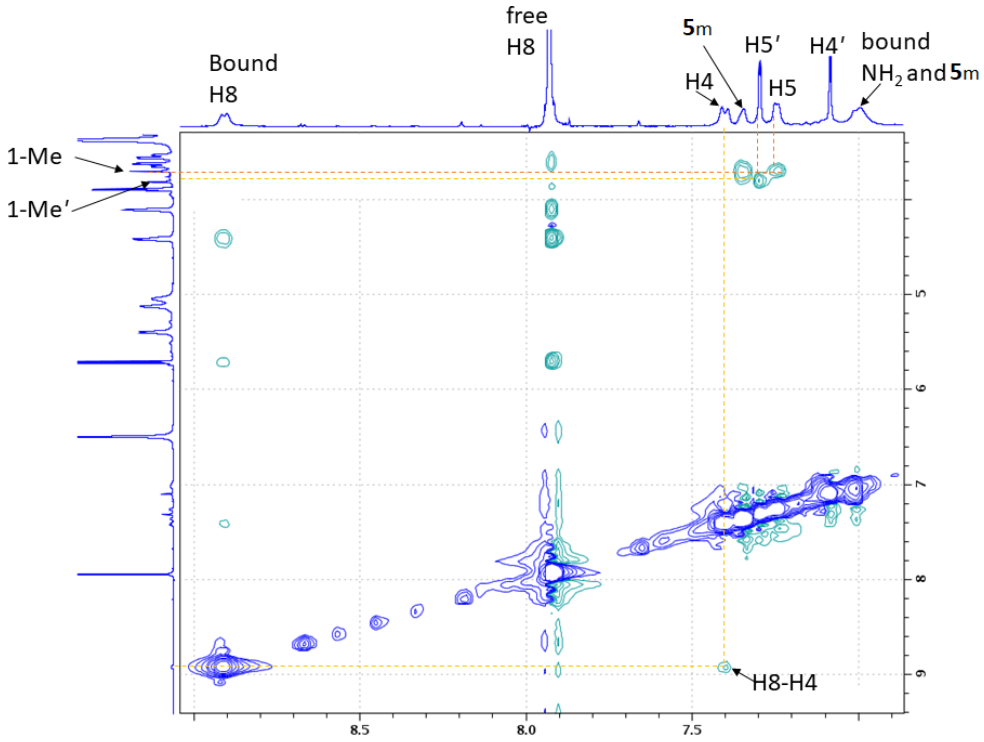

Figure C.11. ^{1}H-^{1}H ROESY spectrum (selected region) of the [Pt(*N*(SO_2Me)1,1′-Me_2dma)(Guo)Cl]$^{+}$ adduct (25 °C, DMSO-d_6, shifts in ppm).

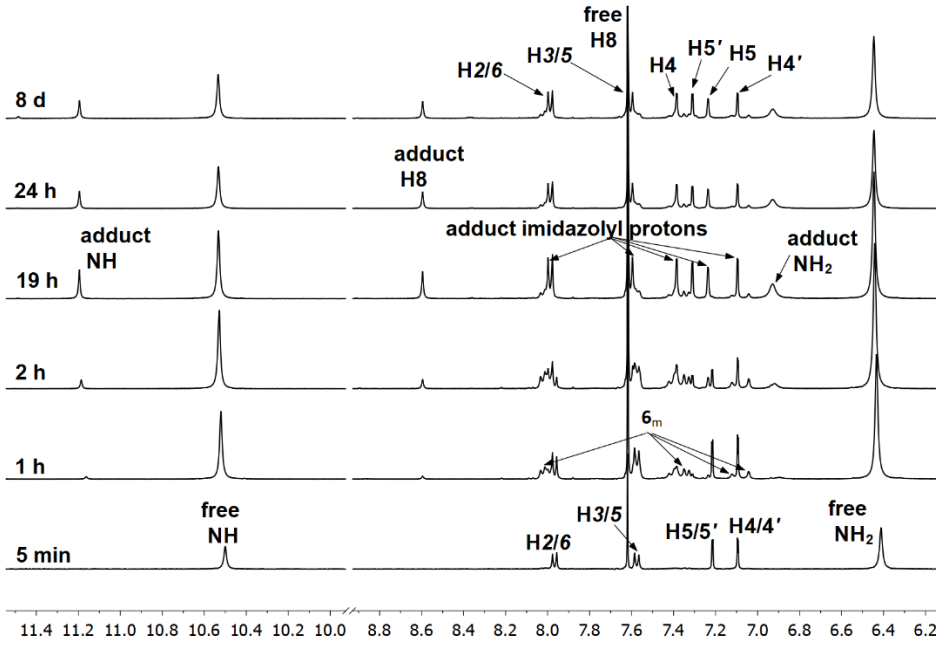

Figure C.12. Selected region of the ^{1}H NMR spectra of the reaction mixture forming [Pt(*N*(SO_2Tol)1,1′-Me_2dma)(9-MeG)Cl]$^{+}$ adduct recorded 5 min, 1 h, 2 h, 19 h, 24 h, and 8 d after addition of 1.9 mg of solid **6** in to a 25 mM solution of 9-MeG (25 °C, DMSO-d_6, shifts in ppm).

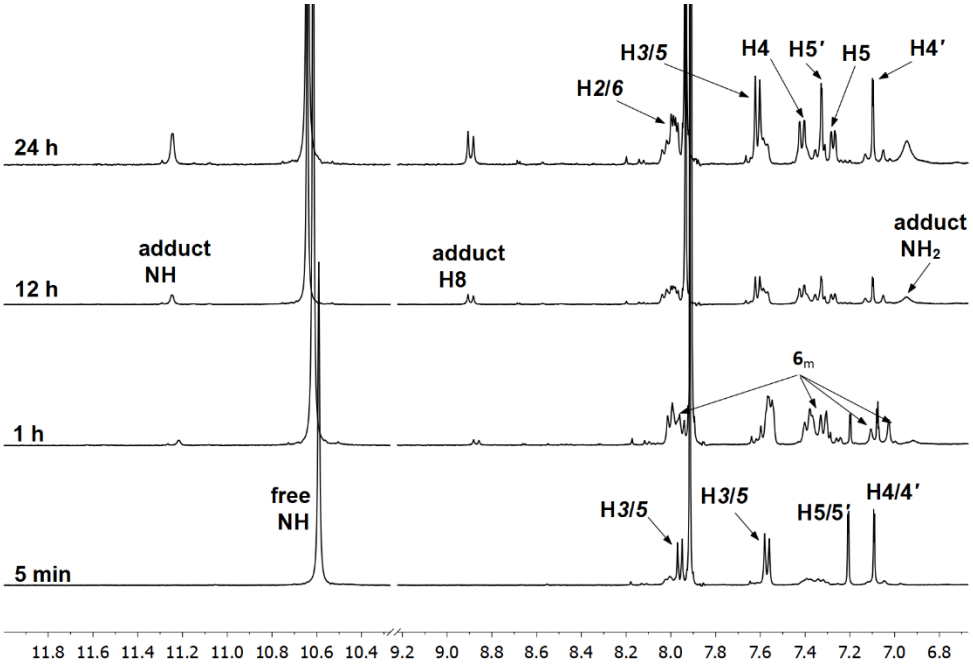

Figure C.13. Selected region of the ^{1}H NMR spectra of the reaction mixture forming [Pt(*N*(SO_2Tol)1,1′-Me_2dma)(Guo)Cl]$^{+}$ adduct recorded 5 min, 1 h, 12 h, and 24 h after addition of 1.9 mg of solid **6** in to a 25 mM solution of Guo (25 °C, DMSO-d_6, shifts in ppm).

APPENDIX D. PERMISSION

Copyright Clearance Center RightsLink®

Home | Account Info | Help

ACS Publications Most Trusted. Most Cited. Most Read.

Logged in as: kokila ranasinghe

LOGOUT

Title: A Very Rare Example of a Structurally Characterized 3′-GMP Metal Complex. NMR and Synthetic Assessment of Adducts Formed by Guanine Derivatives with [Pt(Ltri)Cl]Cl Complexes with an N,N′,N″ Tridentate Ligand (Ltri) Terminated by Imidazole Rings

Author: Kokila Ranasinghe, Svetlana Pakhomova, Patricia A. Marzilli, et al

Publication: Inorganic Chemistry

Publisher: American Chemical Society

Date: Jul 1, 2017

Copyright © 2017, American Chemical Society

PERMISSION/LICENSE IS GRANTED FOR YOUR ORDER AT NO CHARGE

This type of permission/license, instead of the standard Terms & Conditions, is sent to you because no fee is being charged for your order. Please note the following:

- Permission is granted for your request in both print and electronic formats, and translations.
- If figures and/or tables were requested, they may be adapted or used in part.
- Please print this page for your records and send a copy of it to your publisher/graduate school.
- Appropriate credit for the requested material should be given as follows: "Reprinted (adapted) with permission from (COMPLETE REFERENCE CITATION). Copyright (YEAR) American Chemical Society." Insert appropriate information in place of the capitalized words.
- One-time permission is granted only for the use specified in your request. No additional uses are granted (such as derivative works or other editions). For any other uses, please submit a new request.

VITA

Kokila Ranasinghe, eldest daughter of Ajith and Wasantha Ranasinghe, was born in 1987 in Colombo, Sri Lanka. Came from a modest family, she utilized the perks of the government's free education to become the first science graduate in her extended family. She received her school education from Anula Vidyalaya, Nugegoda. Then she entered the University of Sri Jayewardanepura in 2008 and graduated in 2012 with a Bachelor of Science degree majoring in Chemistry. She was one of the first undergraduate students of Dr. Theshini Perera, who inspired Kokila to pursue a career in science.

She entered the doctoral program of chemistry at Louisiana State University and joined the laboratory of Prof. Luigi G. Marzilli in May 2014 as the last graduate student of the group. Kokila was the recipient of the Mary Jo Pribble graduate student award for excellence in inorganic chemistry awarded by the Department of Chemistry, Louisiana State University in 2018. She is a candidate for the degree of Doctor of Philosophy in the Summer Commencement of 2018. Upon graduation, she plans to become a teacher to motivate young sri lankans to pursue and excel in science.